Functional characterisation of FAM40A and FAM40B as novel regulators of the cytoskeleton

Suryavanshi, Narendra Bhupal

Awarding institution:
King's College London

Functional characterisation of FAM40A and FAM40B as novel regulators of the cytoskeleton

by

Narendra Suryavanshi

A thesis submitted to King's College London

for the degree of Doctor of Philosophy, May 2013

Randall Division of Cell and Molecular Biophysics

King's College London

2nd floor New Hunt's House

London SE1 1UL

Abstract

This thesis describes the functional characterisation of the two human FAM40 proteins, FAM40A and FAM40B, in cancer cells and endothelial cells. FAM40A and FAM40B were initially studied in PC3 cells (a prostate cancer cell line) to determine their effects on cell morphology, adhesion and migration. PC3 cells show distinct morphological phenotypes when depleted of FAM40A and FAM40B using RNAi (RNA interference). Knockdown of FAM40A causes cells to have a smaller spread area, but cells depleted of FAM40B are elongated. FAM40-depleted PC3 cells display an adhesion defect, and FAM40B depletion results in a cell spreading defect. Additionally, FAM40B knockdown in PC3 cells leads to a reduction in cell speed.

FAM40A and FAM40B were identified as interacting partners for the CCM3 (cerebral cavernous malformation 3) protein in a previous biochemical study using mass spectrometry. CCM3 is mutated in a subset of patients with cerebral cavernous malformations (CCM). Patients display defects in the vascular endothelium of the central nervous system. The FAM40 proteins were found to form homo- and hetero- dimers, and interact with CCM3 and the serine/threonine kinases MST4 and STK25. Moreover, both FAM40 proteins and CCM3 can be phosphorylated *in vitro* by MST4. Knockdown of FAM40A, FAM40B and CCM3 in endothelial cells by RNAi causes an increase in stress fibres. FAM40B depletion also reduces endothelial barrier function. Furthermore, depletion of FAM40A, FAM40B and CCM3 results in defects in an *in vitro* angiogenesis assay. These results demonstrate the importance of the FAM40 proteins for endothelial cell physiology, and suggest they act as part of the CCM3-containing protein complex.

Taken together, the FAM40 proteins have important roles in cancer cell motility and adhesion, and are regulators of endothelial cell function. In addition to being implicated in CCM, these proteins could regulate two major steps in cancer progression – cancer cell migration, and neovascularisation.

Table of Contents

List of Figures

List of Tables

Supplementary movies

Movie 1	siRNA control PC3 : random migration	Figure 4.6
Movie 2	siRNA FAM40A-1 PC3 : random migration	Figure 4.6
Movie 3	siRNA FAM40A-5 PC3 : random migration	Figure 4.6
Movie 4	siRNA FAM40B-1 PC3 : random migration	Figure 4.6
Movie 5	siRNA FAM40B-4 PC3 : random migration	Figure 4.6
Movie 6	Mock HUVEC : loop assay	Figure 5.19
Movie 7	siRNA control HUVEC : loop assay	Figure 5.19
Movie 8	siRNA FAM40A-3 HUVEC : loop assay	Figure 5.19
Movie 9	siRNA FAM40A-5 HUVEC : loop assay	Figure 5.19
Movie 10	siRNA FAM40B-1 HUVEC : loop assay	Figure 5.19
Movie 11	siRNA FAM40B-5 HUVEC : loop assay	Figure 5.19
Movie 12	siRNA control HUVEC (- Y-27632) : loop assay, ROCK inhibitor rescue	Figure 5.20
Movie 13	siRNA control HUVEC (+ Y-27632) : loop assay, ROCK inhibitor rescue	Figure 5.20
Movie 14	siRNA FAM40A-3 HUVEC (- Y-27632) : loop assay, ROCK inhibitor rescue	Figure 5.20
Movie 15	siRNA FAM40A-3 HUVEC (+ Y-27632) : loop assay, ROCK inhibitor rescue	Figure 5.20
Movie 16	siRNA FAM40B-1 HUVEC (- Y-27632) : loop assay, ROCK inhibitor rescue	Figure 5.20
Movie 17	siRNA FAM40B-1 HUVEC (+ Y-27632) : loop assay, ROCK inhibitor rescue	Figure 5.20

Abbreviations

ADF	actin depolymerising factor
AJ	adherens junction
aPKC	atypical protein kinase C
Arp2/3	actin-related protein 2/3
ATP	adenosine triphosphate
BSA	bovine serum albumin
CCM	cerebral cavernous malformation
CHO	Chinese hamster ovary
CNS	central nervous system
CTTNBP2NL	cortactin binding protein 2 N-terminal like
DAPI	4',6-diamidino-2-phenylindole
DEPC	diethyl pyrocarbonate
DMEM	Dulbecco's modified eagle medium
DMSO	dimethyl sulphoxide
DNA	deoxyribonucleic acid
DTT	dithiothreitol
DUF3402	domain of unknown function 3402
EBM / EGM	endothelial basal medium / endothelial growth medium
EC	enzyme commission
E-cadherin	epithelial cadherin
ECL	enhanced chemiluminescence
ECM	extra-cellular matrix
EDTA	ethylene-diamine-tetra-acetic acid
EGF	epidermal growth factor
EGFP	enhanced green fluorescence protein
ELISA	enzyme-linked immunosorbent assay
EMT	epithelial to mesenchymal transition
ER	endoplasmic reticulum
ERK	extracellular signal regulated kinase
FACS	fluorescence activated cell sorting
F-actin	filamentous actin
FAK	focal adhesion kinase
FAM40	family with sequence similarity 40
FARL-11	factor arrest like-11
FCS	foetal calf serum
FGF	fibroblast growth factor
FH	formin homology
FITC	fluorescein isothiocyanate
G-actin	globular actin
GAP	GTPase activating protein
GAPDH	glyceraldehyde 3-phosphate dehydrogenase
GCKIII	germinal centre kinase III
GDI	guanine nucleotide dissociation inhibitor
GDP	guanosine diphosphate
GEF	guanine nucleotide exchange factor
GEO	gene expression omnibus
GST	glutathione S-transferase
GTP	guanosine triphosphate
HEG1	heart of glass 1
HEK293T	human embryonic kidney 293 T-antigen
HEPES	4-(2-hydroxyethyl)-1-piperazine-ethanesulphonic acid
HRP	horseradish peroxidase

HUVEC	human umbilical vein endothelial cell
ICAP1	integrin cytoplasmic-associated protein 1
IF	immunofluorescence
IP	immunoprecipitation
IPTG	isopropyl β-D-1-thiogalactopyranoside
JAM	junctional adhesion molecule
JNK	c-Jun N-terminal kinase
KLH	keyhole limpet hemocyanin
LB	luria broth
LPA	lysophosphatidic acid
MAPK	mitogen activated protein kinase
mDia	mammalian homologue of Drosophila diaphanous
MHC	myosin heavy chain
MINK1	misshapen like kinase 1
MLC	myosin light chain
mTOR	mammalian target of rapamycin
NDR	nuclear Dbf2-related
ORF	open reading frame
PAK	p21 activated kinase
PBD	p21 binding domain
PBS	phosphate buffered saline
PDGF	platelet-derived growth factor
PECAM-1	platelet endothelial cell adhesion molecule-1
PFA	paraformaldehyde
PI3K	phosphoinositide 3-kinase
PP2A	protein phosphatase 2A
PVDF	polyvinylidene fluoride
Q-PCR	quantitative polymerase chain reaction
RB1	retinoblastoma 1
RBD	Rho-binding domain
RLC	regulatory light chain
RNA	ribonucleic acid
RNAi	RNA interference
ROCK	Rho-associated kinase
ROS	reactive oxygen species
RPMI	Roswell park memorial institute
SDS-PAGE	sodium dodecyl sulphate-polyacrylamide gel electrophoresis
siRNA	small interfering RNA
STRIP	striatin interacting protein
STRIPAK	striatin interacting phosphatase and kinase
TBS	tris buffered saline
TCEP	tris(2-carboxyethyl) phosphine hydrochloride
TEM	trans-endothelial migration
TJ	tight junction
TNFα	tumour necrosis factor α
TORC2	target of rapamycin complex 2
TSP	thrombospondin
VE-cadherin	vascular endothelial cadherin
VEGF(R)	vascular endothelial growth factor (receptor)
VE-PTP	vascular endothelial-protein tyrosine phosphatase
WASP	Wiskott Aldrich syndrome protein
WAVE	WASP-family verprolin homology protein
WB	western blot
ZO	zonula occludens

1 Introduction

1.1 Cancer and cancer metastasis

1.1.1 Cancer: a micro-evolutionary process

The development of cancer can be modelled as a micro-evolutionary process (Alberts et al., 2002), in which the cells in an organism are considered an ecosystem, and must collaborate for the overall good of the organism. A cancer cell is a 'selfish cell' which proliferates at the expense of other cells and so disrupts the cellular ecosystem. Cells send and receive signals from each other and their environment that modulate key processes such as proliferation, differentiation and apoptosis in a manner that ensures the overall good of the organism. Genetic lesions in genes that regulate these pathways may give cells a selective advantage, and along with multiple rounds of mutation be sufficient to cause cancer (Hanahan and Weinberg, 2011)

One model for the mechanism by which cells become cancerous, is that they must obtain certain capabilities or hallmarks in order to overcome cellular control mechanisms that prevent the neoplastic process. These are self-sufficiency in growth signals, insensitivity to growth inhibitory signals, evasion of programmed cell death (apoptosis), limitless replicative potential, sustained angiogenesis, and tissue invasion and metastasis (Hanahan and Weinberg, 2011). Two hallmarks of particular relevance to this thesis include cancer metastasis which is discussed in section 1.1.2 and the link between tumorigenesis and angiogenesis which is discussed further in section 1.1.3.2. Mutations that confer these capabilities occur in genes termed either proto-oncogenes or tumour suppressors. Mutations in proto-oncogenes (resulting in an oncogene) represent 'gain of function' mutations in which the increased activity of the gene confers an increased risk of cancer. These genes usually represent stimulatory components of a regulatory pathway, are inherited as dominant alleles, and include the *Ras* and *Myc* oncogenes. For example, mutations in the *Ras* proto-oncogene which was the first to be indentified (Goldfarb et al., 1982; Pulciani et al., 1982; Shih and Weinberg, 1982) confer 'self-sufficiency in growth signals' and allow cells to proliferate excessively. On the other hand, tumour suppressor genes usually represent inhibitory components of a regulatory pathway and cancer mutations of this class represent

'loss of function' mutations which are recessive in nature. For a cell to become cancerous both copies of the tumour suppressor gene usually have to be mutated, an idea termed the 'two-hit' hypothesis (Knudson, 1971). An example is the *RB1* (retinoblastoma 1) gene which blocks cell proliferation, cell division and regulates cell death (Chau and Wang, 2003).

1.1.2 Cancer metastasis

In the course of the development of a cancer, cells from the primary tumour may attain the capacity to escape the tumour body, invade adjacent tissue and establish distant colonies of tumour cells. This process is termed metastasis (Nguyen et al., 2009). The main cause of mortality in cancer is the dissemination of primary tumours (Hunter et al., 2008) and hence deciphering the underlying mechanisms of this process is important to improve therapeutic intervention.

Metastasis is a complex process and simple oncogenic transformation is not sufficient to gain metastatic capability (Nguyen et al., 2009). While metastasis of solid tumours is a heterogeneous process depending on the cellular origin of a particular tumour, it generally consists of three steps; invasion of surrounding tissue, entry into lymphatic and blood vessels, and exit from blood vessels (reviewed in (Sahai, 2007)). These processes involve cell migration and adhesion which are discussed further in section 1.2. Changes in the expression of multiple genes are necessary to confer these properties. One step in attaining metastatic competency is to gain invasive capacity, and in tumours of epithelial origin this is commonly associated with a loss of E-cadherin (epithelial-cadherin) expression (Cavallaro and Christofori, 2004). E-cadherin is involved in the formation of adherens junctions between adjacent epithelial cells and aids in maintaining the quiescence of these cells (Hanahan and Weinberg, 2011). Loss of its expression allows the cells to escape from their epithelial site of origin and potentiates metastasis.

A developmental program termed 'epithelial to mesenchymal transition' (EMT) is implicated in epithelial cell invasion and dissemination, a common feature of which is a reduction in E-cadherin expression (Yang and Weinberg, 2008). The mesenchymal mode of cell migration is characterised by elongated cell morphology with defined cell polarity and the secretion of proteases to degrade the extra-cellular matrix (ECM) (Friedl and Wolf, 2003). The relevance

of this mode of invasion to metastasis is underlined by a study showing that mesenchymal cells are highly enriched in circulating tumour cells (Yu et al., 2013). Other modes of invasion have been linked to cancer metastasis and these include collective cell migration (discussed in (Friedl et al., 2012) and amoeboid migration in which cells show morphological plasticity and squeeze through gaps in the ECM using contractile force to generate motion (Friedl and Wolf, 2003).

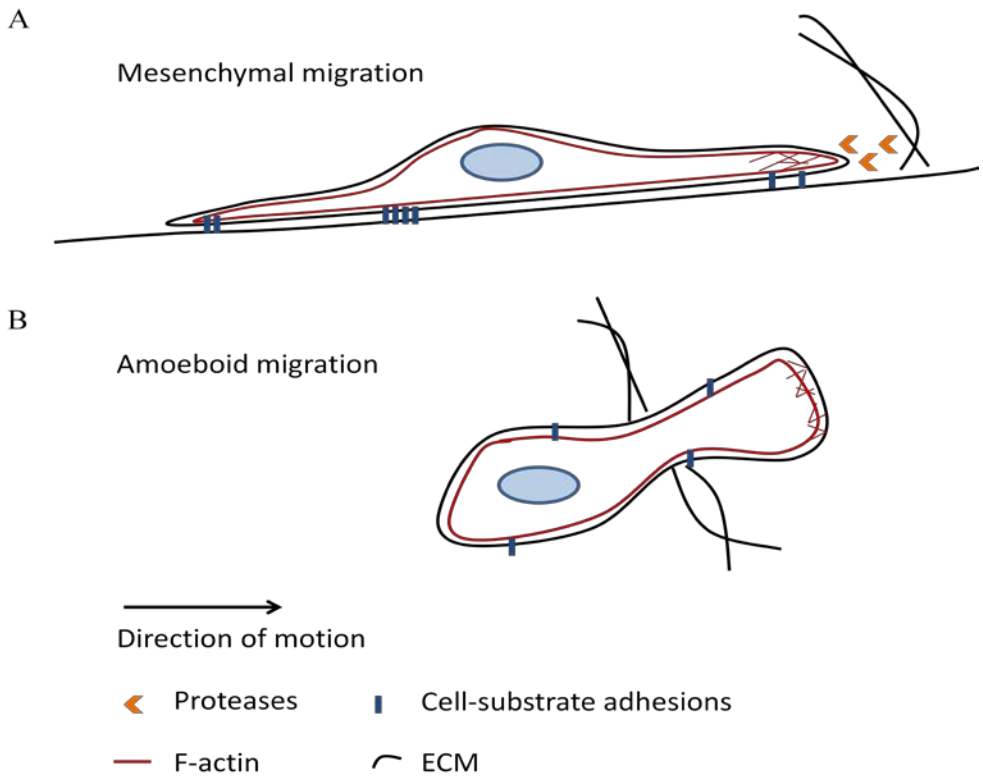

Figure 1.1 Modes of cancer cell invasion
(A) In the mesenchymal mode of migration, cells form strong adhesions to the substrate and migrate by protrusion of a leading edge and degradation of the ECM by protease enzymes. **(B)** In amoeboid migration, cells show morphological plasticity and squeeze through gaps in the ECM using contractile force to generate motion.

Cancer cell invasion relies on multiple interactions with both the surrounding ECM and neighbouring non-cancerous cells generally termed the tumour microenvironment (Calvo and Sahai, 2011). For example, cells of the tumour stroma have been found to secrete the chemokine CCL5 in response to signals from cancer cells. CCL5 acts on cancer cells to promote invasion (Karnoub et al., 2007). Another example is that of macrophages at the periphery of tumours producing matrix-degrading enzymes and so supporting local invasion

(Joyce and Pollard, 2009). These interacting networks could also hold the answer to why cancers of a certain origin can efficiently colonize only specific organs, an idea embodied in the 'seed and soil' hypothesis proposed by Stephen Paget in 1889 and revived by Hart and Fidler in 1980 (Hart and Fidler, 1980). The interaction of cancer cells with tumour-associated vasculature is of particular importance and relevance and is discussed in the following section.

1.1.3 Cancer and the endothelium

Two types of interactions between tumour cells and endothelial cells will be discussed in this section: tumour invasion of the endothelium and tumour angiogenesis.

1.1.3.1 The endothelium plays a central role in cancer metastasis

After cancer cells escape the primary tumour, they enter the vasculature (intravasation), and transit in the blood stream, having to withstand the shear stress caused by blood flow (Dadiani et al., 2006; Wyckoff et al., 2000). Cells then leave the vasculature (extravasation or trans-endothelial migration (TEM)), invade the underling matrix and establish metastases (Nguyen et al., 2009).

Tumour-associated endothelial cells display distinct gene expression profiles when compared to normal endothelial cells. Differences in expressed cell surface markers, adhesion proteins and cell signalling could contribute to the metastatic process (Hanahan and Weinberg, 2011). For example, it was initially thought that cancer cells extravasate at certain sites by being trapped in capillaries due to size restriction (Ito et al., 2001). However, it is now known that this is also an active process in which both the cancer cells and endothelial cells express cell surface adhesion molecules that initiate extravasation. For example, endothelial E-selectin interacts with its ligand PSGL-1, expressed on prostate cancer cells and so favours extravasation (Dimitroff et al., 2005). It is also clear that cancer cells are able to induce signalling events in associated endothelial cells to facilitate extravasation. A recent study illustrates how signalling induced by invasive breast cancer cells results in the disruption of endothelial cell-cell junctions and subsequent endothelial cell retraction (Haidari et al., 2012). Cancer cells can also co-opt other cells to escape the vasculature, for example by recruiting leukocytes and subsequently using them to facilitate

their own exit from blood vessels. CCL2 has been shown to be able to recruit inflammatory monocytes to promote breast cancer metastasis (Qian et al., 2011). In addition, CCL2 produced by tumour cells also increases the permeability of CCR2-expressing endothelium which contributes to increased levels of metastasis (Wolf et al., 2012). These studies point towards an interplay of signalling between cancer cells, endothelial cells and ancillary cells that affect vascular permeability and the invasive potential of tumour cells.

1.1.3.2 Cancer and angiogenesis

Just as normal tissues require oxygen and nutrients from the vasculature for their function and survival, the proximity of cancer cells to the vasculature is crucial for their propagation (Hanahan and Weinberg, 2011). While cancer cells can alter their energy metabolism to adapt to hypoxic conditions found in many tumours, they are usually highly dependent on angiogenesis to sustain themselves (Kroemer and Pouyssegur, 2008). Mechanisms of angiogenesis are discussed in section 1.5. This section deals with aspects of angiogenesis that are relevant to tumour progression.

During embryogenesis, endothelial cells differentiate from stem cells and form blood vessels in a process termed vasculogenesis. In contrast, angiogenesis is the process by which blood vessels sprout from pre-existing ones (Potente et al., 2011). In the adult, the vasculature is largely quiescent except in physiological processes such as wound healing and female endometrial growth. Even in these processes, angiogenesis is induced only transiently. However, during tumour progression, an ‘angiogenic switch’ is almost always turned on highlighting how intricately linked this process is to the neoplastic process (Hanahan and Folkman, 1996). The tumour neovasculature is abnormal in structure and function and endothelial cells lack a cobblestone appearance. Vessels are leaky resulting in poor perfusion, and their loose arrangement facilitates cancer cell invasion and dissemination (Potente et al., 2011). A further interesting consequence is that the poor functioning of these vessels leads to the creation of a hypoxic microenvironment which could drive the selection of more malignant cells and further induces angiogenesis. For example, hypoxia promotes cancer invasion by inducing overexpression of the *Met* proto-oncogene (Pennacchietti et al., 2003).

Tumour angiogenesis is controlled by counter acting pro- and anti- angiogenic signals and an imbalance leads to an angiogenic switch (Bergers and Benjamin, 2003). These signals can either be soluble signalling factors released by cancer cells that bind to receptors on endothelial cells or can be derived from co-opted stromal cells (reviewed in (Hanahan and Weinberg, 2011). Vascular endothelial growth factor-A (VEGF-A) is an important pro-angiogenic factor and a prime target for anti-angiogenic therapy (Ferrara, 2009). Its expression can be upregulated by both hypoxia and oncogene signalling (Carmeliet, 2005). Tumour angiogenesis is highly dependent on VEGF signalling responses which are coordinated to control endothelial cell proliferation/survival, and invasion/migration into surrounding tissue (reviewed in (Claesson-Welsh and Welsh, 2013)). Other pro-angiogenic factors are members of the fibroblast growth factor (FGF) family when their expression is chronically upregulated. Important examples of anti-angiogenic factors include thrombospondin-1 (TSP-1), angiostatin and endostatin. Some of these molecules can be detected in the circulation and could act as physiological regulators or as a defence mechanism against tumour neo-vascularisation (Ribatti, 2009). A range of bone marrow-derived cells also contribute to tumour vascularisation. For example, tumour associated macrophages stimulate angiogenesis by producing VEGF (Lin et al., 2006). Endothelial progenitor cells might also contribute to tumour vascularisation in a manner that resembles vasculogenesis (Patenaude et al., 2010).

1.2 Cell motility and the actin cytoskeleton

Cell migration is a complex process that involves the integration of multiple signals and events both spatially and temporally (reviewed in (Ridley et al., 2003)). Cell motility contributes to many physiological processes such as angiogenesis, tissue repair, immune surveillance, embryonic morphogenesis and foetus implantation. Cell migration also contributes to pathological conditions such as cancer metastasis, chronic inflammation and vascular disease.

Migrating cells need a mechanism by which they sense their environment which contributes to their steering system, an engine to provide the mechanical force that drives locomotion and traction to facilitate these processes and provide adhesive force. Single cells can

migrate using either a mesenchymal or amoeboid mode of migration (described in section 1.1.2). Once cells determine the direction in which they are to move and establish polarity, movement is initiated by the extension of plasma membrane protrusions at the leading edge and the creation of adhesive contacts at the front of the cell by transmembrane adhesion molecules such as the integrins. This is co-ordinated with the detachment of adhesions, cell retraction and actin disassembly at the rear of the cell (Cain and Ridley, 2009).

Protrusions extended at the leading edge include lamellipodia and filopodia (reviewed in (Ridley, 2011)). Lamellipodia are thin, sheet-like protrusions, and the dynamic behaviour of the actin cytoskeleton is central to providing the mechanical force for their extension (reviewed in (Pollard and Borisy, 2003). Actin in its monomeric form (termed globular or G-actin) is soluble but when polymerised, forms insoluble filaments (filamentous or F-actin) (Cory and Ridley, 2002). Actin filaments display polarisation in that they possess a 'fast growing' barbed end and a 'slow growing' pointed end. The localised, directional polymerisation of actin at the leading edge is what drives membrane extension (reviewed in (Ridley et al., 2003). A number of regulatory proteins modulate various aspects of actin dynamics such as filament assembly, branching, bundling and disassembly. The nucleation of actin monomers into a trimer is a rate-limiting step in filament assembly. This process is stimulated by actin nucleators and important examples include the Wiskott Aldrich syndrome protein (WASP) family of proteins. These factors which include WASP itself and WASP-family verprolin homology proteins (WAVEs) bind to and activate the Arp2/3 complex enhancing its capacity to induce actin polymerisation (Cory and Ridley, 2002). The Arp2/3 complex causes branching of the actin network by binding to the sides of existing actin filaments and stimulating the formation of 'dendritic' actin filament networks.

Other important actin nucleators that contribute to lamellipodium extension include members of the formin and Spire families (Ridley, 2011). Formins cause unbranched actin filament extension, and protect barbed ends from capping proteins which restrict actin polymerisation. Similarly, Spire family members cause nucleation of unbranched actin filaments. Additional regulators of actin polymerisation in mediating protrusions include proteins of the ADF/cofilin family, cortactin, filamin A and α-actinin. Cofilin mediates the

severing of existing filaments hence generating new barbed ends that can be used to prime further polymerisation. Profilin prevents self-nucleation of actin monomers by binding to them and also aids in targeting them to barbed ends to facilitate polymerisation. Cortactin stabilises actin branches while filamin A and α-actinin cross link filaments and so stabilise them (Ridley et al., 2003).

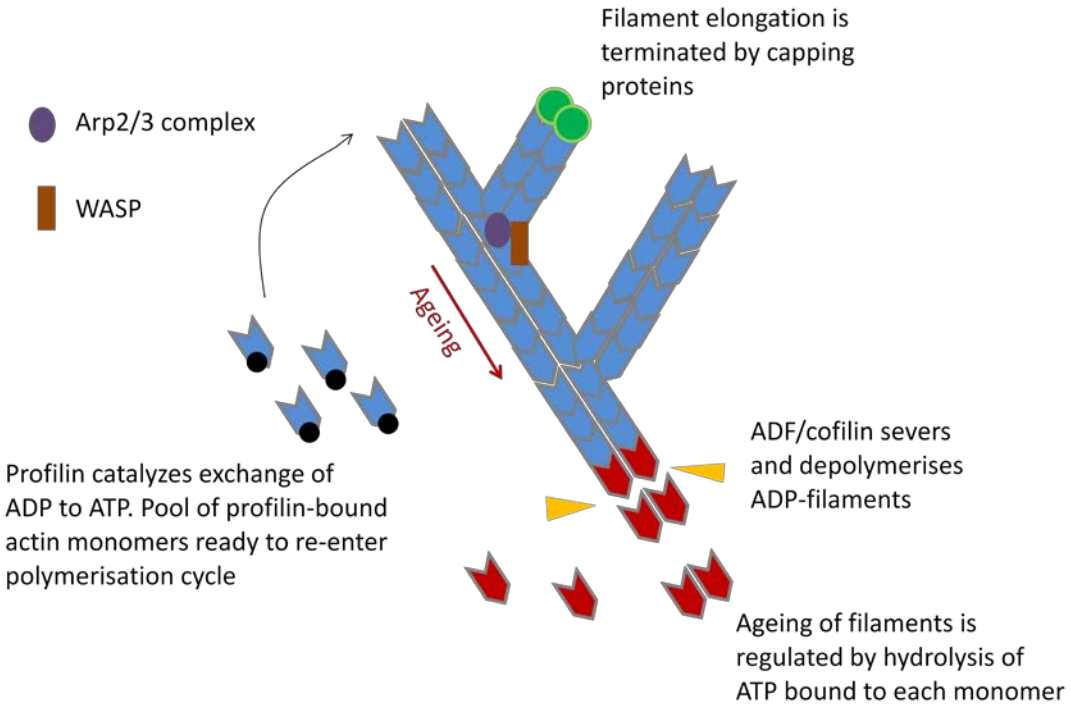

Figure 1.2 Schematic illustrating dynamics of the actin cytoskeleton during membrane protrusion extension
Actin polymerisation and depolymerisation are controlled by multiple actin regulatory proteins (refer to text for details).

Filopodia differ from lamellipodia in that they are exploratory extensions of the plasma membrane that contain parallel bundles of F-actin. Fascin is an actin-bundling protein important for filopodial stability. There is some overlap in the machinery that regulates lamellipodium and filopodium generation. For example formins such as mDia proteins, WASP and the Arp2/3 complex regulate the formation of filopodia (Ridley, 2011).

Protrusions such as lamellipodia and filopodia are stabilised by the formation of adhesions and are coordinated with contraction/retraction events. An important class of adhesion proteins are the integrins which are heterodimeric receptors consisting of α and β chains

(reviewed in (Luo et al., 2007). Integrins connect the cytoskeleton to the extra-cellular matrix and act as mechano-sensors by 'outside-in signalling' and can regulate adhesion by responding to intracellular signalling events referred to as 'inside-out signalling'. Integrins cluster at sites of adhesion and recruit multiple proteins that bind to their cytoplasmic tail. Partners such as talin, vinculin and α-actinin play a role in the integrin-actin connection (Ziegler et al., 2008) while FAK (focal adhesion kinase) is responsible for generating a cascade of integrin-linked signalling (Mitra et al., 2005). Retraction of the rear of the cell is brought about by actomyosin contractility and is coordinated with adhesion disassembly in order for the cell to move forward. The integrin-actin connection plays a central role in transducing the contractile force generated, resulting in cell body contraction and tail retraction. Contractile forces are generated by cross-linking of myosin II and actin filaments. The myosins are a superfamily of molecular motor proteins (reviewed in (Sellers, 2000). Myosin II is a hexamer comprising of two heavy chains (MHC), two essential light chains and two regulatory chains (RLC). Myosin II hexamers assemble to form bipolar filaments which then bind actin at each end. Actomyosin contraction is generated by ATP-dependent sliding of myosin along the actin filaments, pulling the two filaments together. Myosin II activity is regulated by phosphorylation at multiple sites in the RLC. For example, the phosphorylation of the RLC at Threonine 18 and Serine 19 is known to increase actomyosin contractility (Watanabe et al., 2007).

Cells can also use an alternative form of motion based on membrane blebbing. Blebs are membrane protrusions generated due to contractile activity of the actomyosin cortex. They are rapidly produced and retracted and examples of cells in which they are observed include some tumour cells (Sahai and Marshall, 2003) and *Dictyostelium* (Langridge and Kay, 2006). Blebbing is thought to be important for migration in three dimensional matrices, allowing cells to squeeze between ECM filaments (Fackler and Grosse, 2008).

1.3 Rho GTPases: regulators of the cytoskeleton and cell motility

The Rho family guanosine triphosphate (GTP) binding proteins (Rho GTPases) are central regulators of many of the events regulating cell motility that have been described. They are known to regulate actin cytoskeletal dynamics, adhesion organisation and

contraction/retraction events (Ridley et al., 2003). The Rho GTPases belong to the Ras superfamily of small GTPases and bind and hydrolyse GTP (EC 3.6.5.2) (Boulter et al., 2012). These proteins are highly conserved in evolution and have been found in all eukaryotic genomes sequenced so far, including plants and fungi (Boureux et al., 2007; Heasman and Ridley, 2008). Since the discovery of the founding member Rho (Madaule and Axel, 1985) and delineation of its role in cytoskeletal remodelling (Ridley and Hall, 1992), these proteins have been found to be crucial regulators of the cytoskeleton. They also contribute to several other cellular processes such as control of gene transcription, cell cycle progression and cell polarity (Jaffe and Hall, 2005). There are 20 known genes encoding Rho GTPases in the human genome divided into 8 subfamilies based on sequence homology (Boureux et al., 2007).

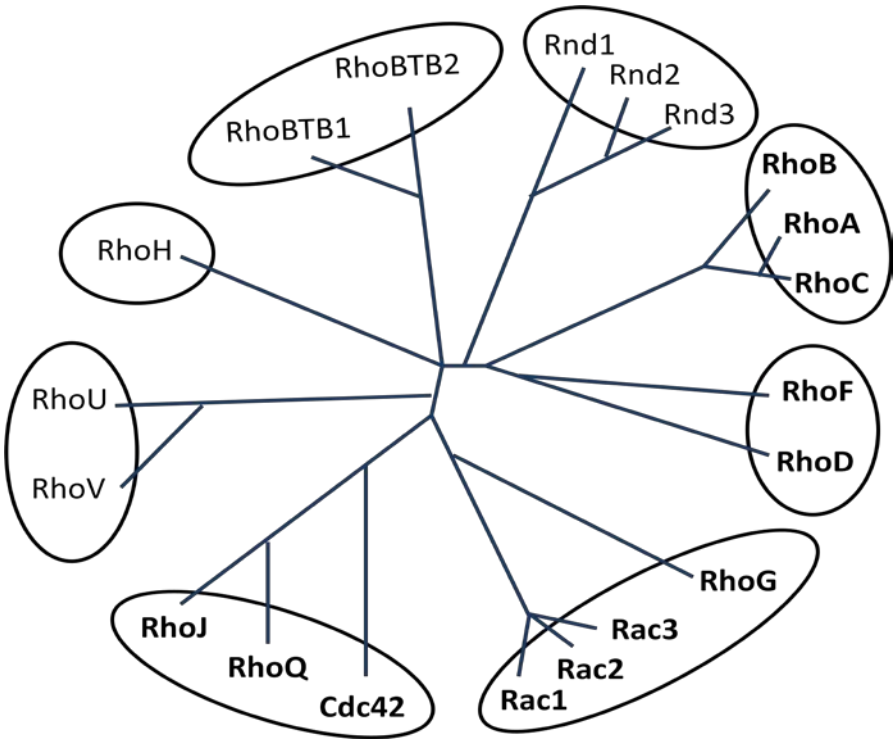

Figure 1.3 The Rho GTPase family tree
The 20 Rho GTPase encoding genes are grouped into 8 subfamilies. Typical members of the family that possess intrinsic GTPase activity are highlighted in bold. The family tree was derived by phylogenetic analysis using human Rho GTPase protein sequences. Adapted from Figure 1 in Boureux et. al., 2007.

1.3.1 Regulation of Rho GTPase activity

Most Rho GTPases act as molecular switches and cycle between an 'active' GTP-bound form and 'inactive' GDP-bound form. In their GTP-bound form, these proteins are able to bind to a variety of downstream effector proteins and so initiate cell signalling. The cycling of the Rho GTPase proteins between GTP and GDP bound forms is regulated by three sets of proteins: guanine nucleotide exchange factors (GEFs), GTPase activating proteins (GAPs) and guanine nucleotide dissociation inhibitors (GDIs). An additional important mechanism of regulation is the post-translational modification of Rho GTPase proteins.

GEFs promote the exchange of bound GDP for GTP by catalysing the release of the GDP molecule and causing the formation of an unstable nucleotide free intermediate. As the cytosolic GTP level is higher than GDP levels, this intermediate is loaded with GTP (Rossman et al., 2005). GAPs downregulate Rho GTPase activity by stimulating GTP hydrolysis. While most Rho GTPases have intrinsic GTPase activity, this is too slow to be physiologically effective, and GAPs serve to accelerate GTP hydrolysis. The regulation of GEFs and GAPs is complex and integrates a variety of upstream signals. An interesting example is cross-talk between different Rho proteins via GEFs and GAPs. For example, active Rac1 can bind to and activate p190RhoGAP and so antagonizes RhoA activity (Bustos et al., 2008).

Most Rho GTPases signal on membranes and to facilitate their localisation to membranes, they are post-translationally modified at the C-terminus by the addition of a lipid group. The CAAX consensus tetrapeptide motif (Cysteine-Aliphatic-Aliphatic-Variable) at the C-terminus of certain Rho GTPase proteins is required for prenylation. This can be a geranylgeranyl or farnesyl lipid. A lack of prenylation causes mislocalisation of Rho GTPase protein to the cytoplasm rendering them functionally inactive (Roberts et al., 2008). Some Rho GTPases are palmitoylated. For example, RhoU and RhoV are palmitoylated instead of being prenylated. The Rho BTBs lack the CAAX box completely (Aspenstrom et al., 2007). The third class of Rho regulatory proteins are GDIs which mask C-terminal prenyl lipid groups, preventing association of Rho GTPases with membranes and thus inhibiting their interaction with downstream effectors (Garcia-Mata et al., 2011).

In addition to lipid modification, Rho proteins can be regulated by various other post-translational modifications. For example, RhoA is phosphorylated at serine 188 which is situated in a conserved polybasic region at the C-terminus. This phosphorylation event negatively regulates RhoA (Ellerbroek et al., 2003). The expression levels of Rho proteins including RhoA and Rac1 can be controlled by means of the ubiquitin-proteasome pathway (Nethe and Hordijk, 2010). In comparison, SUMOylation does not simply turn the Rho switch on or off but instead serves to fine tune the extent of activity. SUMOylation of Rac1 increases the level of GTP loading and stabilises Rac1 activation (Castillo-Lluva et al., 2010). In contrast to other Rho GTPases, atypical members of the Rho family such as Rnd3 and RhoH are constitutively bound to GTP. Their activity is regulated by control of protein levels and phosphorylation (Aspenstrom et al., 2007). For example, RhoH is regulated at the level of transcription (Delestre et al., 2011), and Rnd3 is inactivated by phosphorylation (Riou et al., 2013).

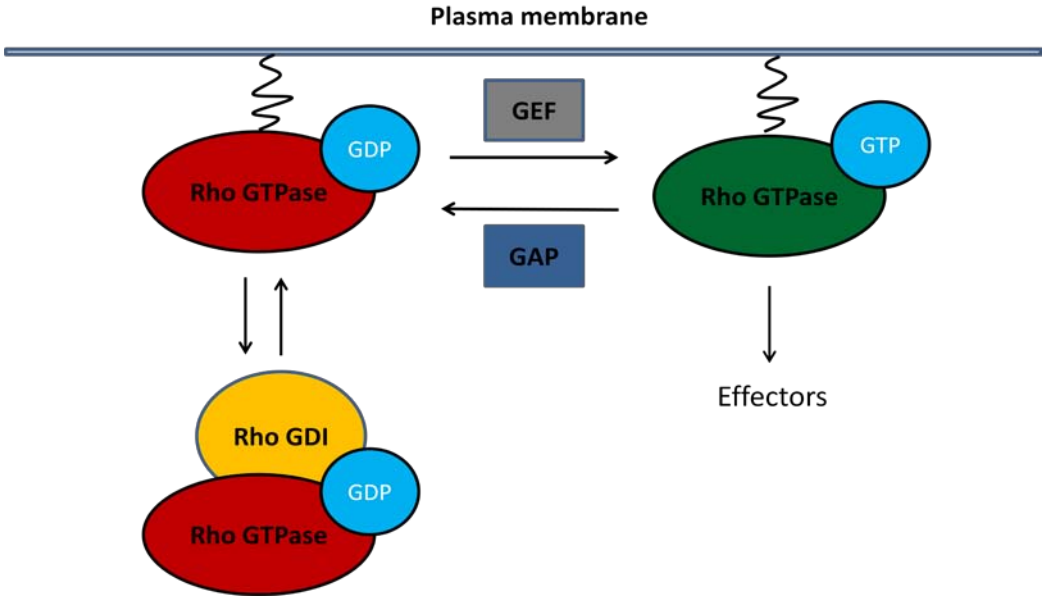

Figure 1.4 Regulation of Rho GTPase activity
Schematic illustrating the regulation of Rho GTPase activity. Typical members of the Rho GTPase family cycle between an 'active' GTP-bound form and an 'inactive' GDP-bound form. GEFs facilitate the conversion of the GDP-bound form to the GTP-bound form. GAPs stimulate GTP hydrolysis and so downregulate Rho GTPase activity. Rho GDIs sequester several Rho proteins in the cytoplasm, preventing their association with membranes which is needed for their signalling.

1.3.2 Rho GTPase signalling

Rho proteins in their GTP-bound active form interact with an array of downstream signalling partners including protein kinases, adapter proteins and actin-regulatory proteins (Bishop and Hall, 2000), and integrate information from a broad spectrum of upstream signals such as growth factors, chemokines and cell adhesion receptors (Sahai and Marshall, 2002). Of the 20 known human Rho GTPases, RhoA, Rac1 and Cdc42 have been the most intensively studied and were also the first to be characterised (Kozma et al., 1995; Nobes and Hall, 1995; Ridley and Hall, 1992; Ridley et al., 1992). This section describes the effects these three proteins have on the actin cytoskeleton. The structure and function of stress fibres (contractile actomyosin filaments) is discussed in greater detail too.

A main function of the Rho GTPases is to regulate the actin cytoskeleton, and as a consequence they are involved in processes that are dependent on the actin cytoskeleton such as cell migration, phagocytosis, vesicle trafficking, axon guidance and cytokinesis (Bishop and Hall, 2000). Initial evidence that RhoA and Rac1 regulate the assembly of actin filaments in response to extracellular cues was provided by studies in serum starved Swiss3T3 fibroblasts. In response to LPA (lysophosphatidic acid) RhoA was shown to be able to induce the formation of contractile actomyosin filaments (stress fibres) and associate focal adhesions (Ridley and Hall, 1992). Focal adhesions are macro-molecular complexes, and are sites of cell adhesion to the ECM. Rac1 was shown to promote the formation of membrane ruffles or lamellipodia in response to PDGF (platelet-derived growth factor), EGF (epidermal growth factor) or insulin. Rac1 was also shown to act via RhoA to induce contractile actomyosin filaments (Ridley et al., 1992). Subsequently, Cdc42 was shown to induce the formation of filopodia as well as indirectly inducing membrane ruffles by the activation of Rac1 (Kozma et al., 1995; Nobes and Hall, 1995).

Even though Rac1 and Cdc42 elicit morphologically different protrusions (lamellipodia and filopodia respectively), they both stimulate actin polymerisation via the Arp2/3 complex (reviewed in (Bishop and Hall, 2000)). Activation of Rac1 is sufficient on its own to induce lamellipodium formation (Wu et al., 2009). Rac1 activates the WAVE complex, following which activated WAVE binds to and activates the Arp2/3 complex which initiates actin

polymerisation. Rac1 also acts via its target PAK (p21-activated kinase) and LIM kinase (LIMK) to phosphorylate and inhibit cofilin. Cofilin disassembles actin filaments, and hence this activity of Rac1 stabilises actin filaments. A model for cofilin action is that its enrichment at the cell membrane results in the generation of new barbed ends, resulting in increased actin polymerisation and extension of membrane protrusions (Tania et al., 2011). In addition, RhoA can either induce or inhibit lamellipodia formation. Loss of RhoA inhibits lamellipodia formation but too much activity at the leading edge stimulates contractility (Ridley, 2011). This indicates the need for precise spatio-temporal regulation of different Rho GTPases to bring about effective cell migration.

Cdc42 also activates Arp2/3 but via WASP and N-WASP (neuronal WASP), and brings about the formation of filopodia. Filopodium formation is thought to require an initial Arp2/3 nucleation step followed by an mDia2-mediated elongation event. However, this picture is complicated by the fact that filopodia can also form independently of the Arp2/3 complex via formins alone (Yang and Svitkina, 2011). Like Rac1, Cdc42 can act via PAK and LIMK to phosphorylate and inhibit cofilin (Bishop and Hall, 2000). Cdc42 also regulates cell polarity acting via its target Par6 and atypical protein kinase C (aPKC) (Etienne-Manneville and Hall, 2003).

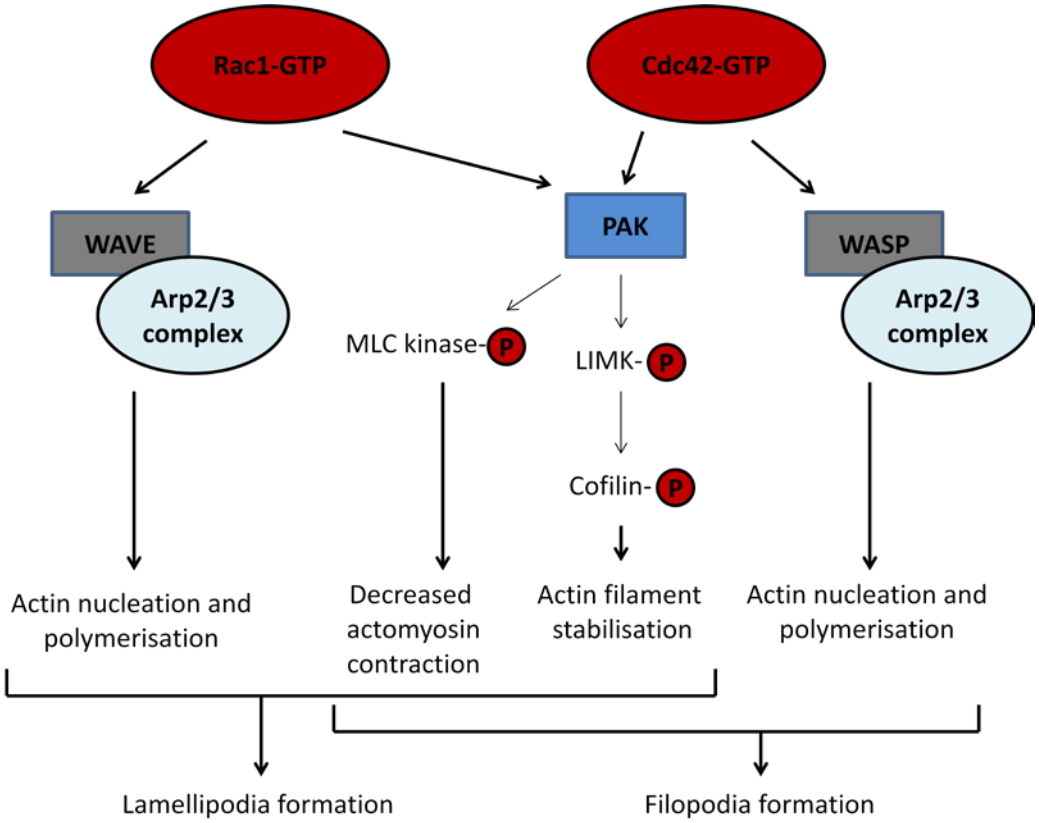

Figure 1.5 Rac1 and Cdc42 signalling involved in the formation of lamellipodia and filopodia
Activated Rac1 and Cdc42 lead to cofilin inactivation via PAK and LIMK which serves to stabilise actin filaments. PAK also phosphorylates and inactivates MLC kinase, resulting in reduced actomyosin contraction. Both Rac1 and Cdc42 bring about actin nucleation and polymerisation via WAVE and WASP respectively.

Stress fibres are a major structure regulated by RhoA signalling. Two effectors are required for RhoA-mediated induction of stress fibres and focal adhesions, ROCK (Rho-associated kinase) and mDia1 (an FH (formin homology) domain containing protein) (reviewed in (Bishop and Hall, 2000)). ROCK is a serine/threonine kinase that is activated upon binding to RhoA-GTP by a disruption of autoinhibitory, intramolecular interactions. There are two ROCK proteins, ROCK1 and ROCK2, and recent observations have indicated that they have different biological roles (Shi et al., 2013; Vega et al., 2011). However, for simplicity they will be referred to as ROCK. Two key substrates of ROCK are myosin light chain (MLC) and the myosin binding subunit of MLC phosphatase. Phosphorylation of MLC at serine 19 by ROCK stimulates the ATPase activity of myosin II and leads to the assembly of actomyosin filaments. ROCK also indirectly increases the pool of phosphorylated MLC (p-MLC) by

phosphorylating and inactivating MLC phosphatase. MLC is also phosphorylated by MLC kinase (MLCK) at threonine 18 and serine 19 (Watanabe et al., 2007). Hence, the phosphorylation of MLC and of MLC phosphatase can be used as a read-out of contractility to some extent. Activation of mDia1 by RhoA leads to it binding to profilin and so contributes to increased polymerisation of actin. A model of mDia1 function is that it initiates actin nucleation in a focal contact contributing to stress fibre extension from the cell membrane (Kovar, 2006). These two effectors are needed together for the assembly of stress fibres. Activation of ROCK alone in the absence of mDia1 results in the formation of thick, stellate stress fibres while mDia1 alone induces thin stress fibres. However, both proteins together induce structures resembling that formed upon Rho activation (Watanabe et al., 1999). Another important target of ROCK is LIMK which phosphorylates and inhibits cofilin. This serves to stabilise actin filaments and also contributes to the formation of stable stress fibres (Bishop and Hall, 2000).

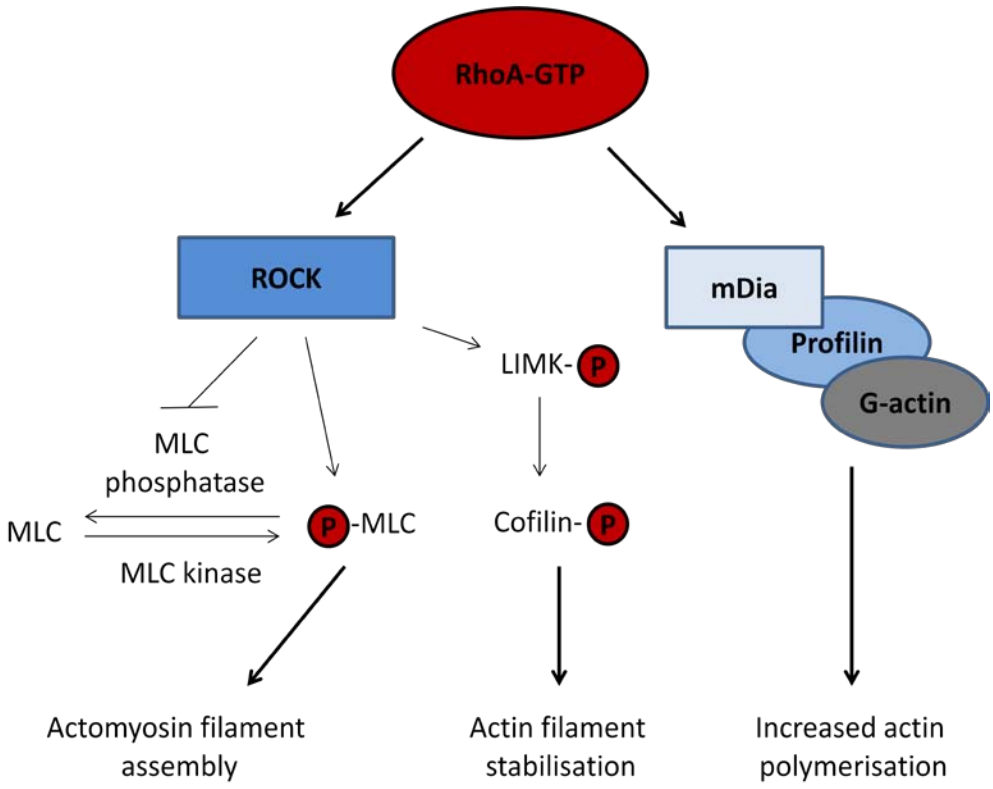

Figure 1.6 Signal transduction during RhoA-mediated stress fibre assembly
RhoA induces stress fibres via its downstream effectors, ROCK and mDia. ROCK increases the pool of p-MLC leading to actomyosin filament assembly. ROCK also leads to cofilin inactivation via LIMK which serves to stabilise actin filaments. mDia activation leads to actin polymerisation.

1.3.2.1 Structure and function of stress fibres

Stress fibres in non-muscle cells are essentially bundles of actomyosin filaments that are comparable to the highly ordered actomyosin structures seen in muscle cells (reviewed in (Pellegrin and Mellor, 2007)). Stress fibres are contractile structures comprising of bundles of about 10-30 actin filaments and myosin II. These filament bundles are held together by actin cross-linking proteins such as α-actinin which is arranged periodically along the bundle (Lazarides and Burridge, 1975). Stress fibres in non-muscle cells differ from muscle sarcomeres significantly with regard to the polarity of actin filaments (Cramer et al., 1997; Mseka et al., 2009). This is an important concept as it determines contractile properties of the bundled actin filaments. In muscle cells, each block of bundled actin filaments shows opposite polarity to the successive block to facilitate sliding contraction. The orientation in non-muscle stress fibres can be much more diverse. However, in motile cells most stress fibres show graded polarity wherein at the ends of the fibre, filament orientation is uniform (barbed ends pointing outwards) and at the centre the filament polarity is more heterogeneous.

Stress fibres can also be classified on the basis of their assembly in relation to the entire cell. (reviewed in (Tojkander et al., 2012)). Ventral stress fibres lie at the base of the cell and are anchored to focal adhesions at each end. Dorsal stress fibres are attached to a focal adhesion at only one end with the other end terminating in a loose meshwork of actin filaments. The third class are transverse arcs which are bundles of actin that form behind the protrusive edge of a migrating cell.

An important question to address in the context of the structure and assembly of stress fibres is what function do stress fibres have? Dorsal stress fibres have uniform polarity as they are formed by filament elongation from a fixed point. Hence, they may not have significant contractile functions and could instead be involved in myosin-based trafficking of vesicle cargos or proteins (DePina and Langford, 1999). They may also contribute to the cell's rigidity and be an intermediate in the formation of ventral fibres. Transverse arcs are not anchored at either end and hence once again it is unclear if they could function as contractile structures. On the other hand ventral fibres are tethered at either end to focal

adhesions and are the major contractile machinery in many cells (Tojkander et al., 2012). For example, this function is necessary for tail retraction in migrating cells, and ventral stress fibres are aligned in the direction of motion in motile fibroblasts (Cramer et al., 1997).

A function for stress fibres particularly relevant to this thesis is their role in the vasculature. In confluent endothelial cell monolayers few focal adhesions are present. Interestingly, adherens junctional complexes can substitute for focal adhesions and anchor stress fibres. Stress fibres form a supra-cellular network that could be important for coordinating endothelial function by providing mechanical linkage (Millan et al., 2010). These concepts and the relation between stress fibres and endothelial junction integrity are discussed further in section 1.4.2.3. Furthermore, stress fibres are induced upon shear stress in endothelial cells (Wojciak-Stothard and Ridley, 2003). They are thought to be required for endothelial cells to remain flat under flow, so reducing shear stress and have been suggested to provide rigidity to resist these forces (Pellegrin and Mellor, 2007).

1.4 The vascular endothelium

The endothelium is the innermost layer of blood and lymphatic vessels and is made up of a single layer of endothelial cells. An important function of the endothelium is to act as a mechanical barrier, separating blood and lymph from surrounding tissue. However, the endothelium has roles beyond this and is involved in the control of leukocyte diapedesis, immune reactions and inflammation, and regulates trans-endothelial passage of soluble macromolecules (Dejana, 2004). An added unique feature of the vascular endothelium is that it is subjected to constant blood flow and associated shear forces. Endothelial cells need to be able to respond to and resist these hemodynamic forces. An interesting example that serves to integrate many of the concepts discussed so far is RhoA and Rac1-mediated polarisation in response to shear stress. Shear stress leads to a RhoA-induced increase in stress fibres, followed by repolarisation of the cell in the direction of the shear force vector which is regulated by RhoA and Rac1 (Wojciak-Stothard and Ridley, 2003). A mechano-sensory system in endothelial cells has been shown to mediate responses to shear stress (Allen et al., 2011; Tzima et al., 2005).

To fulfil these diverse functions, endothelial cells are highly responsive to their surroundings. For example, pro-inflammatory stimuli such as TNFα induce an increase in endothelial permeability (Wojciak-Stothard and Ridley, 2002). Changes in endothelial gene expression and/or surface protein expression in response to extracellular stimuli have also been noted. For example, E-selectin is an inducible endothelial-specific leukocyte adhesion molecule (Bevilacqua et al., 1987). Another example is shear stress-induced activation of the transcription factor c-Fos via RhoA (Shiu et al., 2003). In addition, endothelial cells are heterogeneous to fulfil specialised functions. For example, specialised structures are seen in cells of the renal glomerulus and liver which contain fenestrae, and in cells comprising the blood brain barrier which are enriched in tight junctions (described in section 1.4.1.2).

1.4.1 Endothelial cell-cell junctions

Endothelial cell-cell junctions being regions of contact between adjacent cells have significant roles in mediating endothelial permeability and do not just serve as points of attachment between cells. Furthermore, junction signalling is implicated in mediating angiogenesis, cell proliferation, shear stress responses and leukocyte diapedesis (Dejana, 2004). Endothelial cells have junctional regions corresponding to adherens junctions (AJ) and tight junctions (TJ) and gap junctions (reviewed in (Dejana, 2004)). Junctions between endothelial cells have variable organisation which is less restricted as compared to junctions in epithelial cells. Furthermore, adjacent endothelial cells may overlap resulting in the formation of contact regions in these areas. AJ components in these areas are arranged in reticular domains and are termed reticular AJs (Fernandez-Martin et al., 2012). Adhesion in both AJs and TJs is mediated by transmembrane proteins that are capable of homophilic interactions. These junctional proteins mediate intracellular signalling and link junctions to the cytoskeleton via their cytoplasmic domains. These associations in addition to stabilising cell-cell contacts are required for the dynamic control of vascular permeability (described in section 1.4.2.3).

1.4.1.1 The endothelial adherens junction

VE-cadherin is a key transmembrane component of endothelial adherens junctions and is responsible for providing adhesive capacity by forming homophilic adhesions (reviewed in

(Dejana and Giampietro, 2012)). Single VE-cadherin bonds are of very low strength. VE-cadherin anchorage to the perijunctional actin cytoskeleton is essential for its function and is thought to cluster VE-cadherin and increase its avidity, so stabilising adhesions (Baumgartner et al., 2003). The intracellular domain of VE-cadherin contains binding sites for p120-catenin, β-catenin and plakoglobin. Both β-catenin and plakoglobin can interact with α-catenin. Plakoglobin serves to link VE-cadherin to the vimentin cytoskeleton (Kowalczyk et al., 1998) while it is thought that complexes of VE-cadherin, β-catenin, α-catenin and p120 catenin are involved in connecting to the actin cytoskeleton (Millan et al., 2010). Endothelial cells express other cadherins such as N-cadherin and T-cadherin (Wallez and Huber, 2008). While abundant in the endothelium, N-cadherin is poorly localised to cell-cell junctions (Salomon et al., 1992) and only does so in the absence of VE-cadherin (Navarro et al., 1998). Other studies show that N-cadherin is involved in interactions with perivascular cells like pericytes (Tillet et al., 2005). VE-cadherin-deficient embryos are still able to form electron dense junctions, implying functional redundancy between these different adhesion molecules (Gory-Faure et al., 1999).

Recent observations have shed light on how adherens junctions form and stress the importance of the actin cytoskeleton for both junction formation and junction maintenance/regulation. A study using HUVECs (human umbilical vein endothelial cells) indicates that cell-cell interactions are initiated by lamellipodia of adjacent cells that meet and provides a mechanism by which cell-cell junctions form and mature (Hoelzle and Svitkina, 2012). Subsequent retraction of the lamellipodia results in the formation of filopodium-like bridges with F-actin in these structures bundled by fascin, and VE-cadherin accumulation at points of contact. Following this lamellipodia-filopodia transition, bridges mature into stress fibre-like structures with the incorporation of myosin II. These bridges link adjacent cells and leads to subsequent junction expansion. In epithelial cells, adherens junctions can either exist as linear adherens forming circumferential rings or as dynamic, punctate, discontinuous junctions such as those seen in neoplastic cells (Ayollo et al., 2009). In endothelial cells, a similar situation exists. Discontinuous AJs in endothelial cells are linked to stress fibres and serve to link the cytoskeleton of adjacent cells. This organisation plays an important role in regulating junction permeability and increases stress resistance

(Millan et al., 2010). By contrast, continuous AJs have a linear morphology and are associated with cortical F-actin which is required for the maintenance of mature cell-cell junctions (Garcia et al., 2001). The regulation of vascular permeability and the switch from continuous to discontinuous AJs will be discussed in section 1.4.2.

1.4.1.2 The endothelial tight junction

The major transmembrane, adhesive components of TJs are the claudin proteins. The claudins are a family of more than 20 proteins but only a few are expressed in the endothelium with claudin-5 being highly expressed in most cases (Dejana et al., 2009). These molecules form homophilic and heterophilic (with other claudin subtypes) interactions and low claudin expression is correlated with reduced blood brain barrier function (Nitta et al., 2003). Other transmembrane components of TJs include occludin and JAMs (junctional adhesion molecule). Occludin expression too has been correlated with barrier properties of the endothelium (Wallez and Huber, 2008). Important intracellular signalling mediators linked to claudin and occludin at tight junctions include the ZO proteins (ZO-1, 2 and 3) and afadin which link TJs to the actin cytoskeleton. Occludin has also been shown to be able to directly bind F-actin (Wittchen et al., 1999). ZO-1 can also bind to JAM, the adherens junction protein α-catenin and the gap junction protein connexin-43 (Harhaj and Antonetti, 2004). Hence, it is probable that different junction systems are interconnected and cooperate to regulate barrier integrity.

In addition to these two important junctional structures, the nectin-afadin system contributes to cell-cell contacts. Nectin is a member of the immunoglobulin family of transmembrane proteins and interacts with afadin via its intracellular domain. Afadin interacts with ponsin and actin and so links nectins to the cytoskeleton (Reymond et al., 2001). Ponsin can bind to vinculin (Mandai et al., 1999) and as vinculin is a part of the intracellular cadherin complex (Wallez and Huber, 2008), this provides a link between the cadherin and nectin systems. Other homophilic adhesion molecules include PECAM-1 (platelet endothelial cell adhesion molecule – 1) and S-endo-1 which belong to the immunoglobulin family. These proteins are not part of any specialised junctional structure (Dejana, 2004). PECAM-1 is also found on leukocytes and platelets and is required for leukocyte transmigration (Mamdouh et al.,

2003). A recent study indicates that PECAM-1 coordinates with AJs to maintain barrier function (Fernandez-Martin et al., 2012).

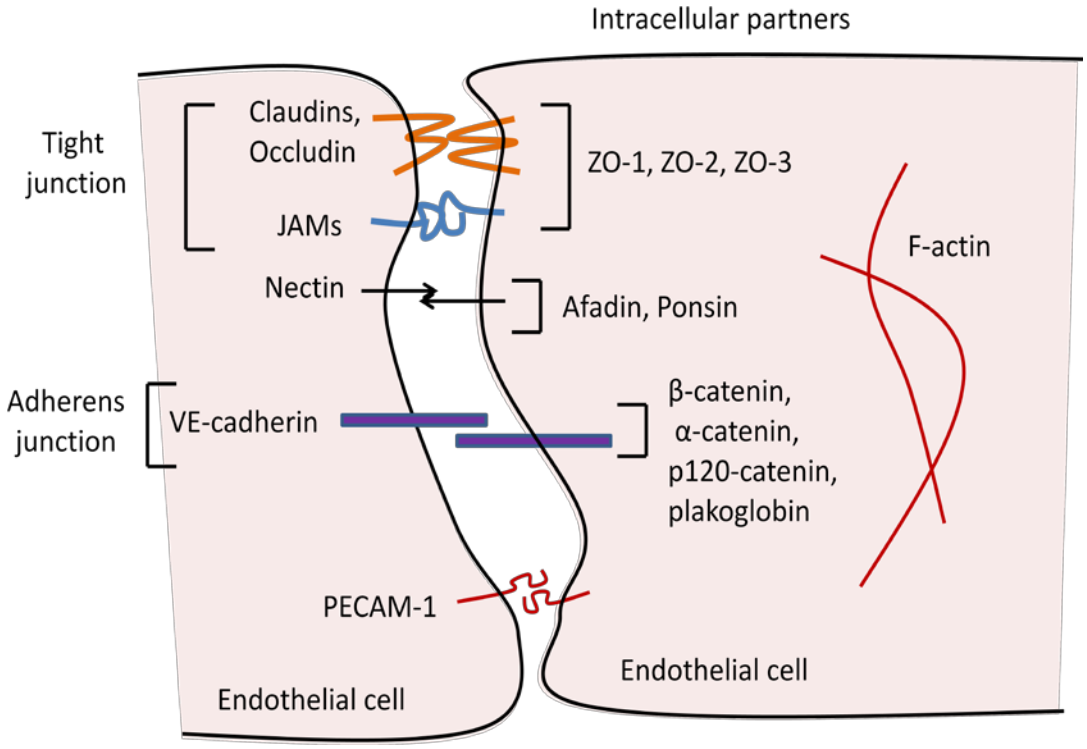

Figure 1.7 Endothelial cell-cell junctions
Junction systems in endothelial cells include tight junctions, adherens junctions, PECAM-1 and the nectin-afadin system. AJs, TJs and nectin link to the actin cytoskeleton by means of intracellular partner molecules.

Endothelial cell-cell junctions mediate cell signalling and respond to multiple inputs as well as inducing downstream signalling responses. For example, AJs are involved in contact inhibition of cell growth/proliferation. This can occur by a modulation of growth factor signalling by VE-cadherin. VE-cadherin in confluent cells is clustered at junctions and forms a complex with VEGFR2 (vascular endothelial growth factor receptor 2) leading to a downregulation of its activity (Grazia Lampugnani et al., 2003). VE-cadherin signalling is also able to protect resting, confluent cells from pro-apoptotic stimuli (Carmeliet et al., 1999)

1.4.2 Mechanisms regulating endothelial permeability

The permeability of the endothelium reflects the extent to which trans-endothelial passage of soluble molecules and/or cells is allowed. The control of permeability is vital to physiological

events such as inflammation. There are two mechanisms by which vascular permeability can be mediated, termed the transcellular and paracellular pathways.

The paracellular route of endothelial permeability regulation is mediated by endothelial cell-cell junction complexes, which act as a barrier to restrict the passage of fluid from the lumen through the intercellular space. The disruption of junctions is also implicated in the passage of cells through the endothelium. This process is regulated by homophilic interactions between molecules present on the endothelial surface and invading cells, which dictates the passage of cells through cell-cell contacts. This is usually accompanied by junction rearrangement and cell retraction (Dejana, 2004).

The transcellular pathway refers to passage through the endothelial cell body and involves vesicular transport systems, fenestrae and biochemical transporters (Dejana et al., 2009). For example, transcellular structures like vesiculo-vacuolar organelles form a series of interconnected vesicles that span the endothelial cell and provide a trans-endothelial passage (Dvorak et al., 1996). Leukocytes too are able to use a transcellular mechanism to achieve diapedesis (Carman and Springer, 2004; Millan et al., 2006). Similarly, cancer cells have been observed to intravasate by the transcellular route (Khuon et al., 2010).

1.4.2.1 Adherens junctions and regulation of vascular permeability

VE-cadherin plays a central role in regulating permeability. This is supported by an increase in vascular permeability in response to an injection of VE-cadherin blocking antibodies in mice (Corada et al., 1999). Phosphorylation of VE-cadherin is an important mechanism by which its function is regulated, and results in disruption of adherens junctions and an increase in monolayer permeability (reviewed in (Harris and Nelson, 2010)). For example, invasive breast cancer cells can induce tyrosine phosphorylation of VE-cadherin to facilitate invasion through the vasculature (Haidari et al., 2012). Hemodynamic forces result in the tyrosine phosphorylation of VE-cadherin via Src kinase in veins, and it is thought that this serves as a priming mechanism to sensitize veins to other permeability inducing agents such as inflammatory cytokines (Orsenigo et al., 2012). Several phosphatases interact with VE-cadherin including VE-PTP (vascular endothelial-protein tyrosine phosphatase). VE-PTP expression enhances VE-cadherin function and reduces vascular permeability (Nawroth et

al., 2002). Phosphorylation of other components of adherens junctions such as p120 catenin, β-catenin and plakoglobin also correlates with increased permeability (Harris and Nelson, 2010).

Regulation of VE-cadherin availability at the cell surface is another way to regulate its function (Harris and Nelson, 2010). The association of p120 catenin with VE-cadherin prevents the endocytosis of VE-cadherin and is needed for maintaining barrier function. VEGF is known to increase vascular permeability by phosphorylation of VE-cadherin on serine 665. Phospho-S665 VE-cadherin is a docking site for β-arrestin which leads to VE-cadherin endocytosis and degradation (Gavard and Gutkind, 2006). In addition, trafficking of VE-cadherin to the cell surface has to be properly accomplished. Myosin-X is a motor protein that transports VE-cadherin along filopodial actin filaments causing accumulation at filopodial tips. Blocking myosin-X activity abolishes VE-cadherin export to cell edges (Almagro et al., 2010).

Furthermore, VE-cadherin function can be regulated by regulation of its expression and proteolytic cleavage. Tumour cells and leukocytes can secrete proteases that digest VE-cadherin and so increase vascular leakage (Dejana et al., 2009).

1.4.2.2 Tight junctions and the regulation of vascular permeability

A wide range of signals including growth factors, cytokines and hormones regulate TJ function to increase vascular permeability (reviewed in (Harhaj and Antonetti, 2004)). Stimulation by inflammatory cytokines like TNFα causes the disruption of TJs. Long term stimulation of endothelial cells with TNFα leads to reduced localisation of occludin and JAM-A at TJs (McKenzie and Ridley, 2007). JAM-C is particularly interesting because unlike other adhesion proteins loss of JAM-C function reduces permeability. JAM-C is thought to regulate permeability by crosstalk with VE-cadherin (Orlova et al., 2006). The claudins too are implicated in vascular permeability. Loss of claudin-5 in mice leads to a size-selective loss in blood brain function against molecules less than 800 kDa in size (Nitta et al., 2003). Finally, phosphorylation of ZO-1 resulting in its reduced localisation to TJs, is linked to enhanced vascular permeability and has been proposed to be one of the ways by which VEGF increases vessel leakage (Antonetti et al., 1999). In summary, the loss of function and/or

mislocalisation of most of the key components of TJs results in increased paracellular permeability.

1.4.2.3 Vascular permeability and the actin cytoskeleton

Endothelial permeability is linked to the cytoskeleton due to the close association between junction complexes and the cytoskeleton. In addition to stress fibres, cortical F-actin is implicated in barrier function. Rho GTPases play a significant role in modulating endothelial permeability (reviewed in (Wojciak-Stothard and Ridley, 2002)). Increased centripetal tension as a result of actomyosin-induced contractility results in the disruption of cell-cell contacts. This is commonly associated with an increase in stress fibres which have been shown to be associated with AJs (Millan et al., 2010). A general model could involve increased contractility of stress fibres and/or of the perijunctional cortical F-actin leading to an increase in tensile force, which subsequently causes a physical breakdown of junctions. The importance of the actin cytoskeleton in mediating permeability is highlighted by F-actin disrupting agents leading to increased permeability, and F-actin stabilising agents that prevent this (McKenzie and Ridley, 2007). In addition, inhibition of ROCK activity increases permeability (McKenzie and Ridley, 2007). These observations point to the requirement of a 'contractile sweet spot' for optimal barrier function. It is likely that too little or too much contractility causes destabilisation of cell-cell junctions.

Thrombin induction of endothelial permeability involves RhoA. RhoA-induced contractility by induction of stress fibres correlates with increased vascular permeability, and is in part responsible for the endothelial response to thrombin (Wojciak-Stothard et al., 2001). RhoA activity spatially associated with actin filaments, is linked to thrombin-induced disruption of junctions (Szulcek et al., 2013). Rac1-mediated control of endothelial permeability is complex, and Rac1 can have barrier-strengthening or barrier-weakening functions. It is likely that the functions of Rac1 are dependent on the stimulus and conditions. For example, Rac1 inhibits thrombin-induced RhoA activation (Rosenfeldt et al., 2006), suggesting a junction strengthening function. Conversely, Rac1 can weaken junctions by inducing VE-cadherin internalisation after VEGF stimulation by PAK activity (Gavard and Gutkind, 2006). Depletion of Rac1 also reduces TNFα-induced permeability (Cain et al., 2010). In addition, Rac1

activity causes loss of VE-cadherin function via ROS (reactive oxygen species) generation (van Wetering et al., 2002).

Other proteins also affect junctions. For example, while dominant negative Cdc42 reduces thrombin-induced stress fibres and contractility, it does not prevent the associated increase in permeability (Wojciak-Stothard et al., 2001). However, its activity is needed for the restoration of junctions after thrombin stimulation *in vitro* and *in vitro* (Kouklis et al., 2004). In some cases, the altered permeability can be independent of associated cytoskeletal changes. A pertinent example is that of TNFα stimulation of endothelial cells. While RhoA-associated contractility results in early changes to F-actin and cell morphology, long term increased permeability instead correlates with the disassembly of tight junctions (McKenzie and Ridley, 2007). Another mechanism by which permeability is mediated involves regulation of cortical F-actin. For example, sphingosine 1-phosphate activates PAK via Rac1, which phosphorylates and activates LIMK. This results in the downregulation of cofilin activity and leads to an enhancement of the F-actin cortical ring, stabilising cell-cell junctions (Garcia et al., 2001). Similarly, the Ras family GTPase Rap1 is thought to control VE-cadherin based junctions by controlling the cortical actin cytoskeleton (Cullere et al., 2005).

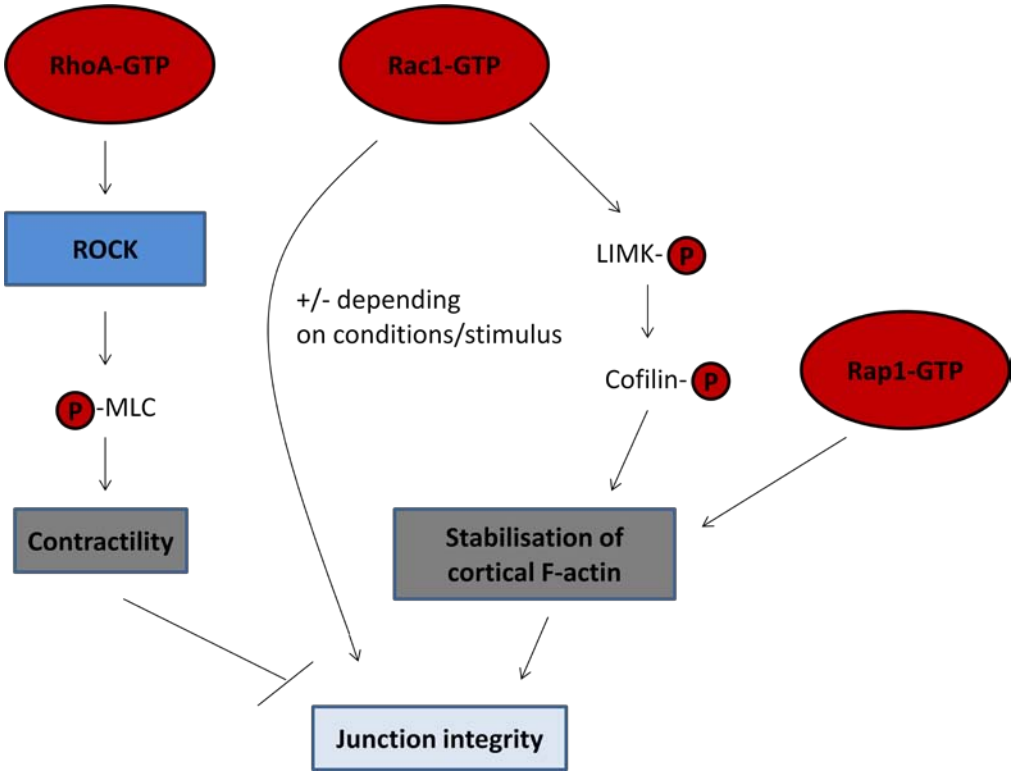

Figure 1.8 Signal transduction pathways regulating junction integrity in endothelial cells
RhoA activation leads to enhanced contractility and is associated with a breakdown of cell-cell junctions. Rac1 can have barrier-strengthening or barrier-weakening functions depending on the conditions/stimulus. Rap1 activity stabilises junctions by mediating cortical F-actin.

1.5 Angiogenesis

Angiogenesis is the process by which new blood vessels form from pre-existing ones and involves endothelial cell activation, proliferation, migration and vessel maturation (reviewed in (Potente et al., 2011)). This section will focus on links between angiogenesis, cell-cell junctions and the cytoskeleton.

In the adult, the vasculature is largely quiescent except in physiological processes such as wound healing and female endometrial growth. Signals that drive angiogenesis are largely derived either from secreted, soluble factors or from the ECM (the role of the ECM in angiogenesis is reviewed in (Senger and Davis, 2011)). VEGF is a 'master regulator' of angiogenesis (Herbert and Stainier, 2011) and is the major angiogenic stimulus in the adult organism. Blood vessels are covered on their basal surface with a basement membrane of which the main constituents are laminin and collagen type IV. One of the first steps in

angiogenesis is the degradation of this membrane so that the underlying endothelial cells are free to enter the sprouting phase. VEGF can induce degradation of the basement membrane (Chang et al., 2009). Cell-cell junctions also have to be destabilised in order for cells to enter the sprouting phase. RhoA and ROCK signalling has been found to mediate vascular hyperpermeability downstream of VEGF (Sun et al., 2006). In addition, VEGF destabilises junctions by promoting VE-cadherin internalisation (Gavard and Gutkind, 2006).

The next stage is termed sprouting angiogenesis and involves two major types of cells, tip cells and stalk cells. Tip cells lead newly sprouting vessels, are highly motile and are induced by VEGF. Stalk cells on the other hand are less motile but proliferate to generate the trunk of the new vessel, establish junctions with neighbouring cells and are subsequently responsible for lumen formation. Tip cells navigate by the extension of filopodia. VEGF stimulation promotes filopodium formation via Cdc42, and also stimulates Rac1 activity at the leading edge promoting lamellipodium extension (De Smet et al., 2009). Endothelial cells in general use mechanisms discussed in section 1.2 to migrate. The p110α catalytic subunit of PI3K (phosphoinositide 3-kinase) is important for endothelial cell motility and regulates tail release of migrating cells through RhoA (Graupera et al., 2008). Another mediator of endothelial cell motility is RhoJ, which is a member of the Cdc42 subfamily of Rho GTPases and highly expressed in endothelial cells (Kaur et al., 2011). Depletion of RhoJ impairs the migration of endothelial cells in a scratch-wound assay.

Sprouting leads initially to the formation of cords which essentially are coalesced chains of endothelial cells. RhoA-mediated formation of stress fibres and induction of spindle morphology is needed for alignment of cells into cords (Liu and Senger, 2004). A lumen has to then form in the vessel trunk which can occur either by cord hollowing (cell shape and cell-cell junctions are altered to create a lumen between adjacent cells and is thought to rely on cytoskeletal contraction) or cell hollowing (intracellular vacuoles coalesce and fuse with vacuoles in other cells to form a lumen) (Potente et al., 2011). Depletion of Rac1, Cdc42 (Koh et al., 2008) and RhoJ (Kaur et al., 2011) impairs endothelial cell tube and lumen formation in *in vitro* assays. Cdc42 is required for cells to acquire apical-basal polarity during lumen formation.

VE-cadherin expressed on the surface of tip cell filopodia is thought to promote anastomosis between different vascular branches leading to the establishment of a vascular plexus. In addition to its importance in junction formation, VE-cadherin signalling has been implicated in the cessation of the sprouting phase. Activation of VE-cadherin signalling by the engagement of junctions leads to increased actomyosin contractility by activation of ROCK and increased levels of p-MLC2 at intercellular junctions. VE-cadherin signalling antagonizes VEGF signalling and so abrogates Rac1-mediated sprouting (Abraham et al., 2009). This is consistent with a study that demonstrates that local downregulation of cortical myosin II activity permits endothelial cell branching and migration (Fischer et al., 2009). Interestingly, ERK (extracellular signal regulated kinase) signalling can downregulate ROCK signalling to promote cell survival and sprouting (Mavria et al., 2006). ERK is a mitogen activated protein kinase (MAPK) involved in cell migration, growth, and proliferation (Roskoski, 2012). Actomyosin contractility induced by VE-cadherin signalling is also needed for the uniform distribution of VE-cadherin itself at cell-cell junctions leading to a positive feedback loop being set up (Abraham et al., 2009).

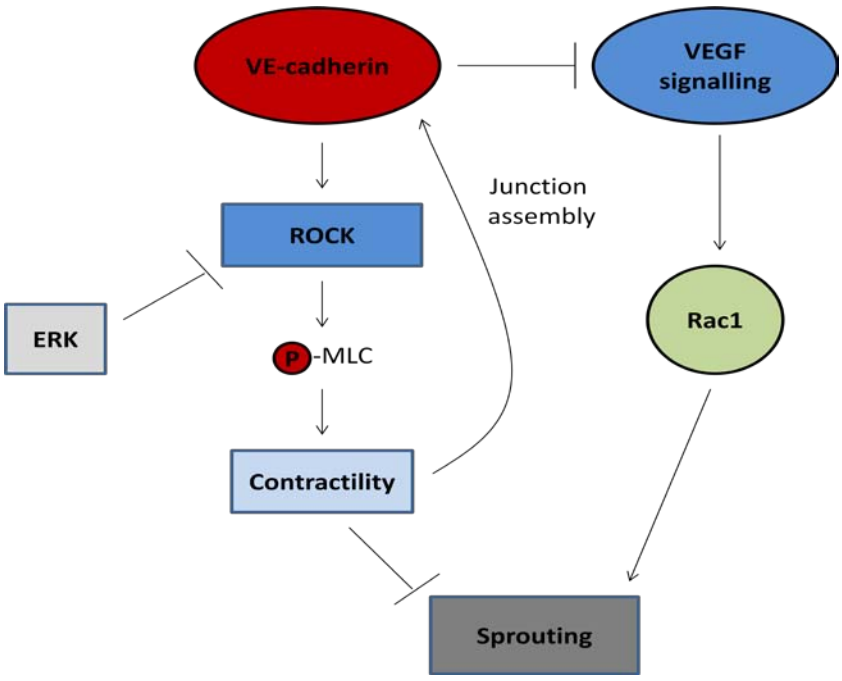

Figure 1.9 Signal transduction involved in the control of sprouting
Interplay between VE-cadherin and VEGF signalling mediates sprouting during angiogenesis. VE-cadherin signals via ROCK to induce contractility and the cessation of sprouting. ERK signals to downregulate ROCK and so promotes sprouting. VEGF signalling drives Rac1-mediated migration and sprouting.

It is likely that precise spatial and temporal regulation of Rac activity determines how it acts in endothelial cells. While Rac1 activity is needed for migration and sprouting, it is also essential for vascular maturation and in quiescent endothelial cells for the proper organisation of cell-cell junctions (Senger and Davis, 2011). For the establishment of a functional vasculature, the vascular network has to mature by pruning and remodelling of branches, while individual endothelial cells become quiescent and acquire a 'phalanx' phenotype in which junctions are strengthened and VEGF signalling is reduced.

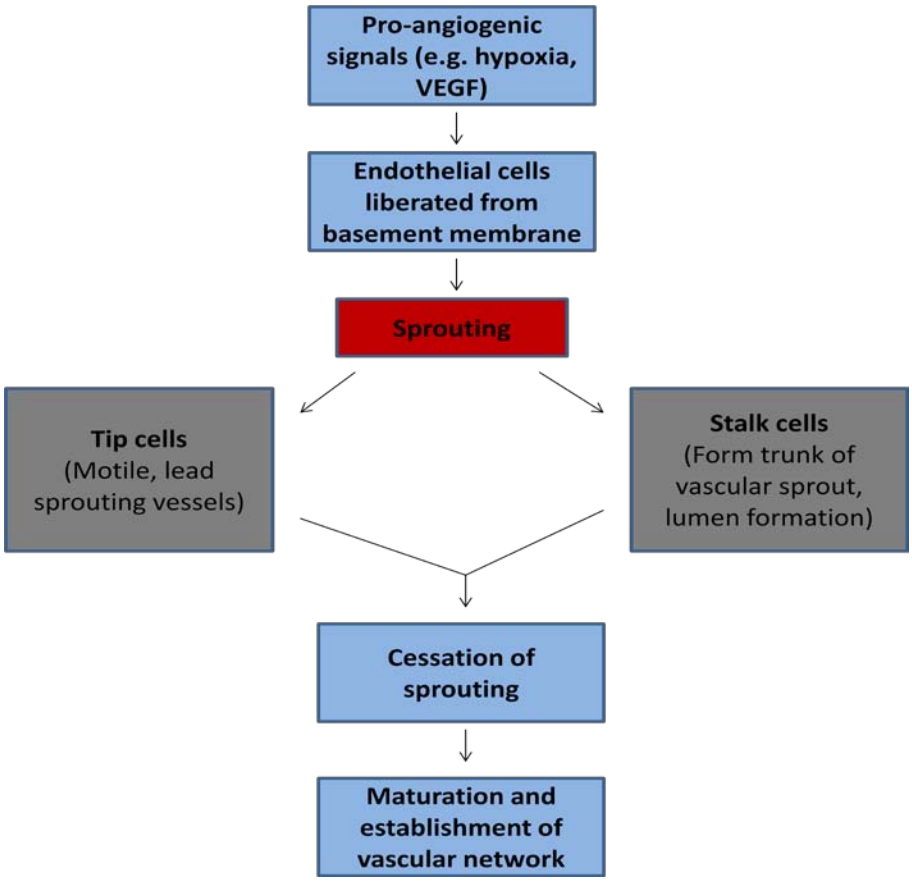

Figure 1.10 Simplified overview of angiogenesis
Schematic highlighting the primary steps in angiogenesis. Endothelial cells respond to pro-angiogenic stimuli leading to formation of vascular sprouts, and the subsequent maturation and establishment of a vascular network (refer to text for details).

1.6 Identification of the FAM40 proteins as regulators of cell morphology and migration

Large-scale RNA interference (RNAi) screens offer a powerful way to identify, and elucidate the functions of novel genes (Mohr and Perrimon, 2012). Phenotypes that arise as a result of

gene expression knockdown using RNAi can provide clues to gene function. This can be achieved by comparing with other genes that induce a similar phenotype. RNAi screen results can be analysed further to construct signalling networks. For example, by comparing the morphologies of cells that were depleted of various Rho GAPs with those of cells overexpressing various Rho GTPases, predictions of Rho GAP/GTPase regulatory pathways could be made (Nir et al., 2010).

The Drosophila FAM40 orthologue was one of many genes identified in a RNAi screen for genes affecting the 'actinome' in Drosophila S2 cells (Rohn et al., 2011). The actinome is defined as the set of genes that contribute to the regulation of the actin cytoskeleton. Members of the known actinome were used to identify novel regulators by comparative screening. Hits in this screen were organised by phenotypic attributes including cell shape, cell size, cell number, actin content/organisation and microtubule content/organisation. To identify a conserved set of actin regulators that performed similar functions across different species, a second RNAi screen was performed in HeLa cells using human orthologues of genes identified as hits in Drosophila. Using data from these two screens a list of conserved novel regulators of the actinome was compiled. For example, the SCF E3 ubiquitin ligase complex, previously not linked to actin regulation was identified as an upstream regulator of actin polymerisation controlled by Rac. S2 cells depleted of the Drosophila FAM40 orthologue (CG11526) present with an 'asymmetric lamella' phenotype. However, CG11526 was not included in the list of conserved regulators of the actinome as knockdown of the human FAM40 orthologues gave a different phenotype as compared to the Drosophila orthologue. FAM40B-depleted HeLa cells present with bright regions of peripheral F-actin associated with lamellipodia and filopodia. A reduction in thick F-actin cortical bundles and in cell-cell adhesions is also observed (Bai et al., 2011).

Data from this initial RNAi screen were used by our laboratory to conduct a second RNAi screen in a cancer cell line, PC3 (derived from prostate cancer metastasis to the bone) to identify novel regulators of cytoskeletal organisation, cell morphology and migration (Bai et al., 2011). The genes selected for this second screen altered the shape of Drosophila S2 cells and had unknown functions in Drosophila. A further bioinformatics and data mining

analysis was done to narrow down this selection to 16 genes. This essentially consisted of evidence of their function (including homologues in other species) from public databases that hinted at a link to cytoskeletal regulation. These 16 Drosophila genes corresponded to 26 homologous human proteins and included human FAM40A and FAM40B. Knockdown of FAM40A and FAM40B in PC3 results in distinct morphological phenotypes. (Bai et al., 2011). These phenotypes will be discussed further in chapter 4. The striking phenotypes they bring about upon RNAi knockdown is why they were selected for further characterisation.

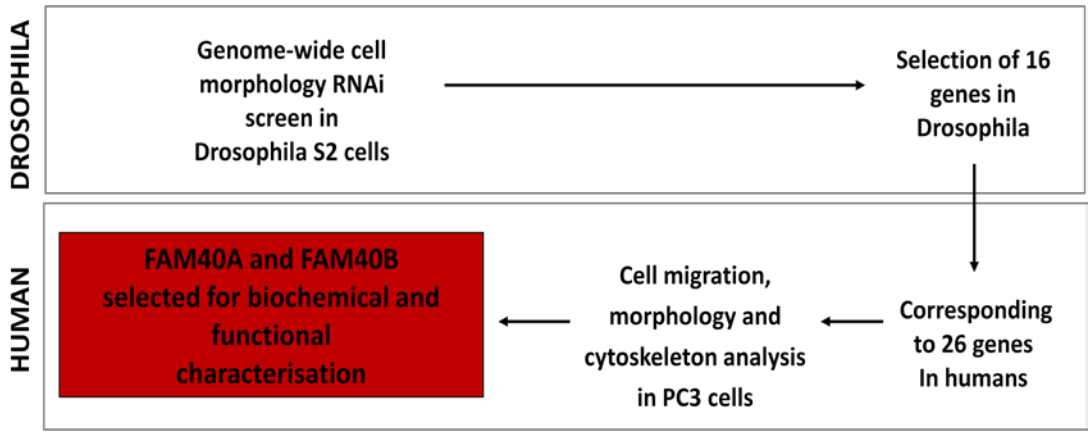

Figure 1.11 Schematic of the procedure used to select FAM40A and FAM40B for functional characterisation
The FAM40 proteins were initially selected for functional characterisation based on their Drosophila orthologue being a hit in a genome-wide cell morphology RNAi screen. A subsequent study in PC3 cells led to effects on cell morphology upon FAM40 depletion.

1.6.1 The FAM40 proteins

The FAM40 (FAMily with sequence similarity 40) proteins are a family of proteins found in many eukaryotes including fungi. Interestingly no homologues could be found in plants. Two FAM40 homologues exist in humans, FAM40A and FAM40B, which also go by the names STRIP1 (striatin interacting protein 1) and STRIP2 respectively. FAM40A and FAM40B have 61% amino acid identity and have the same overall domain architecture. Two domains can be identified in the human FAM40 proteins, the N-terminal N1221-like domain and the C-terminal DUF3402 (domain of unknown function 3402). The sequence of the N-terminal domain is similar to a hypothetical protein product of a yeast ORF (open reading frame)

termed N1221 (conserved domains database, NCBI). Both these domains are functionally uncharacterised and do not bear resemblance to any other known domains. In addition, the N-terminal sequence of FAM40A is proline-rich which could be important for mediating interactions with other proteins (Kay et al., 2000).

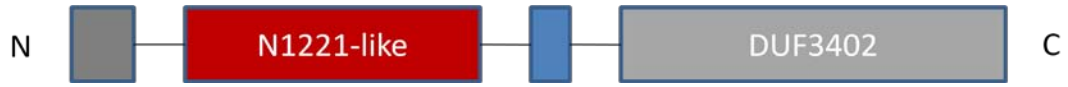

Figure 1.12 Schematic illustrating FAM40 domain architecture
Both FAM40A and FAM40B contain two domains, an N-terminal N1221-like domain and a C-terminal DUF3402 domain.

Functions and interacting partners of FAM40 homologues in other species may be relevant for the understanding of human FAM40 function. The yeast homologue of the FAM40 proteins is Far11 (Factor Arrest 11), which is involved in pheromone signalling in *Saccharomyces cerevisiae* (Kemp and Sprague, 2003). Far11 is part of a multi-protein complex involving other Far proteins (Far3, 7-11) that causes G1 cell cycle arrest in response to pheromone. The exact function of Far11 in the complex is not known but it has been suggested that it may be involved in cell fusion during mating. This is based on an orthologue present in *Neurospora crassa* (Ham2), mutants of which display a significant defect in hyphal fusion (Xiang et al., 2002). A recent study has implicated Far11 in an independent role, as a mediator of human caspase-10 function in *S. cerevisiae*. Heterologously expressed human caspase-10 in *S. cerevisae* requires Far11 for its toxicity. Caspases are proteolytic enzymes and are key regulators of apoptotic cascades in cells. Far11 was shown to be required for the induction of autophagy and regulation of the DNA damage response pathway (Lisa-Santamaria et al., 2012).

Additionally, the Far complex has been shown to antagonise TORC2 (target of rapamycin complex 2) signalling in *S. cerevisae*. Far11 mutants suppress the lethality of TORC2 mutants (Pracheil et al., 2012). TOR kinase is an important regulator of cell growth and metabolism. Knockdown of components of the mammalian equivalent mTORC2 (mammalian TORC2) results in actin cytoskeletal changes in cultured cells and affects cell motility (Cybulski and Hall, 2009). The Far protein complex interacts with Rho4 protein

(determined using BioGRID (Stark et al., 2006)) and thus it is possible it is involved in actin filament polarization and the establishment of cell polarity (Levin, 2005). Additionally Far11 is known to interact with Rom2 (determined using BioGRID (Stark et al., 2006)), which is a GEF for the Rho GTPase Rho1 in *S. cerevisiae* (Ozaki et al., 1996). Rho1 controls polarised actin distribution and cell wall expansion in *S. cerevisiae* (Levin, 2005). The human homolog of Rho1 is Rho, with RhoA being its closest relative.

The *Caenorhabditis elegans* FAM40 homologue is FARL-11 (Factor Arrest Like-11). A mutant for this gene suppresses the lethality of conditional dynein heavy chain mutants in addition to associated spindle length and cytokinesis abnormalities (O'Rourke et al., 2007). This suggests that FARL-11 is a negative regulator of dynein, and hence might be involved in cargo transport along microtubules.

1.6.2 The STRIPAK complex

The FAM40 proteins were identified in an interaction map around the protein phosphatase 2A (PP2A) catalytic subunit by an affinity purification/mass spectrometry approach (Goudreault et al., 2009). Interacting partners identified were in turn cloned and used as baits in subsequent affinity purification steps to construct a high density protein interaction map. This led to the identification of a novel multi-protein complex termed the STRIPAK (striatin interacting phosphatase and kinase) complex of which the FAM40 proteins are a part of. Interestingly, analogues of the human STRIPAK complex are present in other species too. The Far complex in *S. cerevisiae* bears resemblance to the human STRIPAK complex while a Drosophila STRIPAK complex (Ribeiro et al., 2010) and a STRIPAK homologue in filamentous fungi (Bloemendal et al., 2012) have been defined too. This suggests the presence of an evolutionarily conserved protein complex.

PP2A is a serine/threonine phosphatase and has been described to have diverse functions including the control of cell growth, proliferation and differentiation. PP2A is also involved in regulating the cytoskeleton and misregulation of PP2A activity disrupts both the actin and microtubule cytoskeleton (reviewed in (Sontag, 2001)). In addition, PP2A regulates endothelial cell motility (Young et al., 2002), and so might be involved in angiogenesis. The functional PP2A enzyme is a trimer consisting of a catalytic subunit (PP2A C), a scaffolding

subunit (PP2A A) and a regulatory subunit (PP2A B). Two isoforms exist for each of the A and C subunits while 15 B subunits have been identified. It is thought that these regulatory B subunits determine the diversity and specificity of PP2A biological activity, and are important for substrate recruitment (Goudreault et al., 2009). The striatin proteins are a class of regulatory subunit proteins, and striatin (STRN), striatin 3 (STRN3) and striatin 4 (STRN4) are also components of the STRIPAK complex.

Striatins are highly expressed in the nervous system and have been implicated in calcium-dependant neuronal signalling. As they are highly expressed in dendritic spines, it has been suggested that they have a key role in bridging calcium signalling pathways and phosphatase pathways in dendritic spines (Benoist et al., 2006). Mob3 is another component of the STRIPAK assembly and its homologue in filamentous fungi is essential for vegetative cell fusion and sexual development (Bernhards and Poggeler, 2011). The Drosophila Mob3 homologue has been implicated in regulating synapse formation and axonal transport. Mutants also display disrupted microtubule organisation in the nervous system (Schulte et al., 2010). All members of the GCKIII (germinal centre kinase III) family of Ste20 kinases (STK24, STK25 and MST4) are components of this complex and their functions will be elaborated on in section 1.7. In addition, a recent study has identified another germinal centre kinase MINK1 (misshapen like kinase 1) as a component of the STRIPAK complex. MINK1 can interact with STRN4 and is needed for abscission of the cytoplasmic bridge between daughter cells during cytokinesis (Hyodo et al., 2012). The presence of both a phosphatase and a kinase in the same complex could imply the STRIPAK complex acting as an on/off switch in regulating protein phosphorylation and dephosphorylation. On the other hand, the phosphatase and kinases could regulate each other. An example of this has been described wherein PP2A downregulates STK24 activity using striatin as an organising scaffold (Gordon et al., 2011). The other significant component of STRIPAK is CCM3 (cerebral cavernous malformation 3), mutations in which lead to vascular malformations in the brain (Riant et al., 2010). Cerebral cavernous malformations and the role of CCM3 are discussed in section 1.8.

Table 1.1 Key components of the STRIPAK complex

Table derived from (Goudreault et al., 2009) except where indicated.

Protein name	Biological role
FAM40A / FAM40B	Refer to chapter 4 / chapter 5
PP2A	Protein dephosphorylation
GCKIII kinases (STK24, STK25, MST4)	Protein phosphorylation, apoptosis, proliferation, cell migration (refer to section 1.7)
CCM3	Implicated in CCM (refer to section 1.8)
Striatin / Striatin 3 / Striatin 4	Calcium signalling, synaptic function
Mob3	Roles in trafficking, synaptic function
CTTNBP2	Dendritic spinogenesis, synaptic function (Chen et al., 2012)

Insight into the functions of the FAM40 proteins may be obtained by understanding the functions of STRIPAK as a multi-protein complex. For example, the human STRIPAK complex has been implicated in Golgi polarisation. Cells depleted of CCM3 fail to reorient their Golgi apparatus and centrosome towards the wound edge in wound healing assays with SaOS2 cells (derived from primary osteosarcoma) (Fidalgo et al., 2010). CCM3 prevents degradation of the GCKIII kinases via the proteasome. This action stabilises them at the Golgi where STK25 phosphorylates 14-3-3ζ. The authors postulate that this phosphorylation event contributes to the establishment of cell polarity. On a separate note, it is interesting to note that the Drosophila FAM40 homologue binds to aPKC (atypical protein kinase C) (determined using BioGRID (Stark et al., 2006)), a key mediator of cell polarity (Etienne-Manneville and Hall, 2003). Hence, CCM3 could contribute to CCM pathogenesis by regulating endothelial cell migration.

This function of the STRIPAK complex at the Golgi is supported by a second study which demonstrates that MST4 localisation is controlled in opposite ways by CCM3 and striatin (Kean et al., 2011). MST4 is normally localised to the Golgi and to punctate structures in the cytoplasm. Depletion of striatin leads to increased cytosolic localisation of MST4 while

depletion of CCM3 increases its localisation to the Golgi. This control of MST4 localisation correlated with opposite effects on Golgi positioning. The study additionally proposes that striatin acts as a core scaffold in the STRIPAK complex, and can bind both CCM3 and PP2A directly. CCM3 then binds to the GCKIII kinases and recruits them to the complex.

Another theme in STRIPAK function is the control of cell fusion as described in *Sordaria macrospora* (Bloemendal et al., 2012). Furthermore, the *Neurospora crassa* FAM40 orthologue (Ham2), Mob3 orthologue and striatin orthologue (Ham3) have been implicated in cell-cell fusion (Fu et al., 2011). Directed growth of hyphae is required during cell-cell fusion in fungi and hence the STRIPAK complex could mediate this function by affecting Golgi positioning and cell polarity as in human cells.

The Far complex in yeast shows an interesting parallel with the human STRIPAK complex, and could represent a yeast STRIPAK complex. In addition to the FAM40 proteins having a yeast homologue (Far11), Far8 bears resemblance to striatin proteins (Goudreault et al., 2009). Furthermore, Far11 has been shown to interact with the yeast PP2A A subunit Tpd3 (Goudreault et al., 2009; Pracheil et al., 2012)) and the yeast PP2A C subunits Pph21 and Pph22 (Lisa-Santamaria et al., 2012). In budding yeast, a role for this complex in mediating cell fusion has been proposed as well. The Far complex may act to stop premature entry into mitosis by inducing G1 arrest upon pheromone activation, and so allow mating cells enough time to fuse (Kemp and Sprague, 2003).

Finally, the Drosophila STRIPAK complex has been proposed to be the phosphatase complex that antagonizes Hippo signalling. The Hippo pathway consists of a kinase cascade and controls tissue size during development by limiting cell proliferation and promoting apoptosis (Ribeiro et al., 2010).

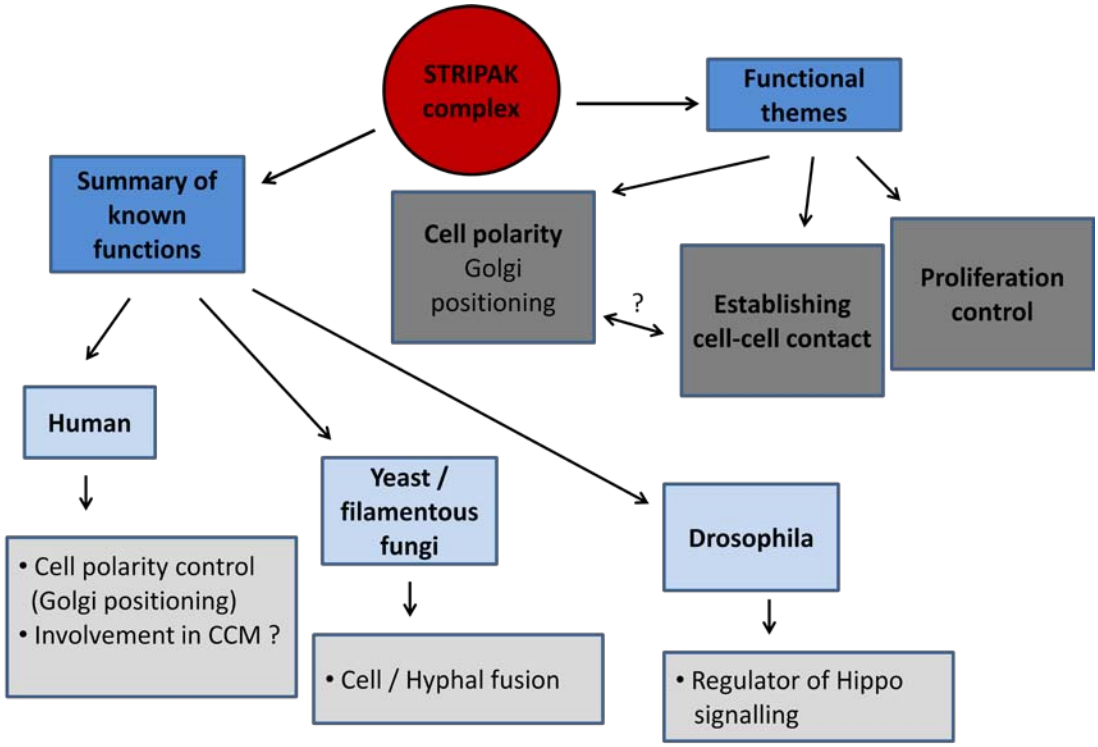

Figure 1.13 Functions of the STRIPAK complex
Schematic illustrating functions of the STRIPAK complex in different species. Based on these observations, three functional themes have been derived. These include control of cell polarity, establishment of cell-cell contact and regulation of cell proliferation.

1.7 The GCKIII family of kinases

The GCKIII group of serine/threonine kinases are a subfamily of the GCK (germinal centre kinase) family of kinases which in turn comprise one of the two subfamilies of mammalian Ste20 kinases (Ling et al., 2008). The Ste20 kinases in yeast are MAP4Ks (mitogen activated kinase kinase kinase kinases) in the mating pathway. The other Ste20 kinase subfamily is the PAK (p21 activated kinase) subfamily. While GCKs and PAKs share homology and are grouped in the same family, they are structurally distinct. For example, the kinase domain in PAKs is at the C-terminus while in GCKs it is at the N-terminus. Furthermore, GCKs do not possess a CRIB (Cdc42/Rac interactive binding) domain and do not interact directly with Rho GTPases.

The GCKIII subfamily comprises the three family members STK24 (also termed MST3), STK25 (also termed SOK1/YSK1) and MST4. Regulation of kinase activity can occur by

autophosphorylation and proteolytic cleavage. For example, autophosphorylation on Thr 178 is essential for STK24 activity and its mutation abolishes kinase activity (Lu et al., 2006). A crystal structure for MST4 with an ATP-mimetic inhibitor suggests dimerisation is involved during autophosphorylation (Record et al., 2010). Caspase-induced cleavage of STK24 during apoptosis increases kinase activity and causes its translocation to the nucleus. By contrast, MST4 is not recognised by caspases (Huang et al., 2002).

Overexpressed STK24 has been shown to be able to activate ERK which mediates cell proliferation and growth (Zhou et al., 2000), but does not activate JNK (c-Jun N-terminal kinase) or p38 MAPK (Schinkmann and Blenis, 1997). JNK, p38 MAPK and ERK are different families of MAPKs (Yang et al., 2013). STK24 can also phosphorylate and activate NDR (nuclear Dbf2-related) kinase which is involved in the control of cell cycle progression and morphology (Stegert et al., 2005). Overexpression of STK25 does not lead to the activation of the JNK, ERK or p38 MAPK pathways (Osada et al., 1997). On the other hand, MST4 has been shown to activate the ERK pathway and can induce cell growth and transformation (Lin et al., 2001). This is supported by another study showing that the interaction of CCM3 with MST4 mediates ERK signalling (Ma et al., 2007). In addition, MST4 plays a role in prostate cancer progression and has been shown to promote the proliferation of prostate cancer cell lines *in vitro* and *in vivo* (Sung et al., 2003).

In addition to controlling growth and proliferation by mediating MAPK signalling, the GCKIII kinases have been implicated in the control of apoptosis. Activation of STK24 is correlated with an induction of apoptosis. Ectopic expression of full length or caspase-cleaved STK24 leads to DNA fragmentation (Huang et al., 2002) and contributes to hypoxia-induced apoptosis (Wu et al., 2011). Similarly, STK25 has been linked with causing apoptosis (Costa et al., 2012; Nogueira et al., 2008; Zhang et al., 2012). Both pro-apoptotic and anti-apoptotic functions have been ascribed to MST4. The interaction between CCM3 and MST4 is implicated in protecting cells from oxidative stress by preventing cell death (Fidalgo et al., 2012). Conversely, a second study suggests a pro-apoptotic function for MST4 (Dan et al., 2002).

The GCKIII kinases are also mediators of cell migration. In general, GCKIII kinase activity negatively regulates migration. Downregulation of STK24 increases the migration of MCF7 breast cancer cells and is associated with a decrease in tyrosine phosphorylation of the focal adhesion protein, paxillin (Lu et al., 2006). Similarly, depletion of STK25 in MCF7 cells enhances their migration and is associated with FAK (focal adhesion kinase) phosphorylation (Chen and Cho, 2011). The orientation of the Golgi is important for cell migration (Mellor, 2004). It is also proposed that STK25 can regulate cell motility by phosphorylating 14-3-3ζ and so affecting Golgi organisation (discussed in section 1.6.2) (Preisinger et al., 2004). MST4 is targeted to the Golgi apparatus and so could mediate cell migration by modulating Golgi function too (Preisinger et al., 2004). The same study reported that wild type MST4 impaired the invasion of HEK293T (human embryonic kidney 293 T-antigen) cells into collagen I.

In summary, the GCKIII kinases have roles in regulating cell proliferation, growth and apoptosis, and are regulators of cell migration.

Table 1.2 Summary of GCKIII kinase functions

GCKIII kinase	Functions
STK24	Activates ERK, induction of apoptosis, impairs cell migration
STK25	Induction of apoptosis, impairs cell migration
MST4	Activates ERK, has pro- and anti- apoptotic functions, impairs cell invasion

1.8 Cerebral Cavernous Malformations (CCM)

Cerebral cavernous malformations are a class of vascular malformations in the central nervous system (CNS) (reviewed in (Cavalcanti et al., 2012; Faurobert and Albiges-Rizo, 2010). CCMs have an incidence of 0.4% - 0.5% in the general population and are responsible for 5% - 15% of all vascular malformations in the CNS. CCM3, one component of the STRIPAK complex, is implicated in this disease and perturbs endothelial physiology.

This provided the rationale to investigate FAM40 function in endothelial cells. Hence, it is important to understand the aetiology and characteristics of CCM in order to put FAM40 function in perspective. This section provides an overview of CCM stressing links with vascular permeability and angiogenesis.

CCMs are 'slow-flow' lesions in the CNS and patients present with densely packed vascular sinusoids surrounded by a collagen matrix. CCM clusters consist of capillary channels that are grossly dilated and lined by a single layer of endothelium. In addition, there is a breakdown of the blood brain barrier, and CCMs lack intact tight junctions (Cavalcanti et al., 2012). Symptoms associated with CCM include haemorrhage, seizures and neurological deficits. Three genes have been linked with this disease termed CCM1, CCM2 and CCM3. CCM can occur both sporadically (~80% of cases) or be inherited in a familial context (~20% of cases). The pattern of inheritance in CCM is autosomal dominant, and it is estimated that about 80% of all CCM patients with a genetic form of CCM harbour a mutation in CCM1, CCM2 or CCM3. These mutations result in a loss of function of the mutated allele (Riant et al., 2010).

All three CCM genes affect vasculogenesis and endothelial development. For example, mice that completely lack CCM2 activity have severely impaired vascular development leading to embryonic death. However, CCM2+/- mice survive into adulthood (Whitehead et al., 2009). CCM usually manifests in adulthood and so it is possible that the functioning of an existing vascular network is affected, in addition to defects in endothelial development (Leblanc et al., 2009). In support of this role for the CCM genes, endothelial cells from CCMs express higher levels of VEGF, display neo-angiogenesis and increased proliferation (Leblanc et al., 2009). VEGF increases paracellular permeability and so could contribute to CCM pathogenesis. These features imply that endothelial cells in CCMs have broken free of control mechanisms that maintain quiescence. Taken together, CCM can be regarded as a disease of vascular development and endothelial quiescence.

CCM1, CCM2 and CCM3 proteins interact physically. CCM1 and CCM3 can both bind to CCM2 but not with each other (Faurobert and Albiges-Rizo, 2010). CCM1 is a Rap1 effector and activation of Rap1 causes association of CCM1 with cell-cell junctions (Glading et al.,

2007), and CCM1 localised at endothelial cell-cell junctions plays a role in mediating vascular permeability (Gingras et al., 2012). This study also suggests that the interaction of CCM2 with CCM1 is important for CCM2 localisation to junctions. Depletion of CCM1 by RNAi in cultured endothelial cells leads to an increase in RhoA activity, p-MLC levels and number of stress fibres and is associated with increased permeability (Stockton et al., 2010). Hence, CCM1 serves to keep RhoA activity in check and prevents an increase in endothelial permeability. CCM2 knockdown induces a similar phenotype, placing both genes upstream of the RhoA/ROCK axis. Furthermore, the two proteins have to interact to carry out these functions and disruption of this interaction abrogates their capacity to maintain junction integrity (Stockton et al., 2010). Like CCM1 and CCM2, CCM3 has been shown to be important for maintaining junction integrity by preventing stress fibre induction and associated contractility (Zheng et al., 2010).

In addition, CCM2 co-immunoprecipitates with Rac1 (Whitehead et al., 2009) and so could facilitate Rac1-mediated stabilisation of cell-cell junctions (Beckers et al., 2010). Depletion of CCM2 also leads to a decrease in levels of activated Cdc42, which along with its effects on the actin cytoskeleton is thought to impair lumen formation during vascular development (Whitehead et al., 2009). Another key molecule in CCM1/CCM2 signalling is HEG1 (heart of glass 1) which is an endothelial-specific transmembrane receptor. Loss of HEG1 function too leads to impairment in lumen formation and disruption of endothelial junctions. HEG1 binds to CCM1 and this interaction has been suggested to be important for CCM1 localisation to junctions, and so facilitates CCM1 function in conserving junction integrity (Gingras et al., 2012). It has been shown that HEG1 couples to CCM2 via CCM1 at endothelial junctions (Kleaveland et al., 2009). CCM2L (CCM2 like), a CCM2 paralog has been recently identified as a novel component of the HEG1-CCM pathway that competes for HEG1 with CCM2 (Rosen et al., 2013; Zheng et al., 2012).

CCM3 differs from the other CCM proteins in that it appears to signal by distinct mechanisms. The GCKIII kinases interact with CCM3 (Ceccarelli et al., 2011), and this interaction is central for CCM3 signalling with GCKIII kinases being downstream effectors of CCM3 function (Zheng et al., 2010). Wild type CCM3 can bind STK24, STK25 and MST4

while mutant CCM3 protein (with a mutation linked to CCM) fails to do so. Expression of mutated CCM3 in zebrafish results in vascular development defects and proves that CCM3 is functionally coupled to the GCKIII kinases. Loss of STK25 and CCM3 function leads to vascular development defects in zebrafish and confers a barrier defect in cultured endothelial cells. The study goes on to demonstrate that STK24 and STK25 act downstream of CCM3 to downregulate RhoA activity, preventing loss of barrier function. However, it is not clear if CCM3 signals via RhoA as a second study failed to detect increased RhoA activity upon CCM3 depletion by RNAi (Chan et al., 2011). This view of an independent CCM3 function is supported by the fact that vascular anomalies observed upon CCM3 knockdown in zebrafish are distinct from those following either CCM1 or CCM2 knockdown (Yoruk et al., 2012). CCM3 could also contribute to CCM through its role in regulating Golgi positioning and organisation via the GCKIII kinases (discussed in section 1.6.2). This function could have implications for junction formation. Furthermore, CCM3 is the only CCM protein that is a member of the STRIPAK complex which again suggests an independent role for it in CCM.

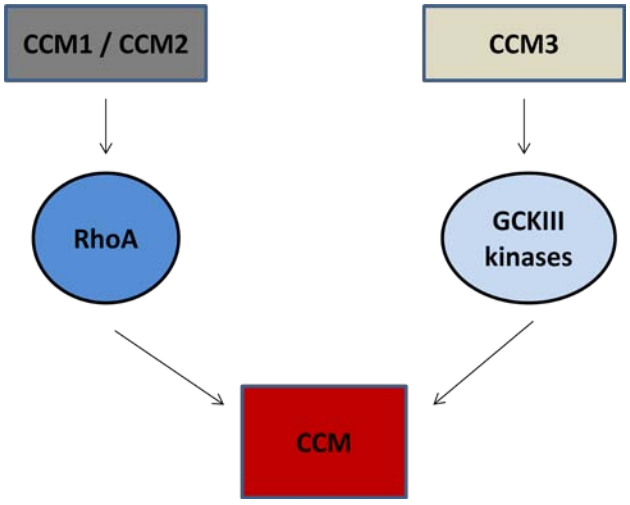

Figure 1.14 A model for CCM gene function
CCM1/CCM2 and CCM3 may signal by independent pathways which converge in yielding a common pathology. It is proposed that CCM1/CCM2 signal via RhoA while CCM3 signals via the GCKIII kinases (Chan et al., 2011).

1.9 Aims

The aim of this project is to investigate the functions and regulation of the human FAM40 proteins.

- The first aim is to carry out a biochemical characterisation of human FAM40A and FAM40B. This includes the identification of interacting partners and protein modifications such as phosphorylation.
- Previous work in our laboratory utilised an RNAi screening approach in PC3 prostate cancer cells to identify the FAM40 proteins as novel regulators of cell morphology and migration. The second aim is to functionally characterise the FAM40 proteins in PC3 cells by investigating their effects on cell morphology, migration and adhesion.
- The FAM40 proteins are members of the STRIPAK complex which also contains CCM3. This led to the hypothesis that the FAM40 proteins are important for endothelial cell physiology. The third aim is to investigate their effects on F-actin organisation, permeability and angiogenesis, using primary endothelial cells as a model system.

2 Materials and Methods

2.1 Materials

Chemicals for solutions were purchased from Sigma-Aldrich unless otherwise stated.

2.1.1 Reagents and kits

Accutase	Millipore
ATP	Calbiochem
[γ-^{32} P]-ATP (# BLU002A500UC)	Perkin-Elmer
Cell permeable C3 transferase	tebu-bio
Cell Tracker ™ Green, CMFDA	Invitrogen
Cell Tracker ™ Orange, CMRA	Invitrogen
Complete, mini EDTA-free protease inhibitor cocktail	Roche Applied Science
Colloidal Coomassie Brilliant Blue-G	Sigma-Aldrich
Coverslips (13 mm)	VWR
Cell dissociation solution	Sigma-Aldrich
Spectra/Por dialysis tubing	Spectrum Laboratories
(MW cut-off 12,000 – 14,000)	
Dulbecco's modified eagle medium (DMEM)	Gibco
(+ 4500 mg/L glucose, + L-Glutamine, + 25 mM HEPES,	
+ 110 mg/L sodium pyruvate)	
Dulbeccos's modified eagle medium (DMEM) : F12	Lonza
(1:1 mix, + L-Glutamine + 15 mM HEPES)	
6X DNA loading dye	Fermentas
DNA-free kit	Ambion
Dried, skimmed milk	Marvel
EBM-2 bullet kits	Lonza
ECL reagent	GE Healthcare
0.4 cm Electroporation cuvettes	Bio-Rad
Foetal calf serum	Invitrogen

Fibronectin	Calbiochem
FITC-dextran (molecular weight 42,000)	Sigma-Aldrich
Fluorescent mounting media	DAKO
Gateway® LR Clonase ™ II Enzyme mix	Invitrogen
Glutathione sepharose beads	GE Healthcare
Immobilon-P PVDF membrane	Millipore
Immobilon-FL PVDF membrane	Millipore
Isopropyl-β-D-thiogalactopyranoside	Sigma-Aldrich
1 kb DNA ladder	Invitrogen
jetPRIME® transfection kit	Polyplus transfection
Lipofectamine ™	Invitrogen
Lysozyme	Sigma-Aldrich
BD Matrigel ™ basement membrane matrix	BD Biosciences
Mouse Anti-HA agarose beads	Sigma-Aldrich
Mouse IgG agarose	Sigma-Aldrich
Recombinant MST4 enzyme (GST tagged)	Invitrogen
Nu PAGE® 4-12 % Bis-Tris Gel	Invitrogen
Oligofectamine ™	Invitrogen
Oligonucleotide primers	Eurogentec
Opti-MEM + GlutaMax ™	Gibco
ORIS™ assay stoppers	Platypus technologies
EndoFree Maxiprep kit	Qiagen
QIAprep Miniprep kit	Qiagen
Phosphate buffered saline (PBS)	Gibco
(-) $CaCl_2$ / $MgCl_2$ or (+) $CaCl_2$ / $MgCl_2$	
Phosphatase inhibitor cocktail (Set 2 and Set 4)	Calbiochem
Penicillin / Streptomycin	Gibco
Precision Master Mix	Primer Design
Precision PlusProtein ™ standards	Bio-Rad
ProQ ® Diamond Phospho-protein blot stain kit	Invitrogen

Rabbit Anti-myc agarose beads	Sigma-Aldrich
Rabbit IgG agarose	Sigma-Aldrich
RNeasy Mini kit	Qiagen
Roswell Park Memorial Institute (RPMI) 1640 media (+ L-Glutamine, + 25 mM HEPES)	Gibco
Streptavidin agarose	Pierce
Sulfo-NHS-Biotin	Pierce
SulfoLink coupling resin	Pierce
SuperScript® VILO ™ cDNA synthesis kit	Invitrogen
Tris(2-carboxyethyl) phosphine hydrochloride (TCEP)	Sigma-Aldrich
Thrombin	Sigma-Aldrich
Transwells (8 µm pore size)	Greiner bio-one
Transwell Permeable Supports, 0.4 µm pore size, 12 mm	Costar
Trizol	Invitrogen
Trypsin / EDTA 0.05%	Gibco
H-1152 Rho Kinase inhibitor	Calbiochem
Y-27632 Rho Kinase inhibitor	Calbiochem
X-ray film	Fujifilm

2.1.2 Buffers and solutions

Table 2.1 Buffers and solutions

Buffer	Composition
IP lysis buffer	20 mM Tris-HCl pH 8.0 1% Triton X-100 130 mM NaCl 1 mM DTT 10 mM NaF Complete mini EDTA-free protease inhibitor Phosphatase inhibitor cocktail
RIPA buffer	20 mM Tris HCl pH 7.5 150mM NaCl 1mM EDTA 1mM DTT 1% NP-40

	0.5% sodium deoxycholate 0.1% SDS 25 mM NaF Complete mini EDTA-free protease inhibitor Phosphatase inhibitor cocktail
Rho lysis buffer	50 mM Tris-HCl pH 7.5 1 mM EDTA 500 mM NaCl 10 mM MgCl2 0.1 % SDS 1 % Triton X-100 10 % Glycerol 0.5% sodium deoxycholate 0.5% β-mercaptoethanol 25 mM NaF 1 mM sodium orthovanadate (Na_3VO_4) 1 mM phenylmethyl sulfonyl fluoride (PMSF) Complete mini EDTA-free protease inhibitor
Laemmli lysis buffer	80 mM Tris-HCl pH 7.5 10% Glycerol 2% SDS 1 mM DTT 10 mM NaF 10 mM glycerol phosphate 1 mM Na_3VO_4 1 mM PMSF Complete mini EDTA-free protease inhibitor
4X SDS sample buffer	4% SDS 160 mM Tris-HCl pH 6.8 20% Glycerol 10 mM DTT 0.006% Bromophenol blue
NuPAGE® MES SDS running buffer	50 mM MES 50 mM Tris base 0.1% SDS 1 mM EDTA pH 7.3
NuPAGE® MOPS SDS running buffer	50 mM MOPS 50 mM Tris base 0.1% SDS 1 mM EDTA pH 7.7
Transfer buffer	25 mM Tris 192 mM Glycine 20% Methanol pH 8.3
Tris-buffered saline with Tween (TBST)	20 mM Tris-HCl pH 7.6 140 mM NaCl 0.1% Tween-20

Stripping buffer	70 mM Tris 20 mM NaCl pH 2.3
STE buffer	10 mM Tris-HCl pH 8.0 150 mM NaCl 1 mM EDTA Complete mini EDTA-free protease inhibitor
50X TAE buffer	2 M Tris 0.05 M EDTA pH 8.0 57.1 ml/L glacial acetic acid
TE buffer	10 mM Tris-HCL pH 8.0 1 mM EDTA
Electroporation buffer	120 mM KCl 10 mM K_2PO_4/$KHPO_4$ pH 7.6 25 mM HEPES pH 7.6 2 mM $MgCl_2$ 0.5% Ficoll 400
Kinase assay buffer	50 mM Tris-HCl pH 7.5 10 mM $MgCl_2$ 1 mM DTT
High salt wash buffer	0.5 M NaCl 10 mM Tris-HCl pH 7.5
FACS buffer	PBS (+) $CaCl_2$ (+) $MgCl_2$ 1% FCS
Peptide affinity chromatography buffers	
Peptide coupling buffer	50 mM Tris 5 mM EDTA pH 8.5
Wash solution	1.0 M NaCl 0.005% NaN_3
Binding buffer	25 mM Tris-HCl pH 7.2 150 mM NaCl
Elution buffer	0.2 M glycine-HCl pH 2.5
Neutralisation buffer	1 M Tris-HCl pH 9.0
ProQ staining solutions	
Fix solution	7% acetic acid 10% methanol
ProQ phosphoprotein blot stain	ProQ reagent (Invitrogen) diluted 1/1000 in ProQ Diamond blot stain buffer (Invitrogen)
Destain solution	50 mM sodium acetate pH 4.0 20% acetonitrile

2.1.3 Antibodies

2.1.3.1 Primary antibodies

Table 2.2 Primary antibodies

Antibody (clone)	Species	Dilution	Supplier and Catalogue number
β1-integrin (18/CD29)	mouse	WB 1/1000	BD Biosciences #610468

β1-integrin (12G10)	mouse	IF 1/100	Abcam #ab30394
Cdc42	rabbit	WB 1/1000	Cell Signaling #2462
FAM40A	rabbit	WB 1/1000	Generated by Genosphere Biotechnologies
FAM40B	rabbit	WB 1/500	Generated by Genosphere Biotechnologies
FAM40B	rabbit	WB 1/250	Sigma-Aldrich #HPA019657
GAPDH	mouse	WB 1/5000	Millipore #MAB374
GFP	rabbit	WB 1/500	Santa Cruz Biotechnology #sc-8334
HA	rabbit	IF 1/200	Santa Cruz Biotechnology #sc-805
HA (3F10)	rat	WB 1/1000 FACS 1/100	Roche #11867423001
c-myc	mouse	IF 1/200	Santa Cruz Biotechnology #sc-40
c-myc	rabbit	WB 1/500	Santa Cruz Biotechnology #sc-789
MLC2	rabbit	WB 1/500	Santa Cruz Biotechnology #sc-15370
MLC2 pSer19	rabbit	IF 1/200	Cell Signaling #3675
MLC2 pThr18/ pSer19	rabbit	WB 1/1000	Cell Signaling #3674s
Rac1 (23A8)	mouse	WB 1/1000	Upstate #05-389
RhoA	mouse	WB 1/500	Santa Cruz Biotechnology #sc-418
α-tubulin	mouse	WB 1/1000	Sigma-Aldrich #T6199
VE-cadherin	mouse	IF 1/100	BD Biosciences #555289
Vinculin	mouse	IF 1/100	Sigma-Aldrich #V9131

2.1.3.2 Secondary antibodies

Table 2.3 Secondary antibodies

Antigen	Species	Conjugate	Dilution	Supplier
mouse IgG	sheep	HRP	1/5000	GE Healthcare #NA931V
rabbit IgG	donkey	HRP	1/5000	GE Healthcare #NA934V

goat IgG	rabbit	HRP	1/5000	DAKO #P0449
mouse IgG (H+L)	goat	AlexaFluor® 488	1/300	Molecular Probes #A11001
mouse IgG (H+L)	goat	AlexaFluor® 647	1/300	Molecular Probes #A21235
rabbit IgG (H+L)	goat	AlexaFluor® 488	1/300	Molecular Probes #A11008
rabbit IgG (H+L)	goat	AlexaFluor® 647	1/1000	Molecular Probes #A21245
phalloidin		AlexaFluor® 546	1/500	Molecular Probes #A22283
DAPI		DAPI	1/10000	Molecular Probes # D3571

2.1.4 siRNA oligonucleotides

Table 2.4 siRNA oligonucleotides

siRNA	Serial number	Sense sequence	Supplier
siControl on target #1	D-001810-01-05	5'-UGGUUUACAUGUCGACUAA-3'	Dharmacon
FAM40A #1 (siGenome)	D-021516-01	5'-GCAGCAAAUUUAUAGGUUA-3'	Dharmacon
FAM40A #2 (siGenome)	D-021516-02	5'-GCAUGAAUGUUCUAAGACA-3'	Dharmacon
FAM40A #3 (siGenome)	D-021516-03	5'-GCUGAUGACUCUCGAGAAG-3'	Dharmacon
FAM40A #4 (siGenome)	D-021516-04	5'-UAGCGGACGUCUUGCCUGA-3'	Dharmacon
FAM40A #5 (siGenome)	D-021516-17	5'-CAGCACAAGUACACGUCGA-3'	Dharmacon
FAM40B #1 (siGenome)	D-025451-01	5'-GAAGGCAACUCCUCACUAA-3'	Dharmacon
FAM40B #2 (siGenome)	D-025451-02	5'-UAAAGCAGCACAAGUAUAU-3'	Dharmacon
FAM40B #3 (siGenome)	D-025451-03	5'-GGGCCAACAUUGAGGCUUU-3'	Dharmacon
FAM40B #4 (siGenome)	D-025451-04	5'-UGCCGGAGCUUACUACUGA-3'	Dharmacon
FAM40B #5 (siGenome)	D-025451-17	5'-UGACUGGGCUUACGGGAAU-3'	Dharmacon

CCM3 #1 (siGenome)	s22176	5'-GUGAUACUCUGAAAACGUAtt-3'	Ambion
CCM3 #2 (siGenome)	s22177	5'-AGAAAAUCCAGGUCUCACAtt-3'	Ambion
FAM40A pool #1 - individual oligos #1 - #4			
FAM40B pool #1 - individual oligos #1 - #4			
FAM40A pool #2 - individual ologos #1, #3, #4, #5			
FAM40B pool #2 - Individual oligos #1, #2, #3, #5			

2.1.5 Primers

2.1.5.1 Q-PCR primers

Table 2.5 Q-PCR primers

Gene	Sequence (5' to 3')	Annealing temp. used	Conc. in reaction
FAM40A	F: ACCTAGATGCCTTCAACGAG R: ATCACTTCATCCCGTTCCAG	60ºC	500 nM
FAM40B (PC3 samples) FAM40B (HUVEC samples)	F: TCAGACAGAAGGACATTGAG R: GATATACTTGTGCTGCTTTAGG F: AGGCCATGCTGCAACTTTAT R: CTTGGAAGTCCCATGGTCTG	65ºC	500 nM
GAPDH	F: GTGAAGGTCGGAGTCAACG R: TGAGGTCAATGAAGGGGTC	60ºC / 65ºC	500 nM
CCM3	F: GAGTATATGATTGAACGACCAGAG R: GCACTAGCTATATCCTTGATTGTC	60ºC	50 nM

2.1.5.2 Sequencing primers

Table 2.6 Sequencing primers

Primer	Sequence (5' to 3')
FAM40A-850rev	CTTCCAGAGCAGCAAGAGAAC
FAM40A-700	CAGACCTTCAGAGCCG
FAM40A-1500	GGAGAAGAAGAAGTTGAG
FAM40A-2000	CAAAGTGGAAGCATTCAAGG
FAM40B-850rev	CAGAGCAGGAGCAGGACC
FAM40B-700	CTGGAGCGAGAGACAGACC
FAM40B-1400	GGACACAGATACATTGGTTGG
FAM40B-2000	GGAGACAACAGCCAGTTCTG
STK24-for	CACCCGAGGTCATCAAACAG
STK24-rev	CTCCACAAACTCCTTGAGGG
STK25-for	CACCTGAGGTCATCAAGCAG
STK25-rev	AGGTCAGAGTTTGGAGGCTC
MST4-for	ATGGCTCCTGAAGTTATTCAACAG

MST4-rev	GAGTTAGGTGGCTCTCCCTT
CCM3-for	ATGAGGATGACAATGGAAGAG
CCM3-rev	GGGACTCCGTGAAGTTAACT

2.1.6 Vectors

Table 2.7 Vectors

Vector	Source
pENTRY-FAM40A (with STOP)	Dr. Stefan Wiemann
pENTRY-FAM40B_long (with STOP)	Dr. Stefan Wiemann
pENTRY-STK24 (with STOP)	Dr. Stefan Wiemann
pENTRY-STK25 (with STOP)	Dr. Stefan Wiemann
pENTRY-MST4 (with STOP)	Dr. Stefan Wiemann
pENTRY-CCM3 (with STOP)	Dr. Stefan Wiemann
pDEST-HA (N-terminal tag)	Dr. Matthias Krause
pDEST-myc (N-terminal tag)	Dr. Matthias Krause
pHA-Ubiquitin	Dr. Matthias Krause
pEGFP-E-cadherin	Dr. Maddy Parsons
pHA-TrkA	Dr. Uwe Drescher
pHA-14-3-3	Dr. Philippe Riou

2.1.7 Software

Table 2.8 Software

Software	Supplier
Illustrator CS4	Adobe
Metamorph	Molecular Devices
ImageJ	National Institutes of Health
LSM + ZEN	Zeiss
Cell Profiler	Broad Institute

2.2 Methods: molecular biology

2.2.1 Transformation of competent *Escherichia coli* (*E. coli*)

100 ng of plasmid DNA or 5 µl of Gateway LR reactions (section 2.2.4) were added to 100 µl of competent DH5α cells (Invitrogen) and the mixture placed on ice for 30 min. The suspension was heat-pulsed at 42ºC for 45 sec and then placed on ice for 5 min. After addition of 500 µl of antibiotic free LB (Luria broth), the cells were allowed to grow at 37ºC for 1 h. 100 µl of transformed plasmid DNA suspensions and the entire amount of Gateway LR reaction suspensions were plated onto LB agar plates containing the appropriate antibiotic for selection (100 µg/ml ampicillin).

2.2.2 Purification of plasmid DNA from bacteria

QIAprep Miniprep kits were used for small scale production of plasmid DNA (used for DNA sequencing (see 2.2.6) and restriction digestion (section 2.2.4)). Steps were carried out at room temperature unless otherwise stated. 5 ml of LB containing antibiotic for selection was inoculated with a single colony from an LB agar plate and incubated overnight at 37°C. Cells from 1.5 ml of this starter culture were pelleted by centrifugation at 17,000 g for 1 min and resuspended in 250 µl of Buffer A (50 mM glucose, 25 mM Tris-HCl, pH 8.0, 10 mM EDTA, 10 µg/ml RNase A). After complete resuspension, 250 µl lysis buffer (200 mM NaOH, 1% SDS) was added and the suspension mixed gently. After 5 min of incubation with lysis buffer, 350 µl neutralisation buffer (3 M KAc, 2 M acetic acid) was added and the suspension mixed thoroughly. Cell debris and proteins were pelleted by centrifugation at 17,000 g for 10 min. The supernatant was added to QIAprep spin columns and centrifuged at 17,000 g for 1 min. Bound DNA was washed with 750 µl wash buffer (750 mM NaCl, 50 mM MOPS, pH 7.0, 15% isopropanol (v/v)) and the DNA eluted with 50 µl water by centrifugation of the column for 1 min at 17,000 g.

Qiagen EndoFree Maxiprep kits were used for larger scale purification of plasmid DNA. A 5 ml starter culture was used to inoculate 200 ml of LB containing antibiotic for selection. After overnight incubation at 37ºC, bacterial cells were pelleted at 4,000 rpm in a Sorvall RC5C centrifuge (Rotor SLA-1500) for 15 min. The bacterial pellet was resuspended, lysed and neutralised as described in the miniprep protocol except that 10 ml volumes of buffers were used in each step. To clarify the lysed cell suspension, the lysate was applied to filter-syringes provided in the kit, left for 10 min and pressed through the filter into 50 ml tubes. 1.5 ml of endotoxin removal buffer was added and the supernatant incubated on ice for 30 min, following which it was applied to columns pre-equilibrated with the equilibration buffer (250 mM NaCl, 50 mM MOPS, pH 7.0, 15% isopropanol (v/v),15% Triton X-100). After washing twice with wash buffer (1 M NaCl, 50 mM MOPS, pH 7.0, 15% isopropanol (v/v)) and DNA elution (elution buffer: 1.25 M NaCl, 50 mM Tris-HCl, pH 8.5, 15% isopropanol), the DNA was precipitated by adding 0.7 volumes of isopropanol (v/v). DNA was pelleted by centrifugation at 2,700 g for 60 min at 4ºC. The pellets were washed with 5 ml 70% ethanol

and air dried. Pellets were resuspended in 200-500 µl of ddH_2O and the DNA concentration determined.

2.2.3 Determining of DNA concentration

DNA concentration was determined spectrophotometrically at 260 nm, using a Nano-Drop system (ND-1000, www.nanodrop.com) to determine optical density. The DNA concentration was determined using the following formula: concentration of DNA= OD_{260} x 50 µg/ml.

2.2.4 Gateway cloning

The Gateway cloning system from Invitrogen utilises the site-specific recombination properties of bacteriophage lambda to move DNA sequences into multiple vector backbones.

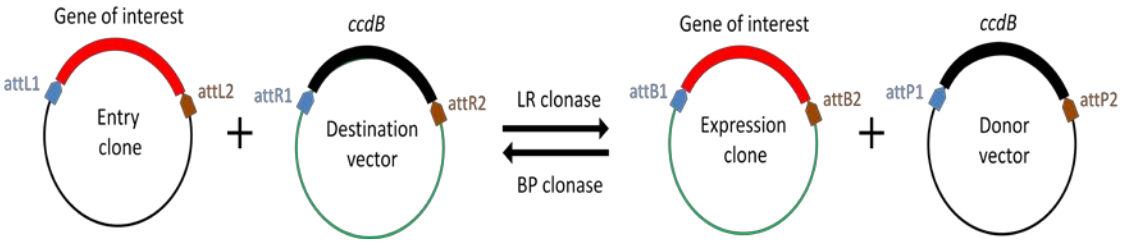

Figure 2.1 Schematic of the Gateway cloning system
The DNA of interest is flanked by specific recombination sequences which allow it to be shuttled across various vector systems in the presence of appropriate recombination enzymes. The toxic gene ccdB is used as a negative selection marker.

The Gateway cloning system was used to generate expression vectors of FAM40A, FAM40B, STK24, STK25 and CCM3 tagged with either HA or myc at the N-terminus. The cDNA of these genes present in an entry clone were made to recombine in a LR reaction with a destination vector containing the required tag (pDEST-HA or pDEST-myc) (see Table 2.7). Gateway LR reactions were set up at room temperature as follows:

Component	Volume
Entry clone (150 ng)	1-7 µl
Destination vector (150 ng/µl)	1 µl
TE buffer, pH 8.0	to 8 µl

The LR clonase II enzyme (provided in the Gateway® LR Clonase ^{TM} II Enzyme mix kit) was thawed on ice for 2 min, vortexed briefly and 2 µl of the enzyme was added to the reaction prepared. The reaction mix was mixed by vortexing gently and incubated at 25ºC for 1 h. 1 µl of Proteinase K solution (provided in the kit) was added to the reaction mix. Incubation at 37ºC for 10 min was done to terminate the reaction. The Gateway cloning technique was used to generate the plasmids pHA-FAM40A, pHA-FAM40B, pmyc-FAM40A, pmyc-FAM40B, pmyc-STK24, pmyc-STK25, pmyc-MST4 and pmyc-CCM3.

The generated expression clones were verified by checking for insert release after digestion with the restriction enzyme BsrGI (New England Biolabs (NEB)) which cuts within the attB sequence. Restriction enzyme reactions were setup using 15 µl miniprep DNA, 2 µl NEB Buffer 2, 2µl BsrGI enzyme and 1 µl H_2O. Restriction reactions were incubated at 37ºC for 1 h and subsequently resolved on a 1% agarose gel.

2.2.5 Agarose gel electrophoresis

A 1% (w/v) agarose gel was made by mixing an appropriate volume of agarose with 1X TAE buffer. The mixture was heated until the agarose was completely dissolved. After the mixture had cooled down, it was supplemented with 0.5 µg/ml ethidium bromide and poured into a gel chamber with a well comb and left to solidify. DNA samples (along with a molecular weight marker) with 1X DNA loading dye were loaded and electrophoresis was performed at 10-15 V/cm^2 until the samples were resolved. DNA bands were visualised using a UV transilluminator.

2.2.6 Sequencing

100 ng of plasmid DNA (in ddH2O) and appropriate sequencing primers (see Table 2.6) at a concentration of 2 pmol/µl in a volume of 15 µl were sent to MWG (www.eurofinsdna.com) for DNA sequencing.

2.2.7 Quantitative PCR

2.2.7.1 Extraction of total RNA and DNase treatment

Quantitative PCR was used to determine the knockdown of gene expression by siRNA. Total RNA was extracted 72 h after siRNA transfection using either the RNeasy mini kit (Qiagen)

according to the manufacturer's instructions or with Trizol. For extraction using Trizol, cells were harvested using trypsin and pelleted by centrifugation in a microfuge tube. 1 ml of Trizol was added to the pellet and incubated for 5 min at room temperature. 200 µl of chloroform was added and the tubes shaken vigorously for 15 sec and left at room temperature for 3 min. Samples were then centrifuged at 17,000 g for 15 min at 4ºC and the upper phase transferred to a fresh tube. 250 µl of isopropanol was added to precipitate the RNA. After 10 min incubation on ice the samples were centrifuged at 17,000 g for 15 min. RNA pellets were washed twice with 75% ethanol following which they were air dried and resuspended in RNase-free water. Samples were incubated at 55ºC for 10 minutes to facilitate solubilisation of RNA. The RNA samples (extracted using Trizol or the RNAeasy mini kit) were then eliminated of genomic DNA using DNase treatment (DNA free kit, Ambion). The purified RNA was incubated with 1X DNase buffer and 1 µl DNase enzyme for 30 min at 37ºC. The enzyme was inactivated by adding 5 µl of DNase inactivation beads followed by incubation at 37°C for 2 min. After centrifugation (10,000 g for 1 min) the supernatant was transferred to a fresh tube and stored at -80°C.

2.2.7.2 cDNA synthesis

The concentration of purified RNA was determined spectrophotometrically at 260 nm, using a Nano-Drop system (ND-1000, www.nanodrop.com) to determine optical density. The RNA concentration was determined using the following formula: concentration of RNA= OD_{260} x 40 µg/ml. The OD_{260}/OD_{280} ratio was used as a measure of RNA purity. The SuperScript® VILO ™ cDNA synthesis kit (Invitrogen) was used to synthesise cDNA using the purified RNA as a template. Reactions were set up on ice as follows:

Component	Volume
5X VILO ™ Reaction mix	4 µl
10X Superscript® Enzyme mix	2 µl
RNA (1 µg)	x µl
DEPC-treated water	to 20µl

The reaction mix was incubated at 25ºC for 10 min and then at 42ºC for 60 min. Reactions were terminated by incubation at 85ºC for 5 min. The cDNA was stored at -20ºC until further use.

2.2.7.3 Q-PCR using SYBR green

The synthesised cDNA was used in Q-PCR reactions to quantitatively determine levels of expression of the gene of interest using SYBR green detection chemistry (mastermix from Primer Design). SYBR green is a fluorescent dye which binds double stranded DNA. Its fluorescent signal is proportional to the amount of double stranded DNA and hence can be used as a measure of DNA quantity. Real-time monitoring of the signal enables the determination of PCR reaction kinetics which is used to quantify the initial amount of template present in the reaction. Reactions set up for each condition (in quadruplicate) included 3 µl of cDNA (diluted 1/65 with RT-PCR grade water (Ambion)), 3 µl primer mix (forward and reverse primers at concentrations specified in Table 2.5) and 6 µl Q-PCR mastermix. GAPDH was used as a reference gene in each reaction. The amplification cycle used was an initial 10 min denaturation at 90ºC, 40 cycles of denaturation (10 sec at 95ºC) and annealing/extension (30 s, refer to Table 2.5 for temperatures used for specific primer pairs). One cycle of 95°C for 15 sec, 60°C for 20 sec and 95°C for 15 sec was used to generate the melting curve.

Data was acquired using either an ABI Prism 7000 system (Applied Biosystems) or the MX3005p system (Agilent technologies) and analysed with ABI7000 SDS analysis software or with MxPro QPCR software respectively. Cycle to threshold (C_T) values were determined for each condition (with GAPDH and gene of interest primers). The C_T value is defined as the PCR cycle number at which the fluorescence signal crosses a certain preset threshold level in the logarithmic amplification phase of the PCR reaction. The C_T value is inversely proportional to the initial amount of template in the reaction. The efficiency of each primer pair was initially assessed by amplification of serial dilutions of cDNA template. To calculate the efficiency, 10-fold dilutions of the cDNA template were made and C_T values for each sample determined. A graph was plotted of the determined C_T values against the dilution factor (logarithmic scale: -1, -2, -3 etc.). The slope of the graph was determined and

efficiency of the primer pair was calculated as (10^(-1/slope) – 1) * 100). PCR efficiencies of between 90% and 110% were considered acceptable (apparent efficiencies of above 100% are an artefact of the manner in which efficiencies are calculated). A melting curve analysis was included to verify the specificity of amplification.

Cycle to threshold values (C_T) were normalised to GAPDH levels and % mRNA expression normalised to control siRNA calculated as (100 / (2 ^ (C_T shift))).

C_T shift = C_T siRNA knockdown sample – C_T siRNA control sample
[C_T siRNA knockdown sample = C_T gene of interest primer – C_T GAPDH primer, C_T siRNA control sample = C_T gene of interest primer – C_T GAPDH primer]

2.3 Methods: cell biology

2.3.1 Cell culture

2.3.1.1 Growing and passaging of cells

PC3 cells were grown in Roswell Park Memorial Institute 1640 medium (RPMI), COS7 cells in Dulbeccco's modified Eagle's medium (DMEM) and CHO cells (Flp-In ^{TM} CHO, Invitrogen provided by Dr. Andrew Beavil) in DMEM:F12 (1:1 mix) medium. Media were supplemented with 10% foetal calf serum (FCS), penicillin (100 IU/ml) and streptomycin (100 µg/ml). Cells were maintained in an incubator at 37ºC and 5% CO2. When the cells reached 80% confluency, they were passaged using trypsin-EDTA. The media was removed and the cells washed once with 1 ml PBS. The PBS was aspirated and 1 ml of trypsin-EDTA per 75 cm^2 tissue culture flask at 37ºC was added for 3 min or until cells detached. Trypsin-EDTA was inactivated by adding 9 ml of media. Cells were split at between 1:2 and 1:10 and the medium changed every 2-3 days.

Pooled human umbilical vein endothelial cells (HUVECs) obtained from Lonza or PromoCell were cultured in EBM-2 medium containing the appropriate growth factors (EGM-2) and supplemented with 2% foetal bovine serum. Cell culture dishes were coated with 10 µg/ml fibronectin for 1 h at 37ºC prior to cell seeding. Cells were passaged when they reached

confluency as described previously and split at between 1:3 and 1:4. Cell medium was changed every 2 days and HUVECs used until passage 4.

2.3.1.2 Freezing and thawing of cells

PC3, COS7 and CHO cells were harvested using trypsin and pelleted by centrifugation at 200 g for 5 min. 2-3 x 10 ^ 6 cells were resuspended in 1 ml of freezing media (90% FCS, 10% DMSO) and aliquoted into cryovials. Cryovials were frozen down at -80ºC in a cryo freezing container overnight to allow gradual cooling. Cryovials were transferred to liquid nitrogen for long term storage.

Cells were thawed by removing cryovials from liquid nitrogen and immersing in a 37ºC waterbath to allow rapid thawing. Contents of each cryovial were transferred to a 75 cm^2 tissue culture flask and 10 ml media added. The medium was removed the next day and fresh medium added to the cells.

2.3.2 siRNA transfection of cells

PC3 cells were reverse transfected with siRNAs (small interfering RNAs) using Lipofectamine 2000. Lipofectamine 2000 and siRNA were diluted separately in Opti-MEM, incubated for 5 min at room temperature, mixed and incubated for a further 20 min at room temperature for lipid-siRNA complexes to form (details in Table 2.9). siRNA was used at a final concentration of 50 nM and lipid-siRNA complexes were allowed to form in tissue culture dishes. Cells for transfection were harvested in parallel, counted and seeded at an appropriate concentration onto the lipid-siRNA complexes in an appropriate volume of medium (details in Table 2.9). Complete growth media was used for the transfections. 24 h later the medium was changed and the cells used for downstream experiments.

Table 2.9 Transfection conditions for PC3 cells

Culture vessel	siRNA (µl of 20µM stock) & Opti-MEM dilution volume (µl)	Lipofectamine 2000 (µl) & Opti-MEM dilution volume (µl)	Cell number per well	Total volume per well (including complexes)
96 well (tissue culture untreated)	0.375 in 25	0.25 in 25	80,000	150 µl
24 well	1.25 in 50	1 in 50	100,000	500 µl

6 well	5 in 250	5 in 250	500,000	2 ml
10 cm dish	12 in 500	18 in 500	700,000	5 ml

HUVECs were transfected using Oligofectamine in wells of a 6 well plate. 24 h before transfection, 10 ^ 5 cells were seeded per well. On the day of transfection, growth medium in each well was replaced with 800 µl of Opti-MEM. Individual siRNAs (20 µM stock) were diluted in Opti-MEM (2.5 µl in 185 µl per condition, 2.5 µl + 2.5 µl in 185 µl for double transfections) so as to reach a concentration of 50 nM in the final transfection mix. Oligofectamine was diluted in Opti-MEM (4 µl in 15 µl) and the two prepared solutions were incubated at room temperature for 5 min. The two solutions were then mixed and lipid-siRNA complexes allowed to form for 20 min at room temperature. This mixture was then added drop-wise to cells in one well (in 800 µl of medium). After 5-6 h, 500 µl of EGM-2 medium containing 12% FCS was added to each well (final FCS concentration of 4%). The following day, medium was changed to EGM-2 containing 2% FCS and the cells used for downstream experiments. Mock transfections in all experiments were performed by replacing siRNA with growth media in the transfection mixes.

2.3.3 DNA transfection of cells

DNA transfection of PC3 cells was done using the jetPRIME® transfection kit (Polyplus transfection) according to the manufacturer's instructions. 30,000 cells were seeded onto Matrigel-coated glass coverslips (100 µg/ml at 37ºC for 1 h) or uncoated glass coverslips the day before transfection. The transfection mix was prepared by adding 0.5 µg of plasmid DNA to 50 µl of jetPRIME® buffer. After vortexing for 10 sec, 1 µl of jetPRIME® transfection reagent was added to the mix. After vortexing further for 10 sec, the mix was incubated at room temperature for 10 min and added to cells on each coverslip in 0.5 ml of medium. After 24 h cells were fixed in 4% PFA at room temperature for 20 min and used for immunofluorescence (section 2.3.13).

DNA/siRNA double transfection of COS7 cells was done using the jetPRIME® transfection kit. 100,000 cells were seeded in each well of a 6 well plate the day before transfection. Cells were transfected with 50 nM of FAM40A or FAM40B targeting siRNA. The transfection mix was prepared by adding 5 µl of siRNA (20 µM stock) to 200 µl of jetPRIME® buffer. After

mixing gently, 4 µl of jetPRIME® transfection reagent was added to the mix. After vortexing for 10 sec, the mix was incubated at room temperature for 10 min and added to cells in each well in 2 ml of medium. After 24 h, cells were transfected with pHA-FAM40A or pHA-FAM40B plasmid DNA. The transfection mix was prepared by adding 500 ng of plasmid DNA to 200 µl of jetPRIME® buffer. After vortexing for 10 sec, 1 µl of jetPRIME® transfection reagent was added to the mix. After vortexing further for 10 sec, the mix was incubated at room temperature for 10 min and added to cells in each well in 2 ml of medium. Medium was changed after 24 h and after a further 24 h cells were used to make lysates for anti-HA immunoblotting.

HUVECs were transfected with plasmid DNA using Amaxa nucleofection. HUVECs were trypsinised and washed once with PBS (+ Ca/Mg) and resuspended in HUVEC electroporation buffer (Amaxa) (10 ^ 6 cells in 100 µl of buffer per condition). 3 µg of plasmid DNA was mixed with the cell suspension and transferred to an electroporation cuvette. Nucleofection was carried out with an Amaxa Nucleofector ^{TM} (Amaxa, Cologne, Germany) using program A-34 according to the manufacturer's instructions. After nucleofection, cells from each sample were transferred to two fibronectin-coated glass coverslips (for confluent monolayers) or four coverslips (for sub-confluent monolayers). In siRNA/DNA co-transfection experiments, 500,000 siRNA-transfected cells were used in each nucleofection and the entire sample transferred to a single coverslip. Cells on coverslips were fixed in 4% PFA at room temperature for 20 min and used for immunofluorescence staining.

2.3.4 Electroporation of COS7 cells

COS7 cells grown in 175 cm^2 flasks were split at a ratio of 1:2 the day before transfection. The cells were detached using trypsin and washed once with electroporation buffer (120 mM KCl, 10 mM K_2PO_4/$KHPO_4$ pH 7.6, 25 mM HEPES pH 7.6, 2 mM $MgCl_2$, 0.5% Ficoll 400). Cells from one 175 cm^2 flask were used for 3 transfections. After the wash, cells for each transfection were resuspended with 250 µl of electroporation buffer and mixed with 3-5 µg of plasmid DNA in a 0.4 cm electroporation cuvette. Cells were left on ice for 10 min and electroporated using a Genepulser II system (Bio-Rad) at 250 V, 975 µF. After electroporation, cells were placed on ice for 5 min and then at room temperature for 5 min.

Electroporated cells were transferred to 10 cm dishes with DMEM medium. Medium was changed after 24 h. Cells were used in downstream experiments 24 h or 48 h after transfection.

2.3.5 Generation of stable CHO cell lines

CHO cells stably expressing HA-FAM40A, HA-FAM40B or EGFP-E-cadherin were generated by transfection with pHA-FAM40B, pHA-FAM40B or pEGFP-E-cadherin respectively. These vectors contained a neomycin resistance gene and selection of stable cell clones was done by treatment with geneticin sulphate (G418).

Cells were seeded in 6 well dishes the day before DNA transfection at a density of 2 x 10 ^ 5 cells per well. Transfection was done using the jetPRIME® transfection kit (Polyplus transfection) according to the manufacturer's instructions. The transfection mix was prepared by adding 2 µg of plasmid DNA to 200 µl of jetPRIME® buffer. After vortexing for 10 sec, 4 µl of jetPRIME® transfection reagent was added to the mix. After vortexing further for 10 sec, the mix was incubated at room temperature for 10 min and added to cells in one well of a 6 well dish in 2 ml of medium. After 24 h, transfected CHO cells were harvested and cells from each well were diluted in 10 ml of medium. Cells from this diluted suspension were seeded sparsely onto individual 10 cm dishes (5 µl, 12 µl and 25 µl volumes) to facilitate picking of individual colonies at a later stage. After a further 24 h, fresh medium was added supplemented with 1 mg/ml G418. Selection with G418 was carried out for 2 weeks with the medium being changed every 3 days. A dish of control CHO cells was included to ensure the efficacy of the antibiotic. At the end of the selection period, resistant cell colonies were picked using trypsin-soaked cloning discs, and validated for stable expression of protein using immunofluorescence (section 2.3.13) and western blotting (section 2.4.2).

2.3.6 Treatment of cells with inhibitors

HUVECs were treated with the ROCK inhibitors H-1152 and Y-27632 in EGM-2 medium. Inhibitors were prepared as stock solutions in sterile water. H-1152 was used at a concentration of 5 µM for 10 min and Y-27632 at 10 µM for 24 h. HUVECs were treated with

4 µg/ml C3 transferase in EGM-2 medium for 2 h. Treatment of HUVECs with thrombin was done for 10 min at a concentration of 1 U/ml.

2.3.7 Migration assays

2.3.7.1 Random migration assay

PC3 cells were transfected with siRNAs targeting FAM40A and FAM40B. 24 h after transfection, cells were harvested and seeded onto wells of a 24 well plate. Tissue culture wells were coated with 100 µg/ml Matrigel for 1 h at 37ºC before cell seeding. 15,000 cells were seeded per well and fresh medium was added which contained 1% FCS. Time-lapse movies were made over a period of 14 h using a Nikon TE2000-E microscope with a Plan Fluor 10X objective (Nikon) and a Hamamatsu Orca-ER digital camera. Image series were captured at 37°C and 5% CO_2 at 10 frame/min using Metamorph software. Cells in movies were tracked using the manual tracker plugin in ImageJ (http://rsb.info.nih.gov/ij/) and the migration velocity calculated using the ibidi chemotaxis and migration plugin in ImageJ (www.ibidi.com).

2.3.7.2 ORIS ^{TM} migration assay

The ORIS^{TM} assay (Platypus technologies) (Figure 2.2) is a migration assay in which stoppers are introduced into a well of a 96-well plate preventing cells from seeding onto a central, annular ‘detection zone’. Stoppers are removed after cells have adhered following which migration is monitored. The extent of migration was quantified by the % area of the central zone that cells have migrated into after certain time periods subsequent to removal of the stoppers.

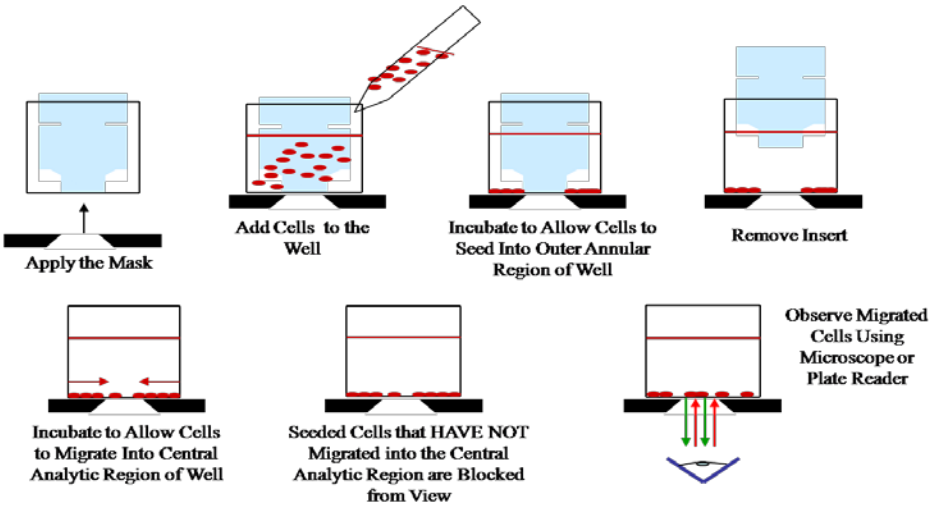

Figure 2.2 Schematic of the ORIS TM assay (adapted from www.platypustech.com)
In the ORIS assay, migration of cells is assessed by measuring their capacity to migrate into a central, annular migration zone that is created by the introduction of cell seeding stoppers.

For ORIS assays with PC3 cells, the cells were stained with Cell Tracker ™ Green, CMFDA (Invitrogen). Cells were stained for 20 min at 37°C (dilution of dye at 1/ 1,000 in PBS + Ca/Mg). Following this, cells were pelleted by centrifugation at 200 g for 5 min and incubated in growth media for a further 20 min. 80,000 stained PC3 cells per condition were transfected in 96-well plates with siRNA pools targeting FAM40A or FAM40B (as detailed in section 2.3.2). After 24 h, cells from each well of the 96-well plate were used to seed two wells of the ORIS plate (with seeding stoppers introduced). Cells were seeded onto Matrigel-coated (100 µg/ml for 1 h at 37ºC) plates in media containing 1% FCS. After a further 24 h, the stoppers were removed and images were acquired of the fluorescent cells at t=0h (point at which stoppers were removed) and t=24h.

ORIS assays with HUVECs were carried out using cells transfected with siRNAs targeting FAM40A and FAM40B. 24 h after transfection, cells were stained with Cell Tracker ™ Orange, CMRA (Invitrogen). Cells were stained for 40 min at 37°C (dilution of dye at 1/400 in growth media). Following this, cells were pelleted by centrifugation at 200 g for 5 min and incubated in growth media for a further 40 min. Stained cells were used to seed wells of the ORIS plate (with seeding stoppers introduced). 30,000 cells were used to seed each well. Cells were seeded onto fibronectin-coated (10 µg/ml for 1 h at 37ºC) plates in growth media.

After a further 24 h, the stoppers were removed and images were acquired of the fluorescent cells at t=0h (point at which stoppers were removed) and t=24h.

Conditions were seeded in triplicate and the mean calculated. Images were acquired using a Nikon TE2000-E microscope with a Plan Fluor 4X objective (Nikon) and a Hamamatsu Orca-ER digital camera.

2.3.8 Adhesion and spreading assays

2.3.8.1 Adhesion assay

For adhesion assays with PC3 cells, cells were transfected with siRNA pools targeting FAM40A and FAM40B. 48 h after transfection, cells were stained with Cell Tracker ™ Green, CMFDA (Invitrogen). Cells were stained for 20 min at 37˚C (dilution of dye at 1/1,000 in PBS + Ca/Mg). Following this, cells were pelleted by centrifugation at 200 g for 5 min and incubated in growth media for a further 20 min. Cells were then detached non-enzymatically (Cell dissociation reagent, Sigma-Aldrich) and resuspended in media containing low serum (1% FCS). Adhesion assays were carried out on Matrigel-coated (100 µg/ml at 37ºC for 1 h) plastic or on uncoated plastic. 25,000 cells were added to each well of a black 96 well plate with a clear bottom. After 15 min adhesion, cells were washed with one change of PBS and fluorescent readings taken as a measure of cell adhesion capacity (using a Perkin Elmer plate reader (PerkinElmer, Cambridge, UK) at 485 nm excitation and 523-535 nm emission). A control where cells were not washed was included to normalise for total cell number. Each condition was done in triplicate and the mean fluorescence calculated.

Adhesion assays with HUVECs were done with cells transfected with siRNAs targeting FAM40A and FAM40B. 72 h after transfection, cells were stained with Cell Tracker ™ Green, CMFDA (Invitrogen). Cells were stained for 40 min at 37˚C (dilution of dye at 1/400 in growth media). Following this, cells were pelleted by centrifugation at 200 g for 5 min and incubated in growth media for a further 40 min. HUVECs were detached by washing with PBS (-Ca/Mg), addition of 250 µl Accutase per well (of a 6 well dish) to just cover the cells, incubation for 3 min. 2 ml medium was added to each well and cells were pelleted by centrifugation at 200 g for 5 minutes. Adhesion assays were carried out on a 1:1 mix of Matrigel and PBS (+ Ca/Mg). 40 µl of this mix was added to each well of a black 96 well

plate with a clear bottom and allowed to polymerise at room temperature for 1.5 h. 25,000 cells were added to each well of the plate and after 5 min adhesion, cells were washed with one change of PBS and fluorescent readings taken as a measure of cell adhesion capacity (using a Perkin Elmer plate reader (PerkinElmer, Cambridge, UK) at 485 nm excitation and 523-535 nm emission). A control where cells were not washed was included to normalise for total cell number. Each condition was done in triplicate and the mean fluorescence calculated.

2.3.8.2 Spreading assay

For spreading assays, PC3 cells transfected with siRNA pools targeting FAM40A or FAM40B were harvested non-enzymatically 72 h after transfection into media containing 1% FCS. 20,000 cells were seeded onto each well of a Matrigel-coated (100 µg/ml at 37ºC for 1 h) 24 well plate. After 30 min incubation at 37 °C, cells were fixed in 4% PFA at room temperature for 20 min and stained with phalloidin-Alexa546 (1/500 in PBS) for 1 h at room temperature. Cells were washed 3 times with PBS and fluorescent images acquired using a Nikon TE2000-E microscope with a Plan Fluor 10X objective (Nikon) and a Hamamatsu Orca-ER digital camera. Cell spread area was determined using ImageJ software and the mean calculated for each condition in each experiment.

2.3.9 Permeability assay with HUVECs

HUVECs were transfected with siRNAs and after 48 h were harvested with trypsin and plated onto fibronectin-coated (10 µg/ml at 37ºC for 1 h). Transwell ™ filters (12 mm diameter, 0.4 µm pore size, Costar) to form confluent monolayers. 10 ^ 5 cells were plated onto each filter and were left to form junctions for 24 h. After 24 h, 1.5 ml of growth media was added to the lower chamber and 0.5 ml of growth media containing 0.1 mg/ml FITC dextran (molecular weight 42 kDa) was added to the apical chamber. A sample of medium (200 µl) was removed from the lower chamber to measure permeability after 80 min and added to wells in a black 96 well plate with a clear bottom. Fluorescence of the removed sample of medium was used as a measure of permeability. Fluorescence was measured using a microplate analyser (Fusion-FA; PerkinElmer; excitation, 485 nm; detection, 523-535 nm). Each condition was performed in triplicate and the mean fluorescence was calculated.

2.3.10 Loop-formation angiogenesis assay

HUVECs were transfected with siRNAs and after 48 h were harvested with trypsin and seeded onto a gel consisting of polymerised Matrigel matrix. To create the Matrigel layer, Matrigel at a concentration of atleast 9 mg/ml was diluted 1:1 with PBS (+ Ca/Mg). 300 µl of this mixture was spread out onto each well of a 6 well dish and allowed to polymerise at room temperature for 1.5 h. HUVECs were seeded onto the Matrigel layer at a density of 2 x 10 ^ 5 cells per well and loops were allowed to form for 24 h. Loops formed were imaged by phase-contrast microscopy or by fluorescence microscopy after staining with Phalloidin-Alexa546 (at a dilution of 1/500 for 1 h at room temperature after cells were fixed with 4% PFA for 20 min and permeabilised with 0.1% Triton X-100 for 1 min, solutions were made in PBS). Loop formation was quantified by counting the number of loops formed per imaged field. The mean value for multiple fields was used for statistical analysis. Images were acquired using a Nikon TE2000-E microscope with a Plan Fluor 4X or 10X objective (Nikon) and a Hamamatsu Orca-ER digital camera. Time-lapse movies were also made by phase-contrast imaging using the 4X objective at 37ºC and 5% CO_2. Images were captured using Metamorph software. A frame rate of 1 frame/30 min was used for 24 h and movies were initiated 1 h after seeding cells onto Matrigel.

2.3.11 CHO cell aggregation assay

CHO cells stably expressing HA-FAM40A, HA-FAM40B, EGFP-E-cadherin and control cells were harvested using non-enzymatic cell dissociation solution (Sigma-Aldrich). Cells were tested for their capacity to aggregate by incubation of cell suspensions at 37ºC and 5% CO_2 for 8 h with gentle mixing every 30 min. Cell suspensions at a density of 2 x 10 ^ 6 cells per ml in a total volume of 2 ml were used. Aggregation assays were carried out in 15 ml polystyrene tubes. A sample containing a heterogeneous mix of HA-FAM40A and HA-FAM40B expressing cells (1:1 mix ratio) was included to test for trans, hetero-dimerisation. At the beginning (t=0 h) and end (t=8 h) of the incubation period, an aliquot of each suspension was taken and loaded into a hemocytometer chamber. Images of random fields were taken using a Nikon Eclipse TS100 microscope with a 10X objective (Nikon) and a QIClick digital camera (QImaging). For each condition in each experiment, 5 individual fields were imaged. The number of ‘particles’ (N) was counted in each image with a ‘particle’

defined as being either a single cell or a clump of multiple cells. The ratio of mean N at t=0 h and mean N at t=8 h (N0 / N8) was used as a measure of cell aggregation in each experiment.

2.3.12 Flow cytometry

COS7 cells were transfected with pDEST-HA, pHA-FAM40A, pHA-FAM40A or pHA-TrkA (used as a positive control). Flow cytometry was used to assess if these proteins were expressed on the cell surface. 24 h or 48 h after transfection, cells (one well of a 6 well dish per condition) were harvested using non-enzymatic cell dissociation solution (Sigma-Aldrich). Cells were washed with FACS buffer (PBS + Ca/Mg with 1% FCS) and pelleted by centrifugation at 200 g for 5 min. Cells were then incubated with the primary antibody (rat anti-HA, Roche, 1/100)) diluted in FACS buffer for 1 h on ice. Cells were washed thrice with FACS buffer using centrifugation at 200 g for 5 min to remove unbound antibody. Incubation of cells with secondary antibody (anti-rat IgG Alexa488, 1/200) diluted in FACS buffer for 1 h on ice was done following which cells were washed 3 times with FACS buffer and centrifugation done at 200 g for 5 min. For each condition, a control was included where cells were stained with secondary antibody alone. The fluorescence of cells was measured using a BD FACSCalibur flow cytometer at an excitation wavelength of 495 nm and an emission wavelength of 519 nm. 10,000 data points were acquired for each condition in each individual experiment. Data was analysed using Flow Jo software.

2.3.13 Immunofluorescence

PC3 cells were seeded onto uncoated glass coverslips or coverslips coated with Matrigel (100 µg/ml at 37ºC for 1 h). Cells treated with siRNA were grown in media containing 1% while other cells were grown in normal growth media (containing 10% FCS). HUVECs were seeded onto glass coverslips coated with fibronectin (10 µg/ml at 37ºC overnight). After attachment of cells and at the point when the experiment was to be terminated, cells were fixed in 4% paraformaldehyde (PFA) for 20 min at room temperature. Fixed cells were washed 3 times in PBS and then permeabilised as required with 0.1% Triton X-100 in PBS for 1 min at room temperature. After washing 3 times with PBS, coverslips were blocked in 3% BSA in PBS for 20 min at room temperature to prevent non-specific binding of

antibodies. Primary antibodies were diluted in 1% BSA (bovine serum albumin) in PBS and 40 µl pipetted onto parafilm. Coverslips were inverted onto the antibody drop and incubated at room temperature for 2 h or at 4ºC overnight. When staining for the active form of β1-integrin (12G10 antibody, Abcam # ab30394), the fixation, permeabilisation and staining steps were performed at 4ºC. Fluorophore-conjugated secondary antibodies, DAPI and phalloidin were prepared in the same way as the primary antibodies. Coverslips were washed 3 times with PBS and inverted onto the secondary antibody drop. Incubation was done at room temperature for 2-3 h. Following this final incubation, coverslips were washed a minimum of 5 times with PBS and mounted onto glass slides using fluorescent mounting medium (DAKO). Slides were incubated at 37ºC for 5 min to allow the mounting media to solidify and then stored at 4ºC until image acquisition.

Table 2.10 Reseeding of siRNA-transfected cells for immunofluorescence

Cell type	Reseeded after transfection at (h)	Number of cells used per coverslip	at 72 h after transfection
PC3	24 h	12,000	sub-confluent
HUVEC	48 h	1.5-2 x 10^5	confluent
HUVEC	48 h	40,000	sub-confluent

For immunofluorescence staining of HUVEC loop assay samples, loops were allowed to form for 24 h (details in section 2.3.10) on 100 µl of matrix in a 8 µl transwell. Samples were fixed with 4% PFA in PBS for 20 min at room temperature and washed 3 times with PBS. Cells were permeabilised with 0.1% Triton X-100 in PBS for 10 min at room temperature. After washing 3 times with PBS, samples were incubated with 3% BSA in PBS for 1 h to reduce background fluorescence. Samples were incubated with phalloidin-Alexa546 and DAPI in 3% BSA in PBS for 2 h at room temperature followed by 3 PBS washes. The filter was then cut away from the transwell and inverted onto a glass coverslip. The coverslip was mounted onto a glass slide and the gap between the coverlip and glass side sealed using a rubber o-ring and microscope grease. Slides were stored at 4ºC until image acquisition.

2.3.14 Confocal microscopy

A Zeiss LSM510 confocal laser-scanning microscope with an EC Plan-Neofluar 40x/1.30 Oil DIC M27 or a Plan-Apochromat 63x/1.40 Oil DIC M27, and ZEN software was used to take

images of fluorescently stained cells. Images were taken at a resolution of 1024X1024 pixels using an average of 2 frames. The range finder function in the ZEN software was used to adjust the gain and offset to avoid saturation and high background in images. Images in each experiment were acquired using the same gain and offset settings if comparison between images was required. Lasers and filters used are shown in Table 2.11.

Table 2.11 Lasers and filters used for confocal microscopy

Fluorophore	Laser	Excitation (nm)	Emission (nm)	Filter (nm)
Alexa 488	Argon	488/494	520/517	Bandpass 505-530
Alexa 546	Helium/Neon	556	573	Bandpass 560-615
Alexa 647	Helium/Neon	650	668	Longpass 650
DAPI	Diode 405-30	405	430	Bandpass 420-480

2.3.15 Analysis of confocal images

2.3.15.1 Analysis of cell morphology using Cell Profiler

The Cell Profiler image analysis software (www.cellprofiler.org) was used to analyse the morphology of FAM40A and FAM40B-depleted cells. A pipeline of individual modules was used to quantify the morphology of cells. Modules are arranged linearly with the output of one module being the input for another. Objects in images were identified by thresholding of the fluorescent signal and by setting appropriate size restrictions. The DAPI staining was initially used to identify locations of individual cells and provides a positional cue. A subsequent module used the F-actin staining to identify cell boundaries using positional cues determined earlier (DAPI staining) as an input. A separate module was then used to compute shape parameters of the identified cells. Values for cell area and eccentricity (a measure of elongation; ratio between foci distance and major axis length) were exported to Microsoft Excel and analysed.

2.3.15.2 Quantification of HUVEC stress fibres

Stress fibres were quantified by manually assigning a subjective score to each cell. Quantification was done by assigning a score to each cell based on the stress fibre content in the centre of the cell; 0 – few or no stress fibres, 1 – upto 50% of the cell centre contains

stress fibres, 2 – 50% to 75% of the cell centre contains stress fibres, 3 – greater than 75% of the cell centre contains stress fibres. Cells were visualised using a Zeiss LSM510 confocal laser-scanning microscope with an EC Plan-Neofluar 40x/1.30 Oil DIC M27 objective and epifluorescence.

2.3.15.3 Analysis of HUVEC focal adhesions using Cell Profiler

Individual cells were first identified using the process detailed in section 2.3.15.1. Vinculin staining was used to identify individual adhesions by thresholding the fluorescent signal and applying appropriate size restrictions. A subsequent module then related the identified adhesions to cells identified earlier. Focal adhesion shape parameters and numbers were then computed by a separate module. Data was exported to Microsoft Excel and analysed.

2.4 Methods: biochemistry

2.4.1 Preparation of cell lysates

Cells in tissue culture dishes were washed twice with cold PBS (+ Ca/Mg) and then lysed on ice in a suitable volume of either IP lysis buffer or RIPA buffer (75 µl per well of a 24 well plate (10 ^ 5 cells seeded the day before lysis), 150 µl per well of a 6 well plate and 800 µl per 10 cm dish). Cells were scraped into microfuge tubes and incubated on ice for 10 min. Samples were cleared by centrifugation at 17,000 g at 4ºC for 30 min and the supernatant transferred to a new microfuge tube. An appropriate volume of 4X SDS sample buffer was added to the lysates, which were then boiled and either used immediately or stored at -20ºC.

Lysis of HUVECs with Laemmli lysis buffer was also used in experiments to check for p-MLC2 (phosphorylated myosin light chain 2) levels by western blotting. Cells in 6 well dishes were lysed by adding 150 µl of lysis buffer to each well on ice. After a 5 min incubation step, cells were scraped into microfuge tubes and snap frozen in liquid nitrogen. Frozen samples were then boiled for 5 min and sonicated on ice (15 sec sonication at an amplitude of 50% (Sonics Vibra VC-130 sonicator)). Samples were cleared by centrifugation at 17,000 g at 4ºC for 30 min and the supernatant transferred to a new microfuge tube. An appropriate volume of 4X SDS sample buffer was added to the lysates which were then boiled and either used immediately or stored at -20ºC.

2.4.2 SDS-PAGE and western blotting

Prepared cell lysates were applied to NuPAGE 4-12% Bis-Tris gels and resolved using a constant voltage of 120 V in either NuPAGE MES or MOPS buffer. After gel electrophoresis, proteins were transferred onto Immobilon-P PVDF membranes (Millipore). Membranes were activated by incubation with 100% methanol for 1 min. The gel and membrane were then equilibrated in 1X transfer buffer and sandwiched between 6 layers of Whatman paper, 2 sponges and inserted into a transfer cassette. The cassette was placed in a Mini-Protean transfer system (Bio-Rad) filled with 1X transfer buffer. Electrophoretic transfer of proteins onto the membrane was achieved at a constant voltage of 100 V for 2 h at 4ºC. After electrophoresis, membranes were blocked in blocking solution (5% skimmed milk powder in TBST or 5% BSA in TBST) for 1 h at room temperature. Incubation with primary antibody was then done (in blocking solution at the appropriate dilution) at room temperature for 1 h or at 4ºC overnight. Membranes were washed 3 times with TBST for 10 min each wash and incubated with the secondary antibody. Secondary antibody (in blocking solution) was incubated at room temperature for 2 h. Unbound antibody was removed by washing 3 times with TBST and the HRP signal determined using an enhanced chemiluminescence (ECL) detection kit according to the manufacturer's instructions and X-ray film (Fujifilm). Bands on immunoblots were quantified by densitometric analysis using ImageJ software.

Stripping of western blots was achieved by washing membranes 3 times with stripping buffer for 10 min for each wash at room temperature. Membranes were subsequently washed 3 times with TBST and blocked, reprobed with primary and secondary antibody and developed according to the described western blotting protocol.

2.4.3 Immunoprecipitation

Immunoprecipitation of overexpressed protein was done using lysates prepared from COS7 cells transfected with plasmid DNA containing the gene of interest tagged with either the HA or myc epitope. 48 h after transfection, COS7 cells in 10 cm dishes were washed twice with cold PBS (+ Ca/Mg) and 800 µl of IP lysis buffer was added. Cells were scraped into microfuge tubes and incubated on ice for 10 min. Samples were cleared by centrifugation at 17,000 g at 4ºC for 30 min and the supernatant transferred to a new microfuge tube. A small

aliquot of the total cell lysate (usually 40 µl) was kept to check total protein levels by immunoblotting. Cell lysates were precleared by incubation with 40 µl of non-immune IgG agarose beads (pre-washed with IP lysis buffer) per sample for 1 h at 4ºC with rotation. Tubes were spun at 17,000 g at 4ºC for 1 min and the supernatant transferred to a new microfuge tube. Lysates were then incubated with 20 µl of anti-HA or anti-myc agarose beads as appropriate (pre-washed with IP lysis buffer) per sample for 3 h at 4ºC with rotation. Beads were washed 5 times with high salt IP lysis buffer (containing 250 mM NaCl) using low speed centrifugation steps (1,000 g for 1 min at 4ºC). After the last wash, protein was eluted from the beads by boiling with 4X SDS sample buffer. These samples were resolved together with total lysate samples by SDS-PAGE and immunoblotted for the HA and/or myc epitope, or processed further as needed.

2.4.4 Rho GTPase activity assays

To detect GTP loading of Rho GTPase proteins, a biochemical affinity method involving the selective pulldown of GTP loaded protein from whole cell lysates was used. A GST fusion of the Rho binding domain of rhotekin (RBD) was used to assess RhoA activity and a GST fusion of the p21-binding domain (PBD) of PAK1 (p21-activated kinase) was used to test Rac1 and Cdc42 activity.

2.4.4.1 Preparation of GST-RBD and GST-PBD beads

Bacteria containing pGEX-2T plasmids encoding either GST-RBD or GST-PBD were inoculated from glycerol stocks into 100 ml of LB containing 100 µg/ml ampicillin (LB-Amp). The culture was allowed to incubate overnight at 37°C with shaking and then diluted 1/20 in fresh LB-Amp. This culture was incubated at 37ºC with shaking until it reached an OD of 1.0. Protein expression was then induced by addition of 0.5 M isopropyl β-D-thiogalactopyranoside (IPTG). Cultures were now incubated at 30ºC for a further 2 h. Bacterial cells were then pelleted in 50 ml tubes by centrifugation at 1,000 g for 30 min at 4ºC. Pellets were stored at -40ºC for future use or were lysed immediately.

For lysis, the required number of bacterial cell pellets was used (e.g. 4 pellets were used for 6 conditions in each assay). Pellets containing the same GST fusion protein were

resuspended in ice cold STE buffer and homogenised by passing repeatedly through a 19G needle. Lysis of cells was initiated by adding 100 µg/ml lysozyme and incubating on ice for 30 min with gentle mixing. Dithiothreitol (DTT) at a concentration of 5 mM, 1% Tween-20 and 0.03% sodium dodecyl sulphate (SDS) was added to the cell suspension which was then mixed gently. The suspension was centrifuged at 16,000 g for 20 min at 4ºC and the supernatant transferred to a fresh tube. 40 µl of glutathione sepharose beads per condition (prewashed in STE buffer) was added to the supernatant and incubated at 4ºC for 1 h with rotation. Beads were then washed 3 times with ice cold STE buffer and finally resuspended in an equal volume (compared to bead bed volume) of STE buffer.

2.4.4.2 Pulldown assay

For assays with PC3 cells, one 10 cm dish was used per condition and for assays with HUVECs, one 6 well plate was used per condition. Cells were lysed with Rho lysis buffer (800 µl per 10 cm dish, 150 µl per well of a 6 well plate) and scraped into microfuge tubes. Lysates were centrifuged at 17,000 g at 4ºC for 30 min and the supernatant transferred to a new tube. A small aliquot of the lysate was kept to immunoblot for total Rho protein as a loading control. Lysates were then incubated with 40 µl of GST-RBD or GST-PBD beads for 1 h at 4ºC with rotation. Beads were pelleted by centrifugation at 1,000 g for 1 min and washed with ice cold Rho lysis buffer. A total of 3 washes were done and protein was eluted from the beads by boiling with 4X SDS sample buffer. These samples were resolved together with total lysate samples by SDS-PAGE and immunoblotted for the Rho protein of interest. Quantification of protein levels on western blots was done by densitometry using the software ImageJ.

2.4.5 Surface biotinylation assay

Sulfo-NHS-Biotin is a water soluble biotinylation reagent and reacts with primary amine groups. The membrane impermeable nature of this molecule makes it suitable to specifically label cell surface proteins, and so can be used to test if a protein is transmembrane. COS7 cells were transfected with pHA-FAM40A, pHA-FAM40B or pHA-14-3-3 (used as a negative control) plasmid DNA. 48 h after transfection, cells were washed twice with cold PBS (+ Ca/Mg) and incubated with 600 µg/ml sulfo-NHS-biotin in PBS (5 ml per 10 cm dish) for 20

min at 4ºC. Cells were washed twice with PBS and blocked with cell culture medium (DMEM with 10% FCS) on ice for 20 min. After a PBS wash, cells were lysed by adding 800 µl of RIPA buffer. Cells were scraped into microfuge tubes and the lysates passed through a 19G needle several times. After 10 min incubation on ice, samples were cleared by centrifugation at 17,000 g at 4ºC for 30 min and the supernatant transferred to a new microfuge tube. A small aliquot of the total cell lysate (40 µl) was kept to check total protein levels by immunoblotting. The remaining supernatant was incubated with glutathione sepharose beads (40 µl per sample, prewashed with RIPA buffer) for 1 h at 4ºC with rotation to reduce non-specific binding. Beads were pelleted by centrifugation at 17,000 g for 1 min at 4ºC and the supernatant transferred to a new microfuge tube. Strepdavidin agarose beads (20 µl per sample, prewashed with RIPA buffer) were added to the supernatants which were then incubated at 4ºC for 2 h with rotation. Beads were washed 5 times with RIPA buffer using low speed centrifugation steps (1,000 g for 1 min). After the last wash, protein was eluted from the beads by boiling with 4X SDS sample buffer. These samples were resolved together with total lysate samples by SDS-PAGE and immunoblotted for the HA epitope.

2.4.6 *In vitro* kinase assays

COS7 cells were electroporated with pHA-FAM40A, pHA-FAM40B or pmyc-CCM3 (2 dishes per condition of which one was used for 'no kinase enzyme' control samples). Electroporation with pDEST-HA or pDEST-myc was also done and lysates from these cells were used in 'kinase enzyme only controls'. 48 h after transfection, cells were lysed and overexpressed protein was immunoprecipitated (section 2.4.3 for details). Beads with immunoprecipitated protein were washed twice with IP lysis buffer, once with high salt wash buffer (0.5 M NaCl, 10 mM Tris-HCl pH 7.5) and twice with kinase assay buffer, with centrifugation at 1,000 g for 1 min between washes. After the final wash, beads were resuspended with kinase mix (20 µl kinase assay buffer, 1 µl of 1 mM ATP, 0.5 µl of [γ-^{32} P]-ATP). In addition, 0.5 µg of recombinant MST4 was added to the mix in the test and 'kinase enzyme only control' samples. Samples were incubated at 30ºC for 30 min with gentle vortexing every 10 min. 20 µl of 4X SDS sample buffer was added and the samples boiled. Samples were resolved by SDS-PAGE and the gels stained with colloidal coomassie to

verify the presence of immunoprecipitated protein (section section 2.4.8). Gels were exposed to X-ray film to detect signal corresponding to phosphorylated protein by autoradiography.

2.4.7 Purification of FAM40A and FAM40B antibodies

Rabbit anti-FAM40 and anti-FAM40B antisera were generated by immunising rabbits with peptide haptens conjugated to keyhole limpet hemocyanin (KLH) (peptide hapten used for anti-FAM40A generation: N-MEPAGGPGPLIVNC, peptide hapten used for anti-FAM40B generation: N-GTGGPPANGNGNGGC). Two individual rabbits were immunised per hapten and the final antisera had an antibody titre > 1:10,000. Antisera were produced by Genosphere Biotechnologies, Paris, France (www.genosphere-biotech.com).

50 ml of antisera was produced per rabbit and 10 ml was used to purify anti-FAM40A and anti-FAM40B antibodies by peptide affinity purification. Peptides used for immunisation were conjugated by means of their terminal cysteine residue to SulfoLink coupling resin (Pierce) to generate the final chromatography resin. This was then used as a bait to isolate anti-FAM40A and anti-FAM40B from total rabbit serum. 1 mg of the peptide was dissolved in 2 ml of coupling buffer and 1.25 mM TCEP (reducing agent) added. The mixture was incubated at room temperature for 30 min. To prepare the chromatography resin, 2 ml of SulfoLink coupling resin (1 ml bed volume) was added to chromatography spin columns. Columns were spun at 1,000 g for 1 min at room temperature to remove the storage buffer. 2 ml of coupling buffer was added and the columns spun as mentioned. This wash step was repeated 2 more times. After the last spin, 2 ml of reduced peptide solution prepared earlier was added to the column. Contents were incubated at room temperature for 15 min with gentle mixing. A further incubation at room temperature for 30 min without mixing was done. The column was washed with 4 changes of 2 ml wash solution and then with 2 changes of coupling buffer. Non-specific binding sites on the resin were blocked by adding 50 mM cysteine in 2 ml of coupling buffer to the column. Contents were incubated at room temperature for 15 min with gentle mixing. A further incubation at room temperature for 30 min without mixing was done. Columns were spun to remove the cysteine solution and

washed 3 times with binding buffer. Columns were stored at 4ºC with addition of 0.05% sodium azide or used immediately.

10 ml of rabbit antiserum was cleared of any particulate matter by centrifugation at 3,000 g at 4ºC for 30 min and the supernatant diluted with 10 ml of binding buffer. The serum was then batch-bound with the prepared chromatography resin in 50 ml tubes at 4ºC overnight. The serum with the resin was then added to the chromatography column and allowed to drain out while the resin was retained in the column. Steps were carried out at 4ºC. The resin in the column was washed a minimum of 5 times with 2 ml of binding buffer. Protein was eluted with 2 ml of elution buffer into tubes containing 100 µl of neutralisation buffer. The elution step was repeated 4 more times (total volume of ~ 10 ml eluted antibody). Eluted antibody was dialysed into binding buffer using a 12,000 – 14,000 cut-off membrane at 4ºC overnight. The purified antibody was concentrated by ammonium sulphate precipitation. 10 ml of saturated ammonium sulphate was added slowly to the 10 ml of antibody solution and the mixture (50% saturation ammonium sulphate) incubated with stirring overnight at 4ºC. Centrifugation at 3,000 g at 4ºC for 30 min was done and the pellet resuspended in 1,000 µl (anti-FAM40A purification) or 500 µl (anti-FAM40B purification) of binding buffer. Dialysis with binding buffer was done overnight as described earlier. Purified antibody solution was resolved by SDS-PAGE along with a BSA protein standard to determine its purity and concentration. The antibody solution was aliquoted and stored at -20ºC.

2.4.8 ProQ staining

COS7 cells were transfected with pHA-FAM40A or pHA-FAM40B plasmid DNA. 48 h after transfection, cells were lysed and total protein resolved by polyacrylamide gel electrophoresis. Proteins in gels were transferred onto Immobilon-FL PVDF membranes (low fluorescence PVDF membrane, Immobilon) as described in section 2.4.2. After electroblotting, membranes were allowed to dry completely, following which they were pre-wet with methanol. Proteins on membranes were fixed by incubation with fix solution for 10 min. Membranes were washed 4 times with distilled water (5 min each wash) following which they were stained using the ProQ phosphoprotein blot stain for 15 min. Membranes were washed in destain solution 3 times (5 min each wash) and after the final wash, allowed to

dry completely. Phosphoproteins on stained blots were visualised by imaging with a UV transilluminator.

2.4.9 Colloidal coomassie staining of gels

After electrophoresis, proteins gels were fixed for 30 minutes in 7% acetic acid, 40% methanol. The colloidal coomassie blue concentrate (Sigma-Aldrich) was diluted 1:5 in deionised water and immediately before staining 4 parts of this solution was combined with 1 part methanol to prepare the working staining solution. Gels were stained overnight at room temperature. Gels were destained for 5 min with 25% methanol, 7% acetic acid and then with 25% methanol, 2% acetic acid until bands appeared in good contrast against the background.

2.5 Methods: statistical analysis

Statistical analysis was carried out using data from 3 or more independent experiments. An unpaired, two-tailed Student's t-test was used as a test of statistical significance and was performed either using Microsoft Excel or GraphPad Prism (www.graphpad.com). A parametric t-test was employed if the data were normally distributed, and a non-parametric t-test was used if the data were not normally distributed.

3 The FAM40 proteins – insights from biochemical and bioinformatics analysis

3.1 Introduction

There are only two reports in the literature that address the biochemical and functional characterisation of human FAM40A and FAM40B (Bai et al., 2011; Goudreault et al., 2009). To understand better the physiological roles of the FAM40 proteins, it is important to understand their biochemical features. This will serve to put their functions in perspective and aid in generating hypotheses as to how they may fulfil these functions. For example, interacting partners and protein modifications such as phosphorylation may be important determinants in cell signalling. This chapter aims to describe the biochemical properties of the human FAM40 proteins. Antibodies targeting the human FAM40 proteins were generated and purified, but they were unable to detect endogenous protein. Hence, the majority of the analysis presented is based on overexpressed proteins tagged with an epitope tag. Furthermore, data available on public databases and computational resources have been used to study the FAM40 proteins. These include data from proteomic analyses.

3.2 Results

3.2.1 The FAM40 proteins interact with members of the STRIPAK complex

The STRIPAK complex was identified by an affinity chromatography/mass spectrometry analysis to generate an interaction network around the catalytic subunit of PP2A (Goudreault et al., 2009). The FAM40 proteins are members of this complex and hence other STRIPAK complex members could be important as FAM40 signalling partners. Co-immunoprecipitation experiments were therefore carried out to determine if FAM40A or FAM40B interact with other members of the STRIPAK complex. Specifically, their interaction with CCM3 and the GCKIII family kinases (STK24, STK25 and MST4) was tested. Using affinity chromatography/mass spectrometry, the interaction of FAM40A with CCM3, STK24, STK25 and MST4 has been previously reported (Goudreault et al., 2009). Hence, this experiment serves to validate these results as well as to test if FAM40B behaves similarly.

As antibodies that recognise endogenous FAM40 proteins were not available, overexpressed proteins tagged with epitope tags were used in these experiments. FAM40A and FAM40B were tagged with HA at the N-terminus while CCM3, STK24, STK25 and MST4 were tagged with myc at the N-terminus. Multiple transcripts exist for both FAM40A and FAM40B (NCBI Protein database, http://www.ncbi.nlm.nih.gov/protein), and the longest isoforms were used in all experiments. COS7 cells were co-transfected with HA-FAM40A or HA-FAM40B and myc-STK24, myc-STK25, myc-MST4 or myc-CCM3. Immunoprecipitation with anti-HA revealed that both FAM40A and FAM40B are capable of interacting with CCM3, STK25 and MST4 (Figure 3.1). No interaction with STK24 was detected with either FAM40A or FAM40B. This could be because only a low level of STK24 expression was achieved. Furthermore, exogenously expressed STK25 and MST4 appeared to be susceptible to degradation indicated by the number of lower molecular weight bands. These results provide a first indication of potential signalling partners for FAM40A and FAM40B.

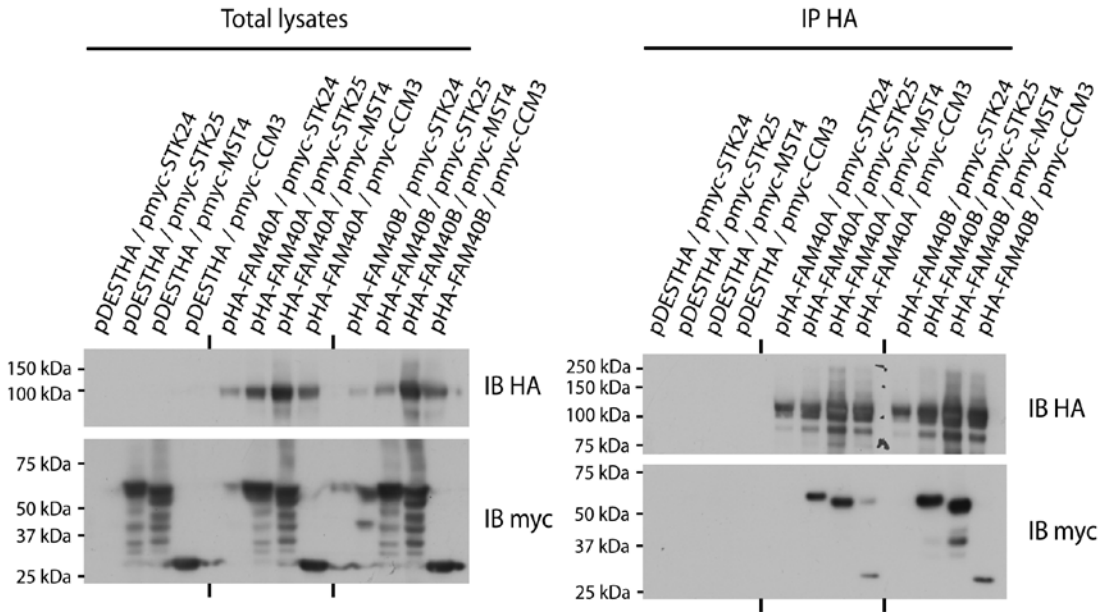

Figure 3.1 FAM40A and FAM40B interact with CCM3 and the GCKIII family kinases, STK25 and MST4

COS7 cells were co-transfected with pDESTHA (empty vector) or pHA-FAM40A or pHA-FAM40B and pmyc-STK24 or pmyc-STK25 or pmyc-MST4 or pmyc-CCM3. After 48 h, cells were lysed and cell lysates were incubated with anti-HA epitope agarose beads. Proteins interacting with the FAM40 proteins were visualized by immunoblotting with an antibody to the myc epitope. Immunoblots are representative of results from 3 independent experiments.

3.2.2 The FAM40 proteins form homodimers and interact with each other

Immunoprecipitation of overexpressed FAM40A and FAM40B revealed a higher molecular weight band (indicated by asterisks in Figure 3.2A and B) in addition to the band that corresponds to full length FAM40A and FAM40B (indicated by arrows in Figure 3.2A and B). This higher molecular weight band had a size approximately twice that of full length protein. Hence, it was hypothesised that this band corresponds to a dimeric form of FAM40A and FAM40B. To validate this, co-immunoprecipitation experiments were carried out with overexpressed FAM40A and FAM40B differentially tagged with the HA and myc epitope. Myc-FAM40A and myc-FAM40B co-immunoprecipitated with HA-FAM40A and HA-FAM40B (Figure 3.2B). These results indicate that both FAM40A and FAM40B form homodimers as well as interact with each other. The fact that the 'dimer band' appeared even under denaturing conditions indicates a strong interaction. Homodimerisation and heterodimerisation can occur simultaneously indicated by the presence of 'dimer bands' in the 'IP lanes' too (Figure 3.2B). Moreover, higher molecular weight bands or smears in addition to the dimer band were observed. These bands could be suggestive of post-translational modifications of the FAM40 proteins.

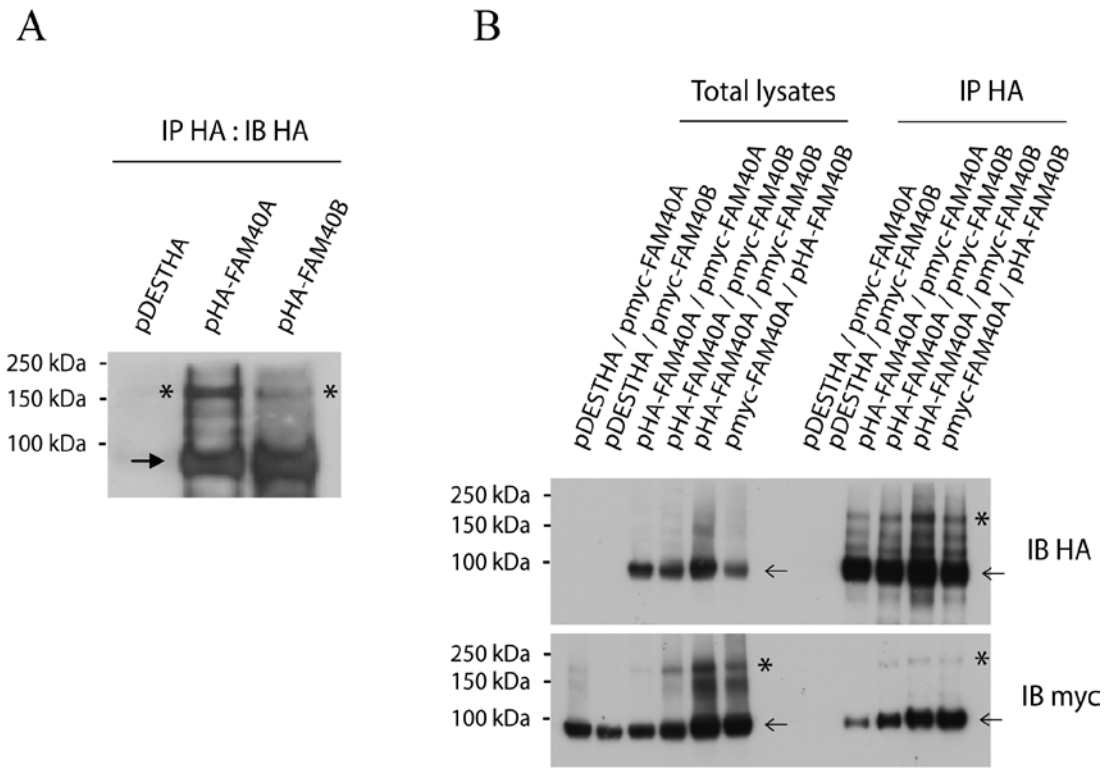

Figure 3.2 FAM40A and FAM40B form homo- and hetero- dimers
(A) COS7 cells were transfected with pDESTHA (empty vector), pHA-FAM40A or pHA-FAM40B. After 48 h cells were lysed and incubated with anti-HA epitope agarose beads. Panel **(B)** shows the results of a co-immunoprecipitation experiment in which COS7 cells were co-transfected with pDESTHA or pHA-FAM40A or pHA-FAM40B and pmyc-FAM40A or pmyc-FAM40B. After 48 h cells were lysed and incubated with anti-HA epitope agarose beads. Dimerising partners were detected by immunoblotting with an antibody to the myc epitope. Monomeric protein is indicated by arrows and the dimeric form is indicated by asterisks. Immunoblots in **(A)** and **(B)** are representative of 3 independent experiments.

3.2.3 The FAM40 proteins are putative transmembrane proteins

Several lines of evidence prompted an investigation into whether the FAM40 proteins could have transmembrane domains. The cellular localisation of proteins has implications for their function and hence is important to determine. Previous studies have predicted that both Far11 (the *S. cerevisae* FAM40 homologue) (Kemp and Sprague, 2003) and Ham2 (the *Neurospora crassa* FAM40 homologue) (Xiang et al., 2002) are putative transmembrane proteins using bioinformatic analysis. In addition, the N-terminal N1221 domain of the human FAM40 proteins is similar to a hypothetical protein product of a yeast ORF which is also predicted to contain several transmembrane regions (conserved domains database, NCBI). Hence, the sequences of both human FAM40A and FAM40B were checked for the presence of transmembrane protein features using publically available prediction software.

The signal peptide is a protein sorting signal that targets proteins for insertion into the endoplasmic reticulum (ER) and subsequent translocation to the plasma membrane. No signal peptide was detected for either FAM40A or FAM40B, as determined by SignalP (http://www.cbs.dtu.dk/services/SignalP/) and MEMSAT-SVM (http://bioinf.cs.ucl.ac.uk/). However, FAM40A was predicted to enter the non-classical secretory pathway or secretion without a signal peptide using SecretomeP (http://www.cbs.dtu.dk/services/SecretomeP/) (Figure 3.3A). In addition, both FAM40A and FAM40B were predicted to contain transmembrane segments by TopPred (http://mobyle.pasteur.fr/), MEMSAT3 (http://bioinf.cs.ucl.ac.uk/), TMPred (http://www.ch.embnet.org/software/TMPRED_form.html), and MEMSAT-SVM (http://bioinf.cs.ucl.ac.uk/). The MEMSAT-SVM program differs in that it attempts to predict both signal peptides and transmembrane topology. A cartoon generated by MEMSAT-SVM is shown in Figure 3.3B and C as an example. These programs were not used to generate a conclusive prediction of FAM40 localisation and topology, but to provide an initial indication to prompt further analysis.

To further investigate the possible transmembrane nature of FAM40A and FAM40B, a cell surface biotinylation assay was used. Briefly, HA-FAM40A and HA-FAM40B were overexpressed in COS7 cells following which all cell surface proteins were labelled using a

membrane-impermeable biotinylation reagent. Labelled proteins were isolated by streptavidin pulldown and probed for the presence of FAM40A and FAM40B. FAM40A and FAM40B were present in the streptavidin pulldown samples (Figure 3.3D), suggesting that certain regions of these proteins are exposed to the cell exterior. 14-3-3 is a cytoplasmic protein (Aitken, 2006) and HA-14-3-3 was used as a negative control. Conversely, HA-TrkA was used as a positive control (TrkA is a neurotrophin receptor (Yoon et al., 1998)). The negative control (HA-14-3-3) was detected in the streptavidin pulldown sample in the experiment shown in Figure 3.3D, and although the intensity of the negative control band was less than that of biotin-labelled HA-FAM40A and HA-FAM40B, and the expression levels of total HA-FAM40A, HA-FAM40B and HA-14-3-3 were similar, this suggests the method might not be working as anticipated. However, HA-TrkA could not be consistently isolated by streptavidin pulldown. Further experiments with this construct need to be performed to determine if HA-TrkA is expressed at the cell surface. Taken together, these results indicate there is a possibility of the FAM40 proteins being transmembrane.

FACS analysis was also performed to determine whether FAM40A or FAM40B were expressed at the cell surface. COS7 cells were transfected with HA-FAM40A or HA-FAM40B, and HA-TrkA expressing cells were used as positive controls. An example FACS plot is shown in (Figure 3.4). HA-TrkA was detected, but FAM40A and FAM40B were not detected on the cell surface. Hence, this technique did not result in the reproducible detection of surface FAM40A and FAM40B which conflicts with results obtained with the bioinformatic (Figure 3.3A, B and C) and biochemical (Figure 3.3D) analysis.

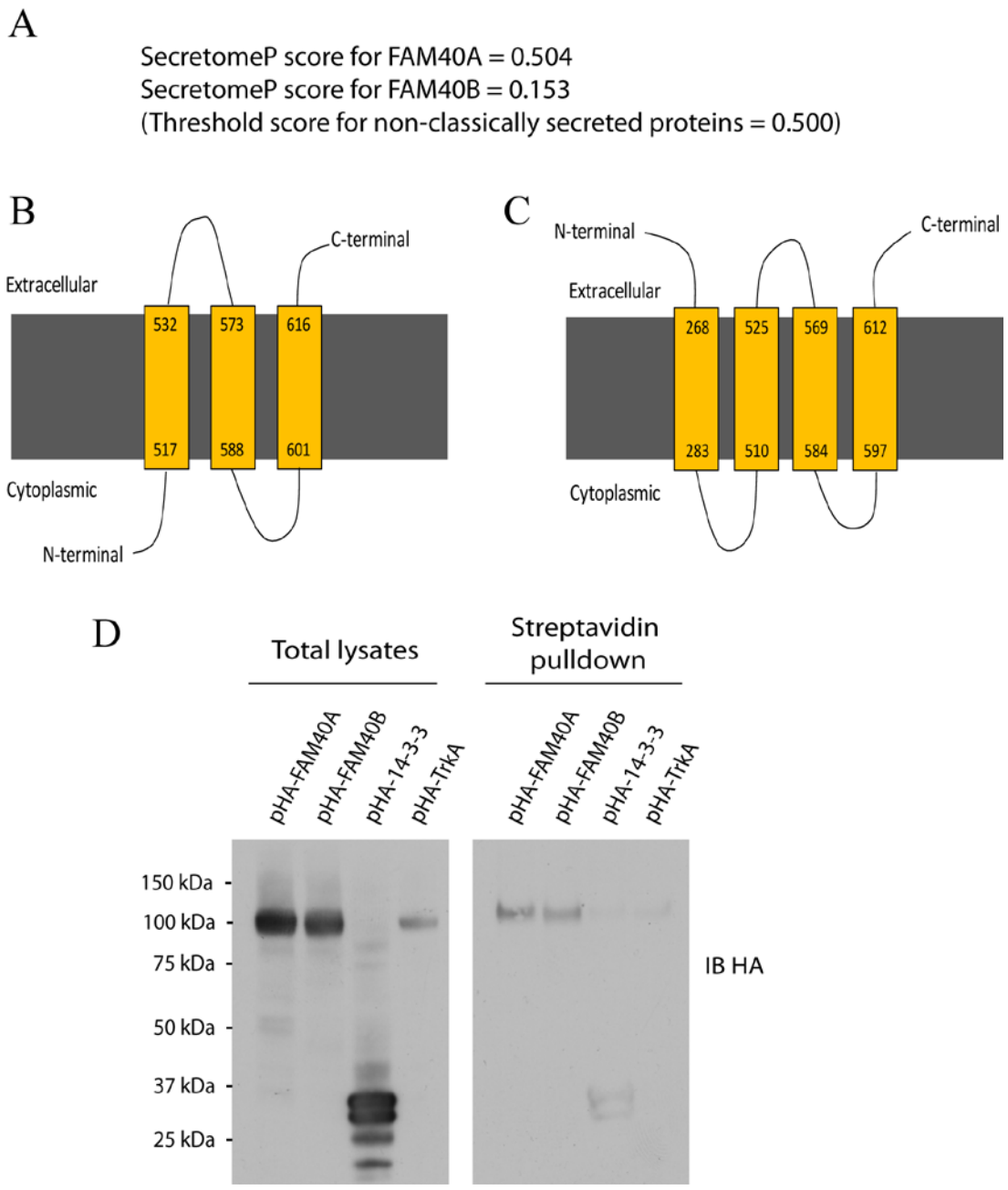

Figure 3.3 FAM40A and FAM40B are putative transmembrane proteins
(A) SecretomeP predictions for FAM40A and FAM40B are shown. MEMSAT-SVM predictions for **(B)** FAM40A and **(C)** FAM40B are shown. **(D)** COS7 cells were transfected with pHA-FAM40A, pHA-FAM40B, pHA-14-3-3 (used as a negative control) or pHA-TrkA (used as a positive control). After 48 h cells were lysed and cell surface proteins labelled with biotin. Cell lysates were subsequently incubated with streptavidin agarose beads. Overexpressed protein was detected by immunoblotting with an antibody against the HA epitope. The immunoblot shown is representative of 3 independent experiments (except for pHA-TrkA, for which an example immunoblot is shown).

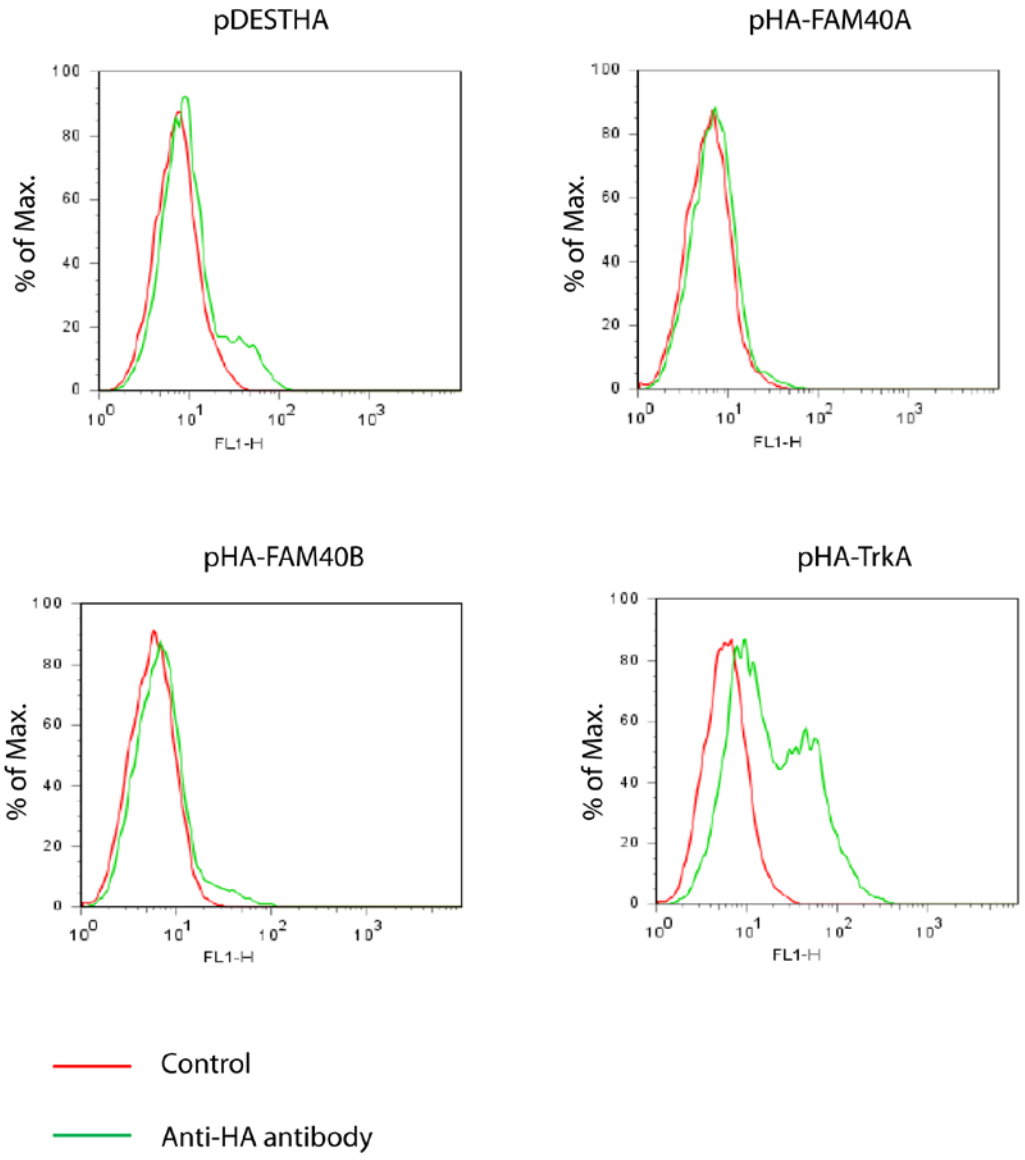

Figure 3.4 FACS does not detect surface FAM40A and FAM40B
COS7 cells were transfected with pDESTHA (empty vector), pHA-FAM40A, pHA-FAM40B or pHA-TrkA (a neurotrophin receptor used as a positive control). After either 24 h or 48 h, cells were harvested non-enzymatically and stained with anti-HA antibody followed by Alexa-488 conjugated secondary antibody. Control samples were stained only with the secondary antibody. Samples were analyzed using a FACSCalibur machine and Cell Quest Pro software (BD Biosciences) and plots generated with Flow Jo software. An example plot is shown (n=5).

3.2.4 Localisation of FAM40A and FAM40B

The cellular localisations of FAM40A and FAM40B were determined by immunofluorescence and confocal microscopy. PC3 cells were transfected with pHA-FAM40A or pHA-FAM40B, and stained for the HA epitope and F-actin. PC3 cells grow as individual cells and exhibit F-actin-rich protrusions at the cell edge (Vega et al., 2011). Both FAM40A and FAM40B showed diffuse localisation in the cytoplasm and were enriched in F-actin-rich protrusions (Figure 3.5). This is suggestive of the FAM40 proteins being proximal to the plasma membrane. However, as cell protrusions can be thicker than adjacent regions of the cell (Abercrombie et al., 1971), it is possible that this contributes to the apparent enrichment of FAM40A and FAM40B in these areas.

In addition, staining for the HA epitope was performed using unpermeabilised cells to determine if the HA tag was present at the cell exterior. Epitope tagging and subsequent assessment of epitope accessibility by immunofluorescence can be used to determine transmembrane protein topology (Covitz et al., 1998). The cells were not permeabilised with detergent to prevent staining of internal HA epitope. Strong foci of staining were observed at F-actin-rich protrusions (Figure 3.6). Negligible staining was observed in the rest of the cell. As the HA tag is present at the N-terminus of FAM40A and FAM40B, these results suggest that the N-terminus of FAM40A and FAM40B is exposed to the cell exterior, and lend support to the hypothesis that these proteins are transmembrane.

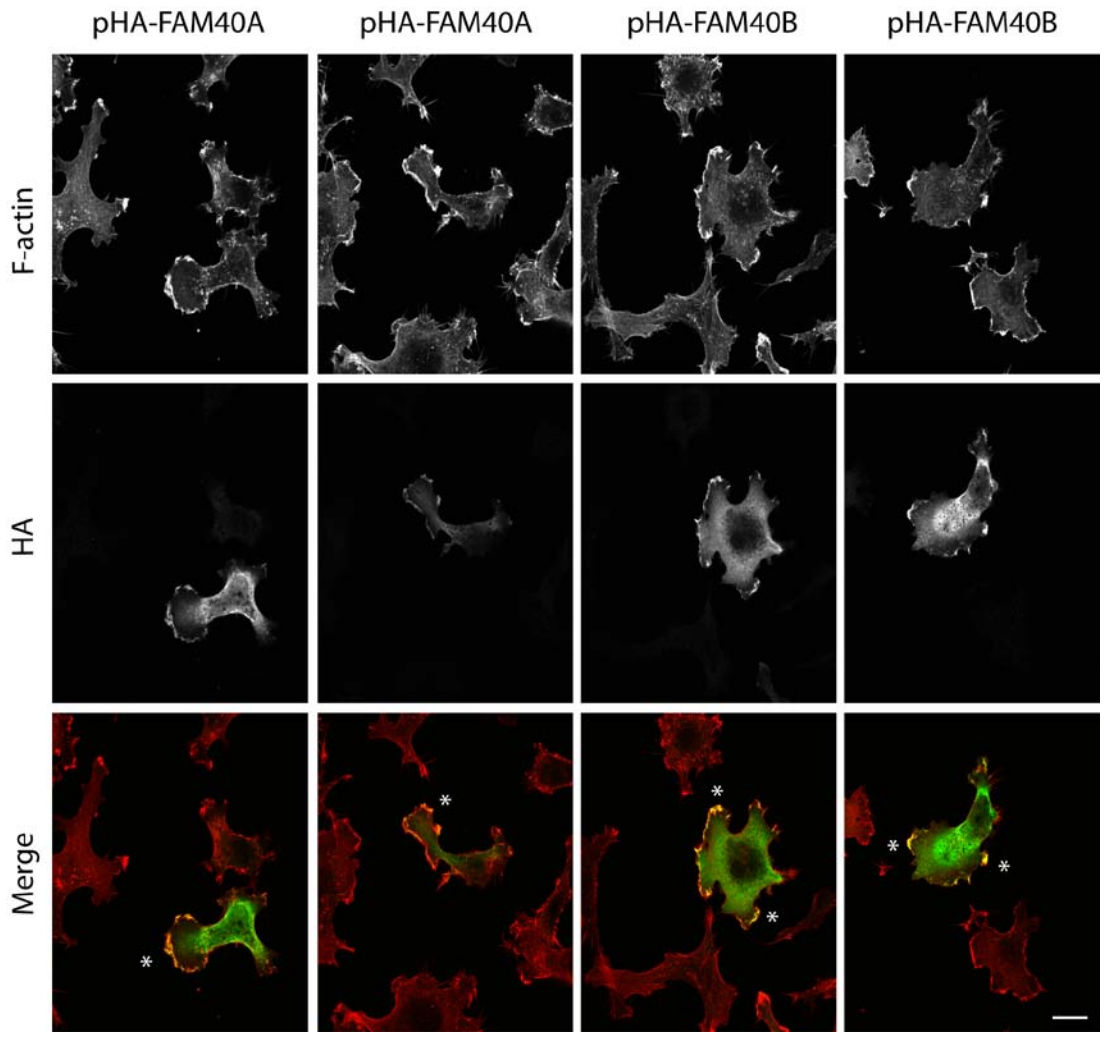

Figure 3.5 Staining for overexpressed FAM40A and FAM40B in permeabilised PC3 cells

PC3 cells on glass coverslips were transfected with pHA-FAM40A or pHA-FAM40B and fixed after 24 h. Cells were stained for F-actin and the HA epitope. Asterisks indicate areas where the HA staining is localised to F-actin-rich protrusions. Scale bar = 20 µm. Images are representative of 3 independent experiments.

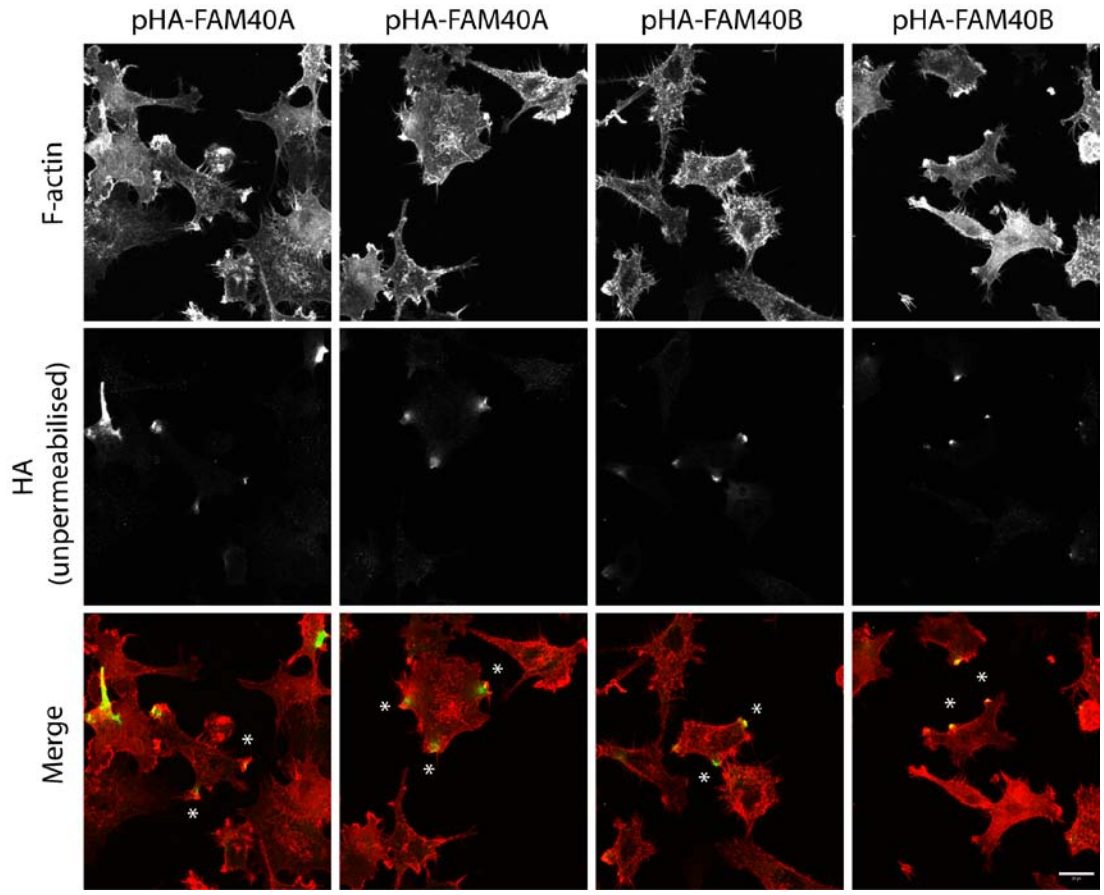

Figure 3.6 Staining for overexpressed FAM40A and FAM40B in unpermeabilised PC3 cells

PC3 cells on glass coverslips were transfected with pHA-FAM40A or pHA-FAM40B and fixed after 24 h. Cells were stained for F-actin and the HA epitope without permeabilisation with Triton. Asterisks indicate areas where the HA staining is localised to F-actin-rich protrusions. Scale bar = 20 µm. Images are representative of 2 independent experiments.

Overall, the results on FAM40A and FAM40B localisation suggest that a portion of total FAM40 protein could be transmembrane.

3.2.5 The FAM40 proteins do not function as cell-cell adhesion proteins

FAM40A and FAM40B form homo- and hetero- dimers and are possible transmembrane proteins. Hence, it was tested if they are capable of trans-dimerisation or of facilitating cell-cell adhesions. Their capacity to form interactions between two adjacent cells is of further interest as they interact with the CCM3 protein (section 3.2.1). CCM3 has been implicated in the pathogenesis of CCM and is known to be important for maintaining endothelial junction integrity (Zheng et al., 2010). The functions of FAM40A and FAM40B in endothelial cells are presented in chapter 5. To determine if the FAM40 proteins can act as cell-cell adhesion proteins, CHO (chinese hamster ovary) cell aggregation assays were carried out. CHO cells stably expressing HA-FAM40A or HA-FAM40B were tested for their capacity to aggregate. Control cells did not clump together and grew as single cells. The presence of a cell adhesion molecule can be detected by the induction of CHO cell clumping (Katsamba et al., 2009). Furthermore, CHO cells can be maintained as suspension cultures making them ideal for this assay. CHO cells were transfected with pHA-FAM40A, pHA-FAM40B or EGFP-E-cadherin (used as a positive control). Cells stably expressing these proteins were selected and validated using immunofluorescence staining and western blotting (Figure 3.7). Both FAM40A and FAM40B exhibited diffuse localisation with enrichment at the cell cortex. Conversely, E-cadherin localised to regions corresponding to cell-cell contacts (Figure 3.7A).

Aggregation assays were carried out with control cells and cells stably expressing HA-FAM40A, HA-FAM40B and EGFP-E-cadherin to determine if these proteins are capable of trans homo-dimerisation. A sample containing a 1:1 mix of HA-FAM40A:HA-FAM40B expressing cells was also included to detect trans hetero-dimerisation. As shown in Figure 3.8, only cells expressing EGFP-E-cadherin aggregated. Hence, neither FAM40A nor FAM40B are capable of acting as cell-cell adhesion proteins. However, this result does not preclude them from being transmembrane proteins.

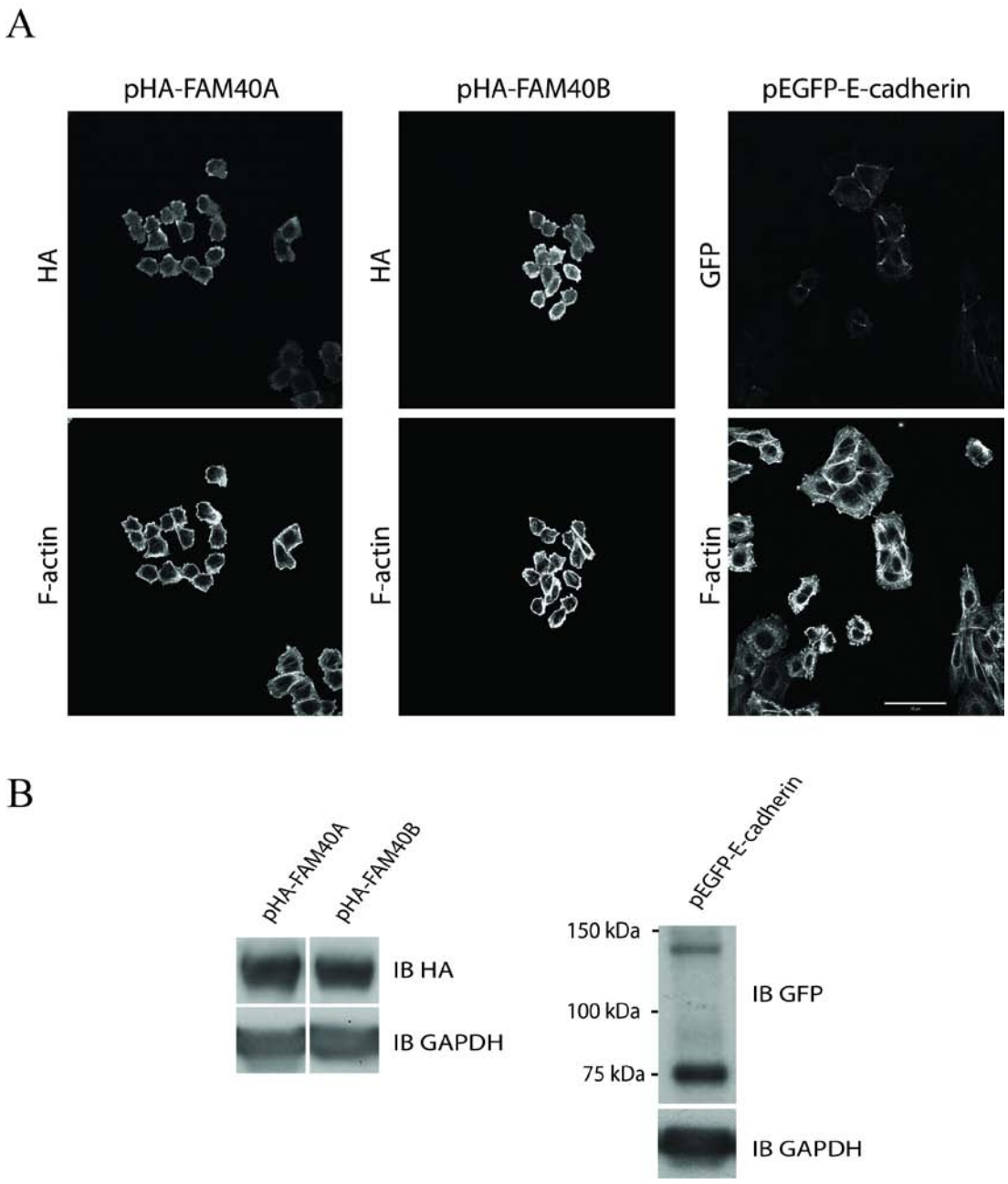

Figure 3.7 Validation of stable CHO cells expressing HA-FAM40A, HA-FAM40B and EGFP-E-cadherin

CHO cells stably expressing HA-FAM40, HA-FAM40B or EGFP-E-cadherin were generated for use in a CHO cell aggregation assay. **(A)** Expression of HA-FAM40A and HA-FAM40B was confirmed by immunofluorescence staining with an antibody against the HA epitope. Expression of EGFP-E-cadherin was confirmed by similarly detecting GFP fluorescence. Scale bar = 50 µm. **(B)** Cell lysates from HA-FAM40A/HA-FAM40B and EGFP-E-cadherin expressing cells were immunoblotted with anti-HA and anti-GFP antibodies respectively to confirm expression of the indicated proteins.

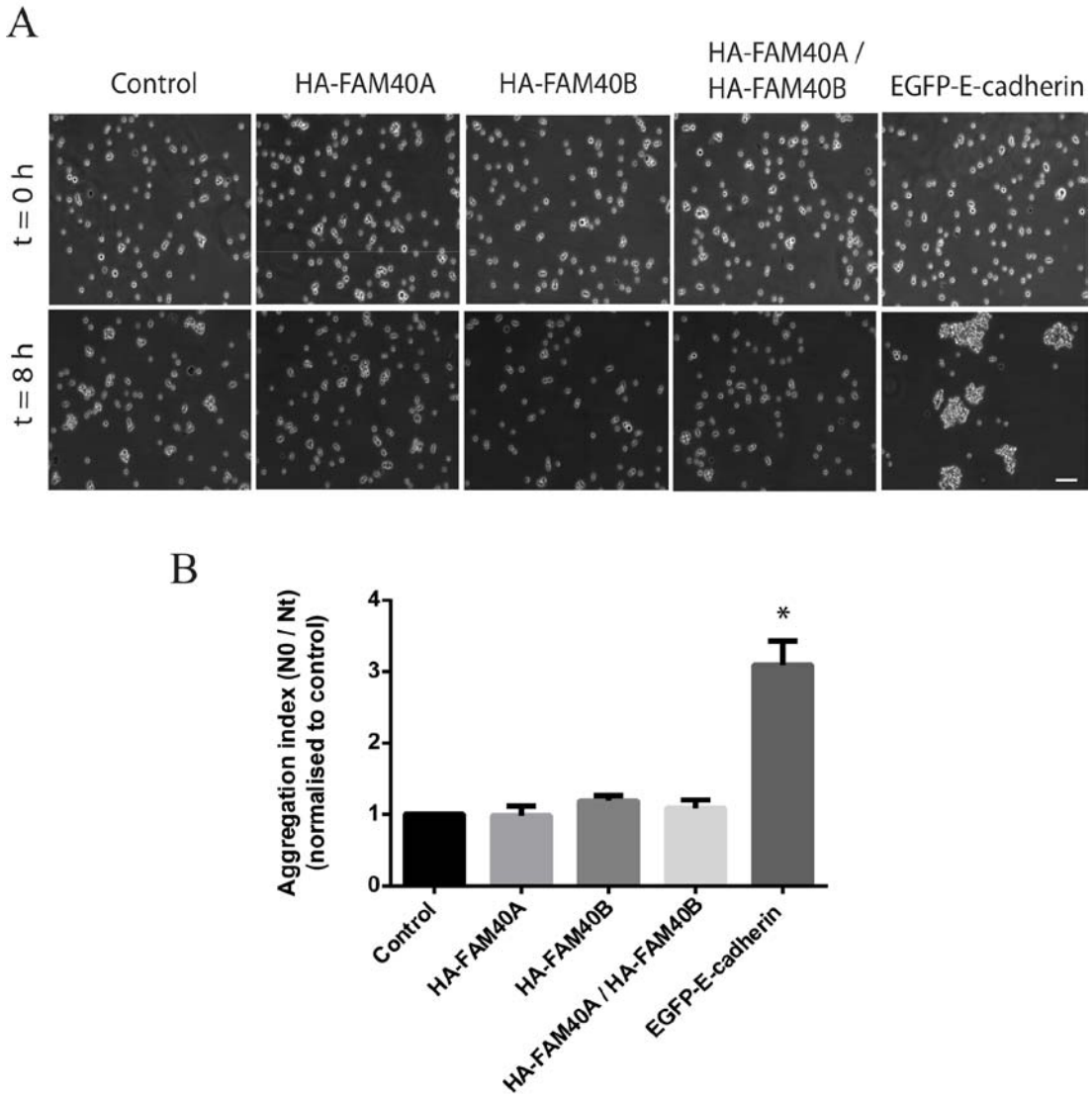

Figure 3.8 The FAM40 proteins do not form cell-cell adhesions as determined by a CHO cell aggregation assay

CHO cells stably expressing HA-FAM40, HA-FAM40B, EGFP-E-cadherin (used as a positive control) and control CHO cells were tested for cell aggregation (8 h aggregation at 37^0C). A sample consisting of a 1:1 mix of cells expressing HA-FAM40A and HA-FAM40B was included to test for trans hetero-dimerisation. Images in **(A)** are representative of 3 independent experiments. Scale bar = 50 µm. Data shown in **(B)** quantify aggregation by a measure of N0 (number of 'particles' at time=0 h) divided by N8 (number of particles at time=8 h), and are the mean of 3 independent experiments ± SEM. Data are presented normalised to control (control = 1). * $p < 0.05$ compared to control and determined by Student's t-test.

3.2.6 The FAM40 proteins are ubiquitinated

Protein modification by ubiquitination is an important determinant in protein degradation and cell signalling. In addition to ubiquitination resulting in the targeting of proteins to degradation either via the proteasome or lysosomes, it plays a central role in other signalling cascades including those implicated in cytoskeletal dynamics, cell adhesion and migration (Schaefer et al., 2012). The presence of higher molecular weight bands in western blots for overexpressed FAM40A and FAM40B, suggest post-translational modifications. Moreover, published proteomic analysis reveals that FAM40A is ubiquitinated on Lysines 742 and 828 while FAM40B is ubiquitinated on Lysine 738 (obtained from PhosphoSitePlus (Hornbeck et al., 2012)). Co-immunoprecipitation assays were carried out with lysates from COS7 cells co-transfected with pHA-ubiquitin and pmyc-FAM40A or pmyc-FAM40B. The 'IB HA' lanes show overexpressed ubiquitin protein (Figure 3.9). Ubiquitin is capable of multimerisation which explains the presence of a smear in these lanes. Both FAM40A and FAM40B were co-immunoprecipitated along with ubiquitin indicating that they are capable of undergoing ubiquitination. Non-ubiquitinated FAM40A and FAM40B are indicated by the asterisk in Figure 3.9. Higher molecular weight bands in the 'IP HA:IB myc' lanes correspond to ubiquitinated FAM40A and FAM40B. Multiple higher molecular weight bands were detected which imply poly-ubiquitination and/or ubiquitination at multiple sites.

It will be additionally important to show that HA-ubiquitin co-immunoprecipitates with myc-FAM40A and myc-FAM40B.

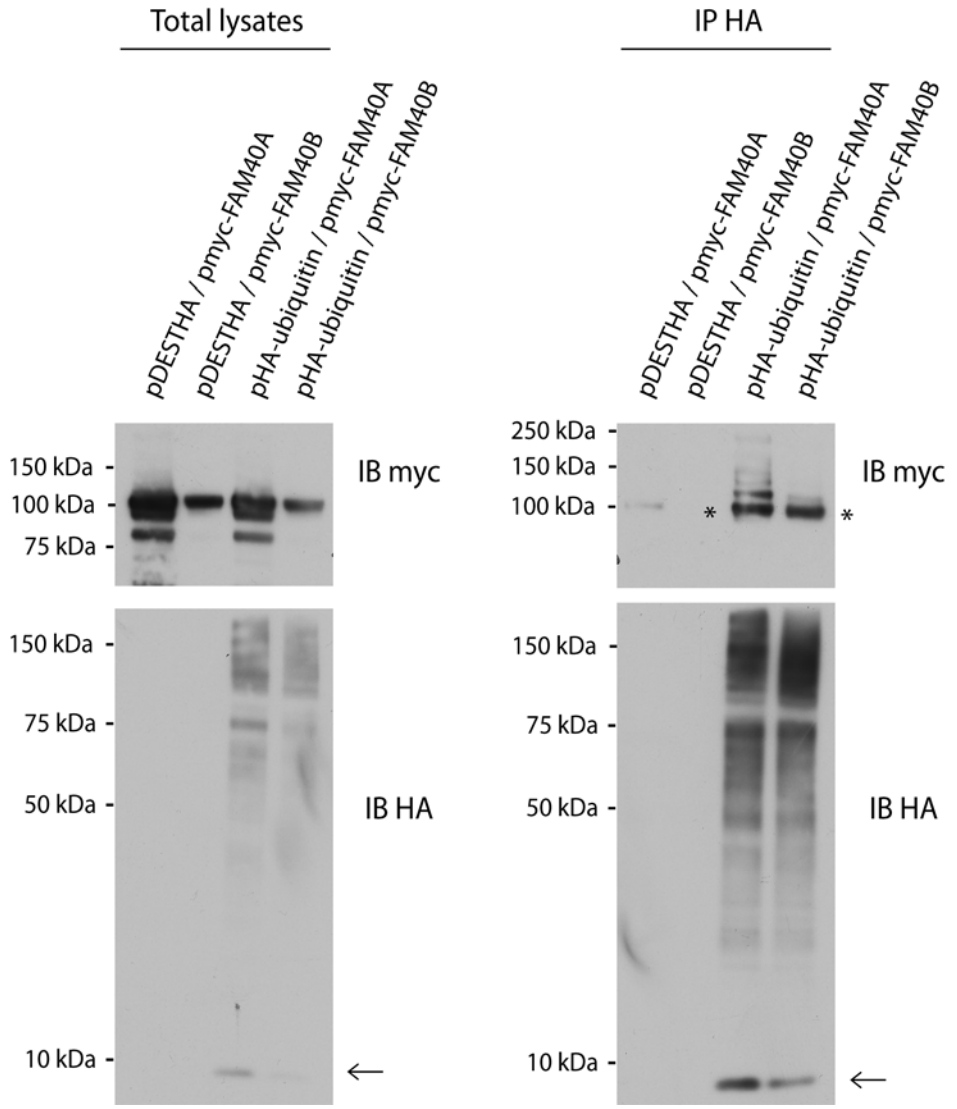

Figure 3.9 FAM40A and FAM40B are ubiquitinated
COS7 cells were co-transfected with pDESTHA (empty vector) or pHA-ubiquitin and pmyc-FAM40A or pmyc-FAM40B. After 48 h cells were lysed and incubated with anti-HA agarose beads. Myc-FAM40A and myc-FAM40B were detected by immunoblotting with an anti-myc antibody. The asterisks indicates signal corresponding to non-ubiquitinated FAM40 protein, while the arrows in the anti-HA blots indicate signal corresponding to monomeric ubiquitin. Immunoblots are representative of 3 independent experiments.

3.2.7 The FAM40 proteins are phosphorylated

Protein phosphorylation is another post-translational modification that can regulate protein function. Phosphorylated amino acids serve to diversify the topology and binding properties of protein surfaces. By doing so, phosphorylation acts as a signalling switch, allowing inducible protein binding and so is a fundamental concept in signal transduction and protein function (Hunter, 2012). The FAM40 proteins reside in a complex that also contains a phosphatase and multiple kinases (Goudreault et al., 2009), and as a consequence phosphorylation may be a mechanism by which FAM40 function is regulated.

Phosphoproteins resolved by gel electrophoresis can be detected by the ProQ staining procedure (Invitrogen) (Schulenberg et al., 2004). Lysates from COS7 cells overexpressing HA-FAM40A or HA-FAM40B were immunoprecipitated with anti-HA epitope agarose beads, and ProQ staining of these samples revealed that both FAM40A and FAM40B are phosphoproteins (Figure 3.10). Proteomic analysis to identify phosphorylated residues on FAM40A and FAM40B was not carried out. However, multiple proteomic studies have been published that document phospho-peptides from which likely phospho-sites may be inferred. FAM40A phospho-sites (Figure 3.11) and FAM40B phospho-sites (Figure 3.12) were compiled from PhosphoSitePlus (Hornbeck et al., 2012). The number of individual experiments which report a particular site, as well as the extent of its evolutionary conservation, indicate the likelihood of it being biologically relevant.

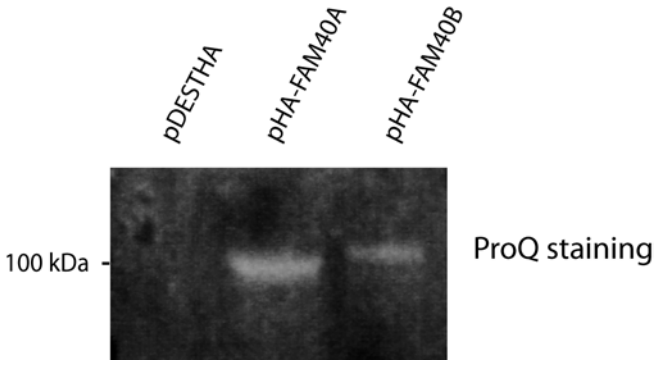

Figure 3.10 FAM40A and FAM40B are phosphorylated as determined by ProQ staining
COS7 cells were transfected with pDESTHA (empty vector), pHA-FAM40A or pHA-FAM40B. After 48 h cells were lysed and cell lysates were incubated with anti-HA agarose beads. ProQ (Invitrogen) staining was done to detect phosphorylated protein. Results are representative of 3 independent experiments.

Protein Acc.	Gene	Organism
NP_149079.2	FAM40A	H.sapiens
XP_524802.3	FAM40A	P.troglodytes
XP_547238.3	FAM40A	C.lupus
NP_705791.2	Fam40a	M.musculus
NP_998686.1	fam40a	D.rerio
AAF477601.1	CG11526	D.melanogaster
NP_014272.3	Far11	S. cerevisae

Figure 3.11 Phospho-sites on FAM40A detected by proteomic analysis
Example phospho-sites on human FAM40A (sequence in bold) detected by proteomic analysis experiments are highlighted in red. These experiments (number of experiments indicated in brackets) have been compiled in PhosphoSitePlus, an online resource for protein modification (www.phosphosite.org). Multiple sequence alignments (generated by MUSCLE (Edgar, 2004)) of homologous sequences indicate the level of evolutionary conservation.

Protein Acc.	Gene	Organism
NP_065755.1	FAM40B	H.sapiens
XP_519374.3	FAM40B	P.troglodytes
XP_849003.1	FAM40B	C.lupus
NP_796178.2	Fam40B	M.musculus
XP_684274.5	LOC556392	D.rerio
AAF47760.1	CG11526	D.melanogaster
NP_014272.3	Far11	S. cerevisae

Figure 3.12 Phospho-sites on FAM40B detected by proteomic analysis
Example phospho-sites on human FAM40B (sequence in bold) detected by proteomic analysis experiments are highlighted in red. These experiments (number of experiments indicated in brackets) have been compiled in PhosphoSitePlus, an online resource for protein modification (www.phosphosite.org). Multiple sequence alignments (generated by MUSCLE (Edgar, 2004)) of homologous sequences indicate the level of evolutionary conservation.

3.2.8 The GCKIII kinase MST4 phosphorylates FAM40A, FAM40B and CCM3

The GCKIII kinase MST4 is a member of the STRIPAK complex and interacts with both FAM40A and FAM40B (section 3.2.1), and with CCM3 (Ceccarelli et al., 2011; Ma et al., 2007). While the GCKIII kinases are downstream mediators of CCM3 function (Ma et al., 2007; Zheng et al., 2010), STK25 (a GCKIII family kinase) has been shown to phosphorylate CCM3 (Voss et al., 2007). Hence, it is possible that CCM3, FAM40A and FAM40B are MST4 substrates. Additionally, determining this would provide a mechanism by which observations in section 3.2.7 could be explained and could have implications for FAM40 cell signalling.

In vitro kinase assays with recombinant MST4 enzyme were carried out using immunoprecipitated HA-FAM40A, HA-FAM40B and myc-CCM3. Recombinant MST4 was found to be able to phosphorylate FAM40A, FAM40B and CCM3 (Figure 3.13). A signal was detected for FAM40B and CCM3 even in the absence of MST4, probably due to association with endogenous kinases. The level of auto-phosphorylated MST4 was reduced in the presence of the substrates FAM40A, FAM40B and CCM3. This could be because of competition with its substrates (FAM40A, FAM40B and CCM3). In summary, these results show that MST4 interacts directly with FAM40A, FAM40B and CCM3 which are also its substrates.

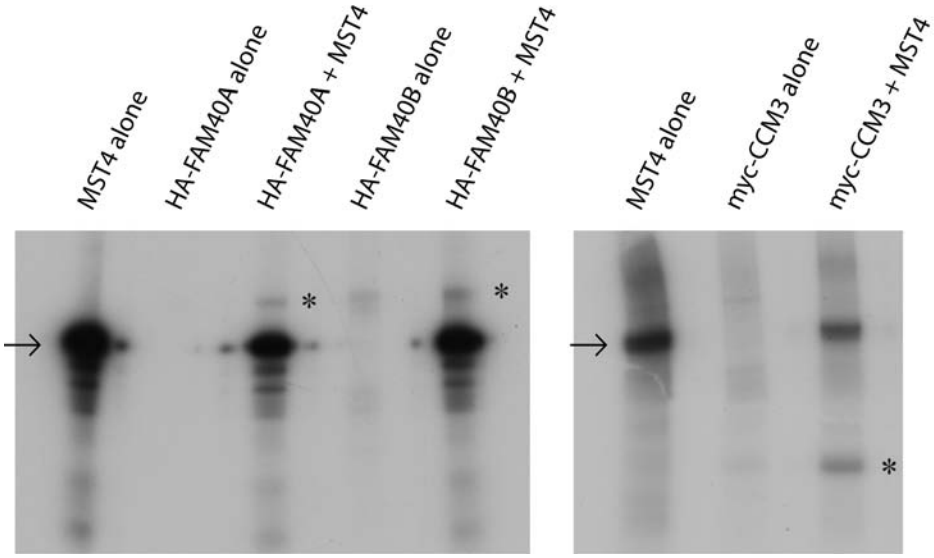

Figure 3.13 *In vitro* kinase assays reveal that MST4 phosphorylates FAM40A, FAM40B and CCM3

COS7 cells were transfected with pHA-FAM40A, pHA-FAM40B or pmyc-CCM3. Cells were lysed 48 h later and cell lysates were incubated with anti-HA agarose beads to precipitate HA-FAM40A and HA-FAM40B or with anti-myc agarose beads to precipitate myc-CCM3. Immunoprecipitated proteins were used in *in vitro* kinase assays with recombinant MST4 and [γ-^{32} P]-ATP. Asterisks indicate signal corresponding to phosphorylated protein while arrows indicate auto-phosphorylated MST4. Results are representative of 3 independent experiments.

3.2.9 Synthesis and purification of anti-FAM40A and anti-FAM40B antibodies produced in rabbit

To facilitate the characterisation of endogenous FAM40A and FAM40B, antibodies against these proteins were generated by immunising rabbits against peptide haptens (generated by Genosphere Biotechnologies, Paris, France (www.genosphere-biotech.com)). Total rabbit antisera obtained were tested by immunoblotting (Figure 3.14) and immunofluorescence staining (Figure 3.15).

For immunoblotting testing (Figure 3.14), lysates from COS7 cells overexpressing HA-FAM40A or HA-FAM40B were used. Incubation of western blots with the antisera had to be performed in the presence of BSA to obtain specific bands with minimal background. Anti-FAM40A antisera detected a major band corresponding to a molecular weight of about 100 kDa. Anti-FAM40B antisera detected a pair of bands proximal to each other at approximately 100 kDa. This molecular weight matches that of full length FAM40A and FAM40B. A number of additional lower molecular weight bands were observed which could be protein degradation products or non-specific bands. A high molecular weight smear was observed in the 'IB FAM40A' lanes which could correspond to protein modifications. Both antisera were specific in that anti-FAM40A antisera did not cross-react with overexpressed FAM40B and vice versa.

Testing of the antisera for immunofluorescence staining (Figure 3.15) was carried out using PC3 cells transfected with pHA-FAM40A or pHA-FAM40B plasmids. The staining pattern of both anti-FAM40A and anti-FAM40B antisera matched very closely that of the respective anti-HA staining pattern. This indicates that these antibodies are capable of recognising their target proteins in their native conformation. Furthermore, staining was detected in cells not expressing HA-tagged protein implying the detection of endogenous protein. However, the specificity of this staining was not checked by knocking down FAM40A and FAM40B by RNAi. Taken together, these results suggest that the generated antisera are suitable for the detection of overexpressed protein in western blots and whole cells.

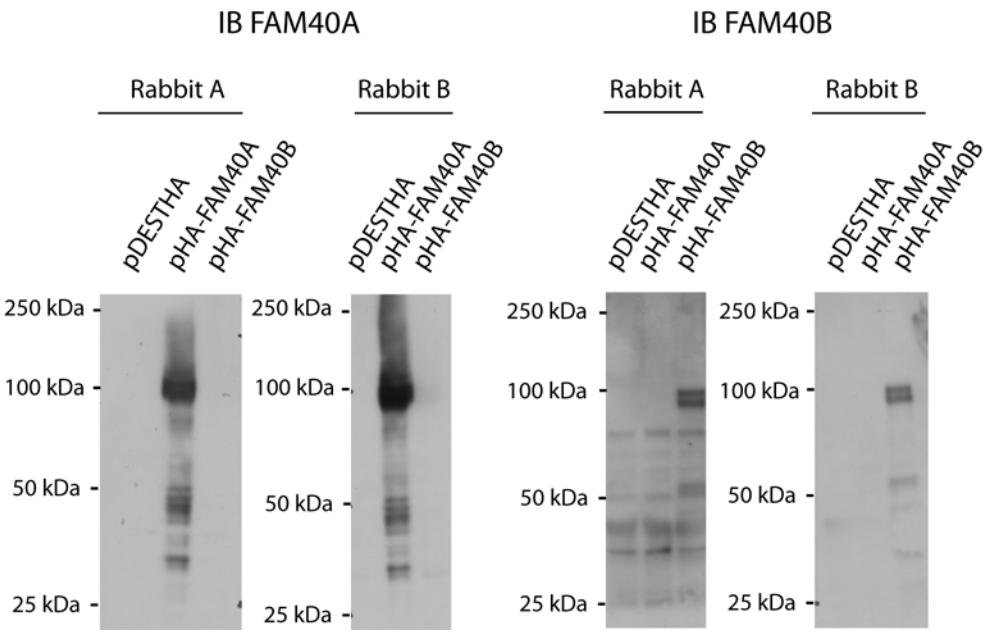

Figure 3.14 Testing anti-FAM40A and anti-FAM40B serum on overexpressed protein for immunoblotting

COS7 cells were transfected with pDESTHA (empty vector), pHA-FAM40A or pHA-FAM40B. Cells were lysed 48 h later and cell lysates incubated with anti-HA agarose beads. Immunoprecipitated protein was used to test anti-FAM40A and anti-FAM40B rabbit sera in western blots.

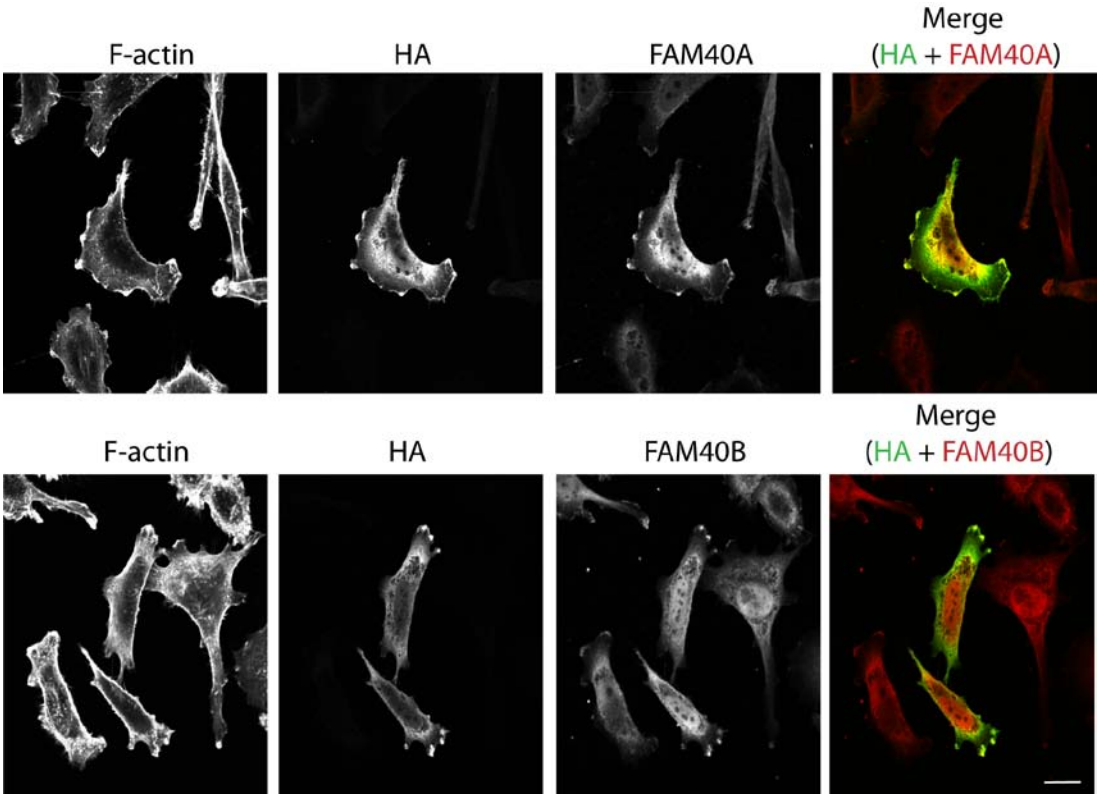

Figure 3.15 Testing anti-FAM40A and FAM40B serum on overexpressed protein for immunofluorescence staining
PC3 cells on glass coverslips were transfected with pHA-FAM40A or pHA-FAM40B. Cells were fixed 24 h later and stained for F-actin, the HA epitope and for FAM40A and FAM40B with anti-FAM40A and anti-FAM40B rabbit sera. Scale bar = 20 µm.

While the generated anti-FAM40A and anti-FAM40B antisera were capable of recognising overexpressed protein, they were unable to detect endogenous protein in western blots. Hence, anti-FAM40A and anti-FAM40B antibodies were purified from total rabbit serum using peptide affinity chromatography. A schematic of the method used is shown in Figure 3.16.

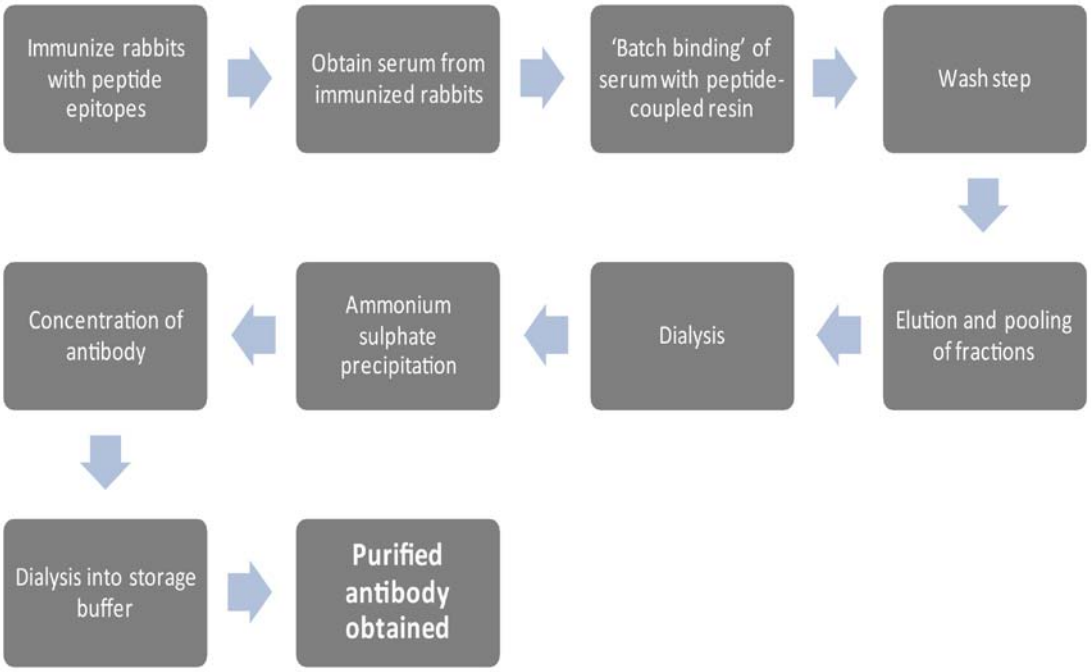

Figure 3.16 Schematic of protocol used to purify anti-FAM40A and anti-FAM40B antibodies from whole rabbit serum
Rabbit antiserum was subjected to affinity chromatography using FAM40A and FAM40B immunisation peptides as the 'bait' to purify anti-FAM40A and anti-FAM40B antibodies. A batch binding technique was used and peptides used for purification were coupled to the chromatography resin by means of a terminal cysteine residue. Eluted antibody was concentrated by ammonium sulphate precipitation.

Coomassie staining of the purified antibodies (Figure 3.17A) allowed the determination of their purity and concentration. The concentration of purified anti-FAM40A was approximately 100 µg/ml while that of purified anti-FAM40B was 40 µg/ml. Both antibodies were able to react specifically with their intended targets as determined by immunoblotting for overexpressed HA-FAM40A and HA-FAM40B (Figure 3.17B). However, the purified antibodies were unable to specifically detect endogenous protein. This was determined by using lysates from HUVECs (Figure 3.17C). Samples in which either FAM40A or FAM40B were depleted by RNAi were included to determine the specificity of the antibodies to their targets. A specific interaction would have resulted in a reproducible decrease in the intensity of the corresponding band in the RNAi lanes. Such a decrease is observed with the oligo siFAM40B-1 in the blot shown in Figure 3.17C but could not be reproduced. The efficiency of knockdown was not confirmed at the mRNA level in these experiments.

In summary, purified anti-FAM40A and anti-FAM40B antibodies were not able to target endogenous protein. However, the generated antiserum contained anti-FAM40A and anti-FAM40B antibodies at an acceptable ELISA (enzyme-linked immunosorbent assay) titre (≥ 1:10,000) which were able to specifically target their intended antigens. A better purification strategy resulting in a more concentrated antibody preparation may yield antibodies that are able to target endogenous protein.

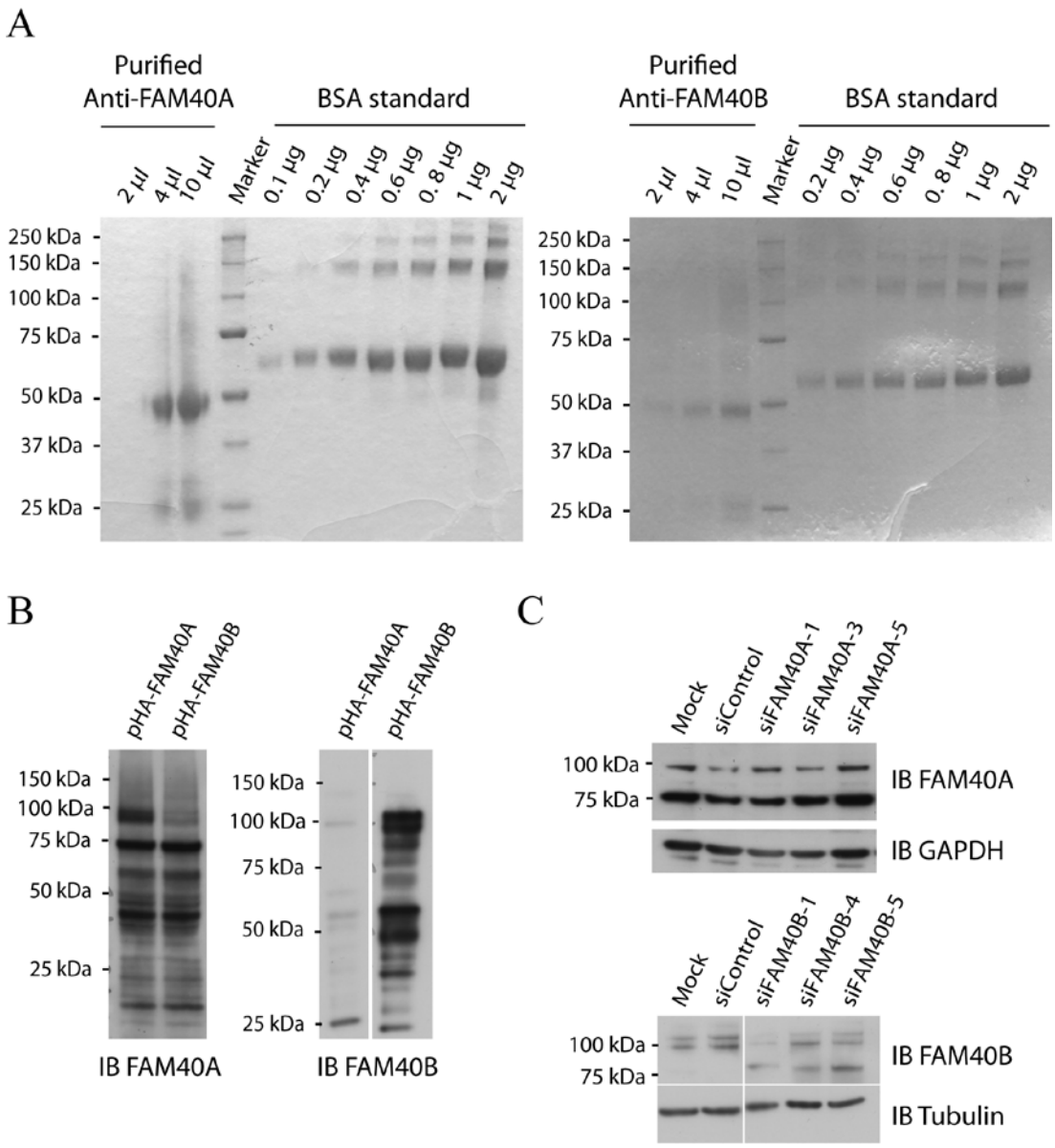

Figure 3.17 Purification and testing of anti-FAM40A and anti-FAM40B antibodies
(A) shows coomassie-stained gels containing purified anti-FAM40A and anti-FAM40B antibodies compared to a BSA protein standard. These gels were used to confirm the purity of the obtained antibody and to determine their concentration. **(B)** COS7 cells were transfected with pHA-FAM40A or pHA-FAM40B. Cells were lysed 48 h later and HA-FAM40A and HA-FAM40B immunoprecipitated using anti-HA agarose beads were used to test purified anti-FAM40A and anti-FAM40B in western blots. **(C)** Lysates from HUVECs depleted of FAM40A or FAM40B using three individual siRNAs for each protein were used to determine the specificity of the purified antibodies by immunoblotting. Blotting for GAPDH or tubulin was used as a loading control. Example immunoblots are shown in **(C)**.

3.3 Discussion

Results presented in this chapter highlight FAM40 interacting partners and provide information on their fundamental biochemical features. These data provide a significant indication of how the FAM40 proteins may function in cells.

3.3.1 FAM40A and FAM40B potentially signal with other members of the STRIPAK complex

A previous biochemical study has shown that both FAM40A and FAM40B are members of the STRIPAK complex (Goudreault et al., 2009). This information was used to provide a first indication of potential signalling partners and to generate hypotheses on how the FAM40 proteins may carry out their cellular functions. Results presented in this chapter indicate that both FAM40A and FAM40B interact with CCM3 and the GCKIII kinases STK25 and MST4 (section 3.2.1), all of which are members of the STRIPAK complex. This is in agreement with previously published data that documents FAM40A interacting partners (Goudreault et al., 2009). Furthermore, FAM40A was reported to interact with other members of the STRIPAK complex including STRN, STRN3, STRN4, Mob3, CTTNBP2, CTTNBP2NL and the GCKIII kinase STK24. The experimental method in this study differs from that used in this thesis in that it utilised affinity chromatography using FAM40A as bait, followed by mass spectrometry to identify interacting partners. Subsequently, these interactions were validated using immunoprecipitation and western blotting. A similar analysis for FAM40B was not performed in this study, and it would be interesting to see if FAM40B also interacts with these proteins.

These data and the results presented in this thesis cannot be used to conclude that these interactions occur directly without the aid of adaptor proteins. Future experiments should attempt to investigate if these interactions occur directly or indirectly. Alternative methods to investigate protein interactions include yeast two-hybrid screening, and GST-pulldown analysis using recombinant protein. These methods have the advantage that they test for direct protein interactions. Furthermore, interactions have been probed so far using overexpressed proteins and future experiments should validate these findings using endogenous proteins. If antibodies targeting only one of the interacting partners are available, an alternative approach in the immunoprecipitation experiments can be used

wherein its interaction with overexpressed, tagged protein is assessed. A drawback with using overexpressed protein is that protein interactions observed may not be physiologically relevant, due to the expression level of the tagged, overexpressed protein being higher than that of endogenous protein. A further disadvantage is that the tag may affect interaction between proteins by decreasing the affinity between individual proteins, or by causing mislocalisation of protein.

These interactions raise several questions as to how FAM40A and FAM40B function in cells. For example, CCM3-GCKIII kinase signalling is known to be required for maintaining junction integrity in endothelial cells and contributes to the development of a mature vascular network (Zheng et al., 2010). This line of thought led to FAM40 function being studied in endothelial cells and is the basis of the work presented in chapter 5. Do FAM40A and FAM40B exist together in the same complex or exist in distinct sub-complexes that carry out different functions? Exogenously expressed FAM40A and FAM40B can form homodimers as well as interact with each other. This is consistent with previously published data in which affinity precipitation/mass spectrometry analysis using FAM40A as a bait resulted in the identification of peptides corresponding to FAM40B (Goudreault et al., 2009). This would suggest that both FAM40 proteins occur in the same complex. However, future experiments will need to show this for endogenous proteins. It would be interesting to determine what consequence dimerisation has for FAM40 function. Perhaps dimerisation results in autoinhibition which is relieved by binding to other interacting partners. Conversely, dimerisation and resultant clustering could enhance FAM40 function.

While both FAM40A and FAM40B share the same overall domain architecture, the N-terminus of FAM40 is proline rich, a feature lacking in FAM40B. Features such as this may be important for determining binding specificities of interacting partners and may explain functional differences between the two FAM40 proteins. For example, affinity precipitation/mass spectrometry using STRN4 and various PP2A subunits as ‘baits’ only identify FAM40A as ‘prey’ while doing the same with Mob3 identifies both FAM40 proteins as prey (Goudreault et al., 2009). It will be important to determine the binding specificities of the two individual domains in FAM40 proteins (N1221-like and DUF3402) as these domains

have not been characterised. The occurrence of these domains in the same order and conservation in FAM40 homologues across different species imply that they perform a role in cells. The roles of these domains can be determined by creating deletion constructs that contain the individual domains, or by performing yeast two-hybrid screens using these domains as baits.

Are any of these interactions mutually exclusive? For example, multiple GCKIII kinases bind to both FAM40 proteins. It is possible that binding to different kinases offers different functionalities to these proteins. Furthermore, what is the stoichiometry of FAM40A and FAM40B in the STRIPAK complex? This may help to explain FAM40 protein function by understanding them as units of a larger multi-protein entity.

In summary, the finding that FAM40A and FAM40B interact with various members of the STRIPAK complex offers important insights into their possible physiological roles and is the impetus for further research into their functions.

3.3.2 FAM40A and FAM40B are putative transmembrane proteins

The subcellular localisation of proteins has consequences for their functions and so significant attention was given to determining the localisation pattern of FAM40A and FAM40B. A combination of biochemical and immunofluorescence analysis in addition to predictions using bioinformatics programs was used. Previous reports suggest that FAM40 homologues in *S. cerevisae* and *N. crassa* are transmembrane proteins (Kemp and Sprague, 2003; Xiang et al., 2002). Hence, bioinformatics software was used to test if the human FAM40 proteins are predicted to be transmembrane. A major concern in using bioinformatics is that of false positives. For example, predicted transmembrane regions may actually be amphipathic helices (Nugent and Jones, 2009). However, this strategy was not used to produce conclusive data on FAM40 localisation but to provide a first indication to complement further analysis.

Transmembrane proteins are commonly targeted to membranes by the presence of a signal peptide sequence (von Heijne and Gavel, 1988). No signal peptides were detected for either FAM40A or FAM40B by using sequence based prediction programs (SignalP and MEMSAT-

SVM). Transmembrane proteins with a signal peptide enter the classical secretory pathway and their translocation occurs via the ER-Golgi network ending with secretory vesicle fusion to the membrane (Bendtsen et al., 2004). However, some secreted proteins can bypass this pathway and enter a non-classical secretory pathway. An example of such a mechanism is where insertion of the protein into the plasma membrane can be mediated solely by transmembrane helices (Renthal, 2010). Hence, the absence of a signal peptide may not preclude the possibility of the FAM40 proteins being transmembrane. FAM40A was predicted to enter this pathway using the program SecretomeP. Immunofluorescence staining of overexpressed FAM40A and FAM40B in PC3 cells showed a diffused staining pattern in the cytoplasm with enrichment in F-actin-rich protrusions. This staining pattern is consistent with proteins that undergo non-classical secretion as a vesicular and/or reticular staining pattern was not observed. Furthermore, enriched localisation in protrusions could imply that the FAM40 proteins are at least proximal to the plasma membrane if not transmembrane. Staining in unpermeabilised cells showed that FAM40 proteins localised at F-actin-rich protrusions, suggesting they could be inserted into the membrane with their N-terminus exposed to the cell exterior. However, the fixation step can produce small holes in the membrane that allow antibody entry and subsequent staining of internal protein. These holes are sufficient to allow phalloidin entry for F-actin staining. Strong foci of FAM40 staining with negligible staining elsewhere in the cells suggests that such non-specific staining was minimal (compared to the F-actin staining). It will be important for future experiments to show that staining in unpermeabilised cells does not stain internal protein, by using a cytoplasmic protein as a negative control. Furthermore, it will be important to determine if the enriched staining observed in F-actin-rich protrusions is an artefact of the staining procedure and/or cell structure. This can be achieved by using a cytoplasmic protein that is known to localise to F-actin-rich protrusions as a negative control. An example is WAVE1 which is known to localise to the edge of cell protrusions (Cory and Ridley, 2002). Additionally, an improved protocol where live cells are stained without fixation can be used.

In addition to these analyses, COS7 cells overexpressing FAM40A or FAM40B were used in surface biotinylation assays and FACS staining to detect surface protein. Positive results were obtained in the biochemical analysis while the FACS data yielded variable results. For

the FACS experiment, cells had to be detached which could have caused internalisation of the protein of interest. A concern with the biotinylation assay is that the experimental manipulation of cells could have compromised their permeability and/or caused lysis of a subset of cells leading to non-specific labelling. A subset of experiments did yield a positive result even with the negative control. This was attributed to non-specific labelling and the experiment was not analysed further. A further concern is that the negative control (HA-14-3-3) being a lower molecular weight protein than HA-FAM40A and HA-FAM40B, is less susceptible to biotinylation. A key assumption made in these experiments was that COS7 cells (derived from monkey cells) contain the necessary cellular machinery to target human FAM40A and FAM40B to the plasma membrane.

While it is tempting to hypothesize the FAM40 proteins as being the transmembrane receptors targeting the STRIPAK signalling complex to the membrane, further experiments need to be done to yield a conclusive result. As a first step cell fractionation experiments can be performed to determine if the FAM40 proteins are present in the membrane fraction. Additionally, the surface biotinylation assay performed can be coupled to mass spectrometry analysis to determine sites of biotin coupling, which can then be concluded to be present at the cell exterior yielding information on protein topology. Other more established techniques can be used to confirm the presence of transmembrane segments. An example is Cys-labelling in which chemical modification of cysteine residues introduced in different regions of the protein using membrane permeable and impermeable reagents is used to deduce topology (Kimura et al., 1997). Another approach to prove that the FAM40 proteins are transmembrane could be to identify extracellular ligands if present.

3.3.3 The FAM40 proteins are post-translationally modified

Both FAM40A and FAM40B are phosphoproteins which suggests that their functions may be regulated by phosphorylation. For example, FAM40 binding to other STRIPAK complex members could be affected by phosphorylation. PP2A and the GCKIII family kinases are members of the STRIPAK complex (Goudreault et al., 2009), and hence the FAM40 proteins could be their substrates. *In vitro* kinase assays revealed that MST4 is able to phosphorylate FAM40A, FAM40B and CCM3. While MST4 shares homology with STK24 and STK25 (other

GCKIII family members) these enzymes can function in distinct ways. For example, CCM3 can be phosphorylated by STK25 but not STK24 (Voss et al., 2007). Hence, it will be important to determine if the other GCKIII kinases can phosphorylate the FAM40 proteins too. The GCKIII kinases have been suggested to be downstream of CCM3 (Zheng et al., 2010) and CCM3 is needed for their stabilisation in cells by preventing their degradation (Fidalgo et al., 2010). Furthermore, CCM3 can increase MST4 kinase activity *in vitro* (Ma et al., 2007). The fact that MST4 can phosphorylate CCM3 indicates there might be a feedback loop. It will be interesting to see if in a similar fashion, the FAM40 proteins can modulate GCKIII kinase activity. This connectivity between different partners by means of phosphorylation may imply shared signalling networks and so is important when considering FAM40 function. While MST4 has been shown to phosphorylate the FAM40 proteins *in vitro*, it will be important to demonstrate this activity *in vivo*. This could be achieved by depleting MST4 using siRNA and assessing FAM40 phosphorylation, or by conducting kinase assays using co-expressed MST4 instead of recombinant enzyme. Finally, the functional consequences of MST4 phosphorylation will need to be studied.

Mass spectrometry analysis was not performed to identify FAM40 phospho-sites and could be considered for future work. However, previously published proteomics data allow the deduction of phospho-sites by detection of FAM40 phospho-peptides (compiled in PhosphoSitePlus (Hornbeck et al., 2012)). To understand how these sites contribute to FAM40 function, phospho-mimetic and phospho-dead mutants can be used. For example, the capacity of these mutants to interact with other STRIPAK complex family members or effects of their overexpression in cells can be tested. The context of the experiments in which these phospho-sites have been reported may offer clues as to how they are important for FAM40 function. A significant number of experiments involved the analysis of the proteome in cancers of different origin (PhosphoSItePlus (Hornbeck et al., 2012)). This may be indicative of FAM40 phosphorylation being involved in or at least a feature of cancer progression. Phosphorylation of the S335 site on FAM40A was detected in studies analysing the mTOR regulated phosphoproteome and phosphorylation dynamics during the DNA damage response (PhosphoSitePlus (Hornbeck et al., 2012)). Interestingly, the *S. cerevisae* FAM40 homologue, Far11 has been shown to be involved in the regulation of the DNA

damage response (Lisa-Santamaria et al., 2012) while the Far complex is implicated in TORC2 signalling (Pracheil et al., 2012). These features point towards the possibility of the FAM40 proteins having functions in the mTOR signalling network.

The FAM40 proteins are also ubiquitinated and this modification may be important for determining FAM40 stability. However, ubiquitination is involved in cellular pathways other than those that mediate protein degradation, including the regulation of protein interactions and signal transduction (Schaefer et al., 2012). Experiments in which cells were treated with MG132 (a proteasome inhibitor) and protein levels subsequently analysed were performed to assess if FAM40A and/or FAM40B are degraded via the proteasome. However, results were variable and hence have not been shown. Future experiments should attempt to identify the functional implications of FAM40 ubiquitination.

4 FAM40 function in prostate cancer cells

4.1 Introduction

FAM40A and FAM40B were identified as novel regulators of cell morphology and migration in an RNAi screen conducted using PC3 cells (Bai et al., 2011). Both FAM40A and FAM40B knockdown were reported to result in morphological changes. FAM40A knockdown resulted in less spread cells while FAM40B knockdown resulted in elongated cells. The control of cell morphology involves dynamic changes to the cytoskeleton (Ridley et al., 2003), and hence the FAM40 proteins could regulate the cytoskeleton. Furthermore, the GCKIII kinase MST4, which interacts with and phosphorylates the FAM40 proteins (section 3.2.7), has been implicated in prostate cancer progression. MST4 has been shown to promote the proliferation of prostate cancer cells (Sung et al., 2003). Additionally, FAM40A expression is increased in primary prostate cancer samples (defined as being clinically localised), as compared to its expression in benign prostate samples (NCBI GEO database, Profile: GDS1439 / 225226_at / FAM40A). This could implicate FAM40A in prostate cancer progression by facilitating the conversion of benign prostate cells to cancerous lesions. Gene function in PC3 cells was primarily studied by depletion of gene expression by RNAi and the subsequent analysis of phenotypes in cell biological assays. As the Rho GTPases are central regulators of the cytoskeleton, biochemical assays to detect changes in their activity were also performed.

PC3 cells are androgen insensitive and were established from prostate cancer metastasis to the bone (Logothetis and Lin, 2005). Their morphology can be described to be mesenchymal and they have been shown to have a high invasive and metastatic potential (Aalinkeel et al., 2004). This feature combined with their androgen insensitivity make them a good system for the study of prostate cancer in its advanced stages. Cancer progression is a heterogeneous process and is dependent on the cellular origin of particular tumours (Nguyen et al., 2009). Hence, results presented in this chapter can only confidently be extrapolated to FAM40 function in prostate cancer cell lines. However, they may be suggestive of wider roles in other cancer cells and more importantly, of fundamental protein function in regulating aspects of cell migration and morphology.

4.2 Results

4.2.1 Verification of siRNA-mediated knockdown of FAM40A and FAM40B in PC3 cells

The functions of FAM40A and FAM40B in PC3 cells were studied using siRNA to knockdown their expression. Individual siRNA oligonucleotides and pools containing a mix of four individual siRNA oligonucleotides were tested for each gene. A control non-targeting siRNA control was used too. Efficient reduction of gene expression was observed after 72 h siRNA transfection for both FAM40A and FAM40B. As antibodies capable of detecting endogenous FAM40A and FAM40B were not available, expression was determined using Q-PCR to quantify relative mRNA levels in control and siRNA-treated samples.

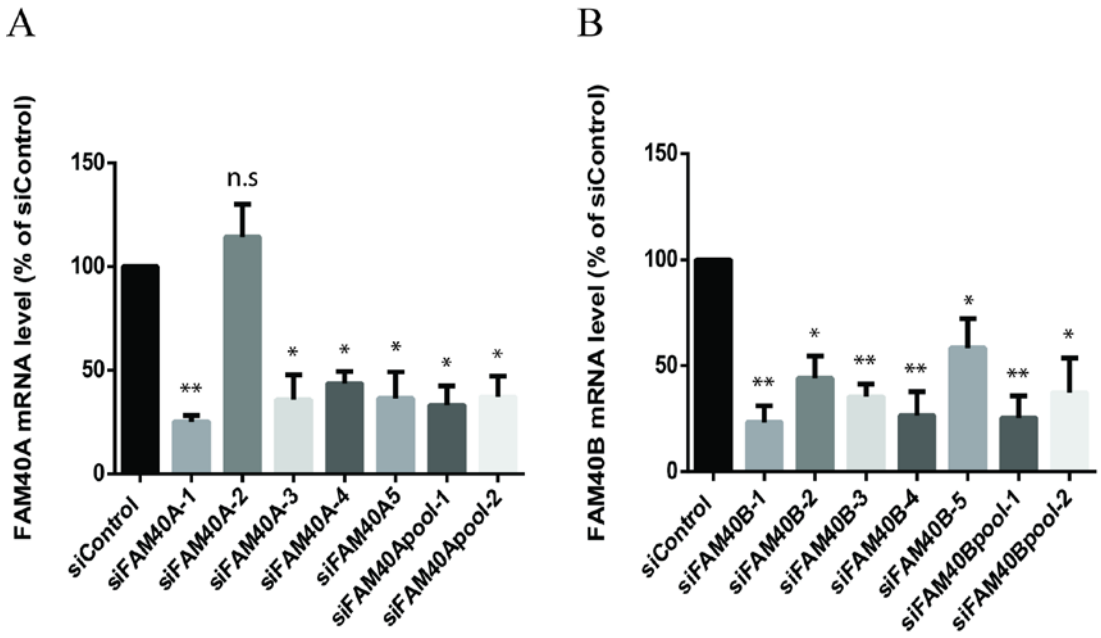

Figure 4.1 siRNA-mediated depletion of FAM40A and FAM40B by quantitative PCR
PC3 cells were transfected with individual and pooled siRNAs for FAM40A or FAM40B. After 72 h, mRNA from these cells was extracted and used to synthesize cDNA. The amount of **(A)** FAM40A and **(B)** FAM40B cDNA was determined by quantitative PCR. Values were normalised to GAPDH cDNA levels. Data are the mean of 3 independent experiments ± SEM. * $p < 0.05$, ** $p < 0.01$ compared to siControl determined by Student's t-test.

4.2.2 Knockdown of FAM40A and FAM40B results in distinct morphological phenotypes in PC3 cells

PC3 cells grew as single cells and did not appear to form stable cell-cell contacts (Figure 4.2). Control cells showed variable morphology with a subset of cells being naturally more elongated. Their morphology can be described to be mesenchymal and multiple F-actin-rich protrusions and enrichment of F-actin staining at the cell edge were observed. Stress fibres were rarely observed.

Knockdown of FAM40A with two individual siRNAs and a siRNA pool reduced cell spread area (Figure 4.2). Targeting FAM40A with the siRNA pool also resulted in a ring of intensely staining cortical F-actin in a subset of cells. This phenotype was not distinguished when using individual siRNAs and may be due to off-target effects. Quantification of cell morphology using Cell Profiler software showed a significant reduction of cell area (Figure 4.3). Knockdown of FAM40B resulted in a reduction in cell area only with one siRNA oligo (siFAM40B-1).

Knockdown of FAM40B with two individual siRNAs and a siRNA pool led to a different phenotype to FAM40A. Cells depleted of FAM40B were elongated and the nucleus was observed to be placed centrally in the elongated cell (Figure 4.2). Quantification of cell morphology using Cell Profiler software showed an increase in cell eccentricity (a measure of elongation) (Figure 4.3), consistent with the observed phenotype. Knockdown of FAM40A with only one oligo (siFAM40A-1) led to a significant reduction in eccentricity, suggesting these cells were more circular in shape compared to control cells. DAPI staining did not show an increased incidence of multi-nucleate cells or other alterations to nuclear structure in either FAM40A or FAM40B knockdown. These results indicate that FAM40A and FAM40B regulate cell morphology and may have distinct cellular functions.

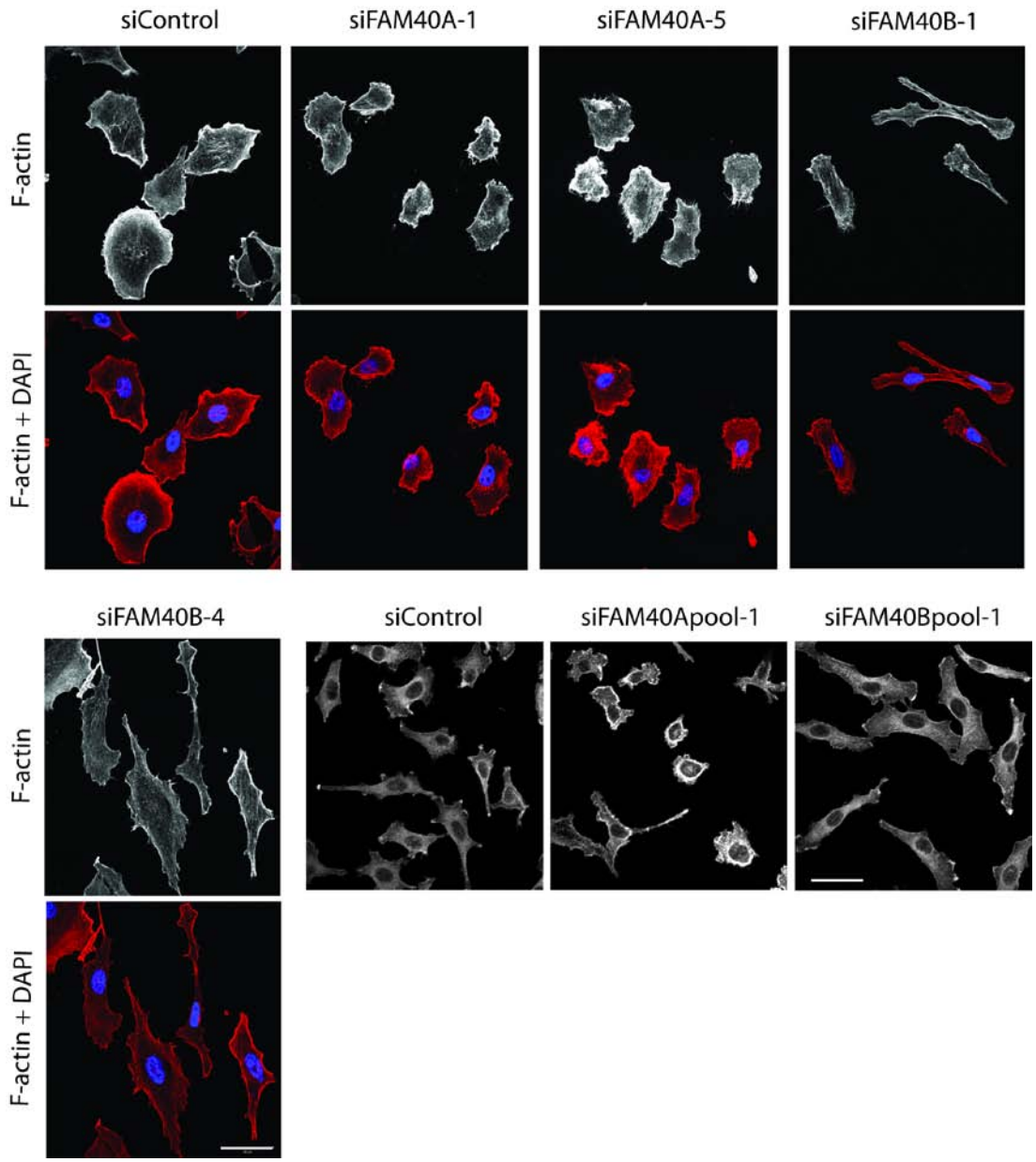

Figure 4.2 Effect of FAM40A and FAM40B depletion on PC3 cell morphology
PC3 cells were transfected with siRNAs for FAM40A or FAM40B. After 24 h cells were harvested and seeded onto glass coverslips coated with Matrigel. After another 48 h, cells were fixed and stained for F-actin and with DAPI. Confocal images were acquired to analyse the effects of FAM40 knockdown on cell morphology and F-actin. Scale bars = 50 µm. Images are representative of 3 independent experiments.

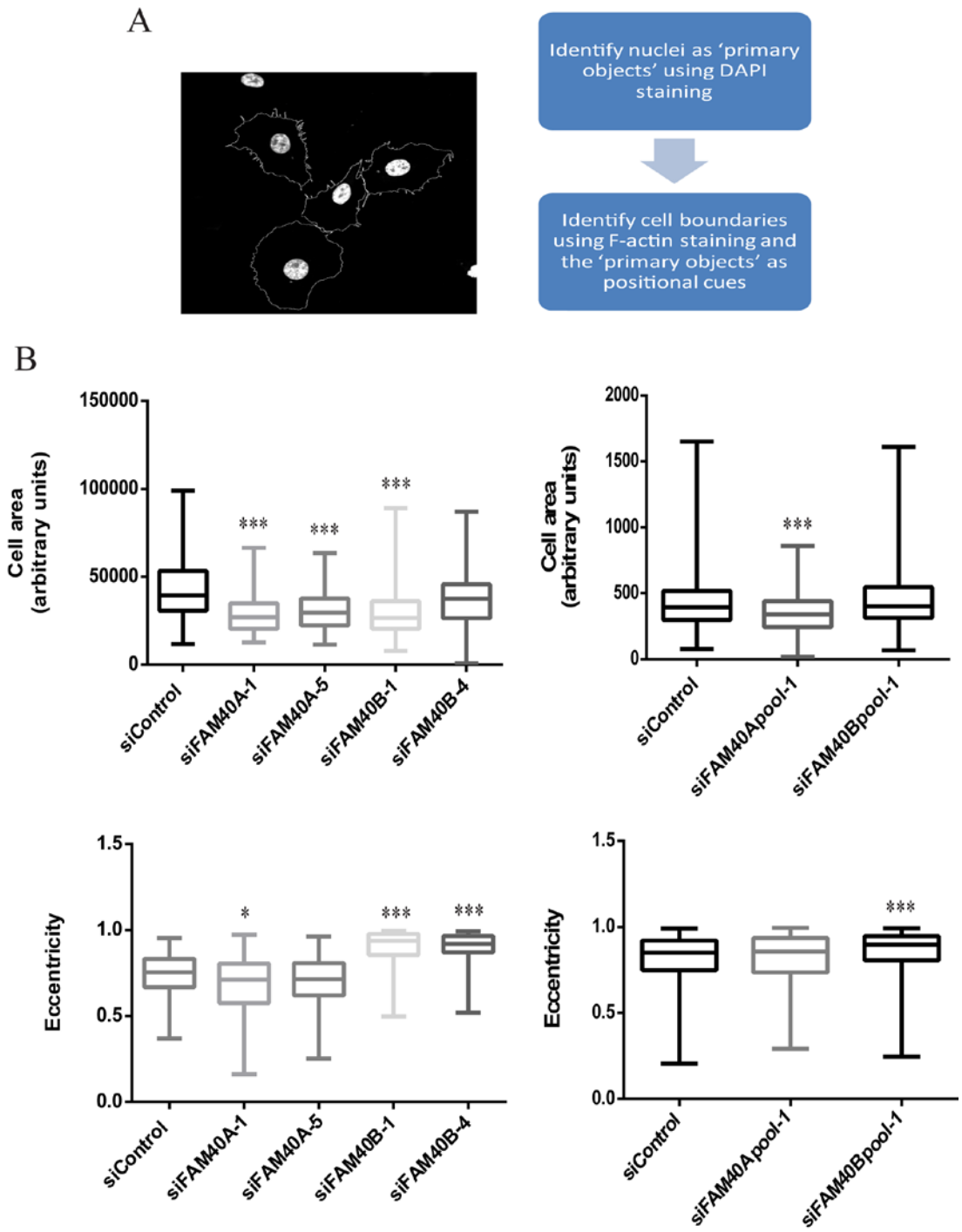

Figure 4.3 Quantification of the morphology of FAM40-depleted PC3 cells
(A) The Cell Profiler software was used to detect individual cells automatically and compute their morphological parameters. DAPI staining was used to identify positions and numbers of individual cells in the images. This positional cue along with the F-actin staining was used to detect cell boundaries. Graphs in **(B)** show computed morphological parameters of the identified cells. The eccentricity has a value between 0 and 1 with a circle having an eccentricity of 0 and a line segment having an eccentricity of 1. n > 50 cells per condition from 3 independent experiments. Boxes of box and whisker plots show median, 25th and 75th percentile. Whiskers show minimum to maximum values. * $p < 0.05$, *** $p < 0.001$ compared to siControl determined by Student's t-test.

4.2.3 The FAM40 proteins affect PC3 cell adhesion and spreading

To test if the FAM40 proteins affect cell adhesion to the substrate, adhesion assays were carried out on uncoated plastic, and Matrigel-coated plastic (Figure 4.4A and B). Matrigel is a basement membrane preparation containing numerous proteins that are constituents of the ECM including collagen IV and laminin (BD Biosciences).

Depletion of FAM40B with a siRNA pool resulted in reduced cell adhesion to both uncoated plastic and Matrigel-coated plastic at 15 min (Figure 4.4A and B). The effect of FAM40A knockdown using a siRNA pool on cell adhesion to uncoated plastic was variable and no significant effect was observed (Figure 4.4A). However, FAM40A depletion resulted in a significant reduction in adhesion to Matrigel-coated plastic (Figure 4.4B). In addition to assays testing for changes in cell adhesion, spreading assays were performed (Figure 4.4C and D). Adhesion and spreading are linked (Price et al., 1998) and possibly reinforce each other. Cells need to adhere to the substrate in order to spread, and reciprocally spreading facilitates cell adhesion. PC3 cells were depleted of FAM40A or FAM40B using siRNA pools and allowed to spread onto Matrigel-coated plastic. The cell spread area was determined after 30 min. Depletion of FAM40A did not change cell spreading despite having caused a reduction of cell area in fully spread cells (Figure 4.2). In contrast, FAM40B depletion reduced cell spreading at 30 min, and it is interesting to note that its depletion led to fully spread cells being elongated (Figure 4.3). These experiments were performed only using siRNA pools and it will be important to additionally test individual siRNAs to validate these results.

In summary, the FAM40 proteins regulate cell adhesion and spreading.

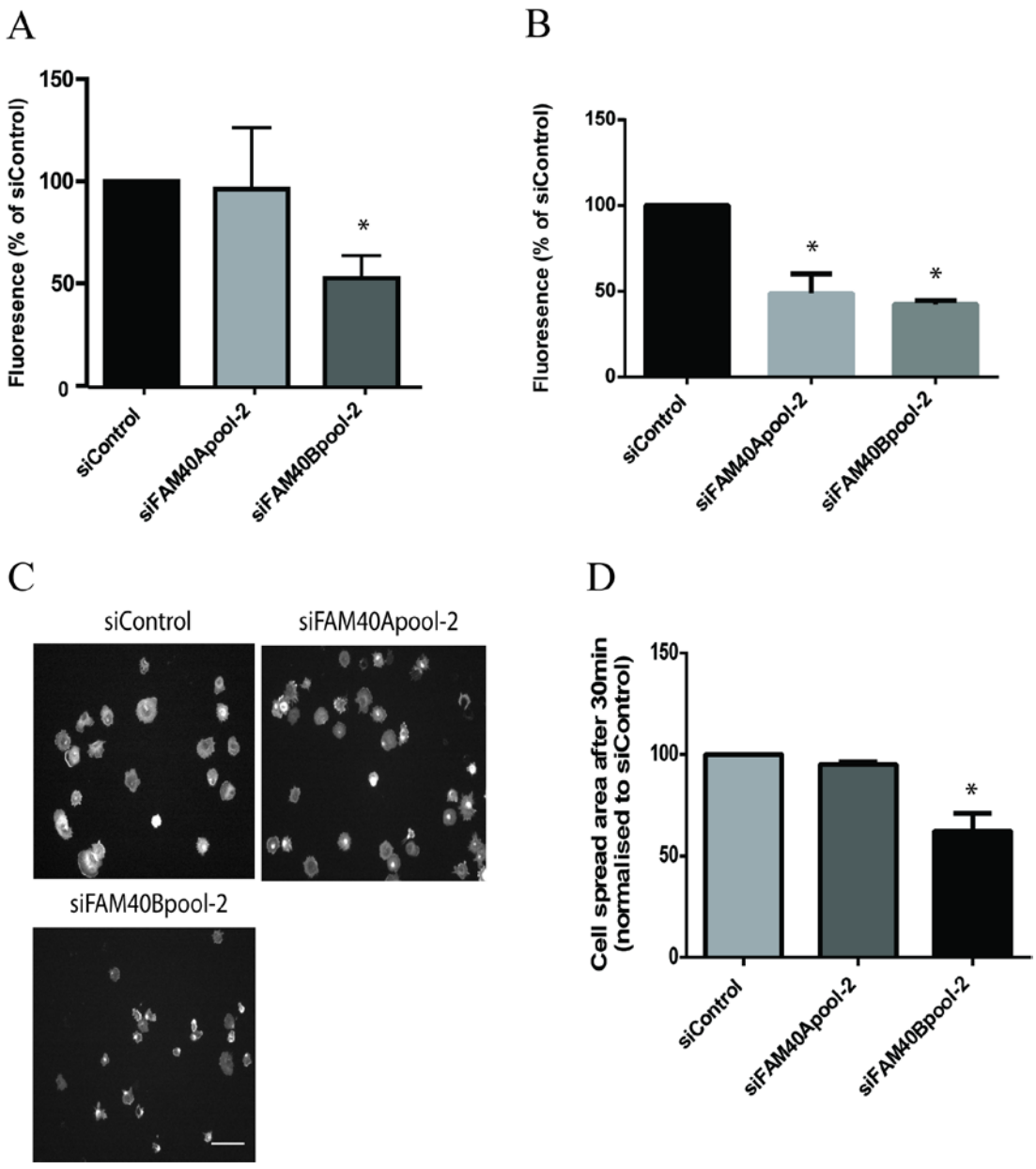

Figure 4.4 Depletion of the FAM40 proteins affects cell adhesion and depletion of FAM40B reduces cell spreading

PC3 cells were transfected with siRNA pools targeting FAM40A or FAM40B. **(A)** and **(B)** show results from adhesion assays. 48 h after transfection cells were labelled with Cell Tracker CMFDA and added onto uncoated plastic **(A)** or onto Matrigel-coated plastic **(B)**. After 15 min adhesion cells were washed to remove unadhered cells and a fluorescence reading was taken as a readout of adhesion capacity. Results in **(A)** are the mean of 4 independent experiments while **(B)** shows the mean 3 independent experiments. **(C)** 72 h after transfection cells were seeded onto Matrigel-coated plastic and allowed to spread for 30 min. Cells were then fixed, stained with Phalloidin-Alexa546 and imaged to determine the extent of spreading by measuring cell area. Scale bar = 50 µm. Atleast 50 cells were considered per condition in each experiment. Results presented in **(D)** are the mean of 3 independent experiments and normalised to siControl (siControl = 100). Error bars indicate SEM values. * $p < 0.05$ compared to siControl determined by Student's t-test.

4.2.4 Effects of FAM40 knockdown on PC3 cell migration

The changes in cell morphology upon FAM40A and FAM40B depletion suggest changes in the regulation of the cytoskeleton and/or associated proteins. These functions may be necessary for cell migration too as there is significant overlap in signalling networks that affect cell morphology and migration. Interestingly, members of the STRIPAK complex, of which the FAM40 proteins are also a part of, have been suggested to regulate cell migration by controlling Golgi orientation and organisation (Fidalgo et al., 2010; Kean et al., 2011).

The effects of the FAM40 proteins on PC3 cell migration were tested using two independent methods, the ORIS assay (Figure 4.5), and time-lapse imaging of randomly migrating cells (Figure 4.6). In the ORIS assay PC3 cells were transfected with siRNA pools targeting FAM40A or FAM40B, and were analysed for their capacity to migrate into a central annular migration zone (described in section 2.3.7.2). Depletion of FAM40A did not affect cell migration in this assay. However, FAM40B knockdown impaired cell migration (Figure 4.5), once again suggesting that the two proteins have distinct functions. Individual siRNAs will have to be tested in future experiments to validate these results.

To understand in more detail how FAM40B knockdown leads to this phenotype, time-lapse movies of PC3 cells depleted of the FAM40 proteins were generated (supplementary movies, movies 1 to 5). Results obtained in this assay matched closely those obtained in the ORIS assay. While FAM40A depletion caused cells to be smaller in size, no observable changes to cell migration were noticed. However, FAM40B knockdown caused a significant reduction in the speed of migrating cells (Figure 4.6). Movies showed that cells appeared elongated and largely oscillated along their axis, resulting in impaired migration capacity. From these observations it can be concluded that FAM40B is required for the efficient migration of PC3 cells.

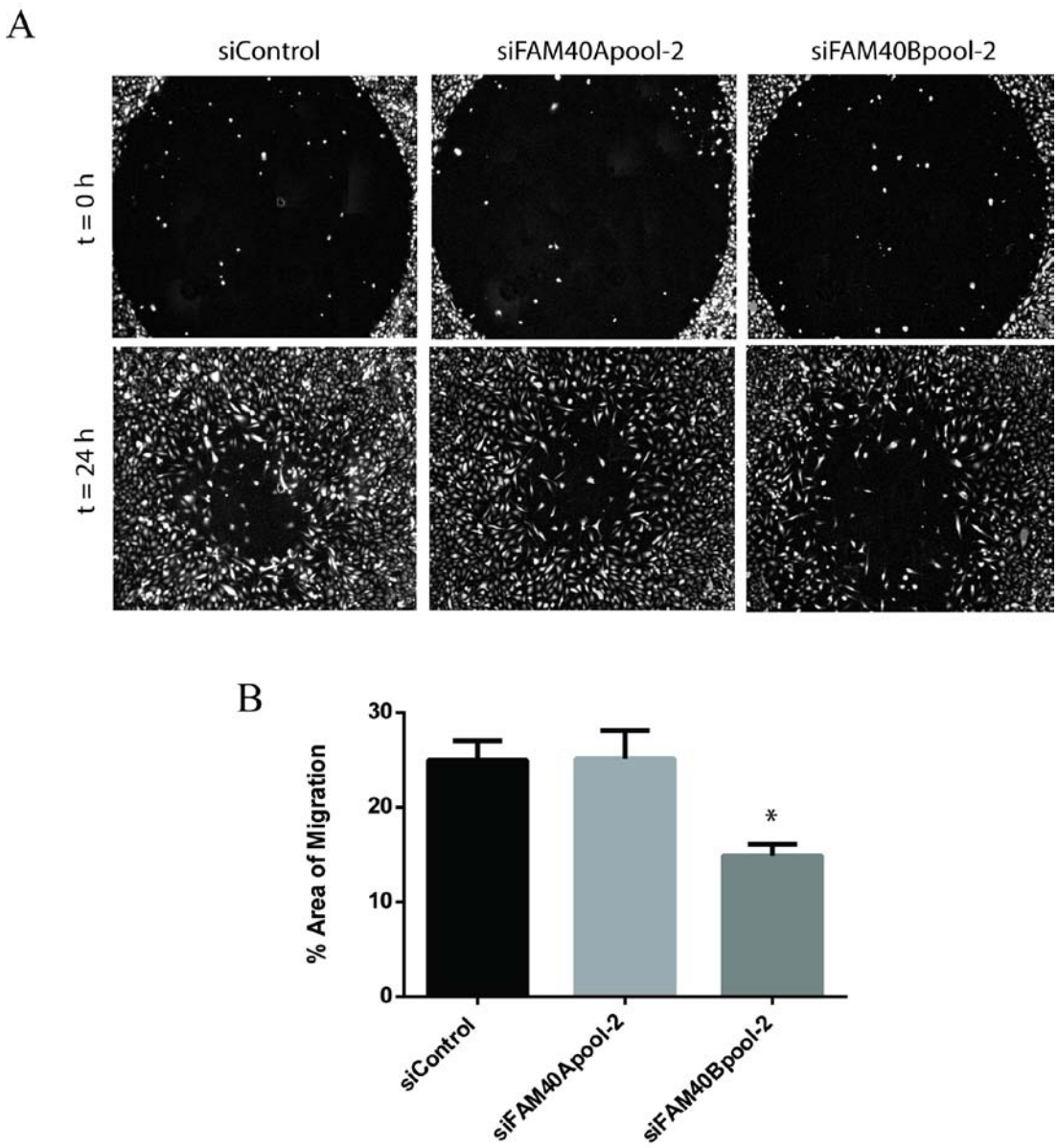

Figure 4.5 FAM40B depletion reduces PC3 cell migration in the ORIS assay
PC3 cells were transfected with siRNA pools targeting FAM40A or FAM40B. After 24 h cells were harvested and seeded onto Matrigel-coated ORIS plates with seeding stoppers. 24 h after cell seeding the stoppers were removed, and the capacity of the cells to migrate was quantified by measuring the percentage area of the central, annular 'detection' zone that cells had migrated into after 24 h (% area of migration). **(A)** shows representative images taken of the ORIS plate at t=0 h and after 24 h migration. Data in **(B)** are the mean of 4 independent experiments ± SEM. * $p < 0.05$ compared to siControl determined by Student's t-test.

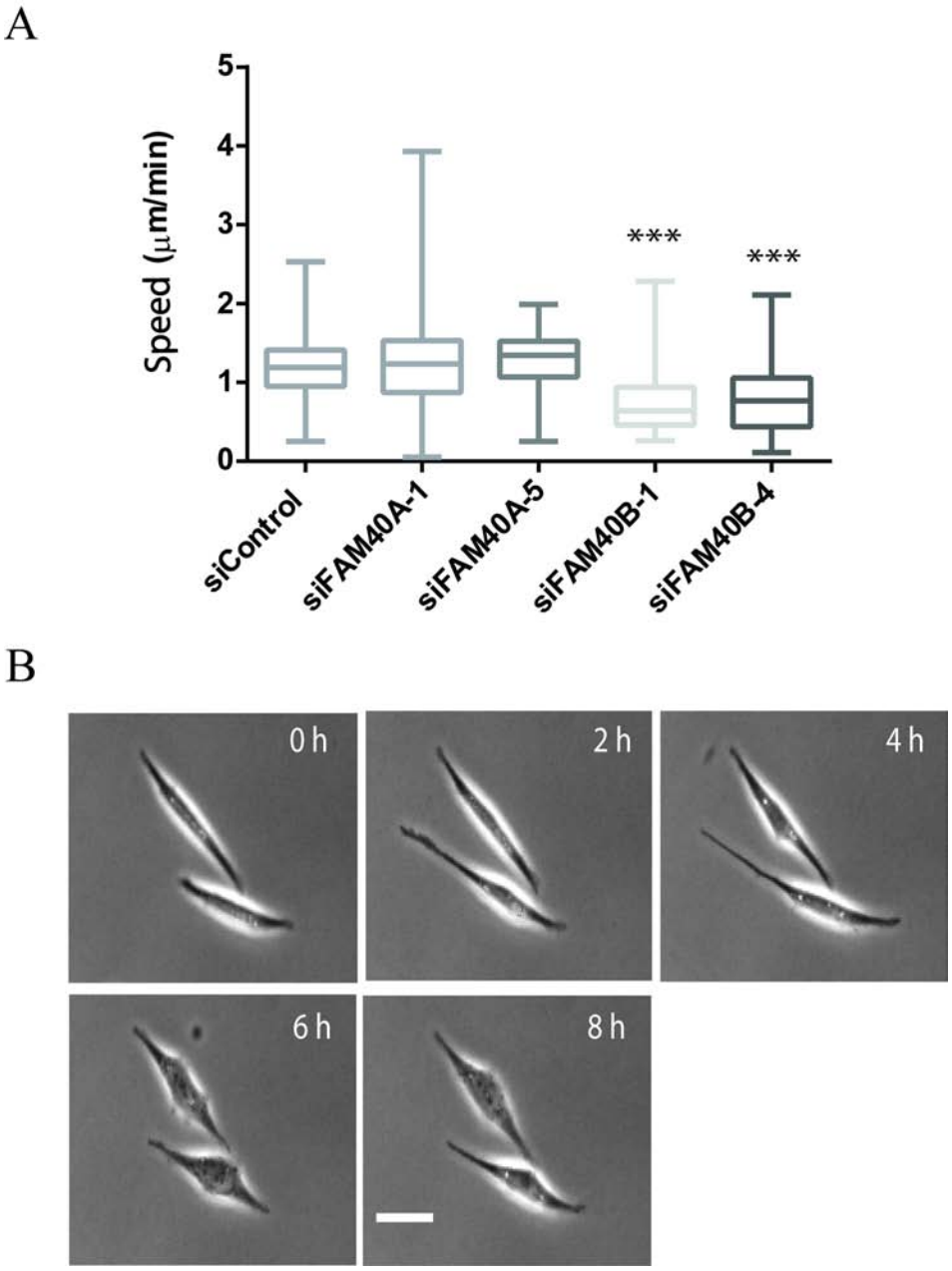

Figure 4.6 Depletion of FAM40B reduces the speed of randomly migrating PC3 cells
PC3 cells were transfected with individual siRNA targeting FAM40A or FAM40B. After 24 h cells were harvested and seeded onto Matrigel-coated plastic. After a further 24 h, time-lapse movies were initiated at 1 frame per 10 min for 14 h (supplementary movies, movies 1 to 5). Data in **(A)** shows speeds of randomly migrating cells determined using ImageJ software. n > 60 cells per condition from 3 independent experiments. Boxes of box and whisker plots show median, 25th and 75th percentile. Whiskers show minimum to maximum values. *** $p < 0.001$ compared to siControl determined by Student's t-test. **(B)** shows frames taken at the indicated time points to illustrate the motility of FAM40B-depleted cells. Scale bar = 100 µm.

4.2.5 Activity levels of the Rho GTPases RhoA and Rac1 upon FAM40 depletion

The Rho GTPases contribute to cell signalling pathways that regulate the cytoskeleton, cell morphology and migration (Ridley et al., 2003). In order to explain the effects of FAM40 depletion on PC3 cell morphology, migration and adhesion/spreading, Rho GTPase activity assays were carried out. The activity of RhoA, Rac1 and Cdc42 on FAM40A and FAM40B knockdown in PC3 cells was determined using a biochemical pulldown approach. In this technique, effectors of the Rho proteins are used to specifically isolate and quantify the active GTP-bound form from whole cell lysates (Ren et al., 1999; Sander et al., 1999; Sander et al., 1998).

Results from the GST-RBD pulldown assay used to quantify RhoA activity were variable and a significant change in RhoA activity was not observed upon either FAM40A or FAM40B knockdown (Figure 4.7B). Only two experiments were carried out to determine RhoA activity on FAM40B knockdown. Further experiments including individual siRNAs need to be conducted before a conclusion can be made on RhoA activity. Knockdown of FAM40B expression with two individual siRNAs resulted in a reduction of Rac1 activity (Figure 4.7C and D) as determined by a GST-PBD pulldown assay. No change in Cdc42 activity was observed upon depletion of FAM40A or FAM40B (assessed using GST-PBD pulldown, results not shown).

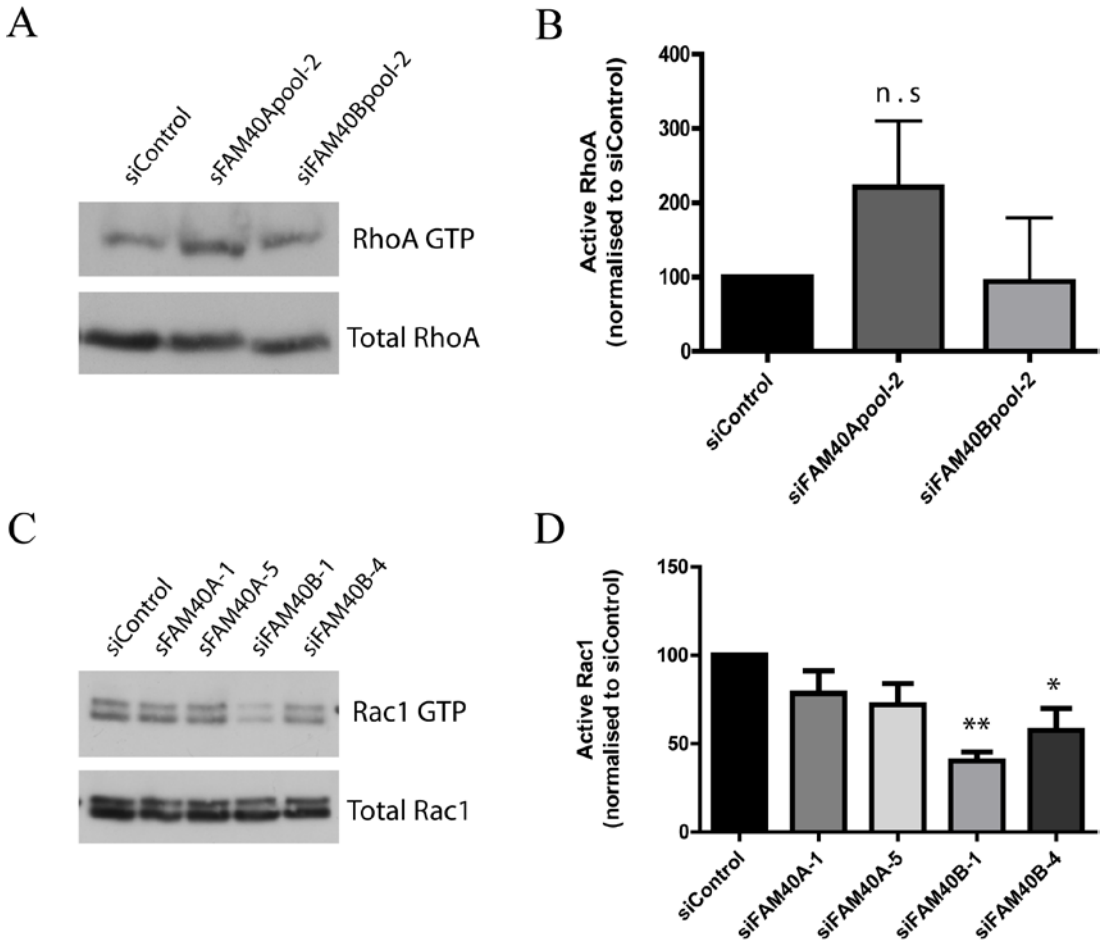

Figure 4.7 Effects of FAM40 knockdown on RhoA and Rac1 activity

PC3 cells were transfected with siRNA targeting FAM40A or FAM40B as indicated. After 72 h cells were lysed and whole cell lysates used in a GST-RBD or GST-PBD pulldown assay to determine levels of GTP-loaded RhoA or Rac1 respectively. **(A)** shows a representative immunoblot for total and GTP-loaded RhoA while **(C)** shows the same for total and GTP-loaded Rac1. Quantification of RhoA and Rac1 activity was performed by normalising the signal from the 'RhoA/Rac1 GTP' lane with that of the 'Total RhoA/Rac1' lane. The graphs represent this normalised signal relative to siControl (siControl = 100) Quantified active RhoA is shown in **(B).** Data shown are the mean of 3 independent experiments for siFAM40A and 2 experiments for siFAM40B. Error bars indicate SD values. Rac1 activity quantification is shown in **(D)**. Data shown are the mean of 4 independent experiments ± SEM. * $p < 0.05$, ** $p < 0.01$ compared to siControl determined by Student's t-test.

4.2.6 Overexpression of FAM40A and FAM40B in PC3 cells

To complement the functional analysis done by siRNA-mediated knockdown of FAM40A and FAM40B, effects of their overexpression were analysed. PC3 cells were transfected with plasmids coding for HA-FAM40A or HA-FAM40B. After 24 h, cells were fixed and stained for the HA epitope. Endogenous FAM40A and FAM40B could not be visualised due to the unavailability of suitable antibodies. Both FAM40A and FAM40B showed diffuse localisation in the cytoplasm and were enriched in F-actin-rich protrusions at the cell edge (Figure 4.8). Neither FAM40A nor FAM40B led to any observable changes to F-actin organisation. Furthermore, no obvious effects on cell morphology were observed. Despite no obvious morphological phenotype being observed, these results provided information on FAM40 localisation within cells (section 3.2.4).

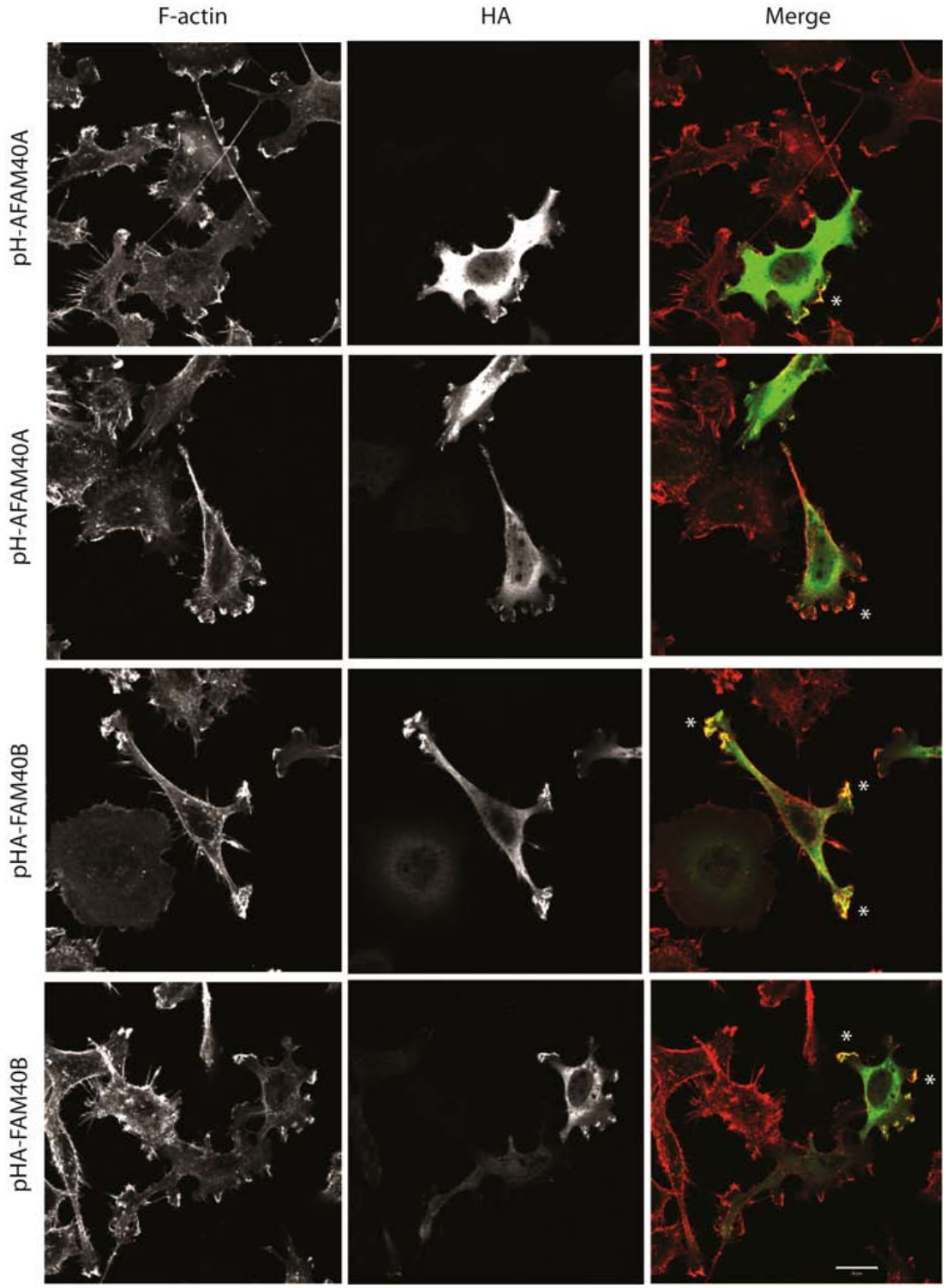

Figure 4.8 Staining for overexpressed FAM40A and FAM40B in PC3 cells
PC3 cells on Matrigel-coated glass coverslips were transfected with pHA-FAM40A or pHA-FAM40B and fixed after 24 h. Cells were stained for F-actin and the HA epitope. Asterisks indicate areas where the HA staining is localised to F-actin-rich protrusions. Scale bar = 20 µm. Images are representative of 3 independent experiments.

4.3 Discussion

This chapter investigated the roles of human FAM40A and FAM40B in PC3 cells, a human prostate cancer cell line. Previously published data used depletion of FAM40A and FAM40B with siRNA pools to suggest that the FAM40 proteins are novel regulators of PC3 migration and morphology (Bai et al., 2011). Here, these results were extended and included analysis using individual siRNAs. Results presented in this chapter show that the FAM40 proteins regulate PC3 cell morphology, migration and adhesion to the substrate. In the light of the biochemical data presented in the previous chapter, mechanisms by which the FAM40 proteins may mediate their functions are proposed. In addition, these results allow the comparison of protein function in two major cell types, epithelial cells and endothelial cells (data presented in chapter 5).

4.3.1 The FAM40 proteins are regulators of PC3 function

FAM40A and FAM40B protein function was studied primarily by using an RNAi approach in PC3 cells. Both individual siRNAs and pools of siRNA were used. Not all experiments were done with the same sets of siRNA, and in some experiments only siRNA pools or individual siRNA were used. In spite of this, these results can be compared as gene expression knockdown was confirmed for all sets of siRNA used. Furthermore, as an indication of different siRNA sets behaving similarly, knockdown of FAM40 function using both a siRNA pool and individual siRNAs resulted in the same morphological phenotype. Future experiments should aim to reproduce these results using individual siRNAs.

Depletion of FAM40A and FAM40B results in distinct morphological phenotypes. FAM40A knockdown using both siRNA pools and individual siRNA caused cells to become less spread with a reduction in cell area, whereas FAM40B knockdown caused cells to become elongated. The different phenotypes suggest functional specialisation. This may be explained by each protein having different signalling partners. For example, only FAM40A is capable of interacting with STRN4 (Goudreault et al., 2009). It was hypothesised that an increase in contractility due to upregulation of RhoA activity could explain the FAM40A depletion phenotype. Additionally, depletion of RhoA in PC3 cells resulted in an elongated phenotype that resembles the FAM40B depletion phenotype (Vega et al., 2011). In a subset

of experiments depletion of FAM40A resulted in an increase in RhoA activity. However, the extent of this effect was variable and no significant difference was obtained. It is likely that more experiments need to be carried out. Nevertheless, it suggests that RhoA activity may be regulated by FAM40A. It might be that RhoA activity is only spatially regulated and hence no strong differences were observed in experiments that analysed activity in whole cell lysates. Imaging using FRET (fluorescence resonance energy transfer) probes may be used to determine spatial regulation of RhoA activity (Nakamura et al., 2006). While only two experiments were performed, no changes in RhoA activity upon FAM40B depletion were observed. The activity of other Rho subfamily members needs to be assessed. For example, depletion of RhoB in PC3 cells results in less spread cells which is similar to the FAM40A phenotype (Vega et al., 2012). Interestingly, similar phenotypes were observed upon FAM40 depletion in MDA-MB-231 cells (epithelial breast cancer cell line) indicating that at least in cancer cells derived from the epithelia, the FAM40 proteins have conserved functions (results not shown). Overexpression of either HA-FAM40A or HA-FAM40B in PC3 cells did not result in any morphological changes. However, overexpression of GFP-FAM40A has been shown to reduce PC3 cell area (Bai et al., 2011). This difference may be due to different tags being utilised. For example, GFP-FAM40A may function as a dominant-negative form, and so lead to a phenotype that resembles the FAM40A depletion phenotype.

FAM40B is required for PC3 cell migration and depletion of FAM40B reduced migration in the ORIS assay and in randomly migrating cells. Time-lapse movies revealed that the cells were elongated, and migration largely occurred along the cell axis. No significant changes to directionality were observed (data not shown), but there was a reduction in mean speed. Depletion of FAM40B resulted in a reduction of Rac1 activity. Rac1 activity is important at the leading edge of cells in regulating actin polymerisation and adhesions (Ridley, 2011). It is possible that the migration defect observed upon FAM40B depletion is due to reduced Rac1 activity. However, the morphology of PC3 cells depleted of Rac1 does not resemble that of FAM40B-depleted cells (Vega et al., 2011). Future experiments should attempt to assess the activity of the other Rac subfamily members, Rac2 and Rac3.

CCM3-GCKIII kinase (STK25, MST4) signalling has been shown to be important for the regulation of Golgi positioning and cell polarisation (Fidalgo et al., 2010; Kean et al., 2011) which is needed for effective cell migration (Mellor, 2004). Additionally, depletion of STK24 (Lu et al., 2006) and STK25 (Chen and Cho, 2011) using RNAi has been shown to enhance the migration of MCF7 breast cancer cells while MST4 overexpression reduces invasion of HEK293T cells into collagen I (Preisinger et al., 2004). In general, GCKIII kinase activity appears to antagonize cell migration and/or invasion. These data suggest that FAM40B signalling could regulate cell migration via CCM3 and/or the GCKIII kinases. For example, FAM40B-depleted cells were elongated and largely exhibited migration along a single axis. Their inability to change their direction of migration could be a result of defects in Golgi positioning. Future experiments should attempt to assess effects of FAM40 depletion on Golgi positioning and localisation.

Depletion of FAM40B resulted in an adhesion defect on both uncoated plastic and Matrigel-coated plastic. FAM40A depletion only caused an adhesion defect on Matrigel. However, results for FAM40A depletion on uncoated plastic were variable and more experiments need to be conducted to determine significance of differences. Moreover, these experiments were performed 48 h after siRNA transfection while mRNA knockdown was only verified after 72 h. Future experiments should verify mRNA depletion at 48 h or these adhesion assays should be reproduced 72 h after transfection. Depletion of FAM40B (72 h after siRNA transfection) additionally resulted in a cell spreading defect on Matrigel-coated plastic, which could cause or be due to the adhesion defect. Further experiments need to be done to tease out how these processes affect each other. Does spreading contribute to adhesion or vice versa, or do both processes reinforce each other?

The reduction in Rac1 activity observed in FAM40B-depleted cells could explain the spreading phenotype as Rac1 has been shown to mediate cell spreading by extension of a broad lamellipodium around the cell edge (Ridley et al., 1992). Interestingly, several members of the STRIPAK complex have been shown to be linked to focal adhesion proteins. Depletion of STK24 leads to a decrease in paxillin phosphorylation at Y118 (Lu et al., 2006) while STK25 depletion leads to an increase in phosphorylation of FAK at Y861 (Chen and

Cho, 2011). Paxillin phosphorylation at Y118 has been linked to integrin activation (Nakamura et al., 2000). Cell adhesion and integrin clustering leads to FAK autophosphorylation and subsequent recruitment of Src kinase which in turn phosphorylates FAK Y861 (Calalb et al., 1996). Additionally, CCM3 can interact with paxillin (Li et al., 2010). These data raise further possibilities as to how the FAM40 proteins may mediate cell adhesion and/or spreading. These roles in mediating cell adhesion could also be behind FAM40 effects on cell migration as the dynamic turnover of cell-substrate adhesions is needed during cell migration (Ridley et al., 2003). Both FAM40A and FAM40B were present in F-actin-rich protrusions where multiple adhesion proteins are localised. Vinculin (results not shown), paxillin (Vega et al., 2012) and β1-integrin (Reymond et al., 2012) are present at these protrusions in PC3 cells. Hence, they are ideally placed to regulate aspects of protrusion and/or adhesion at the leading edge that could affect cell migration. It would be interesting to determine if FAM40A and/or FAM40B can themselves act as adhesion molecules as results presented in chapter 3 (section 3.2.3) suggest that they could be transmembrane proteins.

In summary, these results suggest that the FAM40 proteins could play a role in cancer progression by regulating cell adhesion and migration. Furthermore, the FAM40 proteins may act via members of the STRIPAK complex in mediating their functions in PC3 cells. Future experiments should attempt to uncover these potential functional links.

5 FAM40 function in endothelial cells

5.1 Introduction

Along with FAM40A and FAM40B, CCM3 and all members of the GCKIII kinase family are components of the STRIPAK complex (Goudreault et al., 2009). In addition, data presented in this thesis demonstrate that both FAM40 proteins can interact with CCM3, STK25 and MST4 (section 3.2.1), and are substrates for the MST4 enzyme (section 3.2.8). FAM40A has also been shown to bind to STK24 (Goudreault et al., 2009). This connectivity as a result of protein interactions and phosphorylation suggests a link between the functions of CCM3/GCKIII kinases and the FAM40 proteins. The CCM3-GCKIII signalling axis has been shown to be important for the maintenance of endothelial junction integrity by reducing RhoA activity and the associated increase in stress fibres (Zheng et al., 2010). CCM3-GCKIII signalling is also important for the development of the vascular network as determined by studies in zebrafish (Yoruk et al., 2012; Zheng et al., 2010). CCM3 is one of the genes implicated in CCM pathogenesis and these studies offer insight into how altered CCM3 signalling leads to disease.

As proteins associated with CCM3 and the GCKIII kinases, FAM40A and FAM40B could have functions in the regulation of endothelial physiology. This chapter tests this hypothesis. HUVECs were used as a model system and an RNAi approach was primarily used to study gene function. Their effects on F-actin organisation, endothelial permeability and angiogenesis were assessed. All cases of CCM cannot be explained by the presence of mutations in one of the three identified CCM genes (CCM1, CCM2 and CCM3). In addition, variations are seen in different familial forms of CCM, suggesting that there might be additional genes that contribute to the CCM disease process (Riant et al., 2010). Hence, results presented in this chapter may also have relevance for the understanding of the genetic basis of CCM.

5.2 Results

5.2.1 Verification of siRNA-mediated knockdown of FAM40A and FAM40B in HUVECs

The functions of FAM40A and FAM40B were studied in HUVECs using RNAi-mediated knockdown of gene function. At least two individual siRNA oligonucleotides were used to target each gene. This was done to ensure that phenotypes observed upon gene expression knockdown were not solely due to off-target effects. A control non-targeting siRNA was used too. Antibodies capable of detecting endogenous FAM40 proteins were not available initially, and hence validation of siRNA-mediated knockdown of gene expression was performed by quantifying mRNA levels in control and siRNA-treated samples. Efficient reduction of FAM40A mRNA levels was observed 72 h after siRNA transfection (Figure 5.1A). Reduction of FAM40B mRNA levels could not be detected after siRNA treatment (Figure 5.1B) in contrast to experiments in PC3 cells (section 4.2.1). Multiple pairs of Q-PCR primers and conditions were attempted. It could be that FAM40B siRNAs act differently in endothelial cells compared to PC3 cells. For example, RNA nucleotides can cause translational arrest instead of mRNA degradation (Deleavey and Damha, 2012).

A commercially available antibody (Sigma-Aldrich) that became available subsequently was used to verify FAM40B protein depletion after treatment with siRNAs. HUVECs were transfected with siRNAs targeting FAM40A and FAM40B, and after 72 h protein from whole cell lysates were immunoblotted for FAM40B. A reduction in FAM40B protein levels was observed (Figure 5.1C). This result could only be reproduced twice due to the antibody failing to detect specific bands in subsequent experiments. Further experiments would have to be performed to optimise detection of FAM40B.

To show that siRNAs could reduce protein levels, knockdown of epitope-tagged proteins was tested. COS7 cells were double transfected with siRNAs targeting FAM40A or FAM40B and pHA-FAM40A or pHA-FAM40B. Immunoblotting for the HA tag using whole cell lysates showed that both FAM40A and FAM40B protein levels were efficiently knocked down (Figure 5.1D). Taken together these results suggest that the siRNA oligonucleotides are able to specifically target their intended genes.

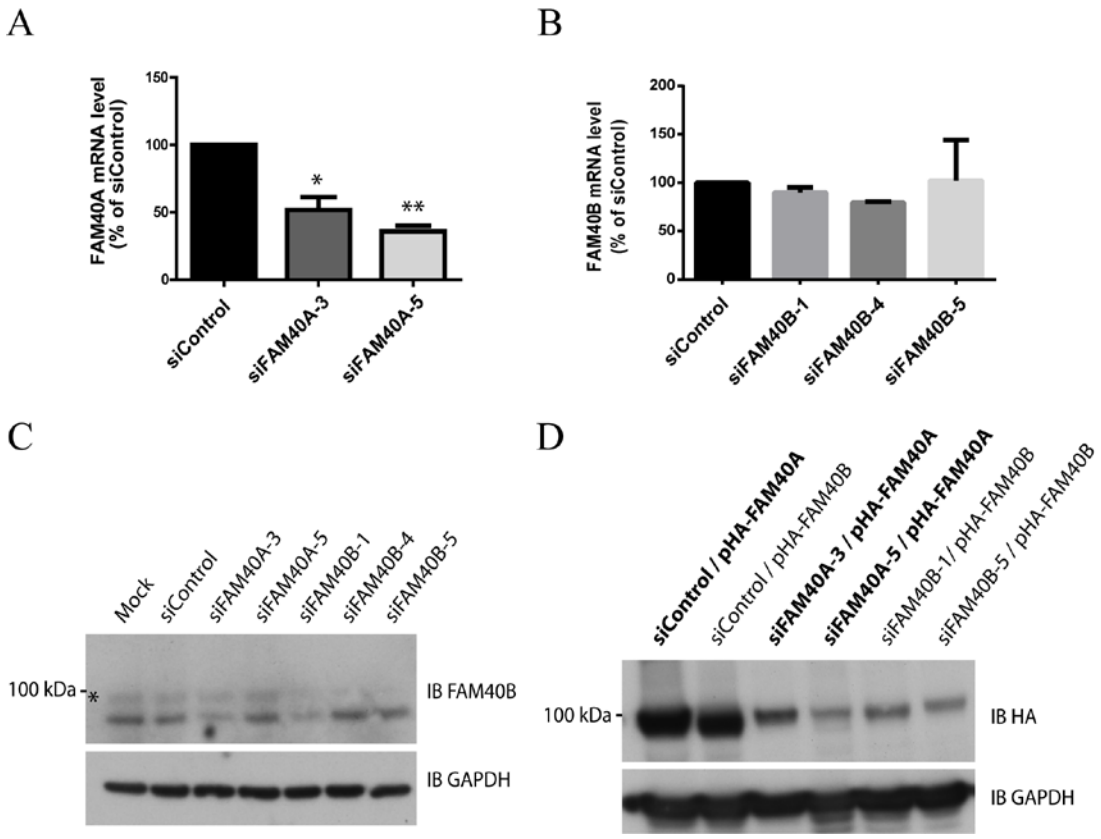

Figure 5.1 siRNA-mediated depletion of FAM40A and FAM40B
HUVECs were transfected with siRNAs targeting FAM40A or FAM40B. After 72 h, mRNA was extracted and used to synthesize cDNA. The amount of **(A)** FAM40A and **(B)** FAM40B cDNA was determined by quantitative PCR. Data are normalised to GAPDH cDNA levels. Data in **(A)** are the mean of 3 independent experiments ± SEM. Data in **(B)** are the mean of 2 independent experiments ± SD. * $p < 0.05$, ** $p < 0.01$ compared to siControl determined by Student's t-test. **(C)** Representative immunoblot of HUVECs at 72 h after transfection with indicated siRNAs (n=2). Cell lysates were immunoblotted for FAM40B and GAPDH as a loading control. The asterisk indicates signal corresponding to FAM40B protein. **(D)** COS7 cells were double transfected with siRNAs targeting FAM40A or FAM40B and pHA-FAM40A or pHA-FAM40B. Cell lysates were immunoblotted for the HA epitope, and GAPDH as a loading control. Results in **(D)** are representative of 3 independent experiments.

5.2.2 The FAM40 proteins do not affect HUVEC migration

Depletion of FAM40B in PC3 cells results in a migration defect (section 4.2.4). In addition, other members of the STRIPAK complex have been suggested to regulate cell migration by controlling Golgi orientation and organisation (Fidalgo et al., 2010; Kean et al., 2011). Migration of endothelial cells is an essential part of vascular development (Potente et al., 2011) and hence is relevant when considering the basis of CCM. As the FAM40 proteins could be functionally linked to CCM3, their effects on endothelial cell migration were tested.

Single cell random migration assays like those carried out with PC3 cells are not physiologically relevant as endothelial cells do not usually exist individually in the body. Hence, the ORIS assay (described in section 2.3.7.2) was used as it provides a better representation of endothelial physiology during processes such as wound healing. HUVECs were transfected with siRNAs targeting FAM40A or FAM40B and assessed for their capacity to migrate into a central annular migration zone in the ORIS plate. FAM40A or FAM40B depletion did not alter migration (Figure 5.2).

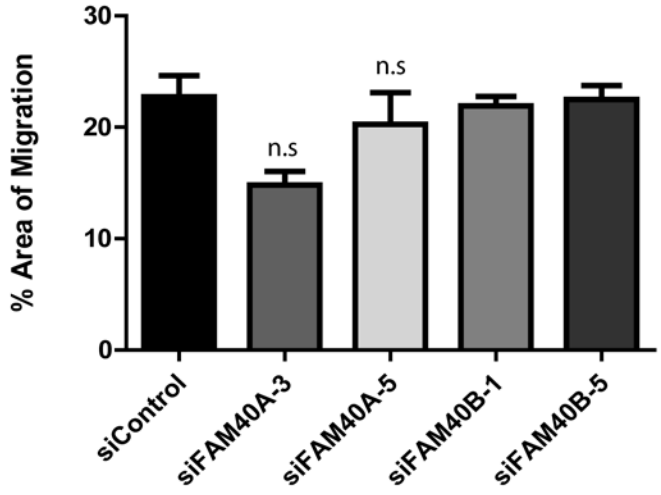

Figure 5.2 Depletion of the FAM40 proteins does not affect HUVEC migration in the ORIS assay

HUVECs were transfected with siRNA targeting FAM40A or FAM40B. After 24 h cells were harvested and seeded onto fibronectin-coated ORIS plates with seeding stoppers. 24 h after cell seeding, the stoppers were removed and the capacity of the cells to migrate was quantified by measuring the area of the central, annular 'detection' zone obscured in 24 h. The graph shows the mean of data from 3 independent experiments for siFAM40A and 2 independent experiments for siFAM40B. Error bars indicate SD values. Student's t-test showed no statistical significance of siFAM40A compared to siControl.

5.2.3 Depletion of FAM40A and FAM40B in HUVECs increases stress fibres

Knockdown of CCM3 expression in endothelial cells results in an increase in stress fibres (Zheng et al., 2010). This function of CCM3 in regulating stress fibres and contractility has been proposed to be behind its involvement in CCM. Hence, the effect of the FAM40 proteins on stress fibres and endothelial junctions was tested. HUVECs were transfected with siRNAs targeting FAM40A or FAM40B and stained for F-actin and VE-cadherin (Figure 5.3A). Control cells exhibited enriched F-actin staining at cell-cell boundaries. These sites were not continuous along cell-cell junctions. Control cells contained few stress fibres traversing the length of the cell. However, a number of stress fibres were present proximal to the cell boundaries. VE-cadherin staining revealed that junctions between adjacent control cells largely occurred as linear, continuous structures. Adjacent cells overlapped in certain regions indicated by a web-like, reticular VE-cadherin staining pattern (Fernandez-Martin et al., 2012).

Depletion of both FAM40A and FAM40B resulted in an increase in stress fibres that traversed the length of the cell (Figure 5.3A and B). The percentage of cells with higher stress fibre content was increased upon FAM40 knockdown (Figure 5.3C). No observable changes to cortical F-actin were observed. VE-cadherin staining revealed regions where cell-cell junctions were discontinuous after FAM40 depletion (prominent with FAM40B depletion (Figure 5.3A)). This occurred at sites where the direction of the stress fibres was perpendicular to the cell edge, and could be indicative of impaired barrier function. Double knockdown of FAM40A and FAM40B resulted in an increase in stress fibres too (Figure 5.4), but it was not higher than single knockdown (Figure 5.4B). Efficiency of siRNA-mediated knockdown of gene expression was not determined in cells double transfected with siRNAs targeting FAM40A and FAM40B, and would have to be performed in future experiments.

In summary, these results indicate that the FAM40 proteins regulate stress fibres in endothelial cells, and suggest a possible functional link between CCM3 and the FAM40 proteins.

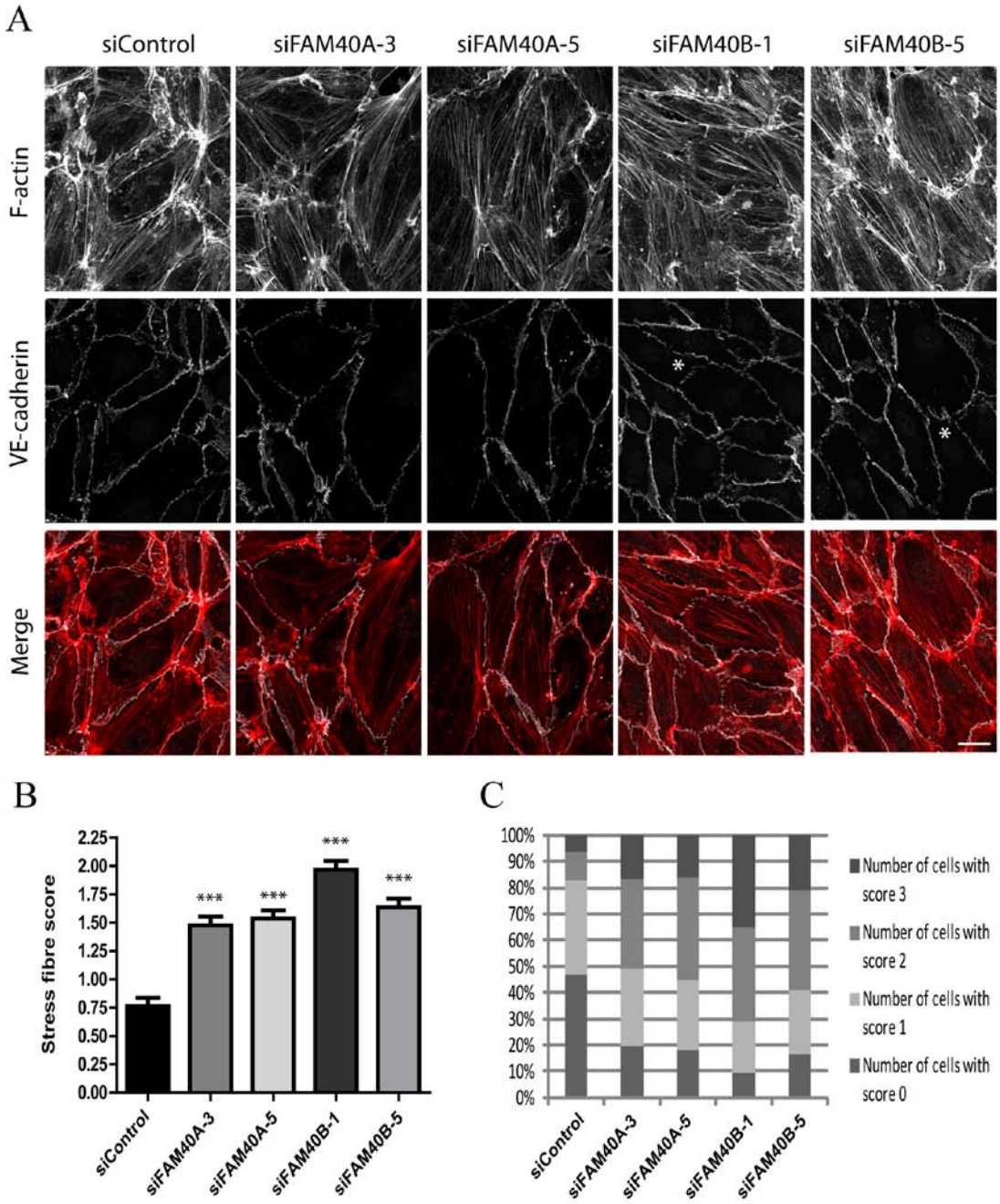

Figure 5.3 FAM40 knockdown increases the number of stress fibres

(A) HUVECs were transfected with siRNAs targeting FAM40A or FAM40B and seeded onto fibronectin-coated glass coverslips to form confluent monolayers. 72 h after transfection cells were fixed and stained for F-actin and VE-cadherin to visualise junctions. Images are compressed stacks of 10-15 z-sections. Scale bar = 40 µm. Asterisks indicate discontinuous adherens junctions. **(B)** Quantification was done by assigning a score to each cell based on the stress fibre content in the centre of the cell; 0 – few or no stress fibres, 1 – upto 50% of the cell centre contains stress fibres, 2 – 50% to 75% of the cell centre contains stress fibres, 3 – greater than 75% of the cell centre contains stress fibres. Results shown are from at least 150 cells per condition from 3 independent experiments. Error bars depict SEM values. *** $p < 0.001$ compared to siControl determined by Student's t-test. The graph in **(C)** represents this data as percentage distributions.

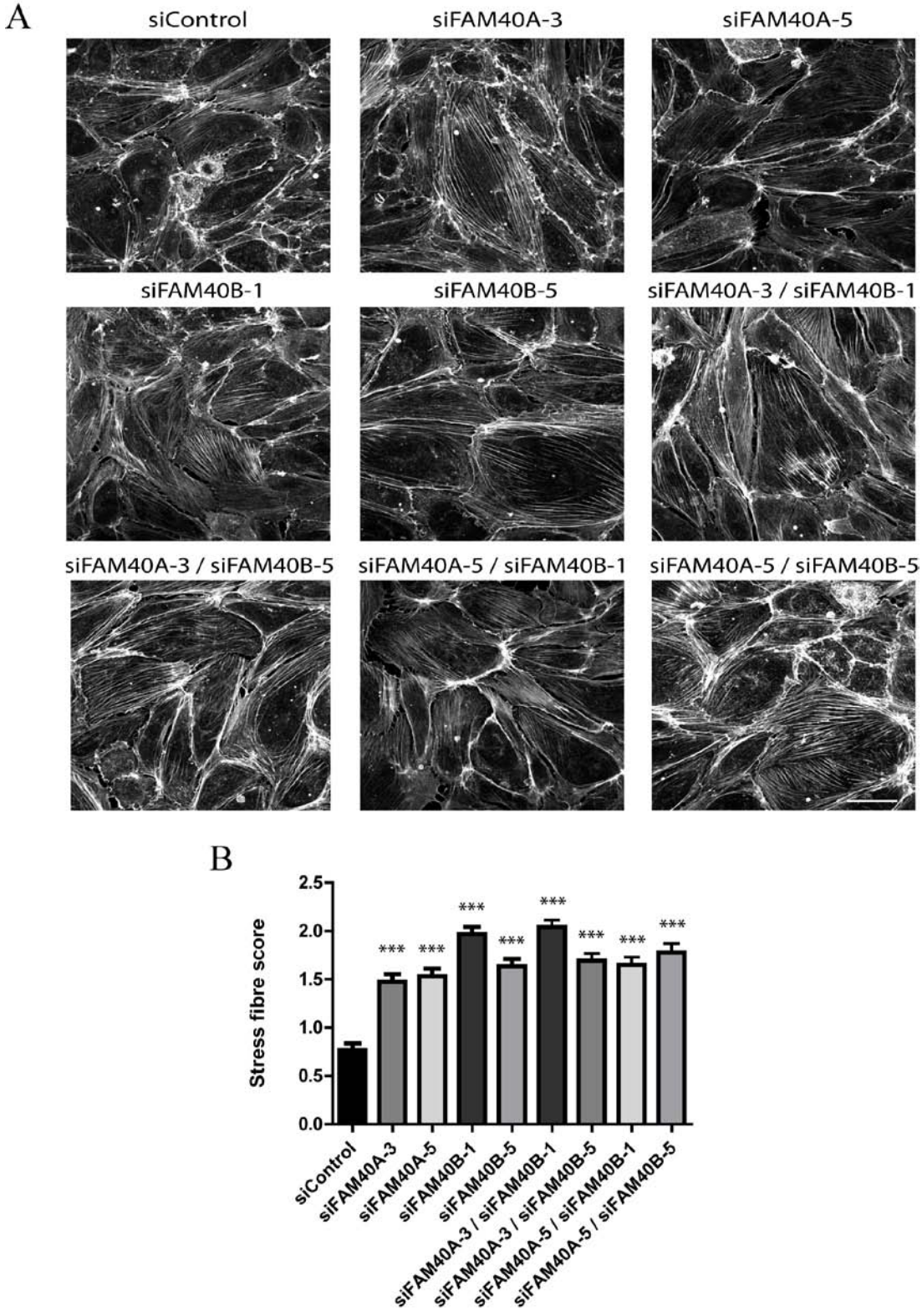

Figure 5.4 Double knockdown of FAM40A and FAM40B increases the number of stress fibres

(A) HUVECs were transfected with siRNAs targeting FAM40A and/or FAM40B as indicated and seeded onto fibronectin-coated glass coverslips to form confluent monolayers. 72 h after transfection cells were fixed and stained for F-actin. Images are compressed stacks of 10-15 z-sections. Scale bar = 40 µm. **(B)** Quantification was done by assigning a score to each cell

based on the stress fibre content in the centre of the cell; 0 – few or no stress fibres, 1 – upto 50% of the cell centre contains stress fibres, 2 – 50% to 75% of the cell centre contains stress fibres, 3 – greater than 75% of the cell centre contains stress fibres. Results shown are from at least 150 cells per condition from 3 independent experiments. Error bars depict SEM values. *** $p < 0.001$ compared to siControl determined by Student's t-test.

5.2.4 Effect of FAM40 knockdown on the permeability of HUVEC monolayers

Stress fibres are linked to adherens junctions in confluent endothelial cells. This provides a mechanical linkage between the actin cytoskeleton and cell-cell junctions, and suggests how contractile force within cells can be transmitted to cell junctions (Millan et al., 2010). It was hypothesised that the increase in stress fibres induced upon FAM40 knockdown leads to increased tensile force, and subsequently could cause a physical breakdown of junctions. Furthermore, depletion of CCM3 and STK25 leads to an increase in endothelial permeability and is associated with an increase in stress fibres (Zheng et al., 2010). Hence, junction function was measured by assessing the permeability of confluent HUVEC monolayers upon FAM40 knockdown. A transwell assay was used in which the amount of FITC-dextran that passes across an endothelial monolayer was used as a readout of endothelial permeability (Figure 5.5A). FAM40B depletion led to an increase in endothelial permeability (Figure 5.5B). However, no significant effects were observed when FAM40A was depleted at 40 min or 80 min after addition of FITC-dextran. These results imply that FAM40B but not FAM40A is needed for the maintenance of HUVEC monolayer integrity.

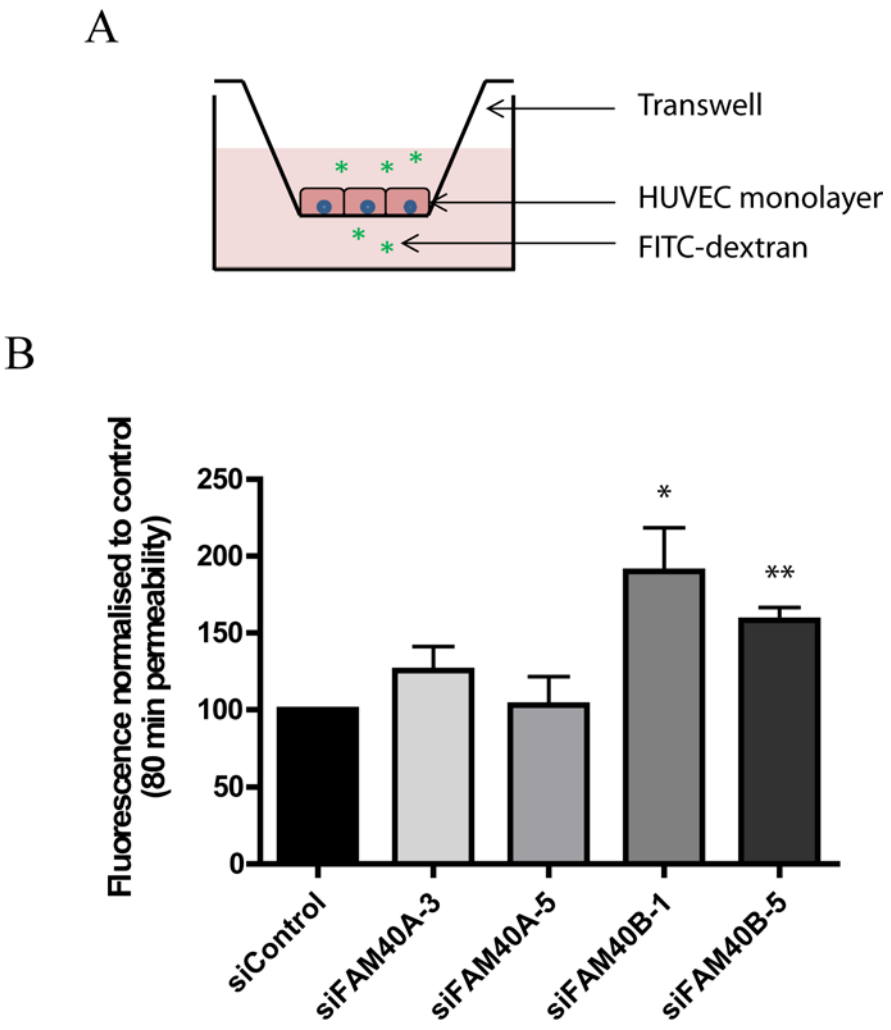

Figure 5.5 FAM40B knockdown increases the permeability of confluent HUVEC monolayers

A transwell permeability assay was used to study effects on cell permeability upon FAM40A and FAM40B depletion **(A)**. HUVECs were depleted of FAM40A and FAM40B using siRNAs and plated at confluency onto transwell inserts. 72 h after transfection, FITC-dextran was added to the upper chamber. After a further 80 min the fluorescence of media in the lower chamber was determined as a measure of permeability. **(B)** shows permeability normalised to siControl (siControl=100). Data are means of 3 independent experiments for siFAM40A and 5 independent experiments for siFAM40B. Error bars indicate SEM values. * $p < 0.05$, ** $p < 0.01$ compared to siControl determined by Student's t-test.

5.2.5 The increase of stress fibres upon FAM40 knockdown is reduced by treatment with ROCK inhibitor and C3 transferase

The Rho-ROCK signalling axis is important for stress fibre formation (Hall and Nobes, 2000). Activated ROCK increases the pool of phosphorylated MLC and causes the assembly of actomyosin filaments (Watanabe et al., 2007). Importantly, all three Rho proteins (RhoA, RhoB and RhoC) can induce the formation of stress fibres in endothelial cells (Gottesbuhren et al., 2013). To determine whether Rho-ROCK signalling mediates induction of stress fibres upon FAM40 depletion, cells were treated with the ROCK inhibitor H-1152 and C3 transferase. The Rho inhibitor C3 transferase is commonly used to study Rho protein function and inhibits Rho proteins by ADP-ribosylation. It specifically inhibits RhoA, RhoB and RhoC and does not target other related GTPases such as Rac1 or Cdc42 (Aktories and Barbieri, 2005).

Treatment with H-1152 reduced the FAM40 depletion-induced increase in stress fibres (Figure 5.6A and B). Different treatment times were tested and 10 min was found to be the optimal time-point. Incubation for longer periods resulted in severe effects on cell morphology and F-actin organisation, while incubation for a shorter time was not sufficient to affect the FAM40 depletion-induced stress fibre response.

Treatment with membrane permeable C3 transferase decreased stress fibres induced by FAM40 depletion (Figure 5.7). The concentration and incubation time used were that described by Cytoskeleton (http://www.cytoskeleton.com/) to yield a ‘moderate phenotype’ (cells retain a well spread morphology in spite of stress fibre disruption). While both H-1152 and C3 transferase treatment resulted in a loss of stress fibres, important differences between the two treatments exist. C3 transferase treatment relatively conserved cell morphology. However, a decrease in F-actin content was observed on C3 transferase treatment. This could be attributed to Rho proteins having other effects in addition to acting on ROCKs. Taken together these results show that inhibition of the Rho-ROCK signalling pathway reduces the induction of stress fibres and associated cell contractility that occurs upon FAM40 depletion.

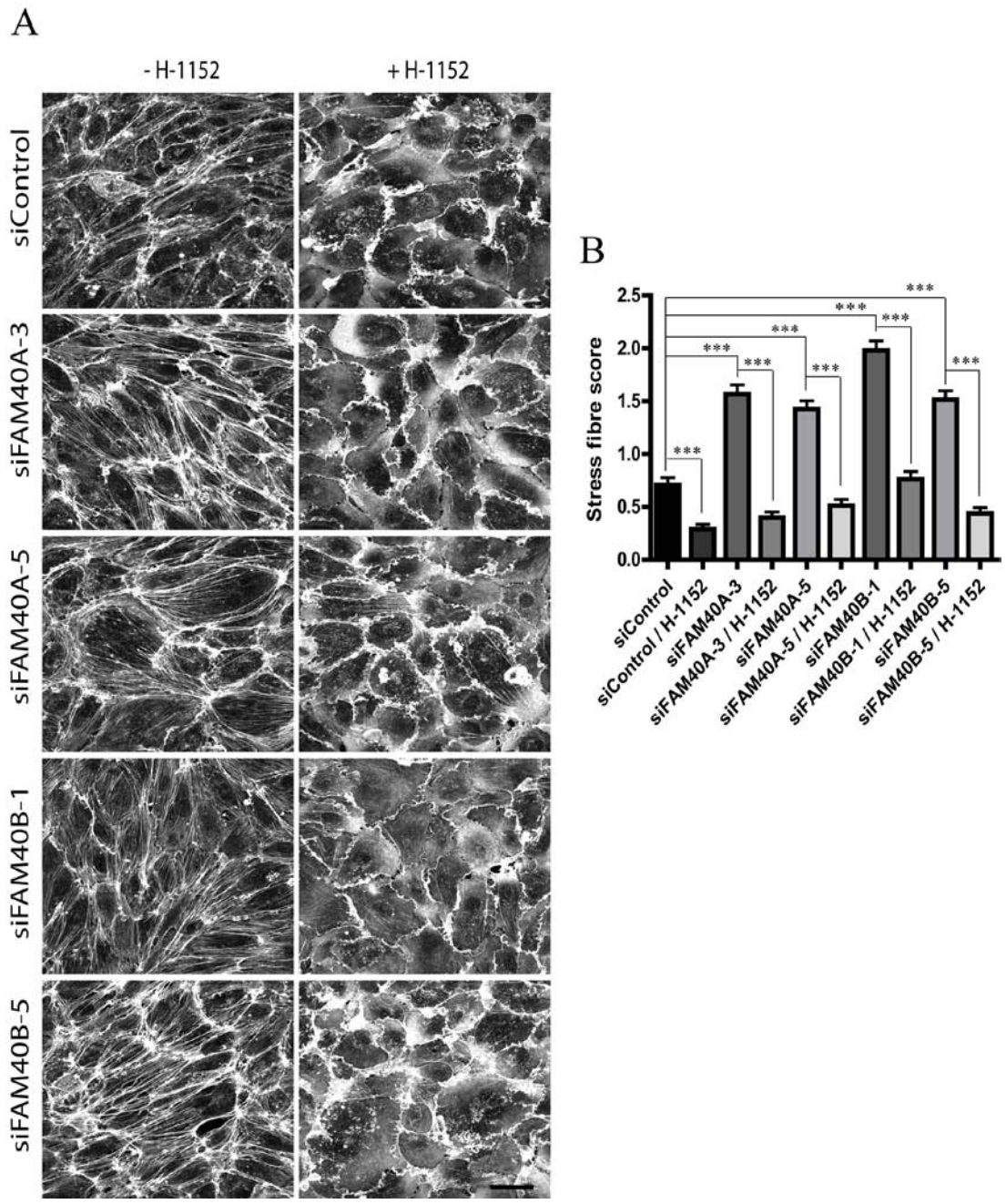

Figure 5.6 Treatment with the ROCK inhibitor H-1152, reduces the increase of stress fibres observed upon FAM40 depletion

(A) HUVECs were transfected with siRNAs targeting FAM40A or FAM40B and seeded onto fibronectin-coated glass coverslips to form confluent monolayers. 72 h after transfection cells were treated with 5 µM H-1152 for 10 min, after which they were fixed and stained for F-actin. Images are compressed stacks of 10-15 z-sections. Scale bar = 40 µm. **(B)** Quantification was done by assigning a score to each cell based on the stress fibre content in the centre of the cell; 0 – few or no stress fibres, 1 – upto 50% of the cell centre contains stress fibres, 2 – 50% to 75% of the cell centre contains stress fibres, 3 – greater than 75% of the cell centre contains stress fibres. Results shown are from at least 150 cells per condition from 3 independent experiments. Error bars depict SEM values. *** $p < 0.001$ determined by Student's t-test.

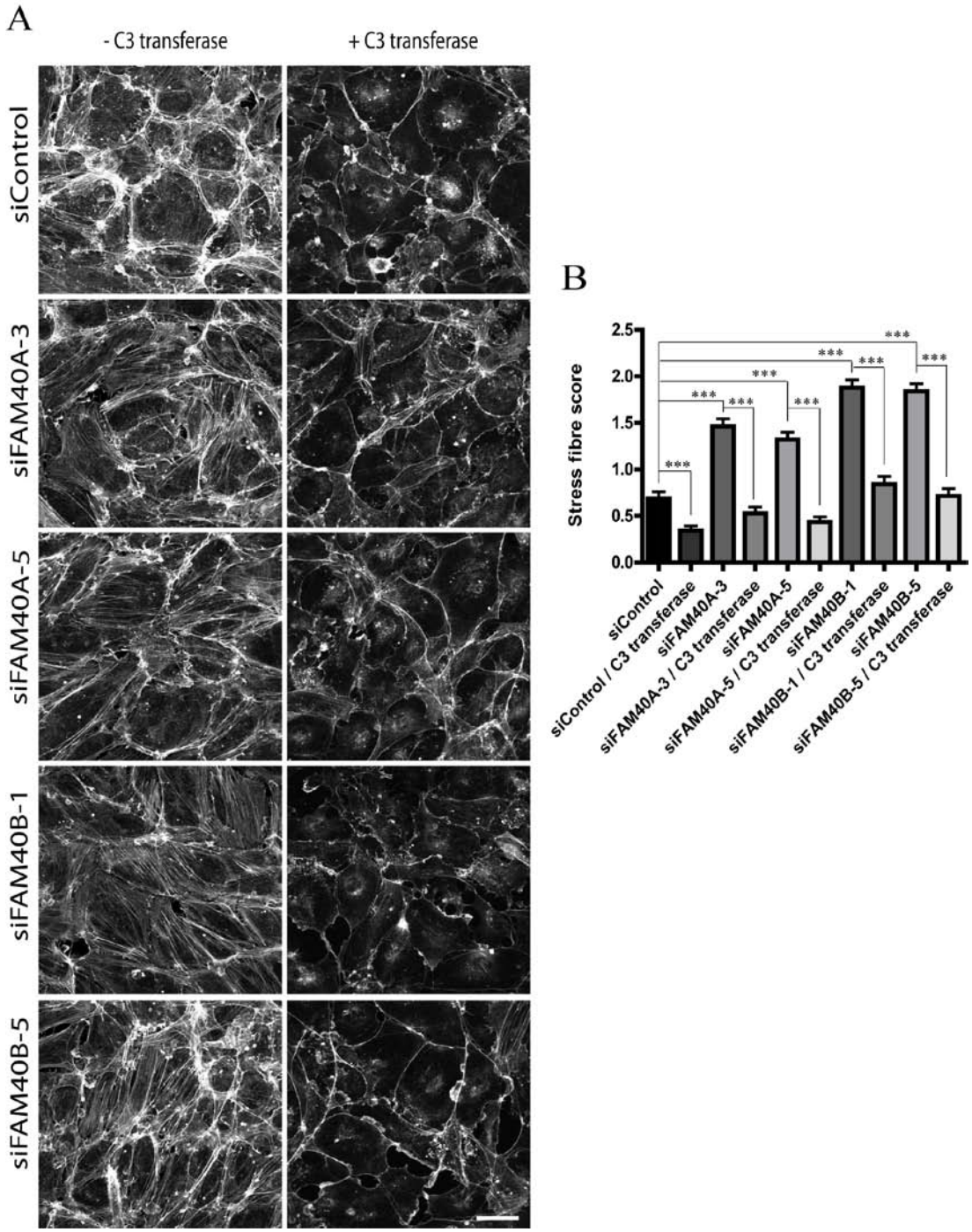

Figure 5.7 Treatment with C3 transferase reduces the increase of stress fibres observed upon FAM40 depletion

(A) HUVECs were transfected with siRNAs targeting FAM40A or FAM40B and seeded onto fibronectin-coated glass coverslips to form confluent monolayers. 72 h after transfection cells were treated with 4 µg/ml C3 transferase for 2 h after which they were fixed and stained for F-actin. Images are compressed stacks of 10-15 z-sections. Scale bar = 40 µm. **(B)** Quantification was done by assigning a score to each cell based on the stress fibre content in the centre of the cell; 0 – few or no stress fibres, 1 – upto 50% of the cell centre contains stress fibres, 2 – 50% to 75% of the cell centre contains stress fibres, 3 – greater than 75% of the cell centre contains stress fibres. Results shown are from at least 150 cells per condition from 3 independent experiments. Error bars depict SEM values. *** $p < 0.001$ determined by Student's t-test.

5.2.6 Effect of FAM40 depletion on RhoA and Rac1 activity

An increase in RhoA activity is known to cause induction of stress fibres (Ridley and Hall, 1992). Rac1 too has been shown to contribute to stress fibre assembly (Ridley et al., 1992). Furthermore, both RhoA and Rac1 are important for mediating endothelial cell permeability (Wojciak-Stothard et al., 2001). The CCM proteins regulate RhoA activity in endothelial cells (Fischer et al., 2013), while previously described results show that FAM40B knockdown in PC3 cells affects Rac1 activity (section 4.2.5). These facts prompted experiments to determine if either RhoA or Rac1 activity was affected upon FAM40 depletion in HUVECs.

HUVECs were transfected with siRNAs targeting the FAM40 proteins and whole cell lysates were used in biochemical pulldown assays to determine levels of active RhoA and Rac1. RhoA activity was found to be variable within and between individual experiments and no reproducible effect was observed. An example blot is shown in Figure 5.8A. Further experiments to optimise experimental conditions could be performed. However, with the data obtained it was concluded that FAM40 depletion does not affect RhoA activity. Furthermore, depletion of FAM40A or FAM40B did not result in significant changes to Rac1 activity (Figure 5.8B). In two out of five experiments, a reduction in Rac1-GTP levels on FAM40B depletion was observed. In summary, these data suggest that FAM40A and FAM40B regulate stress fibre formation and endothelial permeability by mechanisms other than the modulation of global RhoA and Rac1 activity.

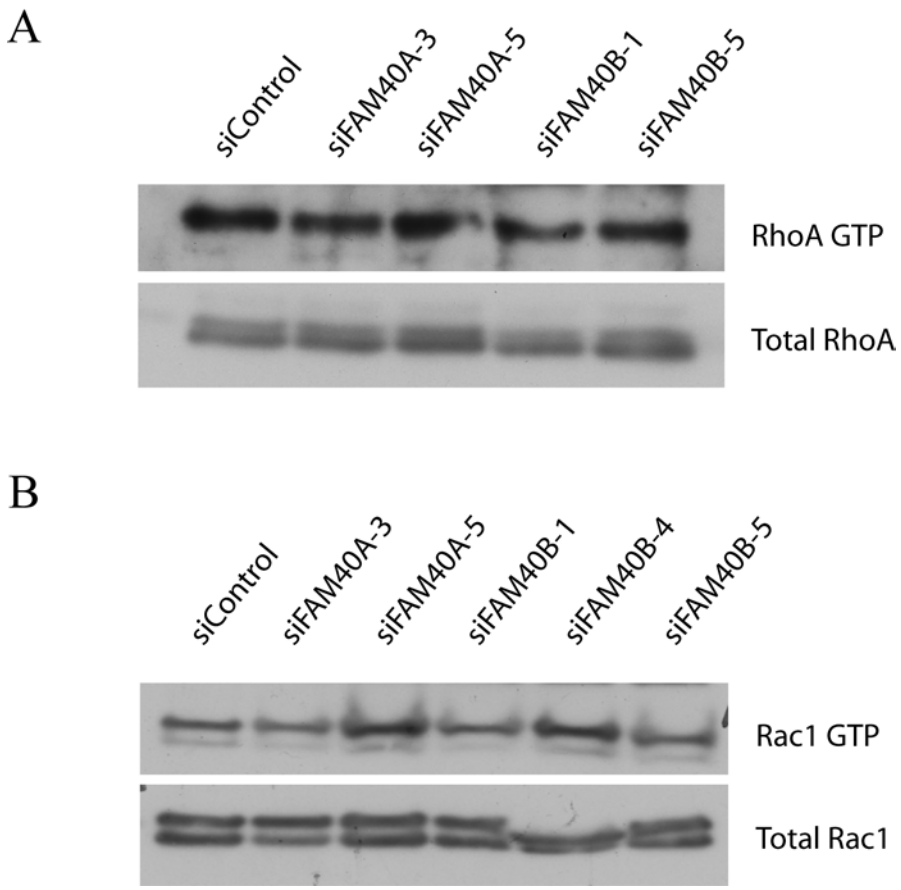

Figure 5.8 FAM40 knockdown does not affect RhoA or Rac1 activity
HUVECs were transfected with siRNA targeting FAM40A or FAM40B. **(A)** After 72 h cells were lysed and whole cell lysates used in a GST- RBD pulldown assay to determine levels of GTP-loaded RhoA (n=3). An example immunoblot for total and GTP-loaded RhoA is shown. **(B)** After 72 h cells were lysed and whole cell lysates used in a GST-PBD pulldown assay to determine levels of GTP-loaded Rac1 (n=5). An example immunoblot for total and GTP-loaded Rac1 is shown.

5.2.7 Effect of FAM40A and FAM40B depletion on p-MLC2

The phosphorylation level of MLC2 is an indication of cell contractility and is associated with the assembly of stress fibres. MLC2 lies downstream of Rho-ROCK and activated ROCK phosphorylates MLC phosphatase and MLC2 at Serine 19. MLC can also be phosphorylated by MLCK at Serine 19 and Threonine 18 (Watanabe et al., 2007). To assess if phosphorylation of MLC2 is affected by FAM40 proteins, lysates from HUVECs depleted of FAM40A and FAM40B were probed for p-MLC2 (serine 19/threonine 18). Neither FAM40A nor FAM40B knockdown resulted in a reproducible effect on p-MLC2 (S/T) levels (Figure 5.9C and D). To ensure that the cells were responsive to p-MLC2 changes, a control experiment was performed in which HUVECs were treated with thrombin which increases p-MLC2 levels (van Nieuw Amerongen et al., 1998) (Figure 5.9A and B). In summary, depletion of FAM40A or FAM40B does not result in changes to p-MLC2 levels, and so MLC2 phosphorylation does not explain the induction of stress fibres.

To complement this analysis, the localisation and distribution of p-MLC2 in FAM40-depleted cells was assessed by immunofluorescence. This experiment was done only twice using one siRNA each for FAM40A and FAM40B, and hence, a definitive conclusion cannot be reached. Moreover, it is difficult to use these images to comment on changes in total p-MLC2 levels as the staining pattern was largely grainy and diffuse. However, these images indicated that p-MLC2 is enriched along stress fibres (Figure 5.10). This is consistent with p-MLC2 causing contractility by stimulating cross-linking of myosin II with actin filaments (Watanabe et al., 2007).

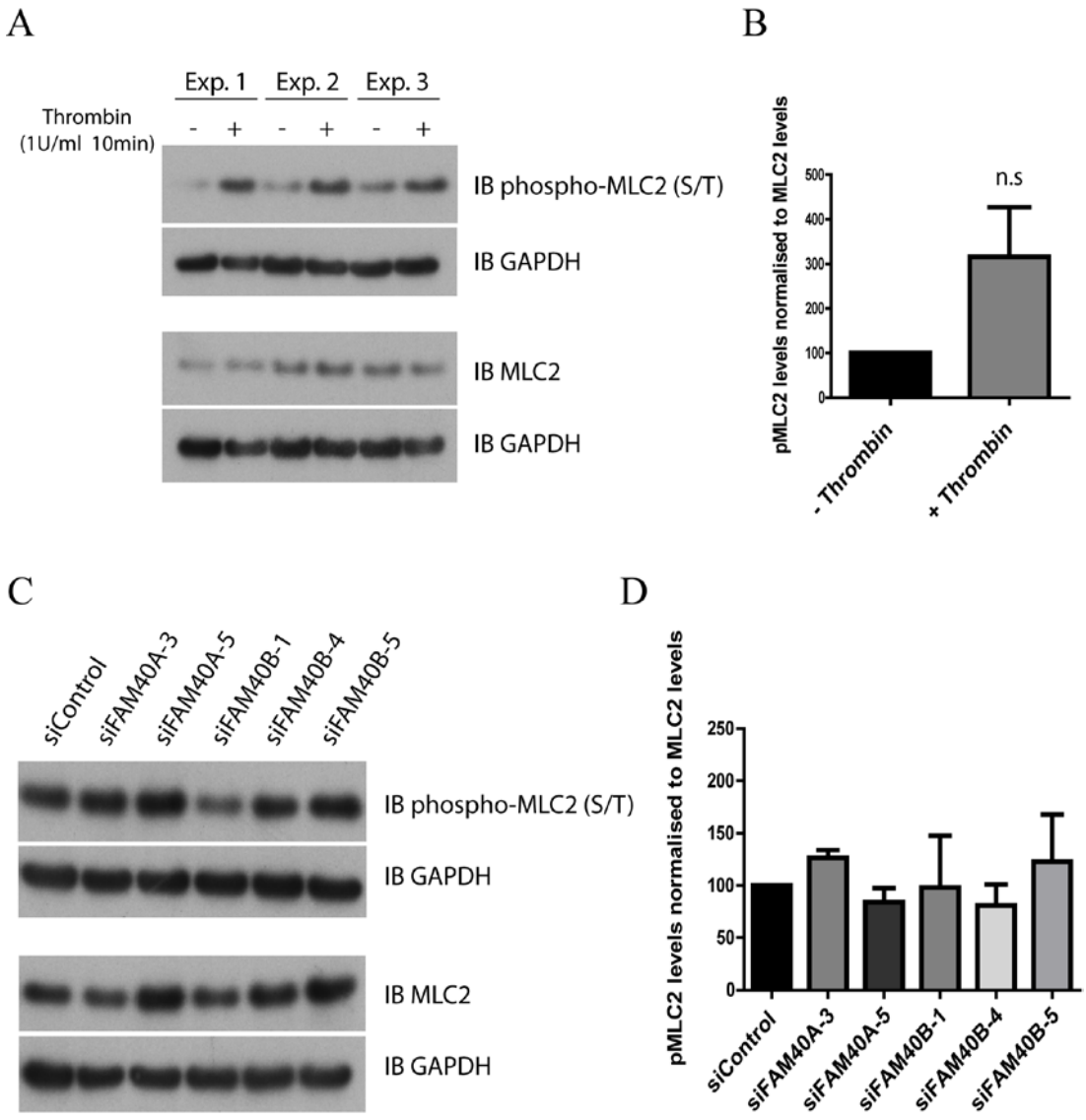

Figure 5.9 FAM40 knockdown does not affect levels of p-MLC2
(A) HUVECs treated with 1 U/ml thrombin for 10 min were used as a control for the p-MLC2 response of cells and immunoblot procedure. After thrombin treatment cells were lysed and lysates used to immunoblot for p-MLC2, MLC2 and GAPDH. **(B)** Quantification was done by first individually normalising p-MLC2 and MLC2 levels to GAPDH levels. The ratio of the normalised p-MLC2 level to the normalised MLC2 level was used as a measure of MLC2 phosphorylation. Data are the mean of 3 independent experiments ± SEM. Statistical significance was determined using Student's t-test. **(C)** HUVECs were transfected for siRNAs targeting FAM40A and FAM40B. 72 h after transfection, cells were lysed and lysates used to immunoblot for p-MLC2, MLC2 and GAPDH. Quantification shown in **(D)** was done as for the thrombin control experiment (described in **(B)**). Data are means of 3 independent experiments ± SEM. Student's t-test showed no statistical significance compared to siControl.

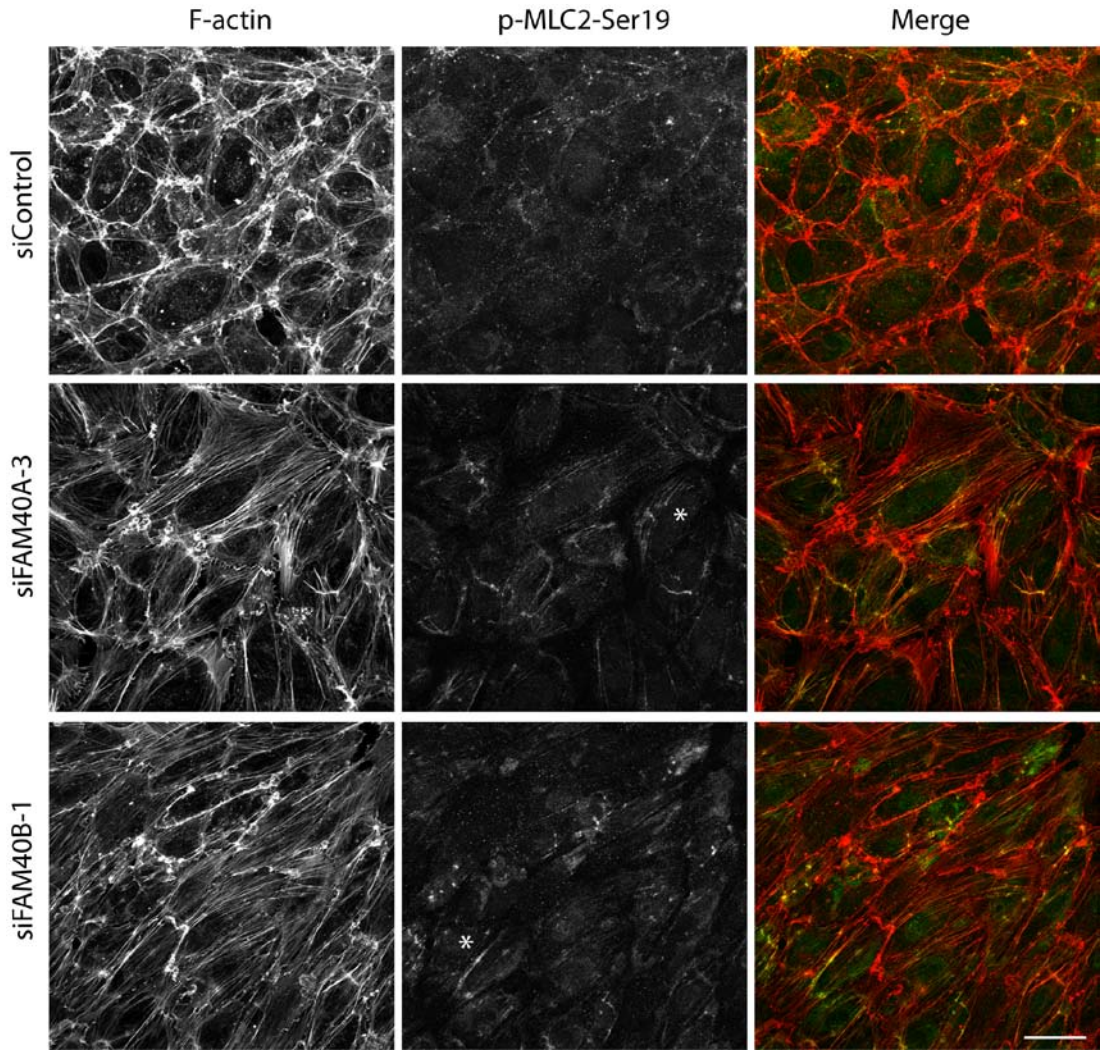

Figure 5.10 Immunofluorescence staining for p-MLC2 in FAM40-depleted HUVECs
HUVECs were transfected with siRNAs targeting FAM40A or FAM40B. 72 h after transfection cells were fixed and stained for p-MLC2 Ser19 and F-actin. Asterisks indicate regions were the p-MLC2 staining co-localises with stress fibres. Representative images from 2 independent experiments are shown. Images shown are compressed stacks of 10-15 z-sections. Scale bar = 40 µm.

5.2.8 The FAM40 proteins do not affect focal adhesion density

Focal adhesions are found at the ends of stress fibres in sub-confluent endothelial cells but few are present in confluent endothelial cells (Millan et al., 2010). Focal adhesions serve to tether stress fibres and are important for the transduction of contractile forces generated within the cell. A correlation is seen between Rho-induced stress fibre assembly and focal adhesion formation (Ridley and Hall, 1992). Contractility generated as a result of stress fibre induction has been suggested to promote focal adhesion assembly (Chrzanowska-Wodnicka and Burridge, 1996).

HUVECs depleted of FAM40A or FAM40B were grown at sub-confluence, and stained for the focal adhesion marker vinculin to assess changes to focal adhesion assembly. Stress fibre content in sub-confluent FAM40-depleted HUVECs was not quantified and would have to be performed in future experiments. However, it was observed that stress fibre induction upon FAM40 depletion was not as pronounced in sub-confluent cells as compared to confluent cells. Vinculin was excluded from the nucleus and exhibited a diffuse staining pattern in the perinuclear region. Additionally, punctate foci of vinculin staining were observed which correspond to cell-substrate adhesions. These puncta were commonly associated with the ends of stress fibres. A large fraction of the stress fibres were linked to vinculin foci at either end suggesting they are ventral stress fibres (Tojkander et al., 2012). No changes to focal adhesion density (number of vinculin puncta per cell normalised to total cell area) were observed on either FAM40A or FAM40B depletion (Figure 5.12). This result indicates that the increase in stress fibre content observed upon FAM40 depletion does not correlate with an increase in focal adhesion assembly as represented by focal adhesion density.

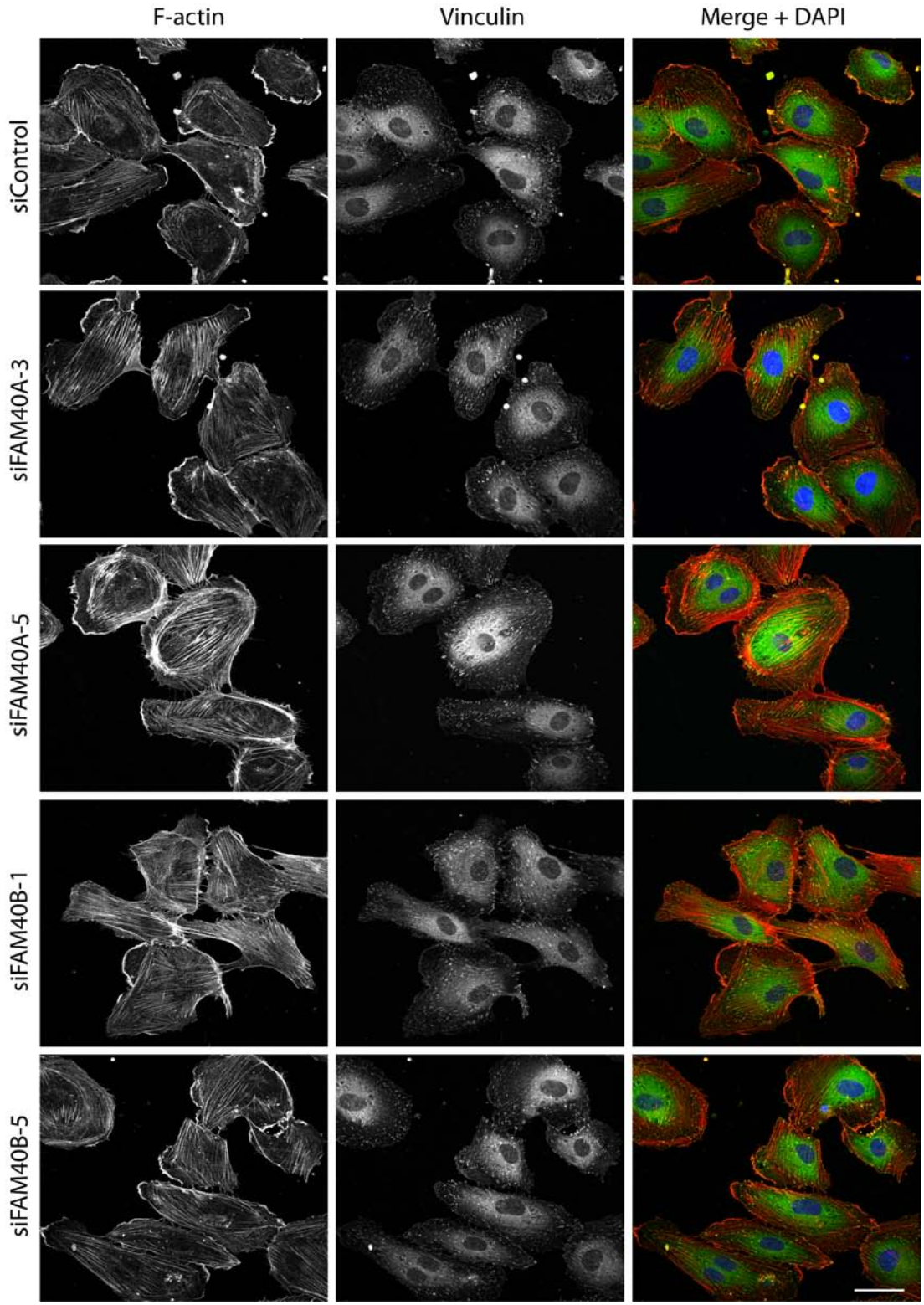

Figure 5.11 Visualising focal adhesions in FAM40-depleted HUVECs by vinculin staining

HUVECs were transfected with siRNAs targeting FAM40A or FAM40B. Cells were then seeded onto fibronectin-coated glass coverslips at sub-confluence. 72 h after transfection cells were fixed and stained for F-actin, vinculin and with DAPI to stain nuclei. Scale bar = 40 µm. Images are compressed stacks of 10-15 z-sections and are representative of 3 independent experiments.

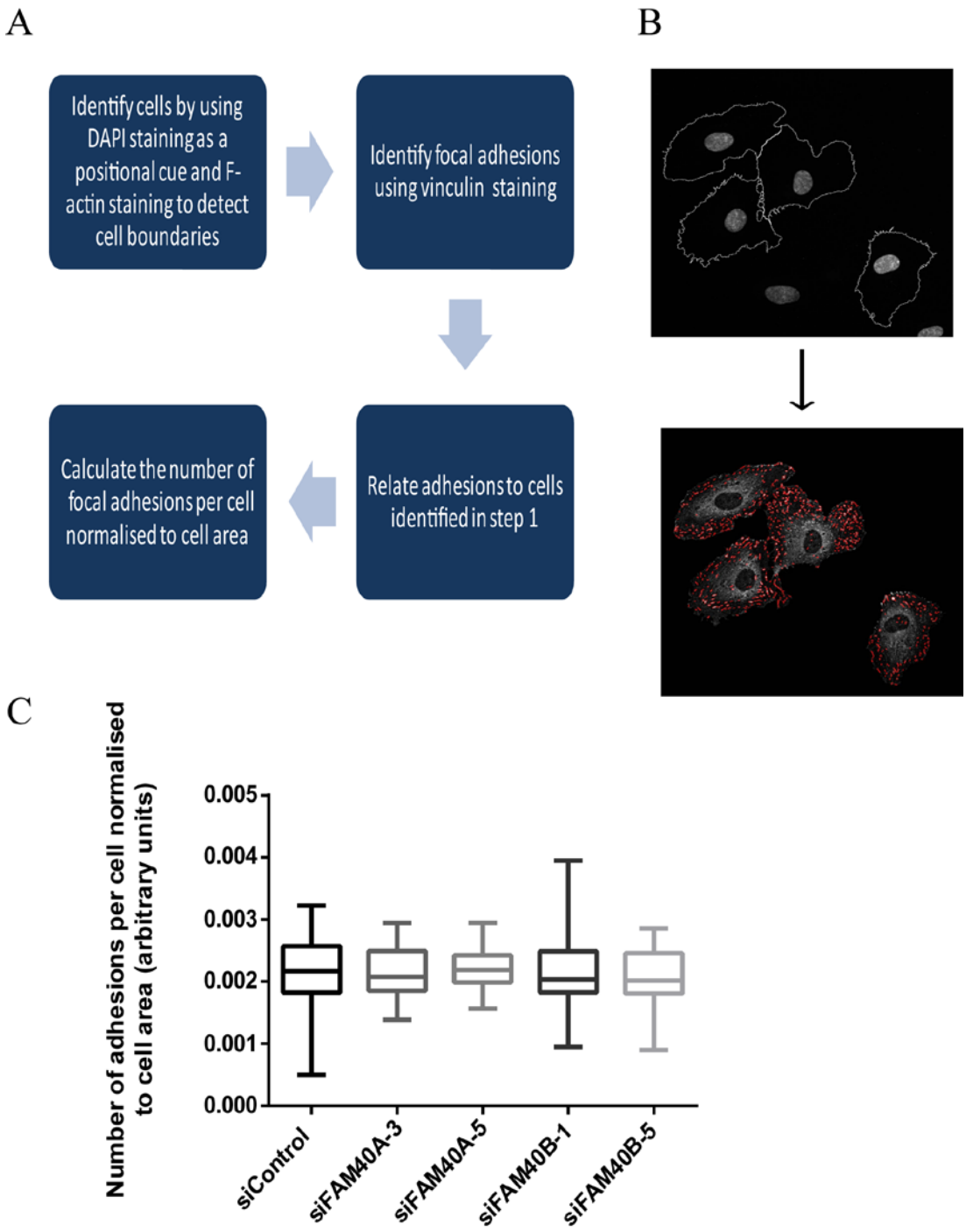

Figure 5.12 Quantification of focal adhesion density in FAM40-depleted HUVECs
(A) Schematic of the pipeline used to calculate focal adhesion density by the software Cell Profiler. DAPI and F-actin staining were used to locate individual cells while the vinculin staining was used to identify individual adhesions. These two parameters were used to link identified adhesions to a particular cell **(B)**. The graph in **(C)** shows the calculated focal adhesion density which is defined as the number of adhesions per cell normalised to total cell area. n≥ 24 cells per condition from 3 independent experiments. Boxes of box and whisker plots show median, 25th and 75th percentile. Whiskers show minimum to maximum values. Student's t-test showed no statistical significance compared to siControl.

5.2.9 The FAM40 proteins do not affect the levels of active or total β1-integrin

To substantiate the analysis performed on focal adhesion density on FAM40 depletion (section 5.2.8), the levels of total and active β1-integrin were assessed. Previous studies have implicated β1-integrin in CCM pathogenesis. ICAP1 (integrin cytoplasmic-associated protein 1) associates with the cytoplasmic region of β1-integrin and suppresses its function (Bouvard et al., 2003). CCM1 competitively binds to ICAP1, restoring β1-integrin function (Liu et al., 2013). As the FAM40 proteins are associated with a CCM protein, effects on β1-integrin function were investigated.

Sub-confluent FAM40-depleted HUVECs were stained with an antibody that specifically detects the activated form of β1-integrin (Figure 5.13A). Active β1-integrin localised to discrete structures in all regions of the cell. These structures commonly had an elongated morphology and many associated with the ends of stress fibres. No differences in the staining pattern could be observed upon FAM40 knockdown though a subset of cells did exhibit small variations in staining intensity. As this experiment was only performed twice, additional experiments would need to be carried out for quantification. FAM40 depletion did not alter the total levels of β1-integrin by immunoblotting (Figure 5.13B and C). In summary, these results suggest that the FAM40 proteins do not regulate the physiology of endothelial cells by modulating β1-integrin levels or activity.

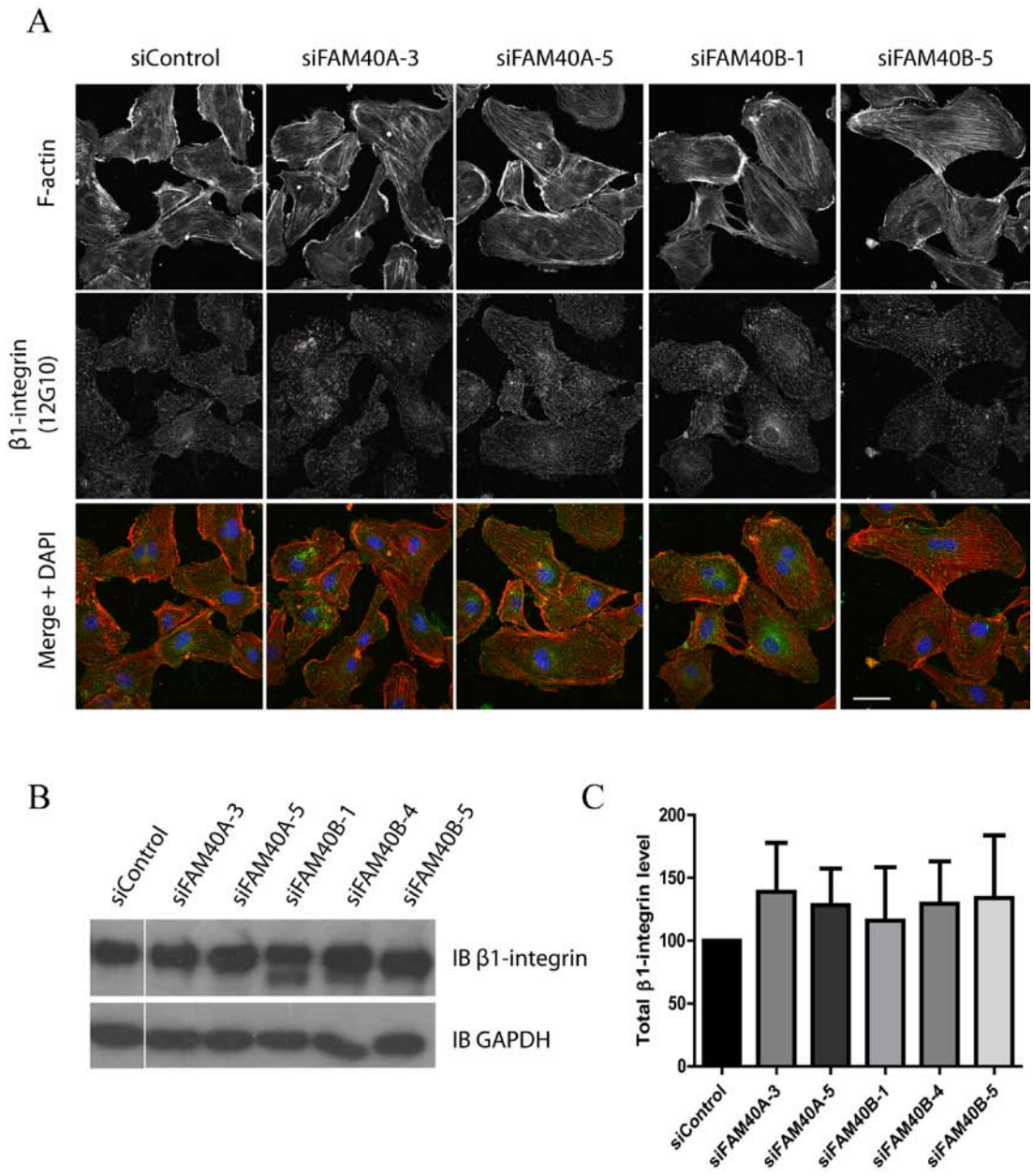

Figure 5.13 Depletion of the FAM40 proteins does not change levels of active or total β1-integrin

(A) HUVECs were transfected with siRNAs targeting FAM40A or FAM40B and seeded onto fibronectin-coated glass coverslips at sub-confluence. 72 h after transfection cells were fixed and stained for F-actin, active β1-integrin (12G10 antibody, Abcam) and with DAPI. Scale bar = 40 µm. Images are compressed stacks of 10-15 z-sections and are representative of 2 independent experiments. **(B)** Total β1-integrin levels on FAM40 depletion was assessed by western blot. 72 h after siRNA transfection, HUVECs were lysed and whole cell lysates used to immunoblot for total β1-integrin and GAPDH (loading control). An example immunoblot from 3 independent experiments is shown. Data in **(C)** show quantification of immunoblots normalised to siControl (siControl=100) and are the mean of 3 independent experiments ± SEM. Student's t-test showed no statistical significance compared to siControl.

5.2.10 Overexpression of FAM40A and FAM40B in HUVECs

The subcellular localisation of proteins can provide an indication of their function. HUVECs were transfected with expression vectors containing HA-FAM40A or HA-FAM40B. After 24 h, cells were stained for the HA epitope and F-actin. Suitable antibodies capable of staining endogenous protein were not available. This experiment also served to identify any cellular effects of FAM40 overexpression. Sub-confluent HUVECs exhibited membrane F-actin-rich protrusions (Figure 5.14A). Both FAM40A and FAM40B were enriched in these regions, and were excluded from the nucleus. Confluent HUVECs do not usually exhibit F-actin-rich membrane protrusions, and in these cells both FAM40A and FAM40B showed a diffuse localisation pattern (Figure 5.14B). Neither FAM40 protein was enriched at cell-cell junctions. No observable changes to VE-cadherin distribution and/or localisation were observed. In addition, no clear changes to F-actin organisation were observed in either sub-confluent or confluent cells.

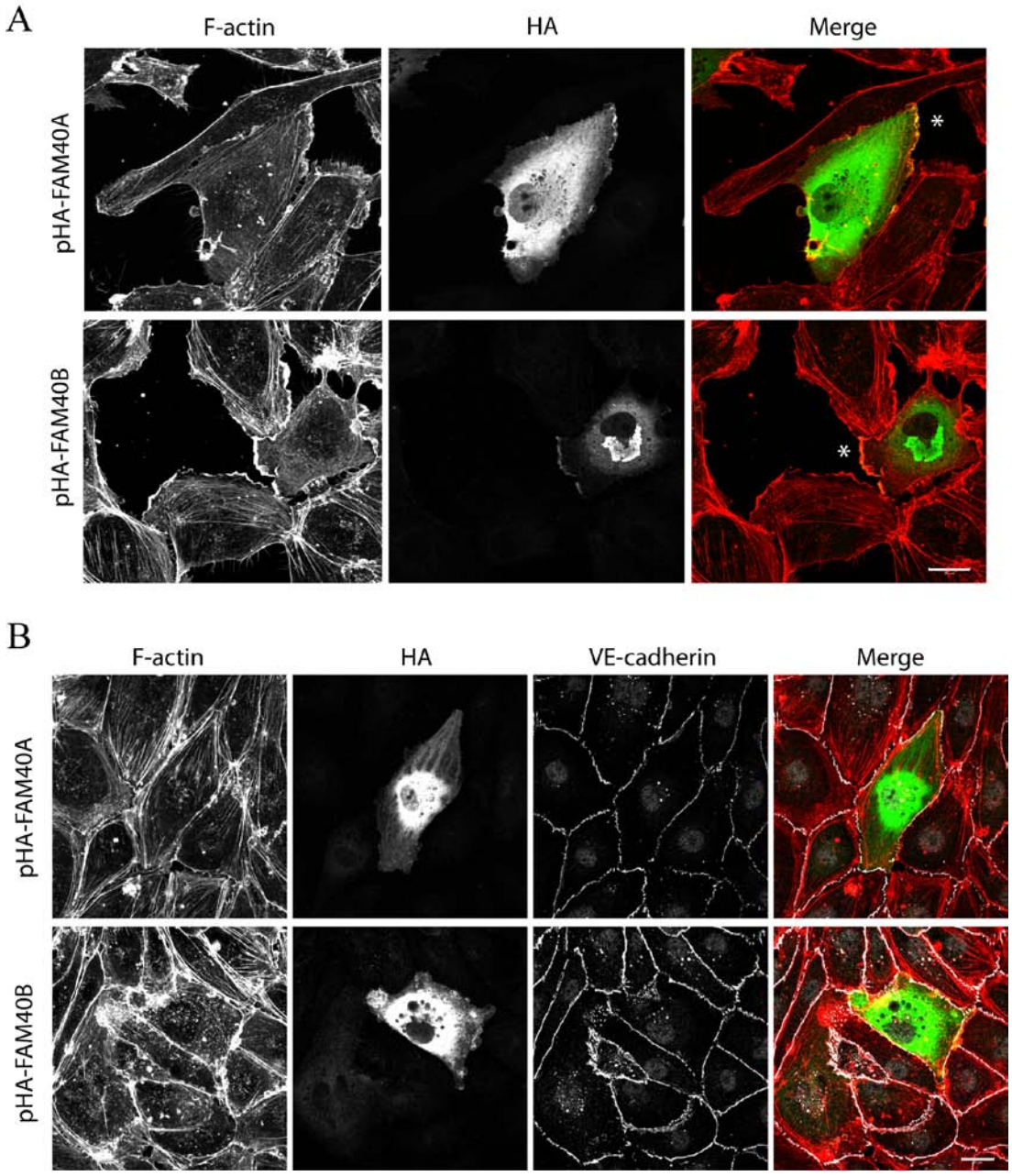

Figure 5.14 Staining for overexpressed FAM40A and FAM40B in HUVECs
HUVECs were transfected with pHA-FAM40A or pHA-FAM40B, seeded onto fibronectin-coated glass coverslips and fixed after 24 h. **(A)** shows FAM40 localisation in sub-confluent cells. Cells were stained for F-actin and the HA epitope. Asterisks indicate regions where the HA staining is localised to F-actin-rich protrusions. **(B)** shows FAM40 localisation in confluent cells. Cells were stained for F-actin, the HA epitope and VE-cadherin to visualise junctions. Images are compressed stacks of 15-20 z-sections and are representative of 2 independent experiments (VE-cadherin staining is from 1 experiment). Scale bars = 20 µm.

5.2.11 Verification of siRNA-mediated knockdown of CCM3 in HUVECs

CCM3 interacts with both FAM40A and FAM40B (section 3.2.1) and as a possible FAM40 signalling partner, its functions in endothelial cells were investigated. Efficient knockdown of CCM3 mRNA by siRNAs was obtained as determined by Q-PCR (Figure 5.15).

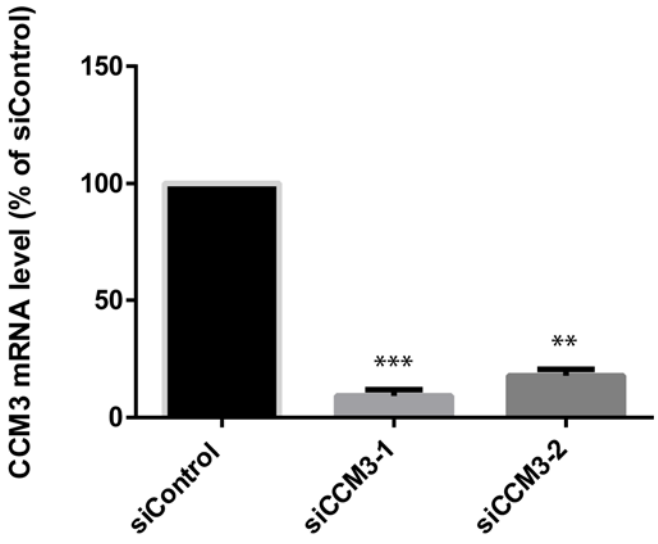

Figure 5.15 Verification of siRNA-mediated depletion of CCM3
HUVECs were transfected with siRNAs targeting CCM3 or with a control siRNA. After 72 h, mRNA from these cells was extracted and used to synthesize cDNA. The amount of CCM3 cDNA was determined by quantitative PCR. Data are normalised to GAPDH cDNA levels and are the mean of 3 independent experiments ± SEM. ** $p < 0.01$, *** $p < 0.001$ compared to siControl determined by Student's t-test.

5.2.12 Knockdown of CCM3 results in an increase in stress fibres in HUVECs

The CCM proteins have been shown to be important for maintaining endothelial homeostasis by regulating cell contractility. Previously published results show that depletion of CCM3 leads to an induction of stress fibres in endothelial cells (Zheng et al., 2010). Consistent with this, HUVECs depleted of CCM3 exhibited increased stress fibres (Figure 5.16, results generated by Joanna Furmston). No observable changes in VE-cadherin localisation or distribution were apparent.

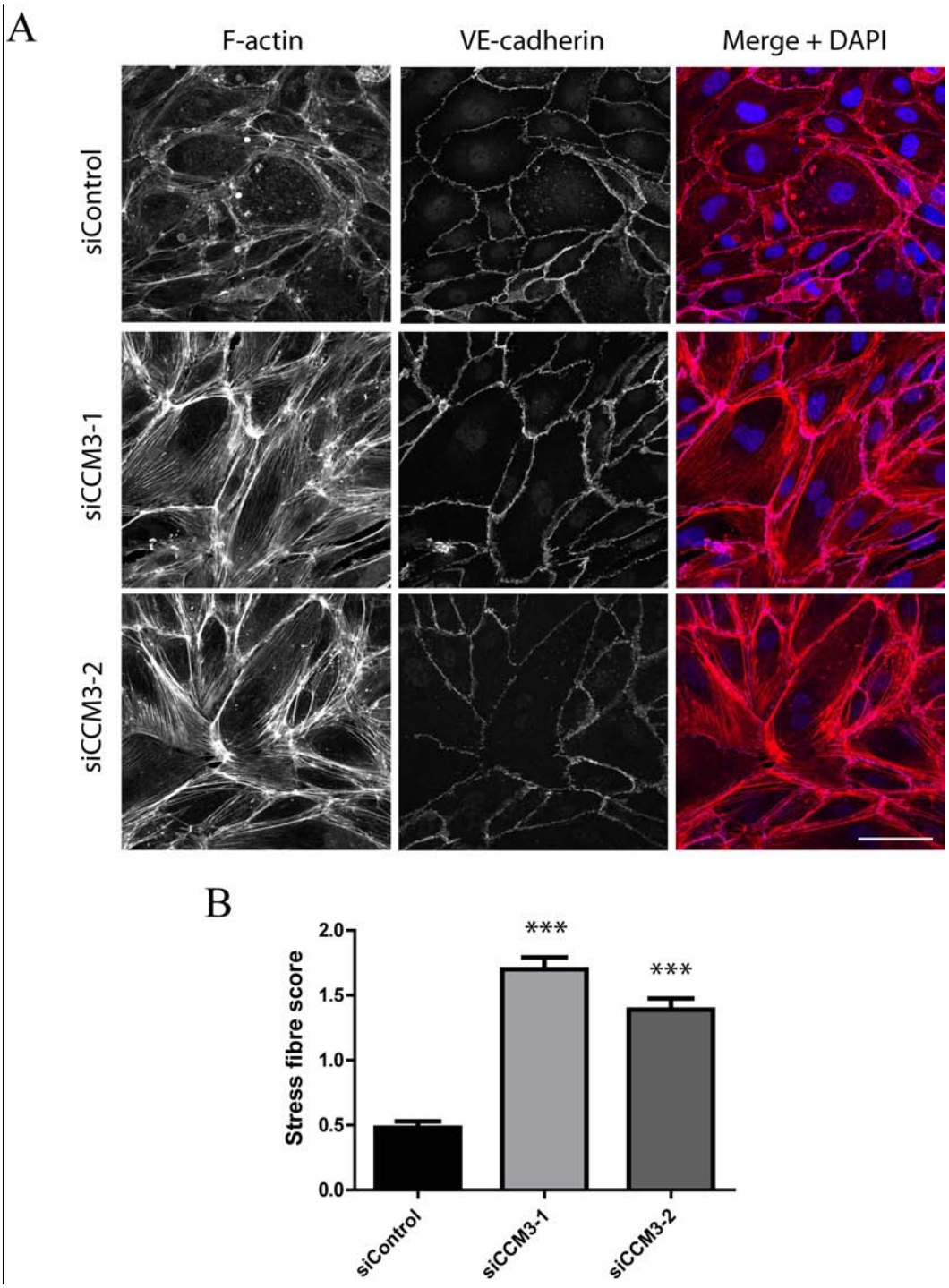

Figure 5.16 CCM3 knockdown increases the number of stress fibres
(*Experiment performed by Joanna Furmston*) **(A)** HUVECs were transfected with siRNAs targeting CCM3 and seeded onto fibronectin-coated glass coverslips to form confluent monolayers. 72 h after transfection cells were fixed and stained for F-actin, VE-cadherin to visualise junctions and with DAPI. Images are compressed stacks of 10-15 z-sections. Scale bar = 40 µm. **(B)** Quantification was done by assigning a score to each cell based on the stress fibre content in the centre of the cell; 0 – few or no stress fibres, 1 – upto 50% of the cell centre contains stress fibres, 2 – 50% to 75% of the cell centre contains stress fibres, 3 – greater than 75% of the cell centre contains stress fibres. Results shown are from at least 150 cells per condition from 3 independent experiments. Error bars depict SEM values. *** $p < 0.001$ compared to siControl determined by Student's t-test.

5.2.13 Overexpression of CCM3 does not rescue the increase of stress fibres induced upon FAM40 depletion

As both FAM40 proteins interact with CCM3 and depletion of all three proteins leads to a similar stress fibre induction phenotype, it is possible that they are functionally linked in endothelial cells. In order to determine if such functional coupling exists in cells, CCM3 was overexpressed against a background of FAM40 depletion.

HUVECs were transfected with siRNAs targeting FAM40A or FAM40B and subsequently transfected with an expression vector containing myc-CCM3. Double transfection with targeting siRNA and plasmid expression vector led to a lower cell density (Figure 5.17A). Experiments with an optimised protocol might reduce the observed loss of cells. Overexpression of CCM3 did not lead to an observable rescue of the stress fibre induction phenotype obtained upon either FAM40A or FAM40B depletion (Figure 5.17B). CCM3 expression did not lead to a reduction in cells with a high stress fibre score. This experiment also provided information on CCM3 localisation in cells. CCM3 was diffusely localised in cells and enriched at F-actin-rich protrusions. No changes in stress fibre content were observed upon CCM3 overexpression.

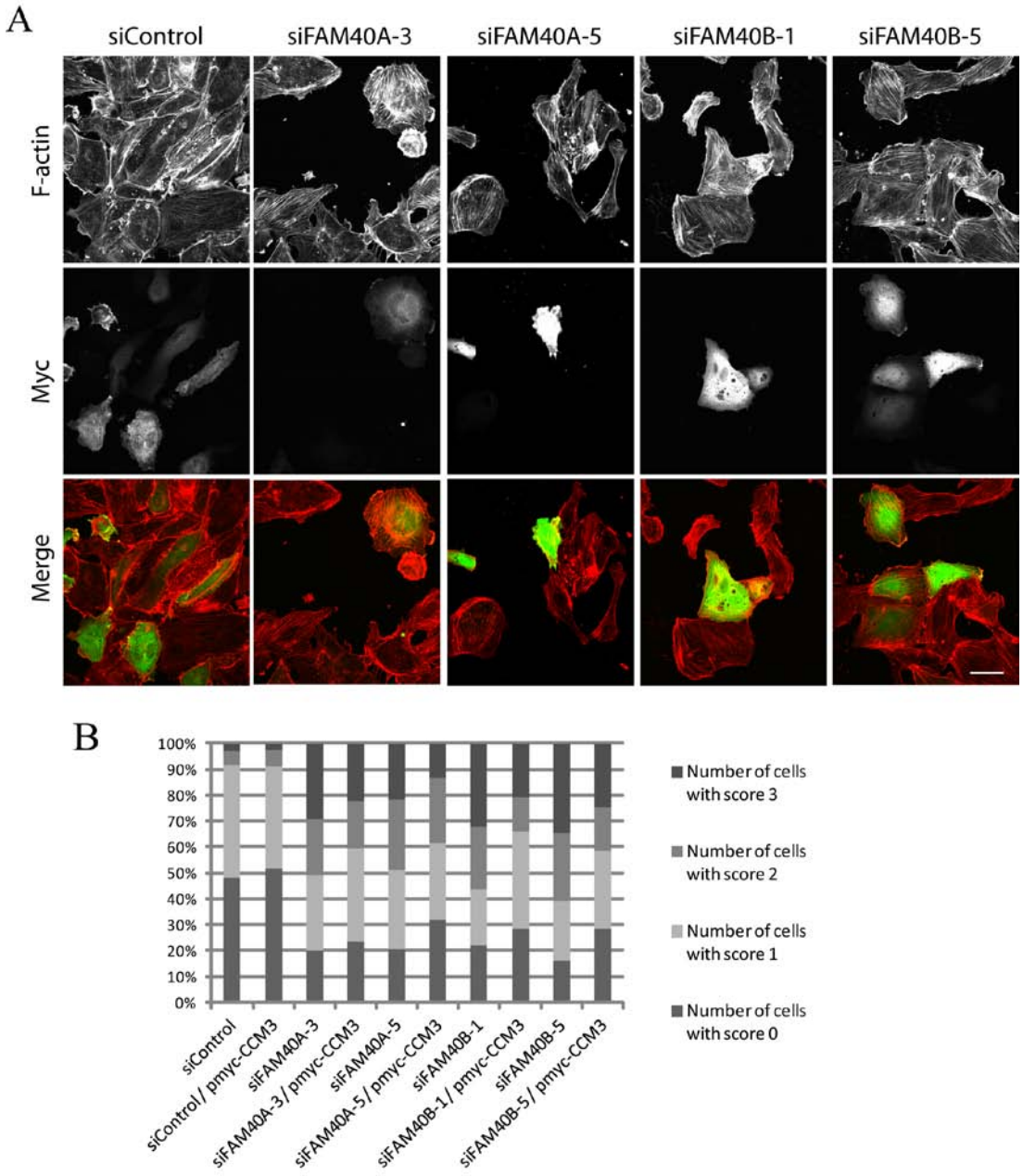

Figure 5.17 FAM40 depletion-induced increase in stress fibres is not rescued by CCM3 overexpression

(A) HUVECs were transfected with siRNAs targeting FAM40A or FAM40B. After 48 h these cells were transfected with pmyc-CCM3 and seeded onto fibronectin-coated glass coverslips. Cells were fixed after 24 h and stained for F-actin and the myc epitope. Images shown are compressed stacks of 10-15 z-sections. Scale bar = 40 µm. **(B)** Quantification was done by assigning a score to each cell based on the stress fibre content in the centre of the cell; 0 – few or no stress fibres, 1 – upto 50% of the cell centre contains stress fibres, 2 – 50% to 75% of the cell centre contains stress fibres, 3 – greater than 75% of the cell centre contains stress fibres. Results are shown as percentage distributions and are from at least 100 cells from 2 independent experiments.

5.2.14 Knockdown of CCM3 results in defects in the loop formation angiogenesis assay

In addition to their roles in maintaining vascular permeability, the CCM proteins are involved in vascular development (Fischer et al., 2013). Hence, HUVECs depleted of CCM3 were used in *in vitro* loop formation assays on Matrigel to provide an indication of their possible roles in angiogenesis. The *in vitro* loop formation assay provides a simplified simulation of angiogenesis and tests the capacity of endothelial cells to network and interact with each other to form ordered loop-like structures. This assay is considered to be representative of the cord formation step in sprouting angiogenesis (Goodwin, 2007). The capacity of CCM3-depleted HUVECs to form loops was severely affected (Figure 5.18).

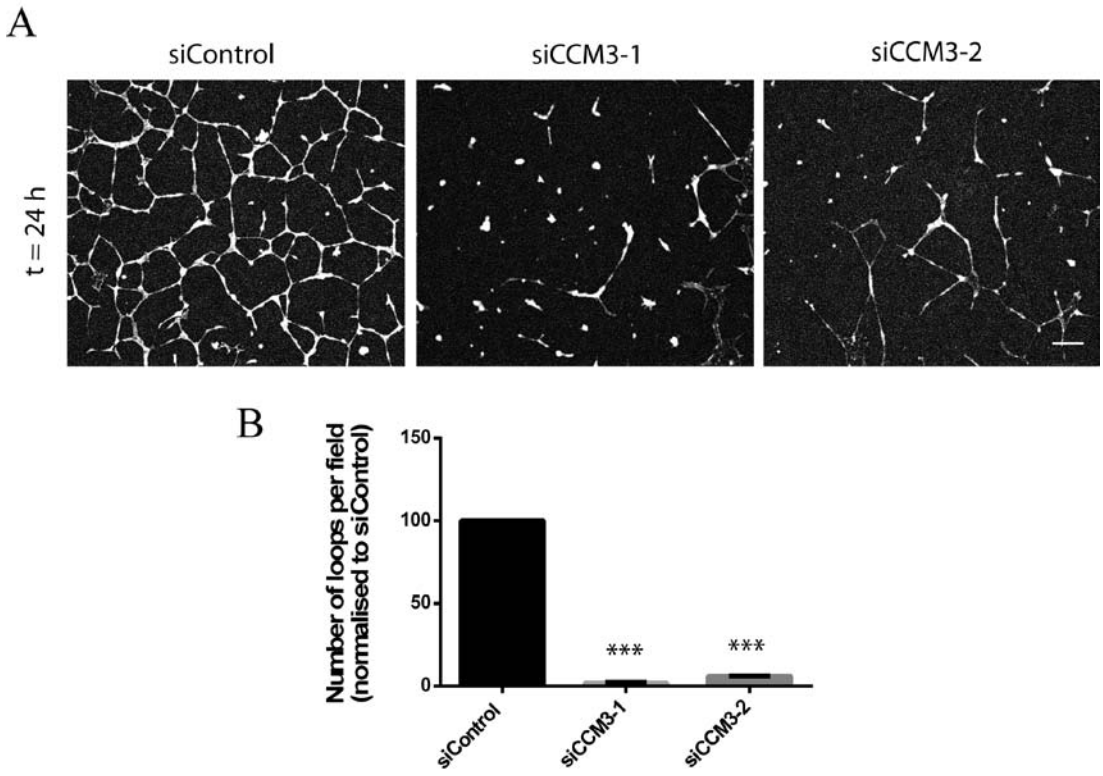

Figure 5.18 Depletion of CCM3 results in defects in the loop formation angiogenesis assay
(A) HUVECs were transfected with siRNAs targeting CCM3. 48 h after transfection cells were seeded onto a gel consisting of polymerised Matrigel. Loops were allowed to form for 24 h. Scale bar = 100 µm. **(B)** Loop formation was quantified by fixing and staining cells with phalloidin-Alexa546, and scoring the number of loops per field using fluorescence images. 6 fields were scored per condition in each experiment. Results are shown normalised to siControl (siControl = 100). Data are the mean of 3 independent experiments ± SEM values. *** $p < 0.001$ compared to siControl determined by Student's t-test.

5.2.15 The FAM40 proteins as mediators of angiogenesis as determined by an *in vitro* loop formation assay

The potential of FAM40A or FAM40B to be regulators of angiogenesis was tested using the *in vitro* loop formation assay. Time-lapse movies were made to monitor loop formation in real time (supplementary movies, movies 6 to 11).

Movies showed that over 24 h control cells were able to interact with each other and form closed loops. After cells were seeded onto Matrigel, they rapidly spread and were highly motile, 'seeking' out other cells to form a well organised network of cells. A subset of cells remained spread and did not acquire a morphology that resembled cords. Depletion of both FAM40A and FAM40B resulted in a more poorly connected network of cells (Figure 5.19A). These cells appeared to have defects in their capacity to spread and adhere to the matrix, and even after 24 h some cells had not spread completely (visualised as being 'phase bright'). While a fraction of cells were able to migrate and associate with other cells to form cords, these networks were largely unstable and significant cell retraction was observed. Interestingly, at some sites of retraction, deformation of the Matrigel substrate could be observed (indicated by arrows in Figure 5.19B). Cells appeared to be contractile, exerting a deforming force on the substrate. The number of loops formed by FAM40-depleted HUVECs was significantly reduced (Figure 5.19C).

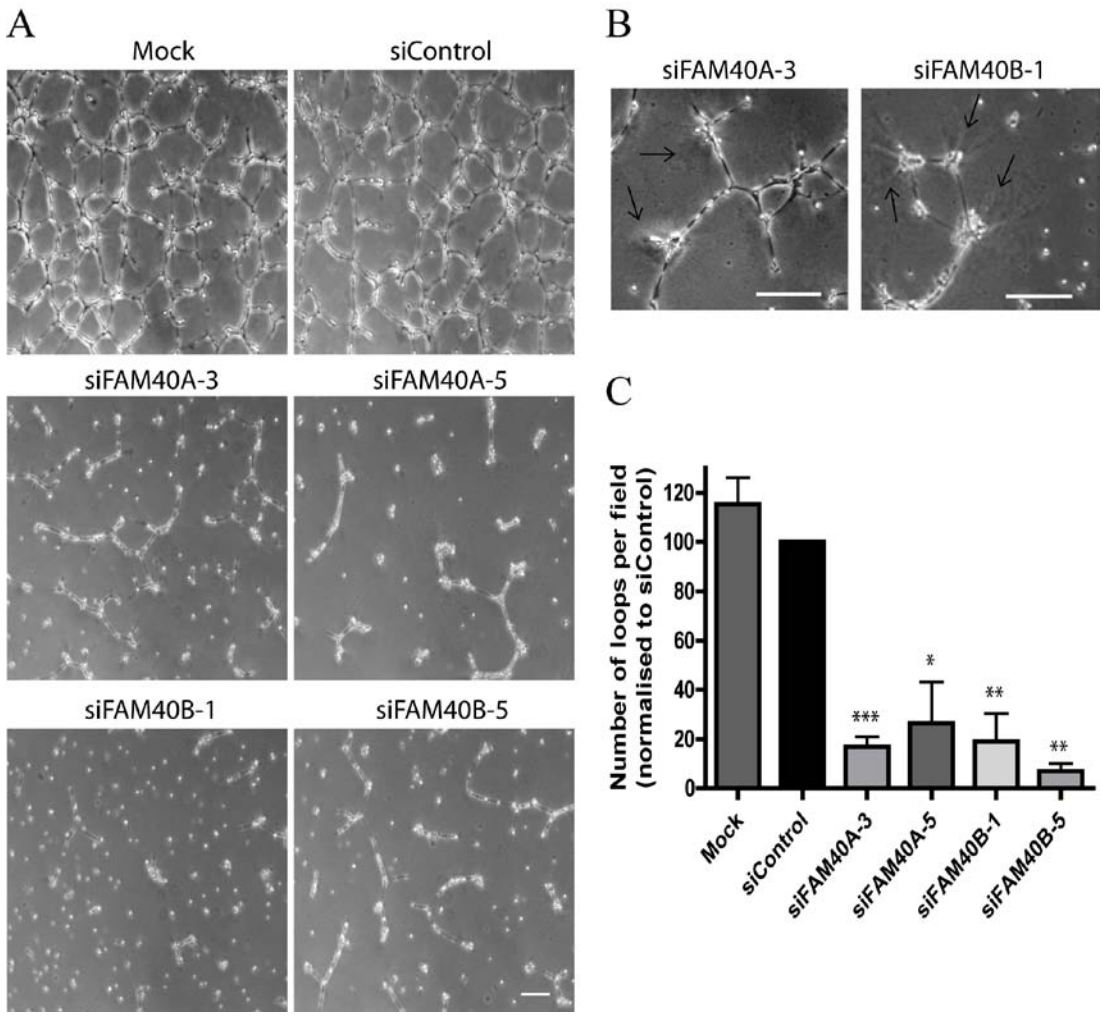

Figure 5.19 Depletion of FAM40A and FAM40B results in defects in the loop formation angiogenesis assay

(A) HUVECs were transfected with siRNAs targeting FAM40A and FAM40B. 48 h after transfection cells were seeded onto a gel consisting of polymerised Matrigel. Loops were allowed to form for 24 h. Scale bar = 200 µm. Arrows in images shown in **(B)** highlight deformation of the Matrigel substrate by FAM40-depleted cells. Scale bars = 200 µm. **(C)** Loop formation was quantified by scoring the number of loops per field. At least 5 fields were scored per condition in each experiment. n=4 for siFAM40A-3, siFAM40A-5 and siFAM40B-1. n=3 for siFAM40B-5. Data show mean ± SEM values and are normalised to siControl (siControl = 100). * $p < 0.05$, ** $p < 0.01$, *** $p < 0.001$ compared to siControl determined by Student's t-test.

Retraction of FAM40-depleted HUVECs observed in movies suggests increased cell contractility. Furthermore, depletion of both FAM40A and FAM40B resulted in the formation of contractile stress fibres in cells (section 5.2.3). The regulation of contractility is important during cell sprouting, and an increase in actomyosin contractility has been shown to cause cessation of sprouting (Abraham et al., 2009). HUVECs depleted of FAM40A or FAM40B were treated with the ROCK inhibitor Y-27632 in an attempt to rescue loop formation defects. Time-lapse movies were made to monitor loop formation in real time (supplementary movies, movies 12 to 17). Treatment of control cells with Y-27632 led to increased loop formation (Figure 5.20), consistent with previously published results that show increased tube formation on Y-27632 treatment (Mavria et al., 2006). Cells also appeared flatter as determined by them being less 'phase-bright'. Treatment of FAM40-depleted HUVECs with Y-27632 was able to rescue their loop formation defects (Figure 5.20B). This result suggests that increased actomyosin contractility upon FAM40 depletion contributes to defects in loop formation.

To complement these analyses, cells forming loops on Matrigel were stained for F-actin and with DAPI to highlight nuclei, and imaged (Figure 5.21). These images showed that cords were composed of multiple endothelial cells arranged linearly. The arrangement of cells was organised and periodic. 'Nodes' in the cell network consisted of multiple cells occurring in groups. Enriched F-actin staining was observed at cell-cell boundaries and at cell tips (indicated by asterisks in Figure 5.21A). Cells in this assay did not form stress fibres, unlike cells cultured in 2D. Depletion of FAM40A and FAM40B resulted in cell cords appearing more disorganised with clumping being regularly observed (Figure 5.21B). The periodic, linear arrangement of cells in cords was disturbed and some cells exhibited micro-spikes (shown in boxed areas in Figure 5.21B), which could be a consequence of cell retraction and collapse.

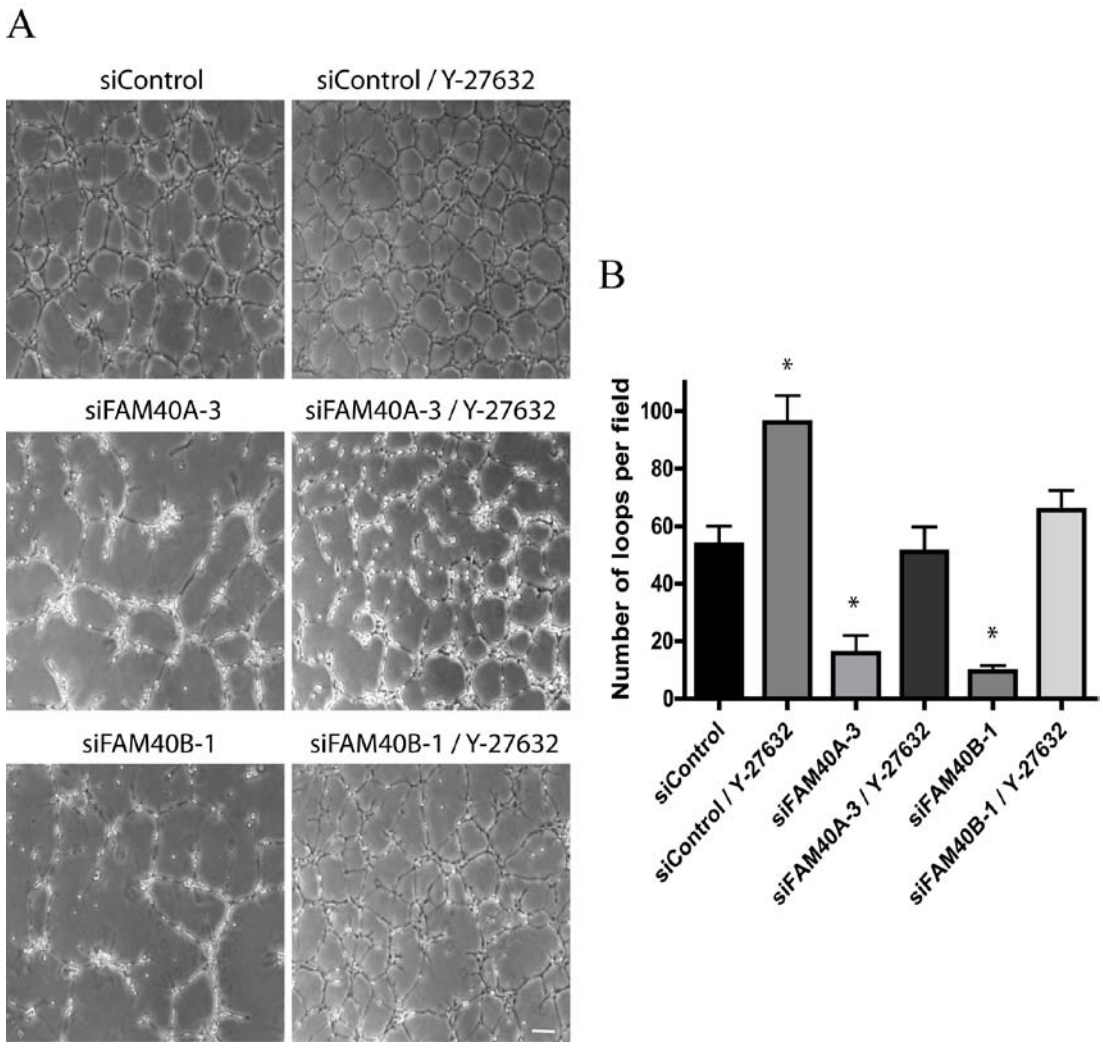

Figure 5.20 FAM40 depletion-induced loop formation defect is rescued by treatment with the ROCK inhibitor, Y-27632

(A) HUVECs were transfected with siRNAs targeting FAM40A and FAM40B. 48 h after transfection cells were seeded onto a gel consisting of polymerised Matrigel. Loops were allowed to form for 24 h. Treatment with 10 µM Y-27632 was done for 24 h. Scale bar = 200 µm. **(B)** Loop formation was quantified by scoring the number of loops per field. At least 4 fields were scored per condition in each experiment. Data are the mean of 3 independent experiments ± SEM values. * $p < 0.05$ compared to siControl determined by Student's t-test.

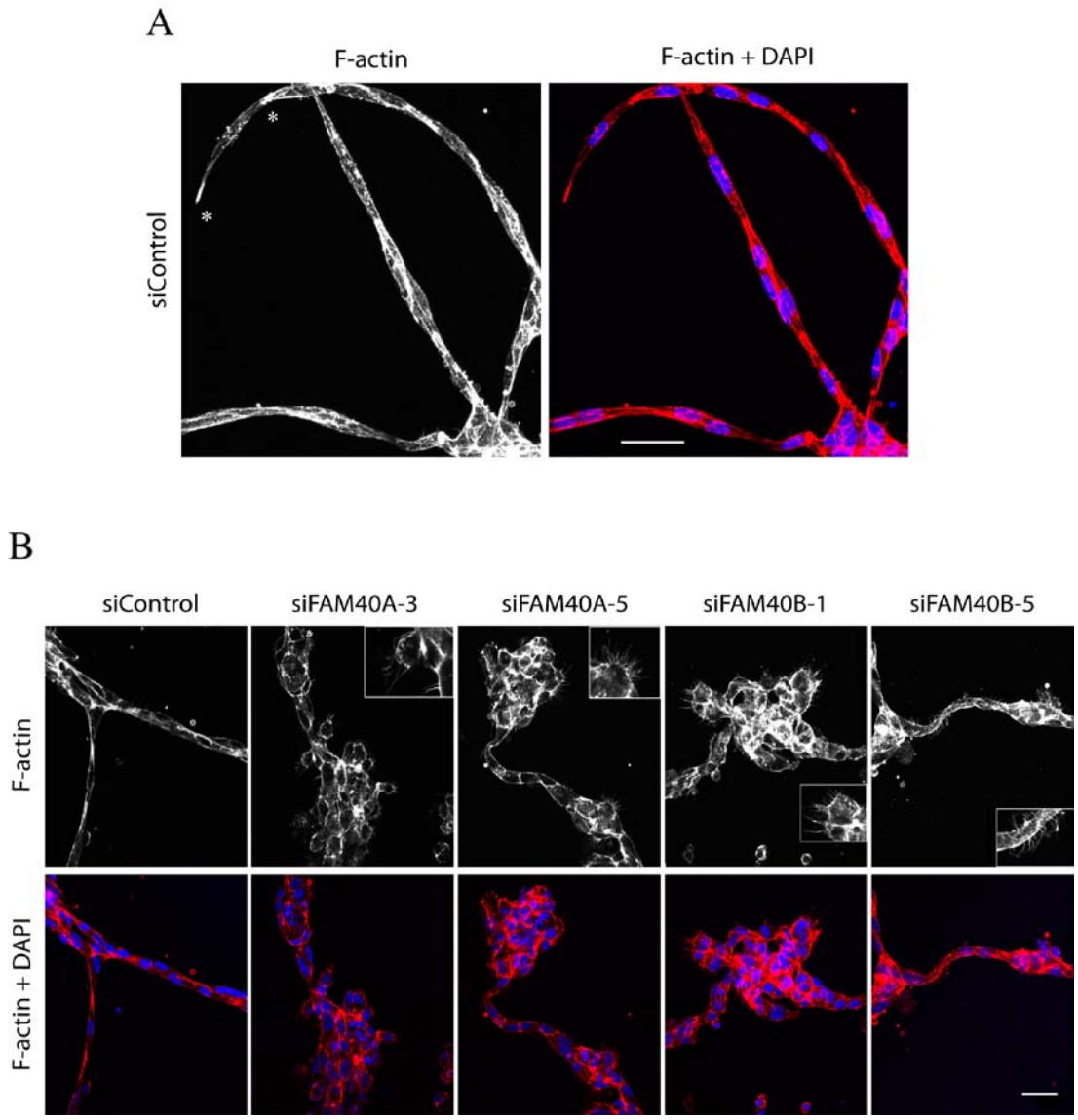

Figure 5.21 Morphology of FAM40-depleted HUVECs forming loops on Matrigel
HUVECs were transfected with siRNAs targeting FAM40A and FAM40B and after 48 h were seeded on polymerised Matrigel for 24 h. Cells were fixed and stained for F-actin and with DAPI to visualise nuclei. Images in **(A)** shows loops formed by control HUVECs and are compressed stacks of 30 z-sections. Asterisks indicate regions of F-actin enrichment at cell tips and cell-cell junctions. Scale bar = 40 µm. Images in **(B)** show loops formed by FAM40-depleted HUVECs. Images are sections taken at a single z-position and are representative of 3 independent experiments. Boxed areas highlight cells with micro-spikes. Scale bar = 40 µm.

HUVECs depleted of FAM40A or FAM40B appeared to exhibit defects in cell spreading and adhesion to the Matrigel substrate, which might subsequently contribute to defects in loop formation. The ability of HUVECs depleted of FAM40A or FAM40B to adhere to polymerised Matrigel was tested. Knockdown of FAM40B resulted in an adhesion defect only with one siRNA oligonucleotide and so could be an off-target effect. However, depletion of FAM40A using two individual siRNAs led to an adhesion defect (Figure 5.22). This reduced adhesion may contribute to the observed loop formation defect.

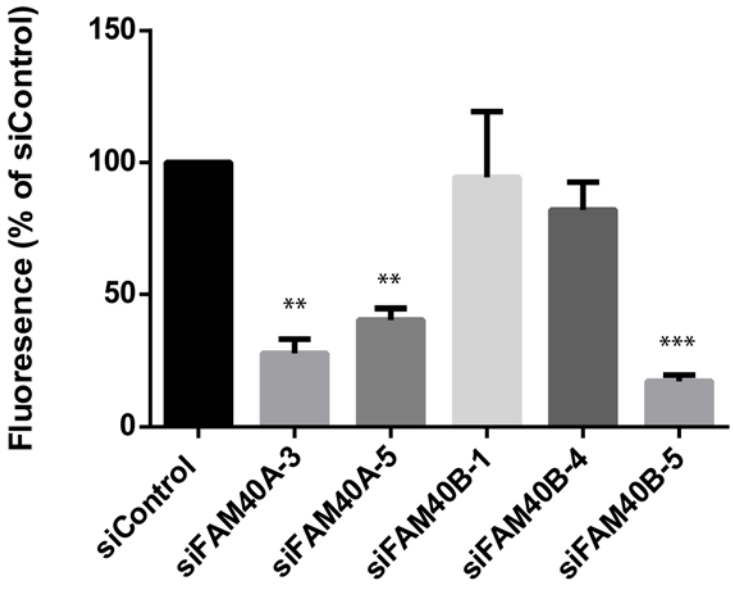

Figure 5.22 FAM40A knockdown affects HUVEC adhesion to Matrigel
HUVECs were transfected with siRNA targeting FAM40A or FAM40B. 72 h after transfection cells were labelled with Cell Tracker CMFDA and added onto a gel of polymerised Matrigel. After 5 min cells were washed to remove unadhered cells and a fluorescence reading was taken as a readout of adhesion. Data are the mean of 3 independent experiments ± SEM values and are normalised to siControl (siControl = 100). ** $p < 0.01$, *** $p < 0.001$ compared to siControl determined by Student's t-test.

In summary, these results show that FAM40A and FAM40B may regulate angiogenesis as determined by the *in vitro* loop formation assay.

5.3 Discussion

The functions of human FAM40A and FAM40B are largely unknown, and analyses presented in this chapter provide for the first time a functional characterisation of these genes in endothelial cells. An RNAi approach was primarily used to asses FAM40 function in HUVECs which were used as an experimental model. Results show that FAM40A and FAM40B are novel regulators of endothelial physiology and affect F-actin organisation, endothelial permeability and angiogenesis.

5.3.1 The FAM40 proteins mediate F-actin organisation

Actomyosin contractility is important in endothelial cells for resisting shear stress and is involved in mediating endothelial permeability. Impaired regulation is implicated in pathological conditions such as oedema, haemorrhagic stroke and vascular malformations (Dejana et al., 2009). Cerebral cavernous malformation is a pathology of the vasculature and is characterised by defects in vascular permeability and development. CCM3 is one of the genetic loci mutated in CCM and depletion of CCM3 in cultured endothelial cells leads to an induction of stress fibres and increased endothelial permeability (Zheng et al., 2010). This phenotype suggested a possible role for the FAM40 proteins in endothelial cells. HUVECs depleted of FAM40A or FAM40B exhibited an increase in stress fibres that traverse the length of the cell. This result combined with the fact that both FAM40A and FAM40B associate with CCM3 (section 3.2.1) provides a strong indication that these genes may be functionally linked in endothelial cells. Overexpression of either FAM40A or FAM40B did not lead to a reduction in stress fibres as would be predicted. Control cells contain few stress fibres that traverse the length of the cell, and so detection of a decrease in stress fibre content would have been difficult to observe. Future work could attempt to ‘sensitize’ the system in order to overcome this limitation. For example, overexpression could be performed in a background of TNFα or thrombin stimulation which are known to increase stress fibre assembly (McKenzie and Ridley, 2007; Wojciak-Stothard et al., 2001). Another explanation is that the FAM40 proteins need to signal with other proteins to regulate stress fibres, and so overexpression of FAM40A or FAM40B alone does not lead to a decrease in stress fibre content.

Multiple signalling pathways are involved in the formation of stress fibres in endothelial cells, including Rho, Rac1 (Tzima et al., 2002; Wojciak-Stothard et al., 2001) and Rnd (Gottesbuhren et al., 2013) signalling. As a consequence, a stress fibre phenotype cannot in itself be used to conclude functional links between two different genes, making it challenging to uncover underlying mechanisms behind FAM40 function. The Rho-ROCK signalling pathway is pivotal in the regulation of stress fibres and RhoA, RhoB and RhoC are capable of inducing stress fibres when overexpressed in endothelial cells (Gottesbuhren et al., 2013). No reproducible changes to RhoA activity were observed. It might be that RhoA activity is only spatially regulated and hence it would be interesting to carry out FRET analysis to determine localised changes in activity (Nakamura et al., 2006). For example, stimulation of endothelial cells with thrombin leads to localised activation of RhoA along stress fibres and is associated with their contraction (Szulcek et al., 2013). It is also possible that RhoA activity is temporally regulated. For example, TNFα only transiently activates RhoA in HUVECs, with RhoA activity subsequently returning to basal levels despite the presence of stress fibres (McKenzie and Ridley, 2007). A similar scenario might exist with FAM40 regulation of stress fibres. As cells were only analysed at 72 h after siRNA treatment, a transient change could have been missed. It would be interesting to conduct a time course experiment of stress fibre induction/RhoA activity after FAM40 siRNA transfection. Furthermore, the activity levels of RhoB and RhoC should be checked as previous studies have reported examples of specific responses to closely related proteins in endothelial cells. Rnd3-mediated induction of stress fibres occurs through RhoB (Gottesbuhren et al., 2013), while it has been suggested that VE-cadherin-mediated regulation of contractility occurs via RhoC during tube formation in culture (Abraham et al., 2009).

Rac1 activity is also implicated in the formation of stress fibres in endothelial cells (Tzima et al., 2002; Wojciak-Stothard et al., 2001) and was assessed after FAM40 depletion. FAM40B depletion resulted in reduced Rac1 activity only in a subset of experiments. Further experiments to assess localised changes of Rac1-GTP levels could be considered. An alternative approach to functionally link these Rho family members with the FAM40 proteins would be to use RNAi to simultaneously deplete either FAM40A or FAM40B along with the Rho GTPase of interest, and assess if the stress fibre phenotype was reversed.

Rho signalling is known to mediate stress fibre assembly by the cooperative activity of two downstream effectors, ROCK and mDia (Watanabe et al., 1999). Activated ROCK has several targets in cells that affect stress fibre formation and the stability of actin filaments, including MLC2 (Riento and Ridley, 2003). Mono and diphosphorylation of MLC2 regulates myosin II-associated contractile activity and so can be used as a measure of contractility (Watanabe et al., 2007). Surprisingly, depletion of FAM40A or FAM40B did not increase p-MLC2 levels. Two extraction strategies using RIPA and Laemmli lysis buffer were performed to ensure that extraction of protein was not a limiting factor in experiments. Immunofluorescence staining for p-MLC2 revealed localisation along stress fibres consistent with its role in mediating contractility. Similar arguments as those used for RhoA activity could explain these results. Like RhoA activity, levels of p-MLC2 are not an absolute indicator of cell contractility and stress fibre induction. TNFα stimulation of endothelial cells leads to only a transient increase in p-MLC2 levels in spite of the presence of stress fibres at later time-points (McKenzie and Ridley, 2007). Another possibility is that the FAM40 proteins affect localised changes to p-MLC2 levels. Activated ROCK also leads to phosphorylation and inactivation of cofilin via LIMK. This activity could additionally stabilise actin filaments as cofilin causes severing of actin filaments (Oser and Condeelis, 2009). Future experiments should investigate if depletion of FAM40A and/or FAM40B alters cofilin phosphorylation. In addition, future experiments should assess effects of FAM40 depletion on mDia signalling.

Treatment with the ROCK inhibitor H-1152, and the Rho inhibitor C3 tranferase reduced stress fibres in FAM40-depleted cells. This result suggests that Rho-ROCK signalling is involved in FAM40 function. While this scenario is consistent with this result, it is not the only explanation. The Rho-ROCK signalling axis is a crucial regulator of contractility and actomyosin filament assembly in endothelial cells. Hence, it is possible that perturbation of its activity would lead to abrogation of stress fibre induction irrespective of the conditions or stimulus. This result therefore cannot be used to conclude that the FAM40 proteins are linearly linked to the Rho-ROCK signalling axis. A compatible alternative is that the Rho-ROCK pathway acts in parallel to FAM40 signalling.

FAM40 depletion did not lead to an increase in focal adhesion density in sub-confluent endothelial cells. This is surprising as in sub-confluent endothelial cells stress fibres are anchored at focal adhesions (Millan et al., 2010). Stress fibre content in sub-confluent HUVECs depleted of FAM40A and FAM40B was not quantified and would have to be performed in future experiments. However, it was observed that stress fibre induction upon FAM40 depletion was not as pronounced in sub-confluent cells as compared to confluent cells, and could explain why no increase in focal adhesion density was observed. Another explanation could be that by using vinculin as a marker for focal adhesions, nascent adhesions may not have been visualised. Vinculin recruitment to focal adhesions lags behind that of paxillin, a marker for nascent adhesions (Pasapera et al., 2010).

In summary, the mechanisms by which the FAM40 proteins regulate stress fibres in cells are not clear and further investigation is needed to resolve this question. It is possible that the FAM40 proteins represent a novel signalling pathway by which contractility and stress fibre assembly is regulated in endothelial cells.

5.3.2 Depletion of FAM40B increases the permeability of endothelial monolayers

Perturbations to the actin cytoskeleton can affect the integrity of endothelial monolayers. Stress fibres in confluent endothelial cells are predominantly linked to adherens junctions (Millan et al., 2010), explaining how tensile force can be communicated to cell-cell junctions. Knockdown of FAM40B resulted in an increase in endothelial permeability. The increase in tensile force as a consequence of stress fibre induction could lead to a physical disruption of junctions. This is supported by discontinuous VE-cadherin staining upon FAM40B depletion. However, depletion of FAM40A did not lead to an increase in endothelial permeability in spite of inducing stress fibre assembly. While a positive correlation exists between stress fibre induction and increased endothelial permeability, this need not be so. For example, TNFα stimulation of endothelial cells leads to stress fibre induction, but long term permeability changes correlate with loss of tight junction proteins (McKenzie and Ridley, 2007). It would therefore be interesting to determine if FAM40 depletion affects tight junctions. This is relevant as endothelial cell interfaces in CCM lesions display a loss of tight junctions (Clatterbuck et al., 2001).

In addition to RhoA and Rac1, Rap1 activity has been reported to be an important regulator of cell-cell junctions in endothelial cells (Kooistra et al., 2007). Interestingly, Rap1 is a CCM1 effector (Glading et al., 2007). However, a preliminary experiment revealed that FAM40 depletion did not change Rap1 activity (results not shown). Neither FAM40A nor FAM40B showed enrichment at cell-cell junctions as determined by immunofluorescence staining of epitope-tagged protein, making it unlikely that they act as cell-cell adhesion proteins.

5.3.3 FAM40A and FAM40B as regulators of angiogenesis

An *in vitro* loop formation angiogenesis assay was used to determine if either FAM40A or FAM40B may regulate angiogenesis *in vivo*. This assay simulates angiogenesis by testing the capacity of endothelial cells to organise into stable networks resulting in the formation of loop-like structures when plated onto polymerised Matrigel.

Angiogenesis *in vivo* involves matrix degradation, endothelial cell proliferation, migration and lumen formation (reviewed in (Potente et al., 2011)). HUVECs in the loop assay form coalesced chains of cells as revealed by staining for F-actin. These structures resemble cords formed *in vivo*, and it is not clear if cells form lumens (Goodwin, 2007). The migration of endothelial cells can be studied by generating time-lapse movies of loop formation. The assay does not test for matrix degradation as plated endothelial cells do not need to invade into the matrix to form loops. The duration of the experiment (24 h) is too short to allow for significant changes in proliferation to be observed. In summary, this assay represents only a part of the process of angiogenesis and so has to be interpreted carefully.

Depletion of both FAM40A and FAM40B led to HUVECs forming fewer loops when plated onto Matrigel. Furthermore, F-actin staining of FAM40-depleted cords revealed a high level of disorganisation, with the ordered periodic arrangement of cells being lost. It is likely that this would impair subsequent tube formation *in vivo*. An inverse correlation between angiogenic sprouting and cell contractility has been shown, and the cessation of sprouting is reliant on MLC2 phosphorylation (Abraham et al., 2009). This could explain the defects in loop formation on FAM40 depletion. Indeed, treatment of FAM40-depleted cells with the ROCK inhibitor Y-27632 rescued loop formation defects. It can be inferred that an optimum degree of contractility is needed during sprouting angiogenesis. Too little leads to excessive

sprouting and increased angiogenesis, while too much leads to a premature abrogation of sprouting. A preliminary experiment probing p-MLC2 levels in FAM40-depleted endothelial cords yielded no observable changes (results not shown). While further experiments will have to be performed to confirm this result, it strengthens the hypothesis that the FAM40 proteins mediate cell contractility by an alternate mechanism. In addition, the coordinated temporal regulation of RhoA and Rac1 activity has been shown to be important during loop formation (Cascone et al., 2003), and it will be interesting to study variations in their activities upon FAM40 depletion in future experiments.

Other processes such as adhesion to the substrate and migration could contribute to defects observed in the loop assay. FAM40A depletion resulted in a reduced capacity of endothelial cells to adhere to the Matrigel matrix. It is likely that this is not a consequence of increased contractility as FAM40B depletion did not cause an adhesion defect. Future experiments should attempt to probe mechanisms underlying FAM40A control of endothelial adhesion to the surrounding matrix. Migration of endothelial cells is important during angiogenesis but neither FAM40A nor FAM40B depletion resulted in migration defects in the ORIS assay. This assay tested migration on fibronectin-coated plastic while loop assays were carried out on polymerised Matrigel. To be comparable, ORIS assays on Matrigel-coated plastic will have to be performed.

The subcellular localisation of FAM40A and FAM40B in subconfluent HUVECs could be extrapolated to localisation in endothelial tip cells leading an angiogenic sprout, as in both scenarios individual cells are not completely surrounded by other cells. Both FAM40A and FAM40B were enriched in F-actin-rich protrusions as determined by immunofluorescence staining of epitope-tagged protein. These regions being located at cell peripheries are involved in the establishment of cell-cell contacts and are sites of junction formation in sprouting cells. It would be interesting to determine if the FAM40 proteins mediate these functions during angiogenesis.

Taken together, these results identify the FAM40 proteins as being novel mediators of sprouting angiogenesis as determined by an *in vitro* loop formation assay, by regulating contractility in endothelial cells. It will be important to use *in vivo* approaches to fully

understand the roles of FAM40A and FAM40B during angiogenesis by addressing questions such as their roles in regulating angiogenesis during embryogenesis, and in maintaining the quiescence of an established vascular network.

5.3.4 FAM40 gene function in endothelial cells in the context of CCM

CCM is a disease of the vasculature of the CNS while results presented in this chapter are based on endothelial cells derived from umbilical veins. Different endothelial cell subtypes may exhibit distinct behaviour. However, assuming that fundamental aspects of cell function such as barrier regulation are conserved across different subtypes, links between the FAM40 proteins and the CCM disease process may be drawn.

Depletion of FAM40A, FAM40B or CCM3 in HUVECs using RNAi led to similar phenotypes in multiple assays. Like with FAM40 depletion, CCM3 depletion resulted in an increase in stress fibres that traversed the length of cells. This is consistent with previously published experiments (Zheng et al., 2010). MST4 was shown to phosphorylate both FAM40 proteins and CCM3 (section 3.2.8). Preliminary experiments revealed that depletion of MST4 by RNAi did not cause induction of stress fibres in HUVECs (results not shown). However, depletion of STK24 and STK25 induces stress fibres in endothelial cells (Zheng et al., 2010). To test for a possible functional link between CCM3 and the FAM40 proteins, overexpression of CCM3 was used to assess if a rescue of the FAM40 depletion-induced stress fibre phenotype occurred. No rescue was observed and if the FAM40 proteins and CCM3 signal together in cells, this result is compatible with two possible scenarios. One possibility is that both CCM3 and FAM40A/FAM40B signal at the same level/node, and so the presence of both proteins is required to prevent excessive stress fibre formation. The other possibility is that CCM3 lies upstream of FAM40A/FAM40B and so in the absence of FAM40A/FAM40B, expression of CCM3 does not affect the numbers of stress fibres.

Furthermore, depletion of CCM3 and STK25 increases endothelial permeability (Zheng et al., 2010), similar to that observed upon FAM40B depletion. This same study showed that depletion of CCM3 or STK25 leads to elevated RhoA activity and uses this to explain CCM3 function in cells. However, it is not entirely clear if elevated RhoA activity is a hallmark of

CCM3 signalling as another study could not reproduce this (Chan et al., 2011). No change to RhoA activity was reproducibly observed upon FAM40 depletion.

The CCM proteins appear to have dual functions as regulators of cell contractility and as mediators of vascular development and angiogenesis. Dysregulation of these functions has been suggested to precipitate CCMs. *In vivo* work using zebrafish has shown that inhibition of CCM3, STK24 and STK25 function leads to vascular anomalies during development (Yoruk et al., 2012; Zheng et al., 2010). Depletion of FAM40A, FAM40B or CCM3 resulted in defects in *in vitro* loop angiogenesis assays. CCM is a disease of endothelial quiescence where cells break free of controls that keep proliferation and neo-angiogenesis in check. Hence, it might be expected that CCM3 depletion would have led to an increase in loop formation. Indeed, endothelial cells derived from CCM patient samples exhibit higher rates of tube formation and express higher levels of VEGF *in vitro* (Zhao et al., 2007). Additionally, knockdown of CCM3 by RNAi causes enhanced migration and sprouting of HUVECs depleted of CCM3 (You et al., 2013). These studies differ from the analyses presented in this chapter in that they assessed angiogenic function in a 3D collagen I tube formation assay and a sprouting assay in fibrin gels respectively. However, another study using 3D collagen tube formation assays reported that HUVECs depleted of CCM3 fail to organise into lumenised networks (Chan et al., 2011), suggesting that CCM3 depletion may result in cells being more angiogenic, but leads to poorly formed vascular networks. One way of reconciling these results with the data presented in this chapter is based on experimental variations due to different assays used. For example, it may be that increased contractility would be perceived as a loop formation defect in the assay used here irrespective of other background factors, such as expression of angiogenic cytokines and/or receptors. In summary, while results from the loop angiogenesis assay highlight a possible functional link between the FAM40 proteins and CCM3, it also underscores the importance of utilising other assays to study angiogenesis in the future.

CCM3 is the least understood of the three CCM genes and appears to signal in a distinct manner. Results presented in this chapter suggest why this may be so. Perhaps the FAM40 proteins are novel, specific signalling partners for CCM3. Depletion of either FAM40 protein

did not lead to changes in the total or active levels of β1-integrin in endothelial cells, a consequence of CCM1 gene function (Liu et al., 2013). This is relevant here as it strengthens the hypothesis that the FAM40 proteins signal specifically with CCM3, and not with other CCM proteins. If this is so, the FAM40 proteins are novel determinants of the CCM disease process and hence future research should be aimed at fully understanding their contributions to CCM pathogenesis. To further this goal, a more detailed functional analysis of the GCKIII kinases will have to be performed. This is especially true for MST4 whose functions in endothelial cells are the least understood. Uncovering their roles in F-actin organisation, regulation of endothelial permeability and angiogenesis will help in comprehending the roles of the CCM3-GCKIII signalling axis, and the FAM40 proteins in CCM. It would be interesting to screen for mutations in the FAM40A and FAM40B genes in CCM patient samples in order to establish genetic links between the FAM40 and CCM genes.

The following model (Figure 5.23) summarises the functional roles of FAM40A and FAM40B in endothelial cells.

5.3.5 Summary

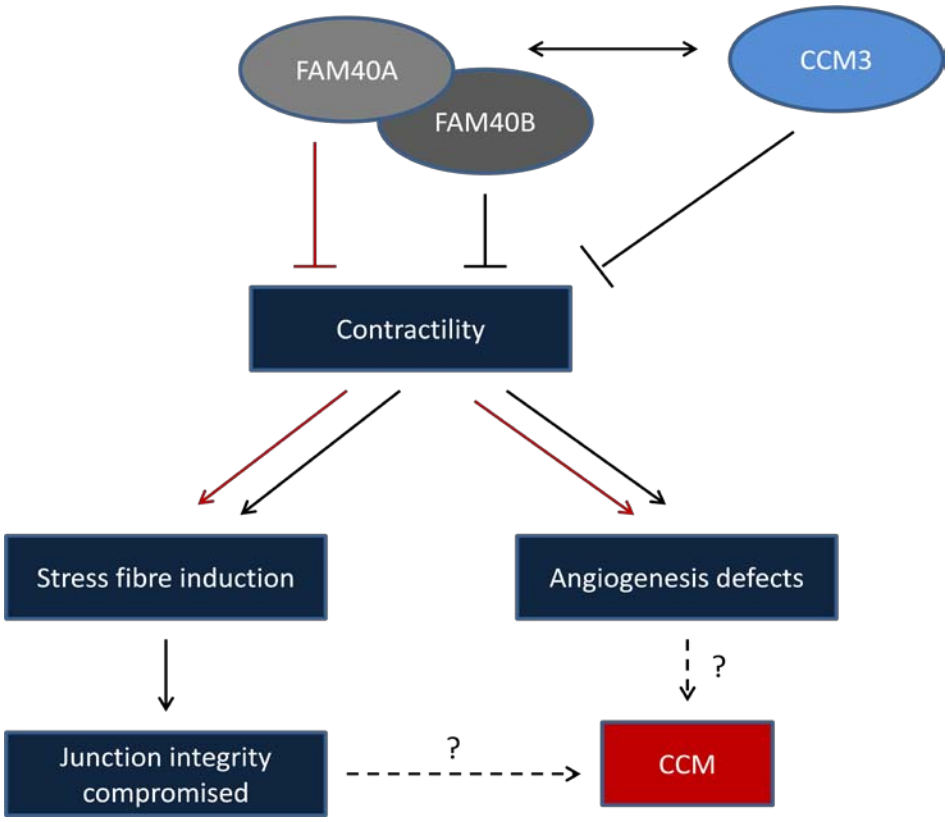

Figure 5.23 Model of FAM40 function in endothelial cells
FAM40A and FAM40B are important for regulating contractility in endothelial cells independently of the regulation of RhoA activity. Loss of their function contributes to stress fibre induction, defects in the *in vitro* loop formation angiogenesis assay and in the case of FAM40B, a decrease in endothelial barrier integrity. In addition to being novel regulators of endothelial cell physiology, the FAM40 proteins may be implicated in CCM pathogenesis by signalling with CCM3.

6 Concluding remarks

The Drosophila FAM40 orthologue was identified in a genome-wide RNAi screen in S2 cells assessing cell morphology (Rohn et al., 2011). Subsequent cell morphology and migration screens in PC3 cells (Bai et al., 2011) led to the identification of human FAM40A and FAM40B as putative novel regulators of the cytoskeleton. FAM40 proteins are present in species ranging from unicellular yeasts to complex higher eukaryotes. Additionally, conservation of their domain architecture points to these proteins carrying out an as yet unidentified role in cells. This study presents for the first time a detailed analysis of FAM40 function. Their roles have been studied in an epithelial cancer cell line (PC3) and in primary endothelial cells (HUVECs). In addition to providing insight on cell specific function, these analyses also allow for the hypothesis of a general role for the FAM40 proteins.

6.1 Comparison of FAM40 function in PC3 cells and HUVECs

Depletion of the FAM40 proteins in PC3 cells and HUVECs affects aspects of cell function as discussed in chapter 4 and chapter 5 respectively. These analyses highlight cell specific functions of the FAM40 proteins in prostate cancer and endothelial cells. It is also of interest to compare their functions in these two different cell types.

PC3 cells and HUVECs differ in several significant ways. PC3 cells are derived from prostate epithelial cells while HUVECs are endothelial cells. Another important difference is that PC3 cells are a cancer-derived cell line while HUVECs are primary cells. These differences may impinge on gene function.

Depletion of the FAM40 proteins in PC3 cells did not cause the induction of stress fibres. Conversely, depletion of the FAM40 proteins in HUVECs caused a marked increase in stress fibre content. From these observations one conclusion that may be reached is that the FAM40 proteins signal by independent means in these two cell types. This could be explained by the presence of cell specific signalling partners. For example, HEG1 is an endothelial specific molecule involved in CCM1/CCM2 signalling (Kleaveland et al., 2009). Another example is that of VE-cadherin which is specific to endothelial cells. However, it may also be that different cell environments cause proteins to express their functions

differently even in the presence of similar signalling partners. If this is true, it serves to highlight how the reduction of gene function may not account fully for an environment/process centric view of gene function (Lippincott-Schwartz, 2000). For example, CCM3 regulation of Golgi positioning may regulate migration in PC3 cells but be important for the establishment of stable cell-cell contacts in HUVECs.

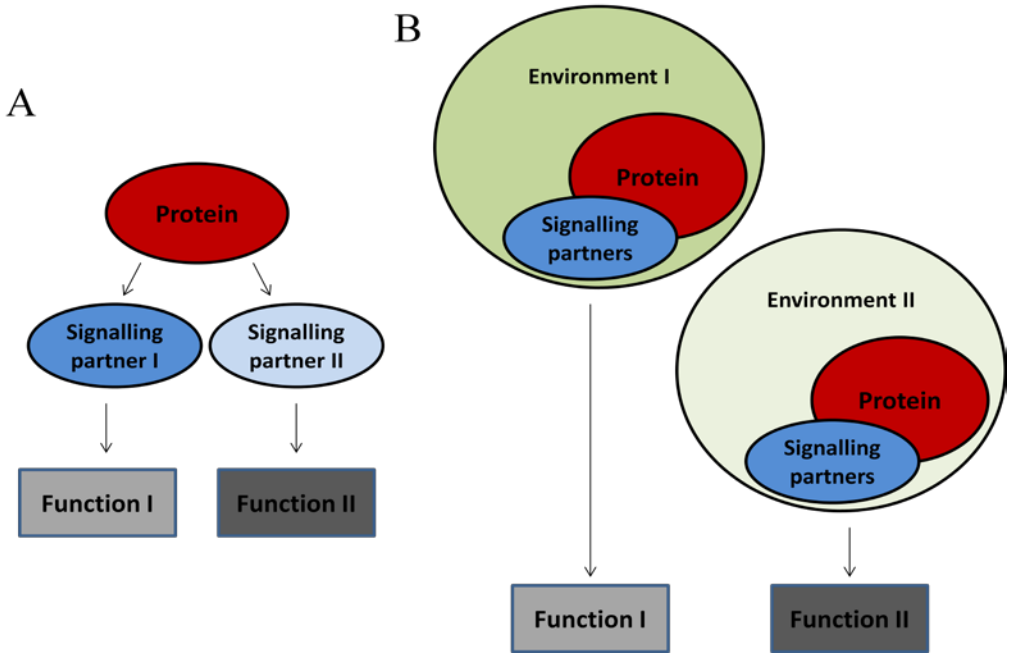

Figure 6.1 A model to explain variable gene function
Proteins may mediate different functions due to the presence of **(A)** different signalling partners, and/or **(B)** different cell environments.

6.2 The FAM40 proteins may contribute to disease

Analysis of FAM40 functions in PC3 cells suggest that they might contribute to prostate cancer progression by regulating cell migration and adhesion. It will be important for future experiments to build on this study by examining FAM40 function in cancers of different origin. Furthermore, *in vivo* models of cancer progression or 3D models for cell migration/invasion will define better the roles of FAM40A and FAM40B in various steps of cancer progression.

Depletion of both FAM40A and FAM40B caused induction of stress fibres in endothelial cells, caused defects in the loop angiogenesis assay, and in the case of FAM40B increased endothelial permeability. These roles fit the functional profiles of the CCM genes (CCM1, CCM2 and CCM3) (Fischer et al., 2013) and both FAM40 proteins interact with CCM3 (section 3.2.1). As discussed in chapter 5, FAM40A and FAM40B may be novel CCM genes. The 'two-hit hypothesis' offers an explanation as to how mutations in the CCM genes manifests specifically as a disorder of the brain endothelium (Gault et al., 2005). According to this, a germline mutation in one CCM allele is augmented by a somatic mutation in the other allele. It would be interesting to ascertain if loss of FAM40 function can act as a '2nd hit'. The FAM40 genes could have roles in endothelium other than that of the CNS. For example, CCM1 mutations can cause cutaneous venous malformations (Toll et al., 2009) showing that CCM patients can display vascular anomalies at secondary sites. Another possibility is that the FAM40 genes are involved in inflammatory responses in endothelial cells. Interestingly, a role for inflammation in CCMs has been proposed (Shenkar et al., 2007).

The interaction of tumour cells with the endothelium is vital to cancer progression and in this context it is interesting that the FAM40 genes have roles in both these cell types. Experiments to probe how the FAM40 genes affect this interaction have not been performed and should be considered for future work. It might be that the FAM40 proteins regulate intravasation and/or extravasation by regulating cancer cell migration/invasion and/or endothelial barrier integrity. Another possibility is that of the FAM40 proteins mediating the vascularisation of tumours. Results presented in this thesis indicate that FAM40 function in endothelial cells might regulate angiogenesis. It will also be important to determine if their functions in cancer cells can cause tumour neovascularisation. A relevant example is that of ROCK function in tumour cells which induces angiogenesis and tumour cell invasion (Croft et al., 2004).

6.3 Why two FAM40 proteins?

The presence of two FAM40 genes in humans (FAM40A and FAM40B) suggests functional specialisation. While it is possible that the two genes have mostly redundant functions, it is important to address this question as differences in functions have been noted in experiments performed. In this thesis depletion of FAM40A and FAM40B in PC3 cells resulted in distinct morphological phenotypes. Furthermore, only FAM40B depletion affected cell migration, spreading and Rac1 activity. A similar functional dichotomy can be observed in HUVECs. Only FAM40B depletion affected endothelial permeability while depletion of only FAM40A resulted in adhesion defects to Matrigel. It might be that FAM40A depletion only induces stress fibres, while FAM40B depletion induces stress fibres and affects junctional proteins. This may explain why only FAM40B depletion caused an increase in permeability. The fact that both FAM40A and FAM40B depletion resulted in stress fibre induction may suggest that both genes signal together to bring about this phenotype. However, endothelial cells have multiple signalling pathways that regulate stress fibre formation.

Taken together, these results suggest that FAM40A and FAM40B may have evolved to fulfil different functions in cells. These differences may be explained by each protein having different signalling partners. For example, only FAM40A is capable of interacting with STRN4 (Goudreault et al., 2009). It is possible that the monomeric form of FAM40A and/or FAM40B represents the functional unit, which is compatible with these observations. However, biochemical analyses presented in chapter 3 indicate that in addition to forming homodimers, both FAM40A and FAM40B are able to interact with each other. This result has to be reconciled with the possibility of FAM40A and FAM40B having independent roles in cells. How can two proteins interact, but yet fulfil individual roles? One possibility is that FAM40A negatively regulates FAM40B signalling and/or vice versa. In this scenario, depletion of FAM40A would lead to increased FAM40B function and/or vice versa. Another possibility is that there is a dynamic equilibrium between FAM40 homodimeric and heterodimeric complexes which form functional units. Depletion of FAM40A would lead to an increase in FAM40B homodimers and associated signalling, and vice versa.

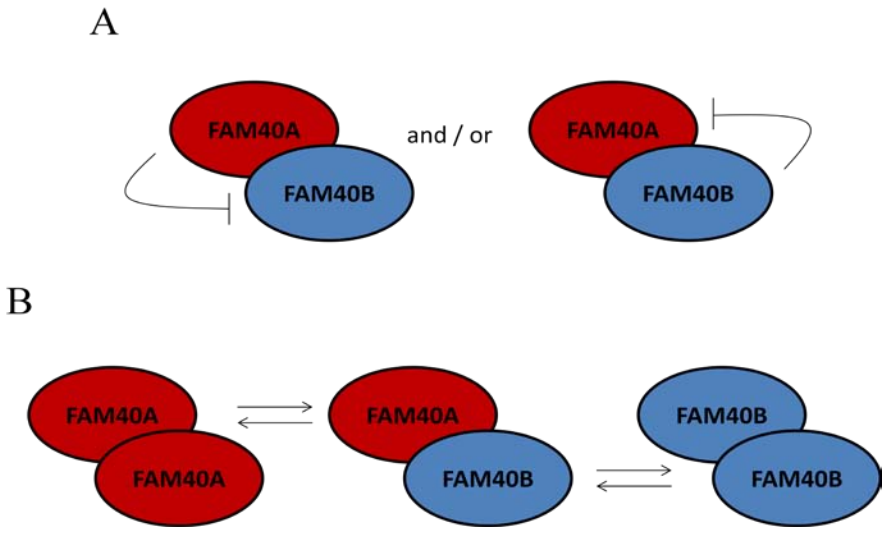

Figure 6.2 A model to explain the divergent roles of FAM40A and FAM40B
FAM40A and FAM40B may associate with each other and still perform independent functions. This can occur by **(A)** FAM40 heterodimerisation being inhibitory, and/or **(B)** the existence of a dynamic equilibrium between FAM40 homodimers/heterodimers.

6.4 A general model for FAM40 gene function

A model for FAM40 function in endothelial cells has been presented in chapter 5 while their roles in cancer cells have been discussed in chapter 4. Based on these findings and data from the literature, can a general model for FAM40 function be put forward?

FAM40A has been shown to interact with members of the STRIPAK complex including CCM3, GCKIII kinases, STRN, STRN3, STRN4, Mob3 and CTTNBP2NL (Goudreault et al., 2009). A common denominator among several of these interacting partners is that they are important for neuronal function. The Drosophila Mob3 homologue is needed for synapse formation and axonal transport (Schulte et al., 2010). Striatins are highly expressed in dendritic spines and have been suggested to function as Ca^{2+} sensors (Benoist et al., 2006), while CTTNBP2 mediates dendritic spinogenesis (Chen et al., 2012). Taken together, these findings imply a role for the STRIPAK complex in synapse formation and signalling. Additionally, FAM40A is highly expressed in the foetal brain (NCBI GEO database, Profile: GDS3113 / 151060 / FAM40A) while FAM40B is upregulated in the retina (NCBI GEO database, Profile: GDS3113 / 152911 / FAM40B). Hence, it would be interesting to study the

functions of FAM40A and FAM40B in neurons and specifically in steps leading to synapse formation.

It has been previously proposed that FAM40B affects endothelial permeability via CCM3 signalling (chapter 5). At the fundamental level, both synapse formation and maintenance of endothelial junction integrity share a common feature – they both involve formation of contacts between adjacent cells. Examples in the literature exist that suggest a role for the STRIPAK complex in mediating cell fusion (section 1.6.2). Perhaps the FAM40 proteins play a fundamental role in mediating cell-cell contact formation in multiple cell types and conditions. It might be that cells use the STRIPAK complex and/or the FAM40 proteins as part of a common tool-kit to facilitate interactions with other cells. Individual components of the complex may have evolved to perform cell specific functions. For example, CCM3 may be important in this respect for contact between endothelial cells, while CTTNBP2NL may act similiarly in neurons. This hypothesis of FAM40 function is supported by the fact that FAM40B depletion in HeLa cells leads to a loss of cell-cell adhesions (Bai et al., 2011). Depletion of CCM3 in neuroglia has been suggested to lead to CCM by affecting interactions within the neurovascular unit (Louvi et al., 2011). In this context, it would be interesting to test if the FAM40 proteins can regulate interactions between the vasculature and neuroglial cells.

The following model presents this hypothesis of FAM40 function, and summarises results presented in this thesis.

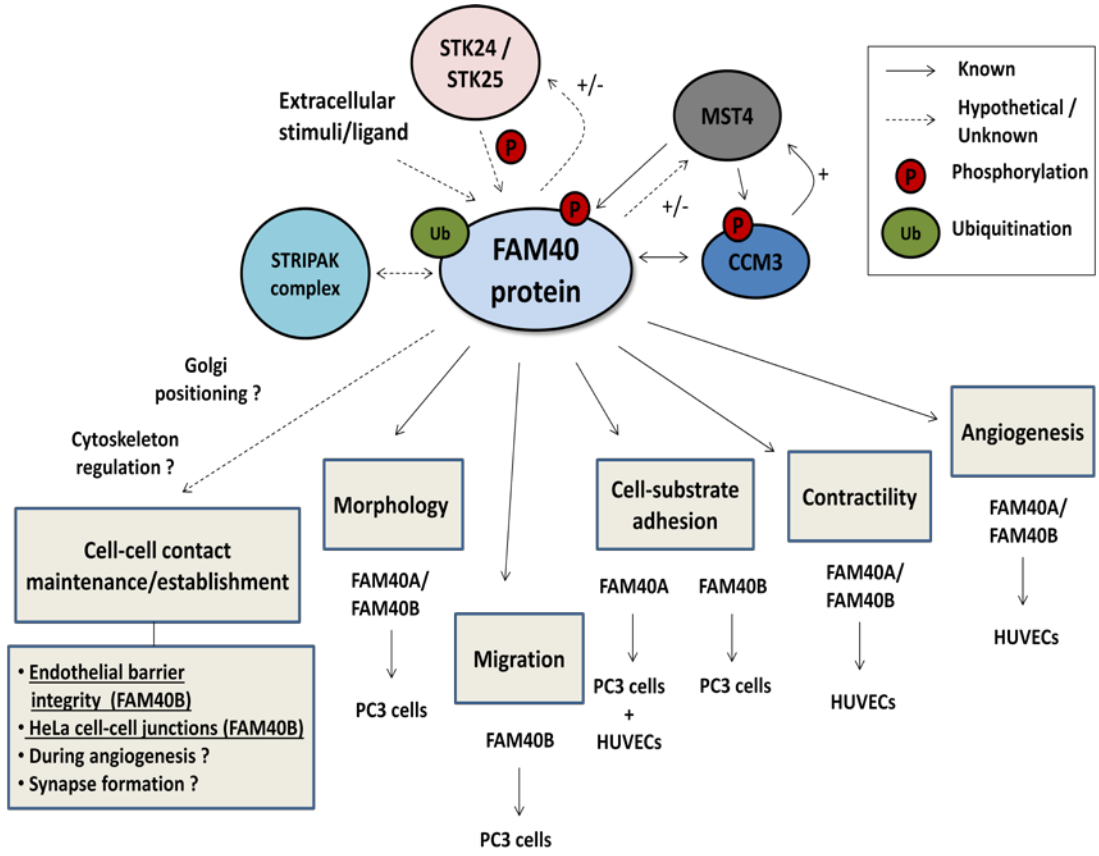

Figure 6.3 A model for FAM40 function

The FAM40 proteins interact with CCM3 and are phosphorylated by MST4 which are components of the STRIPAK complex. It will be important to determine if the FAM40 proteins function only as part of the STRIPAK complex or if they also have independent functions. In scenarios where cell-cell contacts are present, the FAM40 proteins may mediate their maintenance/establishment. Both FAM40 proteins regulate contractility in endothelial cells. A role for FAM40B in endothelial permeability has been demonstrated, while both FAM40A and FAM40B may be important for mediating angiogenesis. FAM40A is important for endothelial cell adhesion to the substrate. In addition, analyses of their functions in PC3 cells have shown that they affect cell morphology, migration and cell-substrate adhesion.

7 References

Aalinkeel, R., Nair, M.P., Sufrin, G., Mahajan, S.D., Chadha, K.C., Chawda, R.P., and Schwartz, S.A. (2004). Gene expression of angiogenic factors correlates with metastatic potential of prostate cancer cells. Cancer Res *64*, 5311-5321.

Abercrombie, M., Heaysman, J.E., and Pegrum, S.M. (1971). The locomotion of fibroblasts in culture. IV. Electron microscopy of the leading lamella. Exp Cell Res *67*, 359-367.

Abraham, S., Yeo, M., Montero-Balaguer, M., Paterson, H., Dejana, E., Marshall, C.J., and Mavria, G. (2009). VE-Cadherin-mediated cell-cell interaction suppresses sprouting via signaling to MLC2 phosphorylation. Current biology : CB *19*, 668-674.

Aitken, A. (2006). 14-3-3 proteins: a historic overview. Semin Cancer Biol *16*, 162-172.

Aktories, K., and Barbieri, J.T. (2005). Bacterial cytotoxins: targeting eukaryotic switches. Nat Rev Microbiol *3*, 397-410.

Alberts, B., Johnson, A., Lewis, J., Raff, M., Roberts, K., and Walter, P. (2002). Molecular Biology of the Cell, 4th edn (New York: Garland Science).

Allen, R.J., Bogle, I.D., and Ridley, A.J. (2011). A model of localised Rac1 activation in endothelial cells due to fluid flow. J Theor Biol *280*, 34-42.

Almagro, S., Durmort, C., Chervin-Petinot, A., Heyraud, S., Dubois, M., Lambert, O., Maillefaud, C., Hewat, E., Schaal, J.P., Huber, P.*, et al.* (2010). The motor protein myosin-X transports VE-cadherin along filopodia to allow the formation of early endothelial cell-cell contacts. Mol Cell Biol *30*, 1703-1717.

Antonetti, D.A., Barber, A.J., Hollinger, L.A., Wolpert, E.B., and Gardner, T.W. (1999). Vascular endothelial growth factor induces rapid phosphorylation of tight junction proteins occludin and zonula occluden 1. A potential mechanism for vascular permeability in diabetic retinopathy and tumors. J Biol Chem *274*, 23463-23467.

Aspenstrom, P., Ruusala, A., and Pacholsky, D. (2007). Taking Rho GTPases to the next level: the cellular functions of atypical Rho GTPases. Experimental cell research *313*, 3673-3679.

Ayollo, D.V., Zhitnyak, I.Y., Vasiliev, J.M., and Gloushankova, N.A. (2009). Rearrangements of the actin cytoskeleton and E-cadherin-based adherens junctions caused by neoplasic transformation change cell-cell interactions. PLoS One *4*, e8027.

Bai, S.W., Herrera-Abreu, M.T., Rohn, J.L., Racine, V., Tajadura, V., Suryavanshi, N., Bechtel, S., Wiemann, S., Baum, B., and Ridley, A.J. (2011). Identification and characterization of a set of conserved and new regulators of cytoskeletal organization, cell morphology and migration. BMC Biol *9*, 54.

Baumgartner, W., Schutz, G.J., Wiegand, J., Golenhofen, N., and Drenckhahn, D. (2003). Cadherin function probed by laser tweezer and single molecule fluorescence in vascular endothelial cells. J Cell Sci *116*, 1001-1011.

Beckers, C.M., van Hinsbergh, V.W., and van Nieuw Amerongen, G.P. (2010). Driving Rho GTPase activity in endothelial cells regulates barrier integrity. Thromb Haemost *103*, 40-55.

Bendtsen, J.D., Jensen, L.J., Blom, N., Von Heijne, G., and Brunak, S. (2004). Feature-based prediction of non-classical and leaderless protein secretion. Protein Eng Des Sel *17*, 349-356.

Benoist, M., Gaillard, S., and Castets, F. (2006). The striatin family: a new signaling platform in dendritic spines. J Physiol Paris *99*, 146-153.

Bergers, G., and Benjamin, L.E. (2003). Tumorigenesis and the angiogenic switch. Nat Rev Cancer *3*, 401-410.

Bernhards, Y., and Poggeler, S. (2011). The phocein homologue SmMOB3 is essential for vegetative cell fusion and sexual development in the filamentous ascomycete Sordaria macrospora. Curr Genet *57*, 133-149.

Bevilacqua, M.P., Pober, J.S., Mendrick, D.L., Cotran, R.S., and Gimbrone, M.A., Jr. (1987). Identification of an inducible endothelial-leukocyte adhesion molecule. Proc Natl Acad Sci U S A *84*, 9238-9242.

Bishop, A.L., and Hall, A. (2000). Rho GTPases and their effector proteins. The Biochemical journal *348 Pt 2*, 241-255.

Bloemendal, S., Bernhards, Y., Bartho, K., Dettmann, A., Voigt, O., Teichert, I., Seiler, S., Wolters, D.A., Poggeler, S., and Kuck, U. (2012). A homologue of the human STRIPAK complex controls sexual development in fungi. Mol Microbiol *84*, 310-323.

Boulter, E., Estrach, S., Garcia-Mata, R., and Feral, C.C. (2012). Off the beaten paths: alternative and crosstalk regulation of Rho GTPases. FASEB J *26*, 469-479.

Boureux, A., Vignal, E., Faure, S., and Fort, P. (2007). Evolution of the Rho family of ras-like GTPases in eukaryotes. Mol Biol Evol *24*, 203-216.

Bouvard, D., Vignoud, L., Dupe-Manet, S., Abed, N., Fournier, H.N., Vincent-Monegat, C., Retta, S.F., Fassler, R., and Block, M.R. (2003). Disruption of focal adhesions by integrin cytoplasmic domain-associated protein-1 alpha. J Biol Chem *278*, 6567-6574.

Bustos, R.I., Forget, M.A., Settleman, J.E., and Hansen, S.H. (2008). Coordination of Rho and Rac GTPase function via p190B RhoGAP. Curr Biol *18*, 1606-1611.

Cain, R.J., and Ridley, A.J. (2009). Phosphoinositide 3-kinases in cell migration. Biology of the cell / under the auspices of the European Cell Biology Organization *101*, 13-29.

Cain, R.J., Vanhaesebroeck, B., and Ridley, A.J. (2010). The PI3K p110alpha isoform regulates endothelial adherens junctions via Pyk2 and Rac1. J Cell Biol *188*, 863-876.

Calalb, M.B., Zhang, X., Polte, T.R., and Hanks, S.K. (1996). Focal adhesion kinase tyrosine-861 is a major site of phosphorylation by Src. Biochem Biophys Res Commun *228*, 662-668.

Calvo, F., and Sahai, E. (2011). Cell communication networks in cancer invasion. Curr Opin Cell Biol *23*, 621-629.

Carman, C.V., and Springer, T.A. (2004). A transmigratory cup in leukocyte diapedesis both through individual vascular endothelial cells and between them. J Cell Biol *167*, 377-388.

Carmeliet, P. (2005). VEGF as a key mediator of angiogenesis in cancer. Oncology *69 Suppl 3*, 4-10.

Carmeliet, P., Lampugnani, M.G., Moons, L., Breviario, F., Compernolle, V., Bono, F., Balconi, G., Spagnuolo, R., Oosthuyse, B., Dewerchin, M.*, et al.* (1999). Targeted deficiency or cytosolic truncation of the VE-cadherin gene in mice impairs VEGF-mediated endothelial survival and angiogenesis. Cell *98*, 147-157.

Cascone, I., Giraudo, E., Caccavari, F., Napione, L., Bertotti, E., Collard, J.G., Serini, G., and Bussolino, F. (2003). Temporal and spatial modulation of Rho GTPases during in vitro formation of capillary vascular network. Adherens junctions and myosin light chain as targets of Rac1 and RhoA. J Biol Chem *278*, 50702-50713.

Castillo-Lluva, S., Tatham, M.H., Jones, R.C., Jaffray, E.G., Edmondson, R.D., Hay, R.T., and Malliri, A. (2010). SUMOylation of the GTPase Rac1 is required for optimal cell migration. Nature cell biology *12*, 1078-1085.

Cavalcanti, D.D., Kalani, M.Y., Martirosyan, N.L., Eales, J., Spetzler, R.F., and Preul, M.C. (2012). Cerebral cavernous malformations: from genes to proteins to disease. J Neurosurg *116*, 122-132.

Cavallaro, U., and Christofori, G. (2004). Cell adhesion and signalling by cadherins and Ig-CAMs in cancer. Nat Rev Cancer *4*, 118-132.

Ceccarelli, D.F., Laister, R.C., Mulligan, V.K., Kean, M.J., Goudreault, M., Scott, I.C., Derry, W.B., Chakrabartty, A., Gingras, A.C., and Sicheri, F. (2011). CCM3/PDCD10 Heterodimerizes with Germinal Center Kinase III (GCKIII) Proteins Using a Mechanism Analogous to CCM3 Homodimerization. The Journal of biological chemistry *286*, 25056-25064.

Chan, A.C., Drakos, S.G., Ruiz, O.E., Smith, A.C., Gibson, C.C., Ling, J., Passi, S.F., Stratman, A.N., Sacharidou, A., Revelo, M.P.*, et al.* (2011). Mutations in 2 distinct genetic pathways result in cerebral cavernous malformations in mice. J Clin Invest *121*, 1871-1881.

Chang, S.H., Kanasaki, K., Gocheva, V., Blum, G., Harper, J., Moses, M.A., Shih, S.C., Nagy, J.A., Joyce, J., Bogyo, M.*, et al.* (2009). VEGF-A induces angiogenesis by perturbing the cathepsin-cysteine protease inhibitor balance in venules, causing basement membrane degradation and mother vessel formation. Cancer Res *69*, 4537-4544.

Chau, B.N., and Wang, J.Y. (2003). Coordinated regulation of life and death by RB. Nat Rev Cancer *3*, 130-138.

Chen, X.D., and Cho, C.Y. (2011). Downregulation of SOK1 promotes the migration of MCF-7 cells. Biochem Biophys Res Commun *407*, 389-392.

Chen, Y.K., Chen, C.Y., Hu, H.T., and Hsueh, Y.P. (2012). CTTNBP2, but not CTTNBP2NL, regulates dendritic spinogenesis and synaptic distribution of the striatin-PP2A complex. Mol Biol Cell *23*, 4383-4392.

Chrzanowska-Wodnicka, M., and Burridge, K. (1996). Rho-stimulated contractility drives the formation of stress fibers and focal adhesions. J Cell Biol *133*, 1403-1415.

Claesson-Welsh, L., and Welsh, M. (2013). VEGFA and tumour angiogenesis. J Intern Med *273*, 114-127.

Clatterbuck, R.E., Eberhart, C.G., Crain, B.J., and Rigamonti, D. (2001). Ultrastructural and immunocytochemical evidence that an incompetent blood-brain barrier is related to the pathophysiology of cavernous malformations. J Neurol Neurosurg Psychiatry *71*, 188-192.

Corada, M., Mariotti, M., Thurston, G., Smith, K., Kunkel, R., Brockhaus, M., Lampugnani, M.G., Martin-Padura, I., Stoppacciaro, A., Ruco, L.*, et al.* (1999). Vascular endothelial-cadherin is an important determinant of microvascular integrity in vivo. Proc Natl Acad Sci U S A *96*, 9815-9820.

Cory, G.O., and Ridley, A.J. (2002). Cell motility: braking WAVEs. Nature *418*, 732-733.

Costa, B., Kean, M.J., Ast, V., Knight, J.D., Mett, A., Levy, Z., Ceccarelli, D.F., Badillo, B.G., Eils, R., Konig, R.*, et al.* (2012). STK25 protein mediates TrkA and CCM2 protein-dependent death in pediatric tumor cells of neural origin. J Biol Chem *287*, 29285-29289.

Covitz, K.M., Amidon, G.L., and Sadee, W. (1998). Membrane topology of the human dipeptide transporter, hPEPT1, determined by epitope insertions. Biochemistry *37*, 15214-15221.

Cramer, L.P., Siebert, M., and Mitchison, T.J. (1997). Identification of novel graded polarity actin filament bundles in locomoting heart fibroblasts: implications for the generation of motile force. J Cell Biol *136*, 1287-1305.

Croft, D.R., Sahai, E., Mavria, G., Li, S., Tsai, J., Lee, W.M., Marshall, C.J., and Olson, M.F. (2004). Conditional ROCK activation in vivo induces tumor cell dissemination and angiogenesis. Cancer Res *64*, 8994-9001.

Cullere, X., Shaw, S.K., Andersson, L., Hirahashi, J., Luscinskas, F.W., and Mayadas, T.N. (2005). Regulation of vascular endothelial barrier function by Epac, a cAMP-activated exchange factor for Rap GTPase. Blood *105*, 1950-1955.

Cybulski, N., and Hall, M.N. (2009). TOR complex 2: a signaling pathway of its own. Trends Biochem Sci *34*, 620-627.

Dadiani, M., Kalchenko, V., Yosepovich, A., Margalit, R., Hassid, Y., Degani, H., and Seger, D. (2006). Real-time imaging of lymphogenic metastasis in orthotopic human breast cancer. Cancer Res *66*, 8037-8041.

Dan, I., Ong, S.E., Watanabe, N.M., Blagoev, B., Nielsen, M.M., Kajikawa, E., Kristiansen, T.Z., Mann, M., and Pandey, A. (2002). Cloning of MASK, a novel member of the mammalian germinal center kinase III subfamily, with apoptosis-inducing properties. J Biol Chem *277*, 5929-5939.

De Smet, F., Segura, I., De Bock, K., Hohensinner, P.J., and Carmeliet, P. (2009). Mechanisms of vessel branching: filopodia on endothelial tip cells lead the way. Arterioscler Thromb Vasc Biol *29*, 639-649.

Dejana, E. (2004). Endothelial cell-cell junctions: happy together. Nat Rev Mol Cell Biol *5*, 261-270.

Dejana, E., and Giampietro, C. (2012). Vascular endothelial-cadherin and vascular stability. Curr Opin Hematol *19*, 218-223.

Dejana, E., Tournier-Lasserve, E., and Weinstein, B.M. (2009). The control of vascular integrity by endothelial cell junctions: molecular basis and pathological implications. Dev Cell *16*, 209-221.

Deleavey, G.F., and Damha, M.J. (2012). Designing chemically modified oligonucleotides for targeted gene silencing. Chem Biol *19*, 937-954.

Delestre, L., Berthon, C., Quesnel, B., Figeac, M., Kerckaert, J.P., Galiegue-Zouitina, S., and Shelley, C.S. (2011). Repression of the RHOH gene by JunD. Biochem J *437*, 75-88.

DePina, A.S., and Langford, G.M. (1999). Vesicle transport: the role of actin filaments and myosin motors. Microsc Res Tech *47*, 93-106.

Dimitroff, C.J., Descheny, L., Trujillo, N., Kim, R., Nguyen, V., Huang, W., Pienta, K.J., Kutok, J.L., and Rubin, M.A. (2005). Identification of leukocyte E-selectin ligands, P-selectin glycoprotein ligand-1 and E-selectin ligand-1, on human metastatic prostate tumor cells. Cancer Res *65*, 5750-5760.

Dvorak, A.M., Kohn, S., Morgan, E.S., Fox, P., Nagy, J.A., and Dvorak, H.F. (1996). The vesiculo-vacuolar organelle (VVO): a distinct endothelial cell structure that provides a transcellular pathway for macromolecular extravasation. J Leukoc Biol *59*, 100-115.

Edgar, R.C. (2004). MUSCLE: multiple sequence alignment with high accuracy and high throughput. Nucleic Acids Res *32*, 1792-1797.

Ellerbroek, S.M., Wennerberg, K., and Burridge, K. (2003). Serine phosphorylation negatively regulates RhoA in vivo. J Biol Chem *278*, 19023-19031.

Etienne-Manneville, S., and Hall, A. (2003). Cell polarity: Par6, aPKC and cytoskeletal crosstalk. Curr Opin Cell Biol *15*, 67-72.

Fackler, O.T., and Grosse, R. (2008). Cell motility through plasma membrane blebbing. J Cell Biol *181*, 879-884.

Faurobert, E., and Albiges-Rizo, C. (2010). Recent insights into cerebral cavernous malformations: a complex jigsaw puzzle under construction. Febs j *277*, 1084-1096.

Fernandez-Martin, L., Marcos-Ramiro, B., Bigarella, C.L., Graupera, M., Cain, R.J., Reglero-Real, N., Jimenez, A., Cernuda-Morollon, E., Correas, I., Cox, S.*, et al.* (2012). Crosstalk between reticular adherens junctions and platelet endothelial cell adhesion molecule-1 regulates endothelial barrier function. Arterioscler Thromb Vasc Biol *32*, e90-102.

Ferrara, N. (2009). Vascular endothelial growth factor. Arterioscler Thromb Vasc Biol *29*, 789-791.

Fidalgo, M., Fraile, M., Pires, A., Force, T., Pombo, C., and Zalvide, J. (2010). CCM3/PDCD10 stabilizes GCKIII proteins to promote Golgi assembly and cell orientation. J Cell Sci *123*, 1274-1284.

Fidalgo, M., Guerrero, A., Fraile, M., Iglesias, C., Pombo, C.M., and Zalvide, J. (2012). Adaptor protein cerebral cavernous malformation 3 (CCM3) mediates phosphorylation of the cytoskeletal proteins ezrin/radixin/moesin by mammalian Ste20-4 to protect cells from oxidative stress. J Biol Chem *287*, 11556-11565.

Fischer, A., Zalvide, J., Faurobert, E., Albiges-Rizo, C., and Tournier-Lasserve, E. (2013). Cerebral cavernous malformations: from CCM genes to endothelial cell homeostasis. Trends Mol Med.

Fischer, R.S., Gardel, M., Ma, X., Adelstein, R.S., and Waterman, C.M. (2009). Local cortical tension by myosin II guides 3D endothelial cell branching. Curr Biol *19*, 260-265.

Friedl, P., Locker, J., Sahai, E., and Segall, J.E. (2012). Classifying collective cancer cell invasion. Nat Cell Biol *14*, 777-783.

Friedl, P., and Wolf, K. (2003). Tumour-cell invasion and migration: diversity and escape mechanisms. Nature reviewsCancer *3*, 362-374.

Fu, C., Iyer, P., Herkal, A., Abdullah, J., Stout, A., and Free, S.J. (2011). Identification and characterization of genes required for cell-to-cell fusion in Neurospora crassa. Eukaryot Cell *10*, 1100-1109.

Garcia, J.G., Liu, F., Verin, A.D., Birukova, A., Dechert, M.A., Gerthoffer, W.T., Bamberg, J.R., and English, D. (2001). Sphingosine 1-phosphate promotes endothelial cell barrier integrity by Edg-dependent cytoskeletal rearrangement. J Clin Invest *108*, 689-701.

Garcia-Mata, R., Boulter, E., and Burridge, K. (2011). The 'invisible hand': regulation of RHO GTPases by RHOGDIs. Nat Rev Mol Cell Biol *12*, 493-504.

Gault, J., Shenkar, R., Recksiek, P., and Awad, I.A. (2005). Biallelic somatic and germ line CCM1 truncating mutations in a cerebral cavernous malformation lesion. Stroke *36*, 872-874.

Gavard, J., and Gutkind, J.S. (2006). VEGF controls endothelial-cell permeability by promoting the beta-arrestin-dependent endocytosis of VE-cadherin. Nat Cell Biol *8*, 1223-1234.

Gingras, A.R., Liu, J.J., and Ginsberg, M.H. (2012). Structural basis of the junctional anchorage of the cerebral cavernous malformations complex. J Cell Biol *199*, 39-48.

Glading, A., Han, J., Stockton, R.A., and Ginsberg, M.H. (2007). KRIT-1/CCM1 is a Rap1 effector that regulates endothelial cell cell junctions. The Journal of cell biology *179*, 247-254.

Goldfarb, M., Shimizu, K., Perucho, M., and Wigler, M. (1982). Isolation and preliminary characterization of a human transforming gene from T24 bladder carcinoma cells. Nature *296*, 404-409.

Goodwin, A.M. (2007). In vitro assays of angiogenesis for assessment of angiogenic and anti-angiogenic agents. Microvasc Res *74*, 172-183.

Gordon, J., Hwang, J., Carrier, K.J., Jones, C.A., Kern, Q.L., Moreno, C.S., Karas, R.H., and Pallas, D.C. (2011). Protein phosphatase 2a (PP2A) binds within the oligomerization domain of striatin and regulates the phosphorylation and activation of the mammalian Ste20-Like kinase Mst3. BMC Biochem *12*, 54.

Gory-Faure, S., Prandini, M.H., Pointu, H., Roullot, V., Pignot-Paintrand, I., Vernet, M., and Huber, P. (1999). Role of vascular endothelial-cadherin in vascular morphogenesis. Development *126*, 2093-2102.

Gottesbuhren, U., Garg, R., Riou, P., McColl, B., Brayson, D., and Ridley, A.J. (2013). Rnd3 induces stress fibres in endothelial cells through RhoB. Biol Open *2*, 210-216.

Goudreault, M., D'Ambrosio, L.M., Kean, M.J., Mullin, M.J., Larsen, B.G., Sanchez, A., Chaudhry, S., Chen, G.I., Sicheri, F., Nesvizhskii, A.I.*, et al.* (2009). A PP2A phosphatase high density interaction network identifies a novel striatin-interacting phosphatase and kinase complex linked to the cerebral cavernous malformation 3 (CCM3) protein. Molecular & cellular proteomics : MCP *8*, 157-171.

Graupera, M., Guillermet-Guibert, J., Foukas, L.C., Phng, L.K., Cain, R.J., Salpekar, A., Pearce, W., Meek, S., Millan, J., Cutillas, P.R.*, et al.* (2008). Angiogenesis selectively requires the p110alpha isoform of PI3K to control endothelial cell migration. Nature *453*, 662-666.

Grazia Lampugnani, M., Zanetti, A., Corada, M., Takahashi, T., Balconi, G., Breviario, F., Orsenigo, F., Cattelino, A., Kemler, R., Daniel, T.O.*, et al.* (2003). Contact inhibition of VEGF-induced proliferation requires vascular endothelial cadherin, beta-catenin, and the phosphatase DEP-1/CD148. J Cell Biol *161*, 793-804.

Haidari, M., Zhang, W., Caivano, A., Chen, Z., Ganjehei, L., Mortazavi, A., Stroud, C., Woodside, D.G., Willerson, J.T., and Dixon, R.A. (2012). Integrin alpha2beta1 mediates tyrosine phosphorylation of vascular endothelial cadherin induced by invasive breast cancer cells. J Biol Chem *287*, 32981-32992.

Hall, A., and Nobes, C.D. (2000). Rho GTPases: molecular switches that control the organization and dynamics of the actin cytoskeleton. Philosophical transactions of the Royal Society of LondonSeries B, Biological sciences *355*, 965-970.

Hanahan, D., and Folkman, J. (1996). Patterns and emerging mechanisms of the angiogenic switch during tumorigenesis. Cell *86*, 353-364.

Hanahan, D., and Weinberg, R.A. (2011). Hallmarks of cancer: the next generation. Cell *144*, 646-674.

Harhaj, N.S., and Antonetti, D.A. (2004). Regulation of tight junctions and loss of barrier function in pathophysiology. Int J Biochem Cell Biol *36*, 1206-1237.

Harris, E.S., and Nelson, W.J. (2010). VE-cadherin: at the front, center, and sides of endothelial cell organization and function. Curr Opin Cell Biol *22*, 651-658.

Hart, I.R., and Fidler, I.J. (1980). Role of organ selectivity in the determination of metastatic patterns of B16 melanoma. Cancer Res *40*, 2281-2287.

Heasman, S.J., and Ridley, A.J. (2008). Mammalian Rho GTPases: new insights into their functions from in vivo studies. Nature reviewsMolecular cell biology *9*, 690-701.

Herbert, S.P., and Stainier, D.Y. (2011). Molecular control of endothelial cell behaviour during blood vessel morphogenesis. Nat Rev Mol Cell Biol *12*, 551-564.

Hirase, T., Kawashima, S., Wong, E.Y., Ueyama, T., Rikitake, Y., Tsukita, S., Yokoyama, M., and Staddon, J.M. (2001). Regulation of tight junction permeability and occludin phosphorylation by Rhoa-p160ROCK-dependent and -independent mechanisms. J Biol Chem *276*, 10423-10431.

Hoelzle, M.K., and Svitkina, T. (2012). The cytoskeletal mechanisms of cell-cell junction formation in endothelial cells. Molecular biology of the cell *23*, 310-323.

Hornbeck, P.V., Kornhauser, J.M., Tkachev, S., Zhang, B., Skrzypek, E., Murray, B., Latham, V., and Sullivan, M. (2012). PhosphoSitePlus: a comprehensive resource for investigating the structure and function of experimentally determined post-translational modifications in man and mouse. Nucleic Acids Res *40*, D261-270.

Huang, C.Y., Wu, Y.M., Hsu, C.Y., Lee, W.S., Lai, M.D., Lu, T.J., Huang, C.L., Leu, T.H., Shih, H.M., Fang, H.I*., et al.* (2002). Caspase activation of mammalian sterile 20-like kinase 3 (Mst3). Nuclear translocation and induction of apoptosis. J Biol Chem *277*, 34367-34374.

Hunter, K.W., Crawford, N.P., and Alsarraj, J. (2008). Mechanisms of metastasis. Breast cancer research : BCR *10 Suppl 1*, S2.

Hunter, T. (2012). Why nature chose phosphate to modify proteins. Philos Trans R Soc Lond B Biol Sci *367*, 2513-2516.

Hyodo, T., Ito, S., Hasegawa, H., Asano, E., Maeda, M., Urano, T., Takahashi, M., Hamaguchi, M., and Senga, T. (2012). Misshapen-like kinase 1 (MINK1) is a novel

component of striatin-interacting phosphatase and kinase (STRIPAK) and is required for the completion of cytokinesis. J Biol Chem *287*, 25019-25029.

Ito, S., Nakanishi, H., Ikehara, Y., Kato, T., Kasai, Y., Ito, K., Akiyama, S., Nakao, A., and Tatematsu, M. (2001). Real-time observation of micrometastasis formation in the living mouse liver using a green fluorescent protein gene-tagged rat tongue carcinoma cell line. Int J Cancer *93*, 212-217.

Jaffe, A.B., and Hall, A. (2005). Rho GTPases: biochemistry and biology. Annu Rev Cell Dev Biol *21*, 247-269.

Joyce, J.A., and Pollard, J.W. (2009). Microenvironmental regulation of metastasis. Nat Rev Cancer *9*, 239-252.

Karnoub, A.E., Dash, A.B., Vo, A.P., Sullivan, A., Brooks, M.W., Bell, G.W., Richardson, A.L., Polyak, K., Tubo, R., and Weinberg, R.A. (2007). Mesenchymal stem cells within tumour stroma promote breast cancer metastasis. Nature *449*, 557-563.

Katsamba, P., Carroll, K., Ahlsen, G., Bahna, F., Vendome, J., Posy, S., Rajebhosale, M., Price, S., Jessell, T.M., Ben-Shaul, A.*, et al.* (2009). Linking molecular affinity and cellular specificity in cadherin-mediated adhesion. Proc Natl Acad Sci U S A *106*, 11594-11599.

Kaur, S., Leszczynska, K., Abraham, S., Scarcia, M., Hiltbrunner, S., Marshall, C.J., Mavria, G., Bicknell, R., and Heath, V.L. (2011). RhoJ/TCL regulates endothelial motility and tube formation and modulates actomyosin contractility and focal adhesion numbers. Arterioscler Thromb Vasc Biol *31*, 657-664.

Kay, B.K., Williamson, M.P., and Sudol, M. (2000). The importance of being proline: the interaction of proline-rich motifs in signaling proteins with their cognate domains. FASEB J *14*, 231-241.

Kean, M.J., Ceccarelli, D.F., Goudreault, M., Sanches, M., Tate, S., Larsen, B., Gibson, L.C., Derry, W.B., Scott, I.C., Pelletier, L.*, et al.* (2011). Structure-function analysis of core STRIPAK Proteins: a signaling complex implicated in Golgi polarization. J Biol Chem *286*, 25065-25075.

Kemp, H.A., and Sprague, G.F., Jr. (2003). Far3 and five interacting proteins prevent premature recovery from pheromone arrest in the budding yeast Saccharomyces cerevisiae. Mol Cell Biol *23*, 1750-1763.

Khuon, S., Liang, L., Dettman, R.W., Sporn, P.H., Wysolmerski, R.B., and Chew, T.L. (2010). Myosin light chain kinase mediates transcellular intravasation of breast cancer cells through the underlying endothelial cells: a three-dimensional FRET study. J Cell Sci *123*, 431-440.

Kimura, T., Ohnuma, M., Sawai, T., and Yamaguchi, A. (1997). Membrane topology of the transposon 10-encoded metal-tetracycline/H+ antiporter as studied by site-directed chemical labeling. J Biol Chem *272*, 580-585.

Kleaveland, B., Zheng, X., Liu, J.J., Blum, Y., Tung, J.J., Zou, Z., Sweeney, S.M., Chen, M., Guo, L., Lu, M.M.*, et al.* (2009). Regulation of cardiovascular development and integrity by the heart of glass-cerebral cavernous malformation protein pathway. Nature medicine *15*, 169-176.

Knudson, A.G., Jr. (1971). Mutation and cancer: statistical study of retinoblastoma. Proc Natl Acad Sci U S A *68*, 820-823.

Koh, W., Mahan, R.D., and Davis, G.E. (2008). Cdc42- and Rac1-mediated endothelial lumen formation requires Pak2, Pak4 and Par3, and PKC-dependent signaling. J Cell Sci *121*, 989-1001.

Kooistra, M.R., Dube, N., and Bos, J.L. (2007). Rap1: a key regulator in cell-cell junction formation. Journal of cell science *120*, 17-22.

Kouklis, P., Konstantoulaki, M., Vogel, S., Broman, M., and Malik, A.B. (2004). Cdc42 regulates the restoration of endothelial barrier function. Circ Res *94*, 159-166.

Kovar, D.R. (2006). Molecular details of formin-mediated actin assembly. Curr Opin Cell Biol *18*, 11-17.

Kowalczyk, A.P., Navarro, P., Dejana, E., Bornslaeger, E.A., Green, K.J., Kopp, D.S., and Borgwardt, J.E. (1998). VE-cadherin and desmoplakin are assembled into dermal microvascular endothelial intercellular junctions: a pivotal role for plakoglobin in the recruitment of desmoplakin to intercellular junctions. J Cell Sci *111 (Pt 20)*, 3045-3057.

Kozma, R., Ahmed, S., Best, A., and Lim, L. (1995). The Ras-related protein Cdc42Hs and bradykinin promote formation of peripheral actin microspikes and filopodia in Swiss 3T3 fibroblasts. Mol Cell Biol *15*, 1942-1952.

Kroemer, G., and Pouyssegur, J. (2008). Tumor cell metabolism: cancer's Achilles' heel. Cancer Cell *13*, 472-482.

Langridge, P.D., and Kay, R.R. (2006). Blebbing of Dictyostelium cells in response to chemoattractant. Exp Cell Res *312*, 2009-2017.

Lazarides, E., and Burridge, K. (1975). Alpha-actinin: immunofluorescent localization of a muscle structural protein in nonmuscle cells. Cell *6*, 289-298.

Leblanc, G.G., Golanov, E., Awad, I.A., and Young, W.L. (2009). Biology of vascular malformations of the brain. Stroke *40*, e694-702.

Levin, D.E. (2005). Cell wall integrity signaling in Saccharomyces cerevisiae. Microbiology and molecular biology reviews : MMBR *69*, 262-291.

Li, X., Zhang, R., Zhang, H., He, Y., Ji, W., Min, W., and Boggon, T.J. (2010). Crystal structure of CCM3, a cerebral cavernous malformation protein critical for vascular integrity. J Biol Chem *285*, 24099-24107.

Lin, E.Y., Li, J.F., Gnatovskiy, L., Deng, Y., Zhu, L., Grzesik, D.A., Qian, H., Xue, X.N., and Pollard, J.W. (2006). Macrophages regulate the angiogenic switch in a mouse model of breast cancer. Cancer Res *66*, 11238-11246.

Lin, J.L., Chen, H.C., Fang, H.I., Robinson, D., Kung, H.J., and Shih, H.M. (2001). MST4, a new Ste20-related kinase that mediates cell growth and transformation via modulating ERK pathway. Oncogene *20*, 6559-6569.

Ling, P., Lu, T.J., Yuan, C.J., and Lai, M.D. (2008). Biosignaling of mammalian Ste20-related kinases. Cellular signalling *20*, 1237-1247.

Lippincott-Schwartz, J. (2000). Doing cell science. J Cell Sci *113 (Pt 9)*, 1499-1500.

Lisa-Santamaria, P., Jimenez, A., and Revuelta, J.L. (2012). The protein factor-arrest 11 (Far11) is essential for the toxicity of human caspase-10 in yeast and participates in the regulation of autophagy and the DNA damage signaling. J Biol Chem *287*, 29636-29647.

Liu, W., Draheim, K.M., Zhang, R., Calderwood, D.A., and Boggon, T.J. (2013). Mechanism for KRIT1 Release of ICAP1-Mediated Suppression of Integrin Activation. Mol Cell *49*, 719-729.

Liu, Y., and Senger, D.R. (2004). Matrix-specific activation of Src and Rho initiates capillary morphogenesis of endothelial cells. FASEB J *18*, 457-468.

Logothetis, C.J., and Lin, S.H. (2005). Osteoblasts in prostate cancer metastasis to bone. Nat Rev Cancer *5*, 21-28.

Louvi, A., Chen, L., Two, A.M., Zhang, H., Min, W., and Gunel, M. (2011). Loss of cerebral cavernous malformation 3 (Ccm3) in neuroglia leads to CCM and vascular pathology. Proc Natl Acad Sci U S A *108*, 3737-3742.

Lu, T.J., Lai, W.Y., Huang, C.Y., Hsieh, W.J., Yu, J.S., Hsieh, Y.J., Chang, W.T., Leu, T.H., Chang, W.C., Chuang, W.J*., et al.* (2006). Inhibition of cell migration by autophosphorylated mammalian sterile 20-like kinase 3 (MST3) involves paxillin and protein-tyrosine phosphatase-PEST. J Biol Chem *281*, 38405-38417.

Luo, B.H., Carman, C.V., and Springer, T.A. (2007). Structural basis of integrin regulation and signaling. Annu Rev Immunol *25*, 619-647.

Ma, X., Zhao, H., Shan, J., Long, F., Chen, Y., Zhang, Y., Han, X., and Ma, D. (2007). PDCD10 interacts with Ste20-related kinase MST4 to promote cell growth and transformation via modulation of the ERK pathway. Molecular biology of the cell *18*, 1965-1978.

Madaule, P., and Axel, R. (1985). A novel ras-related gene family. Cell *41*, 31-40.

Mamdouh, Z., Chen, X., Pierini, L.M., Maxfield, F.R., and Muller, W.A. (2003). Targeted recycling of PECAM from endothelial surface-connected compartments during diapedesis. Nature *421*, 748-753.

Mandai, K., Nakanishi, H., Satoh, A., Takahashi, K., Satoh, K., Nishioka, H., Mizoguchi, A., and Takai, Y. (1999). Ponsin/SH3P12: an l-afadin- and vinculin-binding protein localized at cell-cell and cell-matrix adherens junctions. J Cell Biol *144*, 1001-1017.

Mavria, G., Vercoulen, Y., Yeo, M., Paterson, H., Karasarides, M., Marais, R., Bird, D., and Marshall, C.J. (2006). ERK-MAPK signaling opposes Rho-kinase to promote endothelial cell survival and sprouting during angiogenesis. Cancer Cell *9*, 33-44.

McKenzie, J.A., and Ridley, A.J. (2007). Roles of Rho/ROCK and MLCK in TNF-alpha-induced changes in endothelial morphology and permeability. J Cell Physiol *213*, 221-228.

Mellor, H. (2004). Cell motility: Golgi signalling shapes up to ship out. Curr Biol *14*, R434-435.

Millan, J., Cain, R.J., Reglero-Real, N., Bigarella, C., Marcos-Ramiro, B., Fernandez-Martin, L., Correas, I., and Ridley, A.J. (2010). Adherens junctions connect stress fibres between adjacent endothelial cells. BMC Biol *8*, 11.

Millan, J., Williams, L., and Ridley, A.J. (2006). An in vitro model to study the role of endothelial rho GTPases during leukocyte transendothelial migration. Methods Enzymol *406*, 643-655.

Mitra, S.K., Hanson, D.A., and Schlaepfer, D.D. (2005). Focal adhesion kinase: in command and control of cell motility. Nature reviewsMolecular cell biology *6*, 56-68.

Mohr, S.E., and Perrimon, N. (2012). RNAi screening: new approaches, understandings, and organisms. Wiley Interdiscip Rev RNA *3*, 145-158.

Mseka, T., Coughlin, M., and Cramer, L.P. (2009). Graded actin filament polarity is the organization of oriented actomyosin II filament bundles required for fibroblast polarization. Cell Motil Cytoskeleton *66*, 743-753.

Nakamura, K., Yano, H., Uchida, H., Hashimoto, S., Schaefer, E., and Sabe, H. (2000). Tyrosine phosphorylation of paxillin alpha is involved in temporospatial regulation of paxillin-containing focal adhesion formation and F-actin organization in motile cells. J Biol Chem *275*, 27155-27164.

Nakamura, T., Kurokawa, K., Kiyokawa, E., and Matsuda, M. (2006). Analysis of the spatiotemporal activation of rho GTPases using Raichu probes. Methods in enzymology *406*, 315-332.

Navarro, P., Ruco, L., and Dejana, E. (1998). Differential localization of VE- and N-cadherins in human endothelial cells: VE-cadherin competes with N-cadherin for junctional localization. J Cell Biol *140*, 1475-1484.

Nawroth, R., Poell, G., Ranft, A., Kloep, S., Samulowitz, U., Fachinger, G., Golding, M., Shima, D.T., Deutsch, U., and Vestweber, D. (2002). VE-PTP and VE-cadherin ectodomains interact to facilitate regulation of phosphorylation and cell contacts. EMBO J *21*, 4885-4895.

Nethe, M., and Hordijk, P.L. (2010). The role of ubiquitylation and degradation in RhoGTPase signalling. J Cell Sci *123*, 4011-4018.

Nguyen, D.X., Bos, P.D., and Massague, J. (2009). Metastasis: from dissemination to organ-specific colonization. Nat Rev Cancer *9*, 274-284.

Nir, O., Bakal, C., Perrimon, N., and Berger, B. (2010). Inference of RhoGAP/GTPase regulation using single-cell morphological data from a combinatorial RNAi screen. Genome research *20*, 372-380.

Nitta, T., Hata, M., Gotoh, S., Seo, Y., Sasaki, H., Hashimoto, N., Furuse, M., and Tsukita, S. (2003). Size-selective loosening of the blood-brain barrier in claudin-5-deficient mice. J Cell Biol *161*, 653-660.

Nobes, C.D., and Hall, A. (1995). Rho, rac, and cdc42 GTPases regulate the assembly of multimolecular focal complexes associated with actin stress fibers, lamellipodia, and filopodia. Cell *81*, 53-62.

Nogueira, E., Fidalgo, M., Molnar, A., Kyriakis, J., Force, T., Zalvide, J., and Pombo, C.M. (2008). SOK1 translocates from the Golgi to the nucleus upon chemical anoxia and induces apoptotic cell death. J Biol Chem *283*, 16248-16258.

Nugent, T., and Jones, D.T. (2009). Transmembrane protein topology prediction using support vector machines. BMC Bioinformatics *10*, 159.

O'Rourke, S.M., Dorfman, M.D., Carter, J.C., and Bowerman, B. (2007). Dynein modifiers in C. elegans: light chains suppress conditional heavy chain mutants. PLoS genetics *3*, e128.

Orlova, V.V., Economopoulou, M., Lupu, F., Santoso, S., and Chavakis, T. (2006). Junctional adhesion molecule-C regulates vascular endothelial permeability by modulating VE-cadherin-mediated cell-cell contacts. J Exp Med *203*, 2703-2714.

Orsenigo, F., Giampietro, C., Ferrari, A., Corada, M., Galaup, A., Sigismund, S., Ristagno, G., Maddaluno, L., Young Koh, G., Franco, D*., et al.* (2012). Phosphorylation of VE-cadherin is modulated by haemodynamic forces and contributes to the regulation of vascular permeability in vivo. Nat Commun *3*, 1208.

Osada, S., Izawa, M., Saito, R., Mizuno, K., Suzuki, A., Hirai, S., and Ohno, S. (1997). YSK1, a novel mammalian protein kinase structurally related to Ste20 and SPS1, but is not involved in the known MAPK pathways. Oncogene *14*, 2047-2057.

Oser, M., and Condeelis, J. (2009). The cofilin activity cycle in lamellipodia and invadopodia. J Cell Biochem *108*, 1252-1262.

Ozaki, K., Tanaka, K., Imamura, H., Hihara, T., Kameyama, T., Nonaka, H., Hirano, H., Matsuura, Y., and Takai, Y. (1996). Rom1p and Rom2p are GDP/GTP exchange proteins

(GEPs) for the Rho1p small GTP binding protein in Saccharomyces cerevisiae. EMBO J *15*, 2196-2207.

Pasapera, A.M., Schneider, I.C., Rericha, E., Schlaepfer, D.D., and Waterman, C.M. (2010). Myosin II activity regulates vinculin recruitment to focal adhesions through FAK-mediated paxillin phosphorylation. J Cell Biol *188*, 877-890.

Patenaude, A., Parker, J., and Karsan, A. (2010). Involvement of endothelial progenitor cells in tumor vascularization. Microvasc Res *79*, 217-223.

Pellegrin, S., and Mellor, H. (2007). Actin stress fibres. J Cell Sci *120*, 3491-3499.

Pennacchietti, S., Michieli, P., Galluzzo, M., Mazzone, M., Giordano, S., and Comoglio, P.M. (2003). Hypoxia promotes invasive growth by transcriptional activation of the met protooncogene. Cancer Cell *3*, 347-361.

Pollard, T.D., and Borisy, G.G. (2003). Cellular motility driven by assembly and disassembly of actin filaments. Cell *112*, 453-465.

Potente, M., Gerhardt, H., and Carmeliet, P. (2011). Basic and therapeutic aspects of angiogenesis. Cell *146*, 873-887.

Pracheil, T., Thornton, J., and Liu, Z. (2012). TORC2 signaling is antagonized by protein phosphatase 2A and the Far complex in Saccharomyces cerevisiae. Genetics *190*, 1325-1339.

Preisinger, C., Short, B., De Corte, V., Bruyneel, E., Haas, A., Kopajtich, R., Gettemans, J., and Barr, F.A. (2004). YSK1 is activated by the Golgi matrix protein GM130 and plays a role in cell migration through its substrate 14-3-3zeta. J Cell Biol *164*, 1009-1020.

Price, L.S., Leng, J., Schwartz, M.A., and Bokoch, G.M. (1998). Activation of Rac and Cdc42 by integrins mediates cell spreading. Molecular biology of the cell *9*, 1863-1871.

Pulciani, S., Santos, E., Lauver, A.V., Long, L.K., Robbins, K.C., and Barbacid, M. (1982). Oncogenes in human tumor cell lines: molecular cloning of a transforming gene from human bladder carcinoma cells. Proc Natl Acad Sci U S A *79*, 2845-2849.

Qian, B.Z., Li, J., Zhang, H., Kitamura, T., Zhang, J., Campion, L.R., Kaiser, E.A., Snyder, L.A., and Pollard, J.W. (2011). CCL2 recruits inflammatory monocytes to facilitate breast-tumour metastasis. Nature *475*, 222-225.

Record, C.J., Chaikuad, A., Rellos, P., Das, S., Pike, A.C., Fedorov, O., Marsden, B.D., Knapp, S., and Lee, W.H. (2010). Structural comparison of human mammalian ste20-like kinases. PloS one *5*, e11905.

Ren, X.D., Kiosses, W.B., and Schwartz, M.A. (1999). Regulation of the small GTP-binding protein Rho by cell adhesion and the cytoskeleton. The EMBO journal *18*, 578-585.

Renthal, R. (2010). Helix insertion into bilayers and the evolution of membrane proteins. Cell Mol Life Sci *67*, 1077-1088.

Reymond, N., Fabre, S., Lecocq, E., Adelaide, J., Dubreuil, P., and Lopez, M. (2001). Nectin4/PRR4, a new afadin-associated member of the nectin family that trans-interacts with nectin1/PRR1 through V domain interaction. J Biol Chem *276*, 43205-43215.

Reymond, N., Im, J.H., Garg, R., Vega, F.M., Borda d'Agua, B., Riou, P., Cox, S., Valderrama, F., Muschel, R.J., and Ridley, A.J. (2012). Cdc42 promotes transendothelial migration of cancer cells through 1 integrin. The Journal of Cell Biology *199*, 653-668.

Riant, F., Bergametti, F., Ayrignac, X., Boulday, G., and Tournier-Lasserve, E. (2010). Recent insights into cerebral cavernous malformations: the molecular genetics of CCM. Febs j *277*, 1070-1075.

Ribatti, D. (2009). Endogenous inhibitors of angiogenesis: a historical review. Leuk Res *33*, 638-644.

Ribeiro, P.S., Josue, F., Wepf, A., Wehr, M.C., Rinner, O., Kelly, G., Tapon, N., and Gstaiger, M. (2010). Combined functional genomic and proteomic approaches identify a PP2A complex as a negative regulator of Hippo signaling. Mol Cell *39*, 521-534.

Ridley, A.J. (2011). Life at the leading edge. In Cell (United States: 2011 Elsevier Inc), pp. 1012-1022.

Ridley, A.J., and Hall, A. (1992). The small GTP-binding protein rho regulates the assembly of focal adhesions and actin stress fibers in response to growth factors. Cell *70*, 389-399.

Ridley, A.J., Paterson, H.F., Johnston, C.L., Diekmann, D., and Hall, A. (1992). The small GTP-binding protein rac regulates growth factor-induced membrane ruffling. Cell *70*, 401-410.

Ridley, A.J., Schwartz, M.A., Burridge, K., Firtel, R.A., Ginsberg, M.H., Borisy, G., Parsons, J.T., and Horwitz, A.R. (2003). Cell migration: integrating signals from front to back. Science (New York, NY) *302*, 1704-1709.

Riento, K., and Ridley, A.J. (2003). Rocks: multifunctional kinases in cell behaviour. Nat Rev Mol Cell Biol *4*, 446-456.

Riou, P., Kjaer, S., Garg, R., Purkiss, A., George, R., Cain, R.J., Bineva, G., Reymond, N., McColl, B., Thompson, A.J.*, et al.* (2013). 14-3-3 proteins interact with a hybrid prenyl-phosphorylation motif to inhibit g proteins. Cell *153*, 640-653.

Roberts, P.J., Mitin, N., Keller, P.J., Chenette, E.J., Madigan, J.P., Currin, R.O., Cox, A.D., Wilson, O., Kirschmeier, P., and Der, C.J. (2008). Rho Family GTPase modification and dependence on CAAX motif-signaled posttranslational modification. J Biol Chem *283*, 25150-25163.

Rohn, J.L., Sims, D., Liu, T., Fedorova, M., Schock, F., Dopie, J., Vartiainen, M.K., Kiger, A.A., Perrimon, N., and Baum, B. (2011). Comparative RNAi screening identifies a conserved core metazoan actinome by phenotype. J Cell Biol *194*, 789-805.

Rosen, J.N., Sogah, V.M., Ye, L.Y., and Mably, J.D. (2013). ccm2-like is required for cardiovascular development as a novel component of the Heg-CCM pathway. Dev Biol *376*, 74-85.

Rosenfeldt, H., Castellone, M.D., Randazzo, P.A., and Gutkind, J.S. (2006). Rac inhibits thrombin-induced Rho activation: evidence of a Pak-dependent GTPase crosstalk. J Mol Signal *1*, 8.

Roskoski, R., Jr. (2012). ERK1/2 MAP kinases: structure, function, and regulation. Pharmacol Res *66*, 105-143.

Rossman, K.L., Der, C.J., and Sondek, J. (2005). GEF means go: turning on RHO GTPases with guanine nucleotide-exchange factors. Nat Rev Mol Cell Biol *6*, 167-180.

Sahai, E. (2007). Illuminating the metastatic process. Nature reviewsCancer *7*, 737-749.

Sahai, E., and Marshall, C.J. (2002). RHO-GTPases and cancer. Nature reviewsCancer *2*, 133-142.

Sahai, E., and Marshall, C.J. (2003). Differing modes of tumour cell invasion have distinct requirements for Rho/ROCK signalling and extracellular proteolysis. In Nat Cell Biol (England), pp. 711-719.

Salomon, D., Ayalon, O., Patel-King, R., Hynes, R.O., and Geiger, B. (1992). Extrajunctional distribution of N-cadherin in cultured human endothelial cells. J Cell Sci *102 (Pt 1)*, 7-17.

Sander, E.E., ten Klooster, J.P., van Delft, S., van der Kammen, R.A., and Collard, J.G. (1999). Rac downregulates Rho activity: reciprocal balance between both GTPases determines cellular morphology and migratory behaviour. J Cell Biol *147*, 1009-1022.

Sander, E.E., van Delft, S., ten Klooster, J.P., Reid, T., van der Kammen, R.A., Michiels, F., and Collard, J.G. (1998). Matrix-dependent Tiam1/Rac signaling in epithelial cells promotes either cell-cell adhesion or cell migration and is regulated by phosphatidylinositol 3-kinase. J Cell Biol *143*, 1385-1398.

Schaefer, A., Nethe, M., and Hordijk, P.L. (2012). Ubiquitin links to cytoskeletal dynamics, cell adhesion and migration. Biochem J *442*, 13-25.

Schinkmann, K., and Blenis, J. (1997). Cloning and characterization of a human STE20-like protein kinase with unusual cofactor requirements. J Biol Chem *272*, 28695-28703.

Schulenberg, B., Goodman, T.N., Aggeler, R., Capaldi, R.A., and Patton, W.F. (2004). Characterization of dynamic and steady-state protein phosphorylation using a fluorescent phosphoprotein gel stain and mass spectrometry. Electrophoresis *25*, 2526-2532.

Schulte, J., Sepp, K.J., Jorquera, R.A., Wu, C., Song, Y., Hong, P., and Littleton, J.T. (2010). DMob4/Phocein regulates synapse formation, axonal transport, and microtubule organization. J Neurosci *30*, 5189-5203.

Sellers, J.R. (2000). Myosins: a diverse superfamily. In Biochim Biophys Acta (Netherlands), pp. 3-22.

Senger, D.R., and Davis, G.E. (2011). Angiogenesis. Cold Spring Harb Perspect Biol *3*, a005090.

Shenkar, R., Shi, C., Check, I.J., Lipton, H.L., and Awad, I.A. (2007). Concepts and hypotheses: inflammatory hypothesis in the pathogenesis of cerebral cavernous malformations. Neurosurgery *61*, 693-702; discussion 702-693.

Shi, J., Wu, X., Surma, M., Vemula, S., Zhang, L., Yang, Y., Kapur, R., and Wei, L. (2013). Distinct roles for ROCK1 and ROCK2 in the regulation of cell detachment. Cell Death Dis *4*, e483.

Shih, C., and Weinberg, R.A. (1982). Isolation of a transforming sequence from a human bladder carcinoma cell line. In Cell (United States), pp. 161-169.

Shiu, Y.T., Li, S., Yuan, S., Wang, Y., Nguyen, P., and Chien, S. (2003). Shear stress-induced c-fos activation is mediated by Rho in a calcium-dependent manner. Biochem Biophys Res Commun *303*, 548-555.

Sontag, E. (2001). Protein phosphatase 2A: the Trojan Horse of cellular signaling. Cellular signalling *13*, 7-16.

Stark, C., Breitkreutz, B.J., Reguly, T., Boucher, L., Breitkreutz, A., and Tyers, M. (2006). BioGRID: a general repository for interaction datasets. Nucleic Acids Res *34*, D535-539.

Stegert, M.R., Hergovich, A., Tamaskovic, R., Bichsel, S.J., and Hemmings, B.A. (2005). Regulation of NDR protein kinase by hydrophobic motif phosphorylation mediated by the mammalian Ste20-like kinase MST3. Mol Cell Biol *25*, 11019-11029.

Stockton, R.A., Shenkar, R., Awad, I.A., and Ginsberg, M.H. (2010). Cerebral cavernous malformations proteins inhibit Rho kinase to stabilize vascular integrity. The Journal of experimental medicine *207*, 881-896.

Sun, H., Breslin, J.W., Zhu, J., Yuan, S.Y., and Wu, M.H. (2006). Rho and ROCK signaling in VEGF-induced microvascular endothelial hyperpermeability. Microcirculation *13*, 237-247.

Sung, V., Luo, W., Qian, D., Lee, I., Jallal, B., and Gishizky, M. (2003). The Ste20 kinase MST4 plays a role in prostate cancer progression. Cancer Res *63*, 3356-3363.

Szulcek, R., Beckers, C.M., Hodzic, J., de Wit, J., Chen, Z., Grob, T., Musters, R.J., Minshall, R.D., van Hinsbergh, V.W., and van Nieuw Amerongen, G.P. (2013). Localized RhoA GTPase activity regulates dynamics of endothelial monolayer integrity. Cardiovasc Res.

Tania, N., Prosk, E., Condeelis, J., and Edelstein-Keshet, L. (2011). A temporal model of cofilin regulation and the early peak of actin barbed ends in invasive tumor cells. Biophys J *100*, 1883-1892.

Tillet, E., Vittet, D., Feraud, O., Moore, R., Kemler, R., and Huber, P. (2005). N-cadherin deficiency impairs pericyte recruitment, and not endothelial differentiation or sprouting, in embryonic stem cell-derived angiogenesis. Exp Cell Res *310*, 392-400.

Tojkander, S., Gateva, G., and Lappalainen, P. (2012). Actin stress fibers--assembly, dynamics and biological roles. J Cell Sci *125*, 1855-1864.

Toll, A., Parera, E., Gimenez-Arnau, A.M., Pou, A., Lloreta, J., Limaye, N., Vikkula, M., and Pujol, R.M. (2009). Cutaneous venous malformations in familial cerebral cavernomatosis caused by KRIT1 gene mutations. Dermatology *218*, 307-313.

Tzima, E., Del Pozo, M.A., Kiosses, W.B., Mohamed, S.A., Li, S., Chien, S., and Schwartz, M.A. (2002). Activation of Rac1 by shear stress in endothelial cells mediates both cytoskeletal organisation and effects on gene expression. Embo j *21*, 6791-6800.

Tzima, E., Irani-Tehrani, M., Kiosses, W.B., Dejana, E., Schultz, D.A., Engelhardt, B., Cao, G., DeLisser, H., and Schwartz, M.A. (2005). A mechanosensory complex that mediates the endothelial cell response to fluid shear stress. Nature *437*, 426-431.

van Nieuw Amerongen, G.P., Draijer, R., Vermeer, M.A., and van Hinsbergh, V.W. (1998). Transient and prolonged increase in endothelial permeability induced by histamine and thrombin: role of protein kinases, calcium, and RhoA. Circ Res *83*, 1115-1123.

van Wetering, S., van Buul, J.D., Quik, S., Mul, F.P., Anthony, E.C., ten Klooster, J.P., Collard, J.G., and Hordijk, P.L. (2002). Reactive oxygen species mediate Rac-induced loss of cell-cell adhesion in primary human endothelial cells. J Cell Sci *115*, 1837-1846.

Vega, F.M., Colomba, A., Reymond, N., Thomas, M., and Ridley, A.J. (2012). RhoB regulates cell migration through altered focal adhesion dynamics. Open Biol *2*, 120076.

Vega, F.M., Fruhwirth, G., Ng, T., and Ridley, A.J. (2011). RhoA and RhoC have distinct roles in migration and invasion by acting through different targets. J Cell Biol *193*, 655-665.

von Heijne, G., and Gavel, Y. (1988). Topogenic signals in integral membrane proteins. Eur J Biochem *174*, 671-678.

Voss, K., Stahl, S., Schleider, E., Ullrich, S., Nickel, J., Mueller, T.D., and Felbor, U. (2007). CCM3 interacts with CCM2 indicating common pathogenesis for cerebral cavernous malformations. Neurogenetics *8*, 249-256.

Wallez, Y., and Huber, P. (2008). Endothelial adherens and tight junctions in vascular homeostasis, inflammation and angiogenesis. Biochim Biophys Acta *1778*, 794-809.

Watanabe, N., Kato, T., Fujita, A., Ishizaki, T., and Narumiya, S. (1999). Cooperation between mDia1 and ROCK in Rho-induced actin reorganization. Nature Cell Biology *1*, 136-143.

Watanabe, T., Hosoya, H., and Yonemura, S. (2007). Regulation of myosin II dynamics by phosphorylation and dephosphorylation of its light chain in epithelial cells. Mol Biol Cell *18*, 605-616.

Whitehead, K.J., Chan, A.C., Navankasattusas, S., Koh, W., London, N.R., Ling, J., Mayo, A.H., Drakos, S.G., Jones, C.A., Zhu, W.*, et al.* (2009). The cerebral cavernous malformation signaling pathway promotes vascular integrity via Rho GTPases. Nat Med *15*, 177-184.

Wittchen, E.S., Haskins, J., and Stevenson, B.R. (1999). Protein interactions at the tight junction. Actin has multiple binding partners, and ZO-1 forms independent complexes with ZO-2 and ZO-3. J Biol Chem *274*, 35179-35185.

Wojciak-Stothard, B., Potempa, S., Eichholtz, T., and Ridley, A.J. (2001). Rho and Rac but not Cdc42 regulate endothelial cell permeability. J Cell Sci *114*, 1343-1355.

Wojciak-Stothard, B., and Ridley, A.J. (2002). Rho GTPases and the regulation of endothelial permeability. Vascul Pharmacol *39*, 187-199.

Wojciak-Stothard, B., and Ridley, A.J. (2003). Shear stress-induced endothelial cell polarization is mediated by Rho and Rac but not Cdc42 or PI 3-kinases. J Cell Biol *161*, 429-439.

Wolf, M.J., Hoos, A., Bauer, J., Boettcher, S., Knust, M., Weber, A., Simonavicius, N., Schneider, C., Lang, M., Stürzl, M.*, et al.* (2012). Endothelial CCR2 signaling induced by colon carcinoma cells enables extravasation via the JAK2-Stat5 and p38MAPK pathway. Cancer Cell *22*, 91-105.

Wu, H.Y., Lin, C.Y., Chen, T.C., Pan, S.T., and Yuan, C.J. (2011). Mammalian Ste20-like protein kinase 3 plays a role in hypoxia-induced apoptosis of trophoblast cell line 3A-sub-E. Int J Biochem Cell Biol *43*, 742-750.

Wu, Y.I., Frey, D., Lungu, O.I., Jaehrig, A., Schlichting, I., Kuhlman, B., and Hahn, K.M. (2009). A genetically encoded photoactivatable Rac controls the motility of living cells. Nature *461*, 104-108.

Wyckoff, J.B., Jones, J.G., Condeelis, J.S., and Segall, J.E. (2000). A critical step in metastasis: in vivo analysis of intravasation at the primary tumor. Cancer Res *60*, 2504-2511.

Xiang, Q., Rasmussen, C., and Glass, N.L. (2002). The ham-2 locus, encoding a putative transmembrane protein, is required for hyphal fusion in Neurospora crassa. Genetics *160*, 169-180.

Yang, C., and Svitkina, T. (2011). Filopodia initiation: focus on the Arp2/3 complex and formins. Cell Adh Migr *5*, 402-408.

Yang, J., and Weinberg, R.A. (2008). Epithelial-mesenchymal transition: at the crossroads of development and tumor metastasis. In Dev Cell (United States), pp. 818-829.

Yang, S.H., Sharrocks, A.D., and Whitmarsh, A.J. (2013). MAP kinase signalling cascades and transcriptional regulation. Gene *513*, 1-13.

Yoon, S.O., Casaccia-Bonnefil, P., Carter, B., and Chao, M.V. (1998). Competitive signaling between TrkA and p75 nerve growth factor receptors determines cell survival. J Neurosci *18*, 3273-3281.

Yoruk, B., Gillers, B.S., Chi, N.C., and Scott, I.C. (2012). Ccm3 functions in a manner distinct from Ccm1 and Ccm2 in a zebrafish model of CCM vascular disease. Dev Biol *362*, 121-131.

You, C., Erol Sandalcioglu, I., Dammann, P., Felbor, U., Sure, U., and Zhu, Y. (2013). Loss of CCM3 impairs DLL4-Notch signalling: implication in endothelial angiogenesis and in inherited cerebral cavernous malformations. J Cell Mol Med.

Young, M.R., Kolesiak, K., and Meisinger, J. (2002). Protein phosphatase-2A regulates endothelial cell motility and both the phosphorylation and the stability of focal adhesion complexes. International journal of cancerJournal international du cancer *100*, 276-282.

Yu, M., Bardia, A., Wittner, B.S., Stott, S.L., Smas, M.E., Ting, D.T., Isakoff, S.J., Ciciliano, J.C., Wells, M.N., Shah, A.M.*, et al.* (2013). Circulating Breast Tumor Cells Exhibit Dynamic Changes in Epithelial and Mesenchymal Composition. Science *339*, 580-584.

Zhang, H., Ma, X., Deng, X., Chen, Y., Mo, X., Zhang, Y., Zhao, H., and Ma, D. (2012). PDCD10 interacts with STK25 to accelerate cell apoptosis under oxidative stress. Front Biosci *17*, 2295-2305.

Zhao, Y., Tan, Y.Z., Zhou, L.F., Wang, H.J., and Mao, Y. (2007). Morphological observation and in vitro angiogenesis assay of endothelial cells isolated from human cerebral cavernous malformations. Stroke *38*, 1313-1319.

Zheng, X., Xu, C., Di Lorenzo, A., Kleaveland, B., Zou, Z., Seiler, C., Chen, M., Cheng, L., Xiao, J., He, J.*, et al.* (2010). CCM3 signaling through sterile 20-like kinases plays an essential role during zebrafish cardiovascular development and cerebral cavernous malformations. The Journal of clinical investigation.

Zheng, X., Xu, C., Smith, A.O., Stratman, A.N., Zou, Z., Kleaveland, B., Yuan, L., Didiku, C., Sen, A., Liu, X.*, et al.* (2012). Dynamic regulation of the cerebral cavernous malformation pathway controls vascular stability and growth. Dev Cell *23*, 342-355.

Zhou, T.H., Ling, K., Guo, J., Zhou, H., Wu, Y.L., Jing, Q., Ma, L., and Pei, G. (2000). Identification of a human brain-specific isoform of mammalian STE20-like kinase 3 that is regulated by cAMP-dependent protein kinase. J Biol Chem *275*, 2513-2519.

Ziegler, W.H., Gingras, A.R., Critchley, D.R., and Emsley, J. (2008). Integrin connections to the cytoskeleton through talin and vinculin. In Biochem Soc Trans (England), pp. 235-239.

Acknowledgements

I cannot thank my supervisor, Professor Anne Ridley enough for giving me the opportunity to conduct my Ph.D research in her laboratory. I am very grateful for her guidance, support, limitless patience, and for giving me scientific freedom. The skills and experiences I have gained during the course of my Ph.D will be invaluable for what the future holds.

Many thanks to my second supervisor, Professor Gareth Jones for his scientific input and support.

I would like to thank all past and present members of the Ridley lab., and I am sorry if I have not mentioned everyone individually. Thank you to my fellow Ph.D students Elvira, Barbara, Christina, Silvia M. and Raquel for the friendly chats, and for the great work environment. Special thanks to Ritu for her words of advice and support, and for putting up with my drumming. Many thanks to Francisco, Philippe, Virginia, Nico, Parag, Undine and Sarah for technical advice and scientific discussions. Thank you Audrey and Silvia G. for helpful conversations, and for sharing these three years with me. Thank you Richard for helping make sure my experiments went ahead.

Further thanks go to Fahim, Yolanda and the members of the Sanz Moreno lab. including Jose, Pahini and Cecilia for being great office and lab. mates. Thank you also to Anthony, Simao, Simon, Anna, Vineetha, Shukolpa and Seema. I am grateful to Dr. Ignatius Tavares and Dr. Jonathan Morris for their career advice. Thank you also to Dr. Baljinder Mankoo and Helen Rudkin for helping with the smooth progress of my Ph.D.

Last but most importantly, a big thank you to my parents and brother for being my rock, and for their unquestioning support and encouragement.